

Perturbative Corrections to Hadronic Amplitudes with Heavy Quarks

DISSERTATION
zur Erlangung des akademischen Grades eines Doktors
der Naturwissenschaften

vorgelegt von
M.Sc. Denis Rosenthal

eingereicht bei der Naturwissenschaftlich-Technischen Fakultät
der Universität Siegen

Siegen
September 2015

Gutachter der Dissertation: Prof. Dr. Alexander Khodjamirian

Prof. Dr. Thomas Mannel

Datum der Disputation: 06.11.2015

Prüfungskommission: Prof. Dr. Alexander Khodjamirian

Prof. Dr. Thomas Mannel

Prof. Dr. Alexei A. Pivovarov

Prof. Dr. Ivor Fleck

Für meine Mutter

ABSTRACT

Heavy meson decays are of significant importance for testing the Standard Model of particle physics. They provide possibilities to determine its parameters from experimental data and give hints to physics beyond the Standard Model. In order to exploit the provided data, a deep theoretical understanding of these decays is mandatory. The thesis is devoted to a thorough theoretical analysis of selected aspects of heavy meson flavor physics with the focus on the perturbative QCD effects.

The first part of the thesis is dedicated to the evaluation of leptonic decay constants. Decay constants constitute hadronic quantities, which parametrize transitions of a single meson to the QCD vacuum that are mediated by a local flavor current. They contain the only hadronic information in leptonic weak decays and enter as input parameters into the description of non-leptonic heavy meson decays and mixing processes. We apply the method of QCD sum rules to estimate the decay constants of vector and pseudoscalar heavy-light mesons in their ground state. This method includes the operator product expansion (OPE), which allows for a systematic implementation of perturbative corrections. We calculate perturbative QCD corrections to the leading term of the OPE with next-to-leading order accuracy. To this end, we construct a computation routine for one- and two-loop topologies and present the computational techniques in detail. The effects of $SU(3)$ -flavor violation are also taken into account by including corrections of the strange quark mass. Our results gain highest precision within this approach by including all known perturbative contributions and new corrections to the quark-condensate contribution in the vector-meson channel for the first time.

In the second part we extend the QCD sum rule method, in which, in addition to the ground state contribution, excited states are also included. We present a statistical analysis to determine the decay constants of the first radially excited states of heavy-light mesons.

The final part of the thesis discusses inclusive weak decays of heavy hadrons. We apply the OPE within the heavy quark effective theory (HQET) to determine the total decay rate of such decays. We compute the radiative correction to the coefficient function of the power-suppressed chromomagnetic operator with next-to-leading accuracy. This correction is computed analytically and was up to now unknown. For this purpose, we perform a QCD-HQET-matching calculation and build a computational environment for on-shell two- and three-loop Feynman graphs. For phenomenological applications we also present moments of differential distributions. As a final statement, the influence on the CKM matrix entry $|V_{cb}|$ due to the new correction term is estimated.

ZUSAMMENFASSUNG

Die Zerfälle von schweren Mesonen stellen einen wichtigen Bestandteil zur Verifikation des Standardmodells der Teilchenphysik dar. Mit diesen Zerfällen lassen sich bestimmte Parameter des Standardmodells experimentell überprüfen und können damit Hinweise auf Phänomene jenseits des Standardmodells geben. Zur Auswertung der experimentellen Daten ist ein grundlegendes Verständnis der betrachteten Zerfälle notwendig. In dieser Arbeit werden ausgewählte Aspekte der Flavourphysik mit schweren Mesonen betrachtet, wobei die theoretische Analyse von perturbativen QCD-Effekten im Vordergrund steht.

Der erste Teil dieser Arbeit widmet sich der Bestimmung von leptonischen Zerfallskonstanten. Diese sind hadronische Matrixelemente, welche durch einen lokalen Flavourstrom Übergänge zwischen einem Mesonen und dem QCD-Vakuum vermitteln. Für leptonische Zerfälle beschreiben die Zerfallskonstanten hadronische Effekte. Sie finden ebenso Anwendung bei der Beschreibung von nicht-leptonischen Zerfällen und hadronischen Mischungsprozessen. Um die Zerfallskonstanten von vektoriellen und pseudoskalaren Mesonen in ihrem Grundzustand zu bestimmen, wird die Methode der QCD Summenregeln angewendet. Diese Methode ermöglicht eine systematische Implementierung von perturbativen Korrekturen mit Hilfe der Operatorproduktentwicklung (OPE). In dieser Arbeit wird eine Berechnungsroutine für Ein- und Zweischleifenintegrale verwendet, um den führenden Term der OPE und die nächstführende Ordnung um die starke Kopplung zu berechnen. Des Weiteren werden Korrekturen betrachtet, welche von der Masse des Strange Quarks abhängen. Diese führen zur Brechung der $SU(3)$ -Flavoursymmetrie. Im Rahmen der Methode werden Zerfallskonstanten mit der derzeit höchsten Präzision bestimmt, da alle bekannten perturbativen Beiträge und neue Korrekturen zum Quarkkondensat für Vektormesonen mitberücksichtigt werden.

Im zweiten Teil wird die Methode der QCD Summenregeln erweitert, um Aussagen jenseits der Grundzustandsmesonen treffen zu können. Zu diesem Zweck wird eine statistische Analyse verwendet um die Zerfallskonstanten der radial angeregten Zustände von schweren Mesonen zu bestimmen.

Im letzten Teil werden inklusive Zerfälle von schweren Hadronen betrachtet. Dazu dient die OPE im Rahmen der *Heavy Quark Effective Theory* (HQET) als mathematisches Konstrukt zur Parametrisierung der totalen Zerfallsbreiten solcher Zerfälle. In dieser Arbeit wird die Strahlungskorrektur als Koeffizientenfunktion des zugehörigen massenunterdrückten chromomagnetischen Operators bestimmt und die Korrektur in analytischer Form in nächstführender Ordnung um die starke Kopplung zum ersten Mal berechnet. Die Berechnung wird mit Hilfe eines QCD-HQET-Vergleich (Matching) durchgeführt. Hierfür wurde ein Berechnungsschema zur Bestimmung von Zwei-

und Dreischleifen-Feynmandiagrammen mit dem externen Impuls auf der Massenschale entwickelt. Als Ergebnis werden die totalen Zerfallsbreiten sowie die Momente der differentiellen Zerfallsbreiten angegeben, welche für phenomologische Anwendungen interessant sind. Diese Korrekturen haben Auswirkungen auf den Wert des CKM-Matrixelements $|V_{cb}|$, die abschließend diskutiert werden.

Contents

1	Introduction	1
2	The Standard Model	7
2.1	Outline of the Standard Model	7
2.2	Fundamentals of the Electroweak Theory	11
2.3	The CKM Quark-Mixing Matrix	14
2.4	Fundamentals of QCD	16
2.5	Classification of Heavy-light Mesons	19
2.6	Perturbative QCD: $e^+e^- \rightarrow$ hadrons	19
3	Applications of QCD Sum Rules to Leptonic Decay Constants	23
3.1	Two-Point Correlation Function	25
3.2	Hadronic Representation	26
3.3	Dispersion Relation	27
3.4	Operator Product Expansion	29
3.5	Quark-Hadron Duality and Borel Transformation	36
3.6	Sum rules in the Infinite Heavy-Quark-Mass limit	39
4	Perturbative Corrections to the Two-Point Correlation Functions	43
4.1	Essentials for Loop Computation	44
4.2	Leading Order Contribution	51
4.3	Next-to-Leading Order Contribution	52
4.4	Light-Quark Mass Corrections	55
5	Decay Constants of B and D Mesons from QCD Sum Rules	57
5.1	Numerical analysis of Borel sum rules	57
5.2	Numerical Results of Borel Sum Rules	66
5.3	Alternative Versions of Sum Rules	68
5.4	Discussion of Results	73
6	Decay Constants of Radially Excited B and D Mesons from QCD Sum Rules	79
6.1	Including Radial Excitations in QCD Sum Rules	80
6.2	Strategies and Prerequisites for the Numerical Analysis	82

6.3	Numerical Results of Borel Sum Rules for Radial Excitations	84
6.4	Summary and Concluding Remarks	88
7	Decay Rate of Inclusive Semileptonic B Decays from QCD	91
7.1	Basics of Heavy Quark Effective Theory	94
7.2	Heavy Quark Expansion for the Total Decay Rate	96
7.3	Coefficient Functions of HQE	99
7.4	The Total Width and Moments of the Differential Distribution	108
7.5	Impact on CKM Matrix Element $ V_{cb} $	109
7.6	Discussion of Results	110
8	Technical Aspects of Perturbative Corrections to Inclusive B-Decays	113
8.1	Leading Power Coefficient (Partonic Width)	113
8.2	EOM Operator Coefficient	117
8.3	Chromomagnetic Operator Coefficient	122
8.4	Heavy-quark Current Operator Coefficient	125
9	Summary and Discussion	127
A	General Setup and Properties	131
A.1	Regularization	131
A.2	Definitions and Properties of Feynman Integrals within Dimension Regularization	132
A.3	Renormalization and Quark Masses	133
A.4	Renormalization Group Functions	138
B	OPE and Hadronic Expressions for Two-Point Correlator	141
B.1	Hadronic representation of the two-point correlator	141
B.2	Details about the Dispersion Relation	143
B.3	LiteRed Basis and Master Integrals	144
B.4	Perturbative Spectral Function	147
B.5	Condensate Contributions	149
B.6	Sum rules for Pseudoscalar Quark Currents in the Infinite Heavy-Quark-Mass Limit	151
C	List of Masters of On-Shell Two- and Three-Loop Topology	153
C.1	LiteRed Basis and Master Integrals with Two Masses	153

C.2 LiteRed Basis and Master Integrals	
with One Mass ($m_c = 0$)	159
C.2.1 Two-Loop Prototypes	160
C.2.2 Three-Loop Prototypes	160
C.3 Calculation of N_+ and N_-	162
Bibliography	167
List of Publications	181

CHAPTER 1

Introduction

In the second half of the 20th century the knowledge about physics has reached a new milestone. As a collaborative work of many scientists the *Standard Model* (SM) of elementary particle physics was developed. The SM is a quantum field theory, which includes a multitude of elementary particles as building blocks of matter, and describes three of the four fundamental forces of nature: the electromagnetic, the weak and the strong force. Its success is based on a large number of measurements as a confirmation of the theory's predictions.

The first steps towards the final description of the SM started in the 1950's with Yang's and Mills' work in extending gauge invariance from local to non-local (non-commuting) transformations [1]. This achievement laid the foundations for the unification of electromagnetic and weak interactions, which was developed about ten years later by Glashow [2]. At the same time, three individual groups published a formalism that refers to the generation of mass of the weak gauge bosons [3, 4, 5], the *Higgs mechanism*. A few years later Weinberg and Salam included the Higgs mechanism to the existing theories, which gave the electroweak theory its modern form [6, 7]. 't Hooft and Veltman finally proved that arising divergencies within this theory could be removed by the process of renormalization [8]. This last step enabled precise calculations of particle properties in perturbation theory. The third force is described by the theory of strong interactions, the *Quantum Chromodynamics* (QCD). It was initiated by many scientists in the 1960's such as Gell-Mann, Nishijima, Ne'eman and Zweig, to name only a few. QCD describes the interaction of quarks and gluons inside of hadrons.

Throughout the 1950's and 60's, improvements in collider experiments led to a large variety of observed particles. It became evident that they were built by smaller yet invisible constituents. A notable puzzle in that time was the measured lifetime of "strange" particles. Their lifetimes were much larger as one would have expected for strong and electromagnetic decays. Therefore, in 1953 Gell-Mann introduced an additional quantum number, the *strangeness*, which is carried by *strange* quarks [9]. With this new quantum number, the puzzle about longer lifetimes could be resolved, and

it also explained the appearance of pairs of strange particles in strong interactions. In 1964 the discovery of the Ω -baryon state $|\Omega\rangle = |sss\rangle$ confirmed the existence of the postulated quark [10]. The existence of a baryon with three identical quarks and parallel spins also indicated the necessity of another quantum number, since otherwise the Pauli exclusion principle would be violated. This new quantum number was later referred to as *color*. Electron-positron annihilation in collision experiments also showed that there are exactly three states of this quantum number. Along with Zweig, Gell-Mann explained all known quarks as building blocks of hadrons and carriers of color [11, 12]. The next apparent problem was the mismatch between the predicted and measured branching fraction of neutral kaon decays into muons ($K^0 \rightarrow \mu^+\mu^-$) [13]. In the 1970's this discrepancy was solved by Glashow, Iliopoulos and Maiani by introducing a fourth quark flavor, the charm quark [14]. All contributing effects to the neutral kaon decay result in a significant reduction of the predicted branching fraction, which is compatible to the experimental value. In 1974 the discovery of the J/ψ -particle ($c\bar{c}$) confirmed the existence of the proposed charm quark [15, 16].

The observation of $K_L^0 \rightarrow \pi^+\pi^-$ by Cronin and Fitch [17] has led to another extension of the quark family, a third generation (set) of quark pairs, yielding six quark flavors in total. An explanation for the long-living K_L^0 decaying into two pions was found in the CP violation of weak decays. CP denotes the combination of two discrete symmetries, namely the symmetry under charge conjugation transformation C , transforming a particle into its antiparticle, and the symmetry under parity inversion, which lead to the mirror image of a physical system. In theory at least three quark-flavor generations allow CP-violating decays and, hence, the search for the two postulated quarks was initiated [18]. The confirmation of the third and final generation started in 1977 with the discovery of the bottom quark by the E288 collaboration [19]. In 1995 the top-quark was discovered by the CDF and D0 collaboration [20, 21], which concluded the quark family¹. Kobayashi and Maskawa identified the additional phase parameter in the three-generational theory as the source for observed CP-violation. The final confirmation of the phase parameter was provided by the BaBar and Belle collaboration in 2001 for the evidence of CP-violation in the B^0 system [23, 24]. An integral part of the SM are also the mixing properties between individual quark flavor, as accumulated in a 3×3 matrix (CKM matrix) [25, 18]. This matrix is named after its founders Cabibbo, Kobayashi and Maskawa. Besides, there are three lepton generations that are also characterized by their flavor. Precision measurements of the Z -boson give hints to the number of flavor-generations. Due to the large mass of the Z -boson, it decays

¹A fourth generation is excluded by LHC and Tevatron Higgs data and electroweak precision data [22].

into all kinds of lepton flavor pairs. Its total width strongly indicates the existence of just three lepton flavors with light neutrinos [26].

Recently, the last missing particle of the SM, the *Higgs boson*, was discovered at the *Large Hadron Collider* at CERN [27, 28].

Despite the success of the SM, it is still not a complete theory. An outstanding puzzle is the missing explanation regarding the number and the given arrangement of fundamental particles. Hence, one can examine this established model for problems, which exceed its scope of application. A selection of such unanswered questions and others that are based on evidence from experimental observations, are the following:

- *Neutrino masses.* Neutrinos are considered as massless in the SM. But in 1998 and 2002, the Super-Kamiokande and SNO experiments provided evidence that neutrinos have a small mass due to the relative abundance of atmospheric electron and muon neutrinos [29, 30]. These measurements confirmed the oscillation of neutrinos, changing from one lepton flavor to another. Only massive particles are capable in performing such flavor oscillations.
- *Number of free parameters.* The SM has 19 independent free parameters in total. However, the SM cannot give any insights into their values. Instead, they can only be extracted from specific particle processes.
- *Embedding general relativity.* No theory of gravity is included in the SM. Still, it is unclear how to reconcile the concept of general relativity and renormalizable quantum field theories.
- *Baryon-Asymmetry.* The common expectation is that matter and anti-matter should have been created in equal amount at the Big Bang [31]. After the universe's "cool-down" both forms of matter would have annihilated completely, if the CP-symmetry were preserved. The principles of CP violation based on the SM cannot explain the imbalance of matter and anti-matter [32]. However, from observations we know that CP-violating effects within the SM are too small and new sources of CP violation are necessary to explain the distinct amount of residual matter.
- *Dark matter and energy.* From cosmological observations we know that our universe is not build up by the visible matter. The dynamics of the universe infer the existence of dark matter (unobserved non-luminous matter) and dark energy (hypothetical form of energy with negative pressure and repulsive gravity).

On the basis of these puzzles, there are good reasons to investigate the applicability of the SM and strive for concepts towards a more universal theory. Hence, a deep understanding of this theory is essential. Common strategies for testing the SM are direct and indirect searches for discrepancies between theory predictions and experimental measurements. Both possibilities imply the extension to new physics models beyond the SM (BSM). The direct search includes the production of new particles, which have not been discovered yet. The indirect way is built on precision determination of SM parameters to find deviations between the theoretical description and experimental data at the quantum level. Heavy unknown particles may contribute via underlying virtual effects that influence the SM predictions.

In light of these indirect searches, the phenomenological aspects of weak decays are a rich resource for understanding the nature of elementary particle interactions. The key experiments started more than hundred years ago measuring the energy and momentum spectra for β - and μ -decays at low momentum transfer [33]. Nowadays precision measurements of various weak decays of heavy mesons are used to determine SM parameters. Moreover, they are also the most promising probe for BSM physics. But in order to measure the underlying weak effects, it is crucial to have a thorough understanding of the phenomenology of the strong-interactions as well. The decays of B mesons have some specific properties, which are beneficial for the theoretical description. Heavy-light B mesons consist of a heavy bottom and a light quark $q = \{u, d, s\}$. To some extent these arguments also hold for D mesons, including a heavy charm quark. The structure of charged-current interaction, which are relevant for this thesis, gives rise to three classes of weak B decays:

1. The first class encompasses the leptonic decays of B mesons. Here the valence quarks annihilate and produce a dilepton pair in the final state. As an example, one can consider the decay of $B \rightarrow \tau \bar{\nu}_\tau$, shown in Fig. 1.1(a). At lowest order in the electroweak theory, the decay width is

$$\Gamma(B \rightarrow \tau \bar{\nu}_\tau) = \frac{G_F^2}{8\pi} f_B^2 |V_{bq}|^2 m_\tau^2 m_B \left(1 - \frac{m_\tau^2}{m_B^2}\right)^2, \quad (1.1)$$

where G_F is the Fermi constant, m_τ and m_B are the masses of the tau-lepton and the B mesons, respectively, V_{bq} is the $b \rightarrow q$ transition CKM matrix element and f_B is the decay constant of the B meson. The latter quantity characterizes the meson-to-vacuum transition and contains all information in the realm of strong-interaction effects.

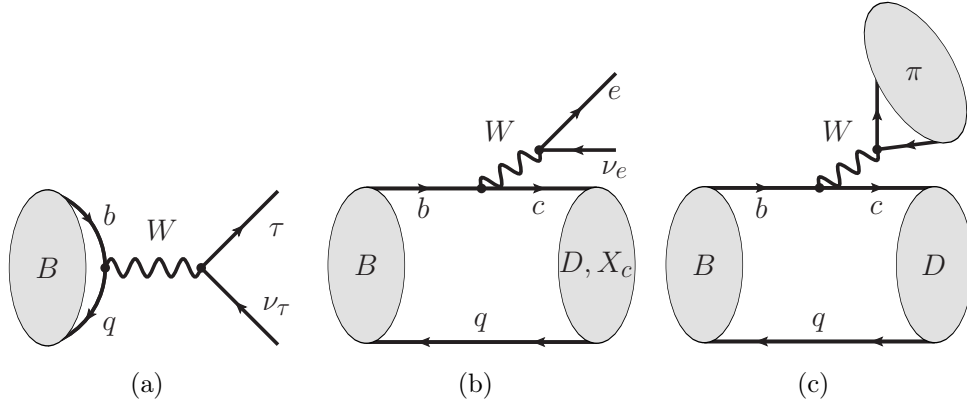


Figure 1.1: Examples of (a) leptonic $B \rightarrow \tau \bar{\nu}_\tau$, (b) exclusive (inclusive) semileptonic $B \rightarrow D e \bar{\nu}_e$ ($B \rightarrow X_c e \bar{\nu}_e$) and (c) hadronic $B \rightarrow D \pi$ decays of B mesons.

- The second class consists of semileptonic decays, in which both leptons and hadrons are in the final state. For exclusive decays, the decay width can be formulated in terms of invariant form factors, which depend on the momentum transfer q^2 between the initial and final meson. For inclusive decays, where we sum over all possible final state mesons, one can apply the *heavy quark expansion* (HQE) to decompose the decay width, see also Fig. 1.1 (b). The formal description of the semileptonic inclusive decay width is

$$\Gamma(B \rightarrow X_q e \bar{\nu}_e) = \Gamma(b \rightarrow q e \bar{\nu}_e) + \frac{1}{m_b} \Delta\Gamma^{(1)} + \frac{1}{m_b^2} \Delta\Gamma^{(2)} + \dots \quad (1.2)$$

Here we consider the B meson decaying into a hadron state, which includes a light quark q , and a dilepton pair, see Fig. 1.1 (c). At leading order the hadronic decay width can be expressed in terms of the partonic width. All other contributions are power-suppressed correction terms.

- The third class considers the decay of B meson into hadrons. The theoretical formalism for processes of this kind is the most recent and the least developed one. Two-body hadronic decays are studied, e.g. in Ref. [34], and studies of three-body hadronic decays are ongoing [35].

In the following, we will focus on the QCD effects of the first two classes.

The structure of this thesis can be outlined as follows: Chapter 2 is dedicated to the SM of particle physics. We outline some basic features of this theory with respect to the gauge symmetry properties and particle content. Further, we discuss the electroweak theory, quark-flavor mixing, fundamentals of the QCD and perturbative QCD in electron-positron annihilation. In the chapters 3–5 we investigate the decay constants of heavy-light mesons, including either a bottom or a charm quark, by using the method of QCD sum rules. We set focus on the perturbative structure of the formalized sum rules and give analytical results for the NLO radiative corrections to the leading OPE contribution. The calculational strategies and tools for computing the resulting master integrals are introduced and discussed. We also perform a detailed numerical study to give updated estimations of the decay constants. Finally, the method itself is tested and compared to alternative versions based on QCD sum rules. Chapter 6 presents the first step for extending the previous study to the extraction of the decay constants of heavy-light mesons beyond their ground state. In our formalism we add the first radial-excited state of the mesons and estimate the decay constants with various strategies within the method of QCD sum rules. The chapters 7 and 8 are dedicated to inclusive semileptonic B decays. We use the heavy quark expansion to expand the total decay rate in powers of $1/m_Q$ and separate the series term-wise into perturbative and non-perturbative expressions. Analytical results for leading power and power-suppressed terms with NLO accuracy are given and strategies for extracting the relevant contributions as well as calculating all master integrals are discussed. The latter terms have not been known yet. A brief discussion on the influence of the new correction term on V_{cb} is also presented. In Appendix B selected intermediate and final results are collected. We also give extended details regarding some basic facts, which are useful for the understanding of this thesis.

The Standard Model

In this chapter we outline the concept of the Standard Model. A detailed review on theoretical aspects and the experimental status is given in Refs. [36, 37, 38].

2.1 Outline of the Standard Model

Particle Content and Fundamental Forces

The Standard Model is built up from a multitude of elementary particles. The spectrum of particles includes 12 fermions (six leptons and six quarks), twelve gauge bosons (three weak bosons, eight gluons and the photon) and a Higgs boson (see Tabs. 2.1 and 2.2). Fermions are of spin $1/2$ and classified into three generations. Only the particles in the first generation build up stable matter. The known particles in the lepton sector are the electron e^- , the muon μ^- and the tau-lepton τ^- . Their electric charge is $Q = -1$ in units of the elementary charge. Each lepton has a corresponding neutrino ν_e , ν_μ and ν_τ that is electrically neutral. In the quark sector there are six flavors of quarks divided into up-type quarks u (up), c (charm) and t (top) with fractional charge $Q = 2/3$ and down-type quarks d (down), s (strange) and b (bottom) with $Q = -1/3$. Note that for each particle there exists an antiparticle with the same mass but opposite quantum numbers. The masses of quarks and leptons have a hierarchical structure, which extends over several magnitudes – as shown in Tab. 2.2.

All fermions are subject to three types of interactions (electromagnetic, weak and strong). Each type of interaction is mediated by its gauge bosons with spin 1. The photon couples to electric-charged particles mediating the electromagnetic interaction. Charged W^\pm and neutral Z bosons couple to fermions. Strong interactions are mediated by eight gluons between color-charged particles. Apart from quarks gluons also carry color, which allows for their mutual interaction. The massive Higgs boson has spin 0 and results from *spontaneous symmetry breaking* of the SM Lagrangian. Due to this breaking mechanism other elementary particles acquire their masses. In the following, we discuss the quantum field theories, in which the particles of the SM are embedded as quantized fields.

Force	Mediator	Affected Particles	Gauge Theory
Electromagnetic	Photon γ	Charged particles	QED
Weak	W^\pm and Z -boson	All fermions	EWT
Strong	Gluon g	Quarks	QCD

Table 2.1: The fundamental forces in nature are described by gauge theories: Quantum electrodynamics (QED), electroweak theory (EWT) – a unification of electromagnetic and weak interaction, Quantum Chromodynamics (QCD).

Gauge Symmetry

The simplest description of a gauge theory is based on $U(1)$ gauge symmetry. To this end, we consider the Lagrangian for free fermion fields ψ :

$$\mathcal{L}_{\text{free}} = \bar{\psi}(i\cancel{D} - m)\psi. \quad (2.1)$$

This Lagrangian is invariant under global $U(1)$ transformations:

$$\psi \rightarrow e^{i\mathbb{Q}\theta}\psi, \quad \bar{\psi} \rightarrow e^{-i\mathbb{Q}\theta}\bar{\psi}, \quad (2.2)$$

where θ is a real constant and \mathbb{Q} is the generator of the $U(1)$ group. If one promotes local dependence to the phase parameter $\theta = \theta(x)$, the Lagrangian for free fermions is no longer invariant under such local phase transformations, which are also called gauge transformations. Invariance of gauge transformations can be achieved by using the covariant derivative

$$D_\mu = \partial_\mu - ig\mathbb{Q}A_\mu. \quad (2.3)$$

The covariant derivative includes the coupling constant g and the gauge field $A_\mu(x)$, transforming as

$$A_\mu(x) \rightarrow A_\mu(x) + \frac{1}{g}\partial_\mu\theta(x). \quad (2.4)$$

We finally obtain the $U(1)$ gauge-invariant Lagrangian for fermions

$$\mathcal{L} = \bar{\psi}(x)(i\cancel{D} - m)\psi(x) - \frac{1}{4}F_{\mu\nu}F^{\mu\nu}. \quad (2.5)$$

Here, we added the kinetic term that includes the field strength tensor

$$F_{\mu\nu} = \partial_\mu A_\nu - \partial_\nu A_\mu = -\frac{i}{g}[D_\mu, D_\nu]. \quad (2.6)$$

Note that the resulting Lagrangian describes the *Quantum electrodynamics* (QED), which is the relativistic quantum field theory of electromagnetism. In this case the generator is the electric charge operator \mathbb{Q} and g the elementary charge. The eigenvalues of \mathbb{Q} are -1 ($+1$) for electrons (positrons).

Yang and Mills extended gauge invariance by including local non-abelian (non-commuting) transformations of the $SU(2)$ group [1], which can be generalized to $SU(n)$. Transformations of a $SU(n)$ gauge group have $n^2 - 1$ generators \mathbf{T}^a . They obey the commutation relations

$$[\mathbf{T}^a, \mathbf{T}^b] = f^{abc}\mathbf{T}^c, \quad (2.7)$$

where f^{abc} are the structure constants of the group. The Lagrangian of a general non-abelian gauge theory with Ψ a multiplet of fermion fields ψ_i ($i = 1, \dots, n$), has the form

$$\mathcal{L}_{\text{YM}} = \bar{\Psi}(i\not{D} - m)\Psi - \frac{1}{4}F_{\mu\nu}^a F_a^{\mu\nu}, \quad (2.8)$$

where

$$F_{\mu\nu}^a = \partial_\mu A_\nu^a - \partial_\nu A_\mu^a - gf^{abc}A_\mu^b A_\nu^c = -\frac{i}{g}[\mathbf{D}_\mu, \mathbf{D}_\nu], \quad (2.9)$$

$$\mathbf{D}_\mu = \partial_\mu \mathbf{I} + i\mathbf{g}\mathbf{T}^a A_\mu^a. \quad (2.10)$$

Here, \mathbf{g} is the coupling constant. Eq. (2.8) is now gauge-invariant under rotations in ψ_i space:

$$\Psi \rightarrow e^{i\mathbf{T}^a \theta^a} \Psi, \quad \bar{\Psi} \rightarrow \bar{\Psi} e^{-i\mathbf{T}^a \theta^a}. \quad (2.11)$$

The gauge symmetry of the SM is a combination of three gauge groups

$$\mathcal{G}_{\text{SM}} = SU(3)_C \otimes SU(2)_L \otimes U(1)_Y. \quad (2.12)$$

These symmetries are reflected in an overall invariance of the SM Lagrangian with regard to transformations within the symmetry groups. The $U(1)_Y$ is associated with

the weak hypercharge (Y). The $SU(2)_L$ symmetry is given for left-handed (two-component) field operators and $SU(3)_C$ denotes the transformation invariance in color space. We leave the discussion of the $SU(2)_L$ and $SU(3)_C$ group to the Sects. 2.2 and 2.4.

Higgs Mechanism

In the previous discussion we did not mention any mass terms of gauge bosons such as $M^2 A_\mu A^\mu$, since they would break gauge invariance. This means that gauge bosons must be massless to guarantee an unbroken theory. In QED and the theory of strong interactions this setup is valid due to massless photons and gluons as mediators, see also Sect. 2.4. However, it is experimentally confirmed that the weak gauge bosons W^\pm and Z are massive. For this purpose, the Higgs mechanism is introduced. It is a description for breaking the gauge symmetry $SU(2)_L \otimes U(1)_Y$ spontaneously and provides gauge-invariant mass terms for gauge bosons. One acquires a scalar *Higgs field* Φ , which is a $SU(2)$ complex doublet with four real degrees of freedom interacting with all gauge bosons of the $SU(2)_L$ and $U(1)_Y$ symmetry groups. By using a distinct minimum of the Higgs potential, the *vacuum expectation value* (vev) of Φ , this leads to the spontaneous symmetry breaking of the ground-state. The Higgs mechanism also implies the existence of the so-called *Goldstone bosons*. They are determined by the number of minima of the Higgs potential. In this case there are three such bosons. The Goldstone bosons become the longitudinal modes of W^\pm and Z and generate their masses. The Higgs mechanism finally leads to

$$SU(3)_C \otimes SU(2)_L \otimes U(1)_Y \rightarrow SU(3)_C \otimes U(1)_{EM}. \quad (2.13)$$

with two remaining gauge symmetries. In addition, the fermions with $SU(2)$ interactions are massless before spontaneous symmetry breaking. This symmetry breaking mechanism also generates fermion masses, see also next section.

Fermions	1 st Generation	2 nd Generation	3 rd Generation	Masses [MeV]		
Leptons	e	μ	τ	0.511	106	1777
	ν_e	ν_μ	ν_τ	$<2 \times 10^{-6}$	<0.19	<18.2
Quarks	u	c	t	2.3	1275	173210
	d	s	b	4.8	95	4180

Table 2.2: List of Standard Model particles (without antiparticles) and their masses. The presented quark masses are in $\overline{\text{MS}}$ scheme at the renormalization scale $\mu = 2 \text{ GeV}$ for $\{u, d, s\}$ and $\mu = m_c, m_b, m_t$ for $\{c, b, t\}$ [36].

2.2 Fundamentals of the Electroweak Theory

The electroweak theory is a unified description of electromagnetism and weak interactions. It is based on the product of gauge symmetry groups $SU(2)_L \otimes U(1)_Y$. The corresponding gauge bosons are $W_\mu^a = \{W^+, W^0, W^-\}$ of weak isospin from $SU(2)_L$ and B_μ is the boson field of weak hypercharge from $U(1)_Y$. We can divide the Lagrangian into four terms:

$$\mathcal{L}_{\text{EWT}} = \mathcal{L}_{\text{Gauge}} + \mathcal{L}_{\text{Higgs}} + \mathcal{L}_{\text{Fermion}} + \mathcal{L}_{\text{Yukawa}}, \quad (2.14)$$

Each of the above terms is invariant under transformations of the Standard Model symmetry group \mathcal{G}_{SM} . The gauge sector describes the mutual interaction between the gauge bosons W_μ^a and B_μ :

$$\mathcal{L}_{\text{Gauge}} = -\frac{1}{4}[W_{\mu\nu}^a W_a^{\mu\nu} + B_{\mu\nu} B^{\mu\nu}]. \quad (2.15)$$

with the field strength tensors $W_{\mu\nu}^a$ and $B_{\mu\nu}$. The Lagrangian of the Higgs doublet Φ is given by

$$\mathcal{L}_{\text{Higgs}} = (\mathbf{D}_\mu \Phi)^\dagger (\mathbf{D}^\mu \Phi) - (\mu^2 \Phi_a^\dagger \Phi^a + \lambda (\Phi_a^\dagger \Phi^a)^2), \quad (2.16)$$

where the covariant derivative is $\mathbf{D}_\mu = \partial_\mu - igW_\mu^a T^a - ig'YB_\mu$. Here, g and g' are the $SU(2)_L$ and $U(1)_Y$ gauge couplings, T^a and Y are the generators of the $SU(2)_L$ and $U(1)_Y$ gauge groups. The first term of Eq. (2.16) contains the coupling of the

Higgs field to the gauge bosons. From this follows that the rotated gauge bosons with diagonalized mass terms that are

$$Z_\mu := \cos \theta_w W_\mu^3 - \sin \theta_w B_\mu, \quad (2.17)$$

$$W_\mu^\pm := \frac{1}{\sqrt{2}}(W_\mu^1 \mp iW_\mu^2), \quad (2.18)$$

$$A_\mu := \sin \theta_w W_\mu^3 + \cos \theta_w B_\mu. \quad (2.19)$$

Here, we introduce the *Weinberg* angle, which can be expressed in terms of the coupling constants according to $\tan \theta_w = g'/g$. The masses of the boson fields are $m_Z = m_W/\cos \theta_w$ and $m_A = 0$. Hence, the photon is massless. The kinetic term of fermions reads

$$\mathcal{L}_{\text{Fermion}} = \bar{Q}_L^i(i\mathcal{D})Q_L^i + \bar{u}_R^i(i\mathcal{D})u_R^i + \bar{d}_R^i(i\mathcal{D})d_R^i + \bar{L}_L^i(i\mathcal{D})L_L^i + \bar{e}_R^i(i\mathcal{D})e_R^i, \quad (2.20)$$

where the index i denotes the three generations of $SU(2)$ doublet pairs of either quarks or leptons. The right-handed $SU(2)$ singlets are labelled by the first-generation particle, see Tab. 2.3. Mass terms of fermion fields are generated through the coupling to the Higgs field. This is the so-called *Yukawa interaction*. In the following we restrict ourself to the quark sector. However, in general the lepton terms have an analogous structure. The Yukawa term of quarks is given by

$$\mathcal{L}_{\text{Yukawa}} = -Y_{ij}^d \bar{Q}^i \Phi d_R^j - Y_{ij}^u \bar{Q}^i (i\sigma_2 \Phi^*) u_R^j + \text{h.c.} \quad (2.21)$$

In the equation above, we introduce 3×3 Yukawa matrices Y_{ij}^u and Y_{ij}^d . After spontaneous symmetry breaking, one obtains the quark mass terms as

$$\mathcal{L}_{\text{mass}} = -m_j^d \bar{d}_L^j d_R^j - m_j^u \bar{u}_L^j u_R^j + \text{h.c.} \quad (2.22)$$

after diagonalizing the Yukawa matrices. The parameters m_j^d and m_j^u are the diagonal elements of the diagonalized Yukawa matrices

$$M_d = U_d^\dagger Y_d V_d, \quad M_u = U_u^\dagger Y_u V_u, \quad (2.23)$$

where U_u , U_d , V_u and V_d as unitary matrices. In order to diagonalize the Yukawa matrices we change from the original flavor basis to the mass basis by $d_R \rightarrow V_d d_R$, $u_R \rightarrow V_u u_R$, $u_L \rightarrow U_u u_L$ and $d_L \rightarrow U_d d_L$. This change of basis also affects the kinetic term, whereas the other terms in the electroweak Lagrangian, see Eq. (2.14),

are invariant. Hence, the symmetry-broken Lagrangian in the mass-basis is

$$\begin{aligned}
 \mathcal{L}_{\text{EWT}}^{(\text{broken, mass-basis})} &= -m_j^d \left(\bar{d}_L^j d_R^j + \bar{d}_R^j d_L^j \right) - m_j^u \left(\bar{u}_L^j u_R^j + \bar{u}_R^j u_L^j \right) \\
 &+ \frac{e}{\sin \theta_w} Z_\mu J_Z^\mu + e A_\mu J_{\text{EM}}^\mu \\
 &+ \frac{e}{\sqrt{2} \sin \theta_w} \left[W_\mu^+ \bar{u}_L^i \gamma^\mu (V_{\text{CKM}})^{ij} d_L^j + W_\mu^- \bar{d}_L^i \gamma^\mu (V_{\text{CKM}}^\dagger)^{ij} u_L^j \right] + \dots
 \end{aligned} \tag{2.24}$$

Here, we use the electromagnetic coupling strength $e = g \sin \theta_w = g' \cos \theta_w$ and the neutral currents J_Z^μ and J_{EM}^μ describing the coupling to the Z boson and the photon with

$$J_Z^\mu = \frac{1}{\cos \theta_w} \left(\sum_i \bar{\psi}_i^L \gamma^\mu T^3 \psi_i^L - \sin^2 \theta_w J_{\text{EM}}^\mu \right), \tag{2.25}$$

$$J_{\text{EM}}^\mu = \sum_i Q_i \left(\bar{\psi}_i^L \gamma^\mu \psi_i^L + \bar{\psi}_i^R \gamma^\mu \psi_i^R \right), \tag{2.26}$$

where ψ_i^L and ψ_i^R are the left- and right-handed fermion fields. In Eq. 2.26 we also use the *Gell-Mann–Nishijima formula* $Q_i = T^3 + Y$. The Lagrangian in the mass basis now has flavor mixing terms describing the coupling to the charged W^\pm bosons. Moreover, the mixing effects are determined by a single unitary matrix

$$V_{\text{CKM}} := U_u^\dagger U_d, \tag{2.27}$$

the *Cabibbo-Kobayashi-Maskawa (CKM) matrix*. In the next section the CKM matrix is described in more detail.

To summarize Eq. (2.24), we have formalized a unified theory including the electromagnetic and electroweak interactions. Three gauge bosons, W^\pm and Z , became massive by spontaneous symmetry breaking whereas one boson, the photon, is massless. All mass terms (for gauge bosons and fermions) are gauge-invariant under the SM gauge group transformations.

Leptons				$(SU(3)_C, SU(2)_L)_{U(1)_Y}$
L_L^i	$\begin{pmatrix} e \\ \nu_e \end{pmatrix}_L$	$\begin{pmatrix} \mu \\ \nu_\mu \end{pmatrix}_L$	$\begin{pmatrix} \tau \\ \nu_\tau \end{pmatrix}_L$	$(\mathbf{1}, \mathbf{2})_{-\frac{1}{2}}$
e_R^i	e_R	μ_R	τ_R	$(\mathbf{1}, \mathbf{1})_{-1}$
Quarks				$(SU(3)_C, SU(2)_L)_{U(1)_Y}$
Q_L^i	$\begin{pmatrix} u \\ d \end{pmatrix}_L$	$\begin{pmatrix} c \\ s \end{pmatrix}_L$	$\begin{pmatrix} t \\ b \end{pmatrix}_L$	$(\mathbf{3}, \mathbf{2})_{\frac{1}{6}}$
u_R^i	u_R	c_R	t_R	$(\mathbf{3}, \mathbf{1})_{\frac{2}{3}}$
d_R^i	d_R	s_R	b_R	$(\mathbf{3}, \mathbf{1})_{-\frac{1}{3}}$

Table 2.3: Fermion fields in the SM Lagrangian. The final column shows the representation under the SM gauge group \mathcal{G}_{SM} .

2.3 The CKM Quark-Mixing Matrix

In the previous section we showed that flavor-changing W^\pm -transitions are accompanied by the mixing matrix V_{CKM} . By construction, it is a 3×3 unitary matrix with four independent physical parameters [36]: three Euler angles θ_{12} , θ_{23} , θ_{13} and one complex phase factor $e^{-i\delta}$. Due to this phase δ the matrix V_{CKM} is a source of CP violation. From experiments we know that the entries of the CKM matrix have a hierarchical structure with the largest values along the diagonal entries. This hierarchy implies a preference for transitions within generations (CKM-favored) while cross-generational flavor transitions are disfavored (CKM-suppressed). One common representation of the CKM matrix is the *Wolfenstein parametrization* in terms of four parameters: λ , A , ρ and η [39]. The expanded form in terms of

$$\lambda = \sin \theta_{12}, \quad (2.28)$$

$$A\lambda^2 = \sin \theta_{23}, \quad (2.29)$$

$$A\lambda^3(\rho - i\eta) = \sin \theta_{13} e^{-i\delta}. \quad (2.30)$$

is

$$V_{\text{CKM}} = \begin{pmatrix} 1 - \lambda^2/2 & \lambda & A\lambda^3(\rho - i\eta) \\ -\lambda & 1 - \lambda^2/2 & A\lambda^2 \\ A\lambda^3(1 - \rho - i\eta) & -A\lambda^2 & 1 \end{pmatrix} + \mathcal{O}(\lambda^4). \quad (2.31)$$

From measurements we know that $\lambda \simeq 0.23$ (and $A, \rho, \eta = \mathcal{O}(1)$), which manifests the aforementioned hierarchy. The current CKM entries are [36]

$$\begin{aligned} & |V_{\text{CKM}}| \\ &= \begin{pmatrix} |V_{ud}| & |V_{us}| & |V_{ub}| \\ |V_{cd}| & |V_{cs}| & |V_{cb}| \\ |V_{td}| & |V_{ts}| & |V_{tb}| \end{pmatrix} = \begin{pmatrix} 0.97425 \pm 0.00022 & 0.2252 \pm 0.0009 & 0.00389 \pm 0.00044 \\ 0.230 \pm 0.011 & 1.023 \pm 0.036 & 0.00406 \pm 0.0013 \\ 0.0084 \pm 0.0006 & 0.0387 \pm 0.0021 & 0.88 \pm 0.07 \end{pmatrix}. \end{aligned} \quad (2.32)$$

The numbers show that unitarity holds within the stated uncertainties. Furthermore, unitarity also implies that the rows of V_{CKM} are orthonormal, as are the columns; that is

$$\sum_i V_{ij} V_{ik}^* = \delta_{jk} \quad (i, k = 1, 2, 3). \quad (2.33)$$

A standard choice is the relation

$$V_{ud}V_{ub}^* + V_{cd}V_{cb}^* + V_{td}V_{tb}^* = 0, \quad (2.34)$$

where each term is of the same magnitude $\mathcal{O}(\lambda^3)$. Dividing by the best measured combination of CKM elements $V_{cd}V_{cb}^*$ leads to the common normalized unitarity relation. Eq. (2.34) can also be graphically represented as a triangle in the complex plane shown in Fig. 2.1(a). Current measurements give strong constraints on the shape of this (normalized) unitarity triangle, see Fig. 2.1(b).

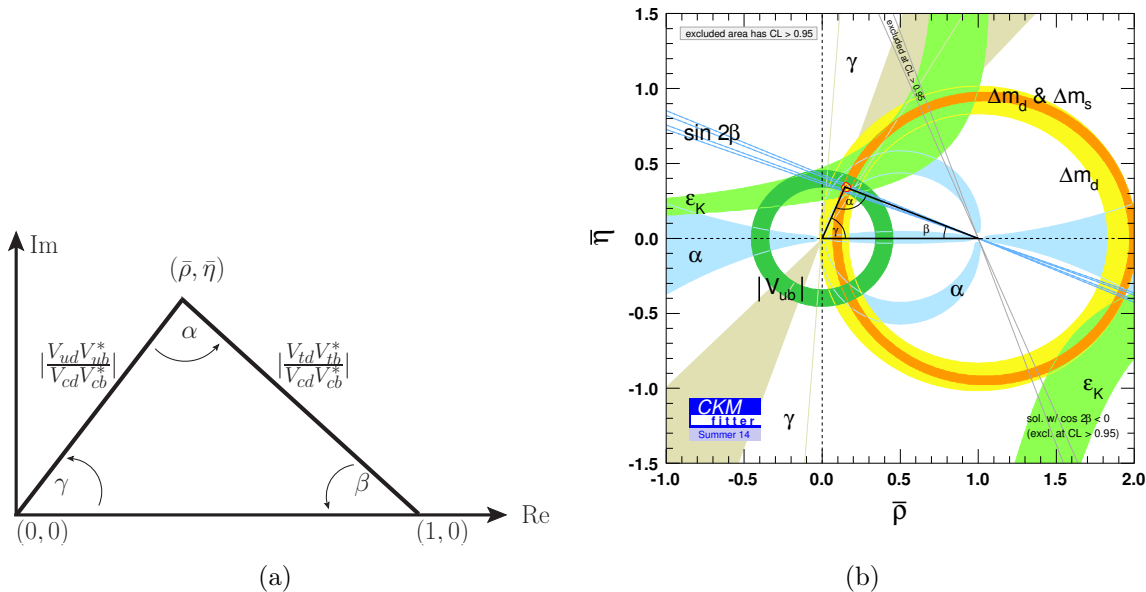


Figure 2.1: The unitarity triangle of Eq. (2.34) is shown on the right-hand side. All edges of the triangle are divided by $V_{cd}V_{cb}^*$ and, hence, the bottom edge is normalized to 1. The right-hand side shows the precision flavor measurements collected and mapped to the normalized unitarity triangle [40].

2.4 Fundamentals of QCD

Quantum Chromodynamics describes strong interactions between color-charged particles, namely quarks and gluons. It is subject to the $SU(3)_C$ gauge symmetry group. In QCD each quark with color $i = 1, 2, 3$ and flavor q is described by a quark field operator ψ_q^i . For simplification one can adopt a vector notation in the fundamental representation of the $SU(3)_C$ color space, i.e. $\psi_q^T := (\psi_q^1, \psi_q^2, \psi_q^3)$. The corresponding QCD Lagrangian can be divided into two parts, which are each invariant under local gauge transformations of $SU(3)_C$:

$$\mathcal{L}_{\text{QCD}} = \mathcal{L}_{\text{quark}} + \mathcal{L}_{\text{gauge}}. \quad (2.35)$$

The first term describes the propagation of quarks and their interaction with gluons

$$\mathcal{L}_{\text{quark}} = \sum_q \bar{\psi}_q (i\not{D} - m_q) \psi_q, \quad (2.36)$$

where the covariant derivative reads $D_\mu := \partial_\mu - ig_s G_\mu(x)$. Here, quark-gluon interactions are encoded in the coupling to the gauge field $G_\mu = G_\mu^a t^a$, $a = 1, \dots, 8$ describing the eight gluons. The parameter g_s denotes the strong coupling. The gauge-invariant kinetic term for the gluon fields is determined through the corresponding field strength tensor

$$G_{\mu\nu}(x) = t^a G_{\mu\nu}^a(x) := \frac{i}{g_s} [D_\mu, D_\nu]. \quad (2.37)$$

We end up with the final form of the kinetic term

$$\mathcal{L}_{\text{gauge}} = -\frac{1}{4} G_a^{\mu\nu} G_{\mu\nu}^a. \quad (2.38)$$

The QCD has a non-abelian gauge structure, i.e. the generators t^a of its gauge group do not commute. They satisfy the commutation relation

$$[t^a, t^b] = i f^{abc} t^c, \quad (2.39)$$

where f^{abc} is the $SU(3)_C$ structure constant. In other words, gluons are also color charged and, hence, the kinetic term $\mathcal{L}_{\text{gauge}}$ also generates three- and four-gluon interaction terms. Note that additional terms must be added, which are related to the fact that massless gluons have only two polarization states, whereas the gluon fields have four degrees of freedom. To this end, a gauge-fixing term $\mathcal{L}_{\text{gf}} = -\frac{1}{2\xi} (\partial^\mu G_\mu)(\partial^\nu G_\nu)$ (in Feynman gauge $\xi = 1$) has to be added to subtract the additional (unphysical) degrees of freedom. Moreover, gluonic loop-diagrams are also possible in QCD, which require *Faddeev-Popov ghost fields* for proper quantization of gauge fields [41].

Apart from the general structure of the QCD Lagrangian that determines the dynamics of strong-interacting processes, we should consider the coupling constant of the strong interaction which differ from particles interacting either electromagnetically or weakly. Due to the additional contributions from gluon self-interaction the leading order coefficient of the β -function¹ results in

$$\beta_0 = \frac{11}{3} N_C - \frac{2}{3} n_f. \quad (2.40)$$

One obtains a negative β -function for three colors $N_C = 3$ and six (active) quark flavors $n_f = 6$ in maximum (see also Eq. (A.19)). As a consequence, the strong

¹The β -function is defined in Eq. (A.19).

coupling constant is

$$\alpha_s(q^2) = \frac{g_s^2(q^2)}{4\pi}, \quad (2.41)$$

which decreases for increasing momentum scales q^2 . It also changes more drastically compared to the electromagnetic coupling constant. In the limit $q^2 \rightarrow \infty$, the coupling vanishes and reveals that color-charged particles are asymptotically free. We can now rescale α_s by solving the *renormalization-group equation* (RGE), see Appendix A.3. To leading order we obtain

$$\alpha_s(q^2) = \frac{4\pi}{\beta_0 \ln\left(\frac{q^2}{\Lambda_{\text{QCD}}^2}\right)}. \quad (2.42)$$

The scale-dependence of α_s has been confirmed by measurements (see Fig. 2.2). At a the scale $\Lambda_{\text{QCD}} \sim 200 - 300$ MeV the coupling diverges and perturbation theory breaks down. From experiments we know that bound (color singlet) states, the so-called *hadron* states, exist in this regime. The spacial size of such states is about 10^{-15} m ($\sim 1/\Lambda_{\text{QCD}}$). One can show that just specific combinations of quarks q and antiquarks \bar{q} are allowed and stable enough to form such singlet state, namely the quark-antiquark (*meson*) $|M\rangle = \frac{1}{\sqrt{3}}|\bar{q}_\alpha q_\alpha\rangle$ and triple-quark (*baryon*) state $|B\rangle = \frac{1}{\sqrt{6}}\varepsilon^{\alpha\beta\gamma}|q_\alpha q_\beta q_\gamma\rangle$, where $\varepsilon^{\alpha\beta\gamma}$ is the total antisymmetric tensor. The formation of quarks to hadrons and the non-observability of free quarks is commonly known as the *confinement principle*.

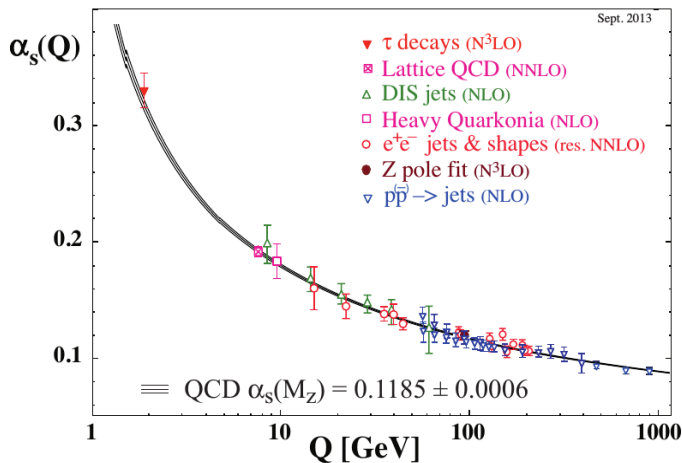


Figure 2.2: Summary of measurements of the strong coupling α_s as a function of the momentum scale Q and the state-of-the-art value of $\alpha_s(M_Z)$ [36].

2.5 Classification of Heavy-light Mesons

A specific type of mesons are heavy-light mesons, which are relevant for this thesis. They are built up by a heavy quark Q and a light valence quark q . The mass of the heavy quark is much larger compared to the hadronization scale ($m_Q \gg \Lambda_{\text{QCD}}$), whereas quarks are light if their mass is much smaller than this scale ($m_q \ll \Lambda_{\text{QCD}}$). Mesons can be classified by the quantum numbers of the heavy and light degrees of freedom, e.g. their flavor, spin and parity. Characteristics, which are not related to the heavy quark, are defined as light degrees of freedom and vice versa. The essential degrees of freedom in a meson system are combined to the quantum numbers of the valence quarks. The quantum numbers result from the summed total angular momentum operator of the heavy J_Q and light quark J_q , respectively,

$$J = J_Q + J_q. \quad (2.43)$$

The numbers j , j_Q and j_q are the eigenvalues of J^2 , J_Q^2 and J_q^2 in the meson state. Since J and J_Q are conserved operators, J_q is also separately conserved. Hence, meson states can be characterized by the quantum numbers resulting from the operators of both quarks (J_Q, J_q). The short-handed notation J^P (spin-parity) combines the total angular momentum and the parity P of the particle.

Excited meson states have larger masses than their ground-state but the same quark-flavor content as well as spin-parity. In non-relativistic quark models, one can distinguish between radial and orbitally excited states following the principles of the Schrödinger equation in a central potential, c.f. the hydrogen atom. In QCD hadrons form a relativistic bound of the valence quarks and, hence, we characterize all resonances with the same flavor content and J^P , but larger masses as radial excitations of their ground state.

2.6 Perturbative QCD: $e^+e^- \rightarrow$ hadrons

In the previous section, basic aspects of QCD are presented. We note that there are two specific regimes to distinguish, which depend on the momentum scale of the strong coupling. For large momentum-transfer we know that the coupling decreases and at some point the approximation of processes by essentially free quarks is reasonable. This is a characteristic feature of QCD, which is called *asymptotic freedom*. In the regime of asymptotic freedom quark-gluon interactions are of short-distances and a

perturbative treatment in terms of $\alpha_s(q^2)$ is justified. If q^2 approaches the hadronic scale, the coupling diverges and signals the hadronization process of quarks. In this regime non-perturbative methods are necessary. A prominent phenomenological setup for testing QCD is e^+e^- annihilation at high energies, which provides virtual photons of high momenta. For $q^2 \gg \Lambda_{\text{QCD}}^2$ these photons are a source for perturbatively interacting quark-antiquark pairs within QCD. A fundamental experimental observable is the total cross section $\sigma_{\text{tot}}(s)$ depending on the squared center-of-mass energy $s = (p_{e^+} + p_{e^-})^2$. This corresponds to the virtuality of the photon that produces a hadronic state at an average distance of $\mathcal{O}(1/\sqrt{s})$. For $\sqrt{s} \gg \Lambda_{\text{QCD}}$ the cross-section for hadron production can be reliably estimated by the sum of quark-antiquark cross-sections of all flavors with masses $m_q \ll \sqrt{s}$ [42]

$$\sigma_{\text{tot}}^{e^+e^- \rightarrow h}(s) = \sum_{q=u,d,s,\dots} \sigma^{e^+e^- \rightarrow q\bar{q}}(s). \quad (2.44)$$

The detection of high-energetic back-to-back hadron jets in collider experiments initiated from quark-antiquark pairs provides an indication for the reliability of a free-quark approximation. The total cross section is defined by

$$\sigma_{\text{tot}}^{e^+e^- \rightarrow h}(s) = \frac{1}{2s} \sum_n |\langle e^+e^- | \hat{T} | h_n \rangle|^2. \quad (2.45)$$

Here, we introduce the sum over all possible hadronic states $|h_n\rangle$. From unitarity of the scattering matrix $\hat{S} = 1 + i\hat{T}$ follows the optical theorem

$$2 \text{Im} \hat{T} = \hat{T}^\dagger \hat{T}, \quad (2.46)$$

where \hat{T} is the transition operator describing the interaction part of the annihilation process. We are now able to rewrite Eq. (2.45) as

$$\sigma_{\text{tot}}^{e^+e^- \rightarrow h}(s) = \frac{1}{s} \times \text{Im} \langle e^+e^- | \hat{T} | e^+e^- \rangle \quad (2.47)$$

$$= -\frac{(4\pi\alpha_{\text{em}})^2}{s^2} \bar{\psi}_e \gamma^\mu \psi_e (\text{Im} \Pi_{\mu\nu}(q)) \bar{\psi}_e \gamma^\nu \psi_e \Big|_{q^2=s>0}, \quad (2.48)$$

with ψ_e as the spinor of an electron and α_{em} as the electromagnetic coupling constant. The non-trivial kernel of the last equation is the *correlation function* or *correlator* which describes the dynamics of $j^{\text{em}} \rightarrow h \rightarrow j^{\text{em}}$ transitions. $\Pi_{\mu\nu}$ has no hadrons in

the initial and final states and, hence, it is given by the vacuum expectation value

$$\Pi_{\mu\nu}(q) = i \int d^4x e^{iqx} \langle 0 | \mathcal{T} \{ j_\mu^{\text{em}}(x) j_\nu^{\text{em}}(0) \} | 0 \rangle = (q_\mu q_\nu - q^2 g_{\mu\nu}) \Pi(q^2). \quad (2.49)$$

The correlation function depends on just one invariant amplitude $\Pi(q^2)$, since the current operator $j_\mu^{\text{em}} = \sum_i Q_i \bar{q}_i \gamma_\mu q_i$ is conserved, where we sum over all quark flavors with charge Q_i . In the limit of high center-of-mass energy ($\sqrt{s} \rightarrow \Lambda_{\text{QCD}}$) one can argue that the free quarks are only subject to ordinary QED interactions. The calculation of $\Pi(q^2)$ is identical to the cross section calculation of muon-pair production in e^+e^- annihilation. Thus, in this limit we obtain

$$\sigma_{\text{tot}}^{e^+e^- \rightarrow h}(s) = N_C \frac{4\pi\alpha_{\text{em}}^2}{3s} \sum_i^{n_f} Q_i^2. \quad (2.50)$$

The number of active quark flavors n_f is determined by the threshold energy. Later on we will also see that experiments determine the color factor as $N_C = 3$. Using the normalization condition $\sigma^{e^+e^- \rightarrow \mu^+\mu^-}(s) = 4\pi\alpha_{\text{em}}^2/(3s)$ one can define the ratio

$$R(s) = \frac{\sigma_{\text{tot}}^{e^+e^- \rightarrow h}(s)}{\sigma^{e^+e^- \rightarrow \mu^+\mu^-}(s)} \rightarrow 3 \sum_i^{n_f} Q_i^2. \quad (2.51)$$

Experimental measurements of the R -ratio show that the plateaus are well described by the high-energy approximation, see Fig. 2.3. This behavior confirms the description of the hadronic picture by quark-gluon interactions, the *quark-hadron duality* [43]. In the vicinity of resonance peaks, i.e. at the threshold of bound states such as ρ , J/ψ or Υ , the theoretical description does not directly reflect the spectrum. However, the quark picture is still in good agreement if the R -ratio is averaged over the resonance region. For more precision of the predicted spectrum one has to consider correction terms. They can be of perturbative nature around the high-energy scales, but we can also include effects that scale close to Λ_{QCD} , namely soft quark-interactions, where perturbation theory breaks down. These correction terms can be treated systematically by the *operator product expansion* (OPE). As a part of the thesis, this expansion method will be elaborated in Chap. 3 in the context of *QCD sum rules* for heavy meson productions from certain interpolating quark currents. The key point of the evaluation of $R(s)$ is to relate the correlation function $\Pi(q^2)$ in the regime of spacelike $q^2 < 0$ to timelike $q^2 = s > 0$ in terms of a *dispersion relation*. Based on this idea, the picture of free quarks can be connected to the actual hadronic spectrum. The next-

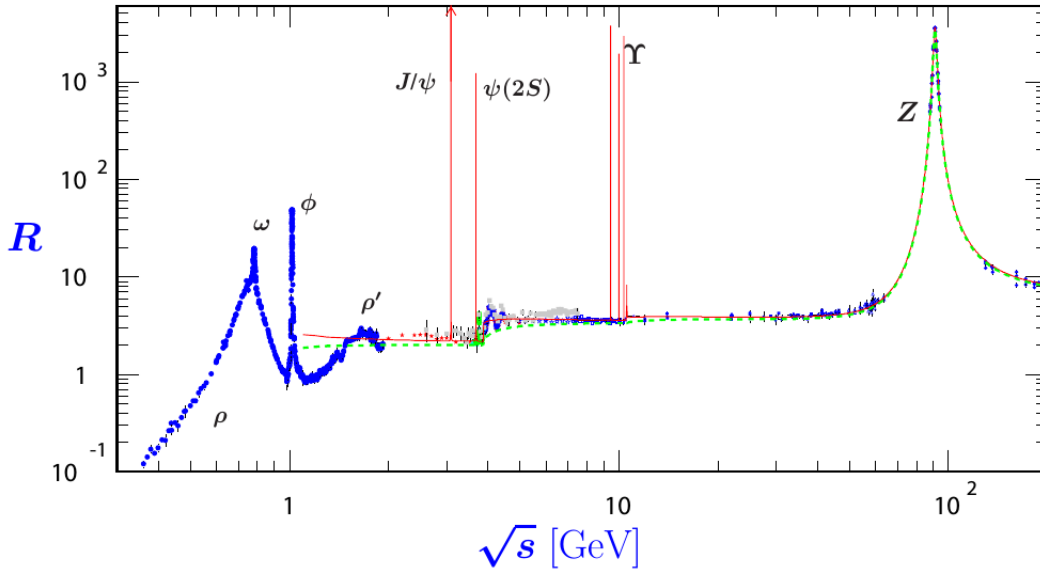


Figure 2.3: World data on the ratio $R(s) = \sigma_{\text{tot}}^{e^+e^- \rightarrow h}(s) / (\sigma^{e^+e^- \rightarrow \mu^+\mu^-}(s))$. The green (dashed) line shows the approximation at high threshold limit. The red (solid) line is the three-loop perturbative QCD prediction [36].

to-leading order contribution from an additional gluon radiation modifies the ratio to [44]

$$R(s, q^2) \rightarrow 3 \sum_i^{n_f} Q_i^2 \left(1 + \frac{\alpha_s(q^2)}{\pi} \right). \quad (2.52)$$

The radiative correction to the ratio improves its agreement between the theoretical description and experiment.

Applications of QCD Sum Rules to Leptonic Decay Constants

Matrix elements of interpolating quark currents between the QCD vacuum and a one-meson state give rise to the simplest non-perturbative hadronic matrix elements in flavor physics. These matrix elements are parametrized in terms of the decay constant f_H of the meson H . The following chapter is dedicated to the evaluation of decay constants of heavy-light mesons in particular.

A reliable method to approach non-perturbative QCD quantities was established by Shifman, Vainshtein and Zakharov in 1979 [45], the so-called SVZ- or QCD sum rules. Decay constants enter in various processes. They contain information on the hadronic dynamics in decay or scattering processes. In case of weak leptonic decays such as $D_s \rightarrow \mu\nu_\mu$ and $B \rightarrow \tau\nu_\tau$ all information on QCD dynamics is encoded in $f_{D(s)}$ and f_B , respectively. In 2012/13 the LHCb and CMS collaboration published the first evidence of $B_{s(d)} \rightarrow \mu^+\mu^-$ [46, 47, 48]. This leptonic flavor-changing neutral current (FCNC) decay channel is an essential probe to BSM physics, on the other hand a strong test of the SM requiring very accurate determinations of $f_{B_{s(d)}}$. Apart from the interest on the experimental side, many high precision predictions of B and D meson decay constants are available. There are many computations within lattice QCD [49, 50, 51, 52] as well as predictions based on the sum rules method [53, 54, 55]. A profound understanding of vector mesons such as B^* and D^* are also desirable. QCD processes including B^* cannot be measured directly as it decays predominately via electromagnetic interaction $B^* \rightarrow B\gamma$. An important application of f_{B^*} (f_{D^*}) is their use in determining the $BB^*\pi$ ($DD^*\pi$) strong coupling constants [56]. Furthermore, the deviation of $f_{B^*(D^*)}$ compared to $f_{B(D)}$ give a measure for heavy-quark spin symmetry violation, whereas ratios of $f_{B_s(D_s)}$ and $f_{B(D)}$ determine the violation of the $SU(3)_F$ symmetry.

In continuum QCD the hadronic decay constants can be determined via the method of QCD sum rules. This method is based on the OPE of two-point correlation functions, including quark currents of a specific spin-parity. Correlation functions also obey a

hadronic dispersion relation [57, 58]. Then both representations are matched assuming quark-hadron duality [59, 60]. The OPE is a double expansion in the difference of the heavy quark mass and the transfer momentum $(m_Q^2 - q^2)^{-1}$ as well as the strong coupling α_s . As such, it is also a local expansion around small spatial-time distances $x = 0$ separating short- and long-distance effects at a specified scale. Short-distance interactions are incorporated in coefficient functions (*Wilson coefficients*) that are subject to QCD perturbation theory. Effects of long-distance interactions are expressed via non-perturbative quantities, so-called *condensates*, which describe fluctuations of the QCD vacuum. In addition to evaluations within full QCD, other approaches exist, using the heavy-quark expansion [61] or heavy-quark effective theory (HQET) [62, 63, 64]. Radiative corrections to the leading contribution in the OPE (PT part) at next-to-leading order (NLO) were computed in Ref. [65, 66]. At this level of accuracy, the decay constants of heavy-light mesons were also estimated, e.g. in [67]. Another substantial refinement of the correlation function was obtained by Chetyrkin and Steinhäuser, who computed the next-to-next-to-leading order (NNLO) contribution of the PT part in a semi-numerical way [68]. While the perturbative QCD corrections to the quark condensate in the pseudoscalar two-point correlation function are known [53], we obtain such corrections for the vector correlation function for the first time [A1].

We investigate the QCD sum rules for heavy-light bottom and charmed meson decay constants. In chapters 3-5 the following aspects will be presented:

- In this chapter we recapitulate the basics about QCD sum rules in the context of decay constants, starting with the description of two-point correlation functions. We also reparametrize the sum rules to a special form suited for a $1/m_Q$ -expansion. This allows us to assess the infinite quark mass limit of the ratios f_{H^*}/f_H , and the corresponding heavy-quark corrections that explicitly break the heavy-quark spin symmetry.
- Chapter 4 presents the analytic calculation of the PT part for the vector and pseudoscalar meson channel with NLO accuracy. To this end, we also discuss how to compute the required master integrals.
- In chapter 5 the numerical analysis is carried out give central values of vector and pseudoscalar $B(D)$ meson decay constants and their upper bounds. The accuracy of the sum rules for vector meson decay constants has been upgraded by including perturbative corrections to the quark condensate, which we present in Refs. [A1, 69]. At the same time, we give a major update to the pseudoscalar counterpart.

In order to scale the systematic uncertainty of our method, we employ certain modifications of the sum rules with different weights in the dispersion integrals and their power moments.

The main results of these chapters have also been published in Ref. [A1].

3.1 Two-Point Correlation Function

We consider the two-point correlation function, a time-ordered product of interpolating quark-current operators, $j_\Gamma(x) = \bar{q}\Gamma Q(x)$, at two space-time points. The currents include quantized field operators of the heavy and light quark, with $Q = \{b, c\}$ and $q = \{u, d, s\}$, and a certain Dirac gamma structure Γ . In the following, all color indices are implied in field operators and omitted for the sake of brevity. At first, we choose such a current that the quark content and quantum numbers match the vector meson $H^* = \{B^*, D^*\}$, i.e. $j_\mu(x) = \bar{q}\gamma_\mu Q(x)$. The corresponding correlation function is formally defined in momentum space as

$$\Pi_{\mu\nu}(q) = i \int d^4x e^{iqx} \langle 0 | T \{ j_\mu(x), j_\nu^\dagger(0) \} | 0 \rangle \quad (3.1)$$

$$= (q_\mu q_\nu - q^2 g_{\mu\nu}) \tilde{\Pi}_t(q^2) + q_\mu q_\nu \Pi_l(q^2), \quad (3.2)$$

where the kinematical structure of $\Pi_{\mu\nu}(q)$ is decomposed into the transverse (t) and longitudinal (l) components. These components are multiplied by the invariant amplitudes $\tilde{\Pi}_t(q^2)$ and $\Pi_l(q^2)$. To avoid a kinematical singularity, we redefine the transverse invariant amplitudes as

$$\Pi_t(q^2) \equiv q^2 \tilde{\Pi}_t(q^2). \quad (3.3)$$

The correlation function for pseudoscalar heavy-light currents reads

$$\Pi_5(q) = i \int d^4x e^{iqx} \langle 0 | T \{ j_5(x), j_5^\dagger(0) \} | 0 \rangle, \quad (3.4)$$

where the interpolating current is $j_5 = (m_Q + m_q) \bar{q} i \gamma_5 Q$. Decay constants are defined as transitions from QCD vacuum to a single hadronic state (on its mass-shell $p^2 = m_{H^*}^2$) that are mediated by the interpolating currents:

$$m_{H^*} f_{H^*} \varepsilon_\mu(\lambda) e^{-ipx} \equiv \langle 0 | \bar{q} \gamma_\mu Q(x) | H^*(p, \lambda) \rangle, \quad (3.5)$$

$$m_H^2 f_H e^{-ipx} \equiv \langle 0 | \bar{q} \gamma_5 Q(x) | H(p) \rangle. \quad (3.6)$$

In Eq. (3.5) the four-vector ε_μ is the polarization vector for polarization $\lambda = 0, \pm 1$ of the H^* -meson.

3.2 Hadronic Representation

In the domain of $q^2 \geq m_Q^2$ the correlation functions cannot be computed analytically due to arising divergences, which can be interpreted as the formation of hadrons. Hence, we need to quantify the hadronic content of $\Pi_{\mu\nu}$ and Π_5 . A more detailed description is also presented in Appendix B.1. To determine the correlation functions in this domain, we insert the unity operator between the interpolating quark-current operators of (3.1) and (3.4). The unity operator is as a complete set of hadronic Fock states

$$\int d\tau_h |h(p_h)\rangle\langle h(p_h)| = \mathbf{1}_h, \quad (3.7)$$

which matches the quantum numbers of either H^* and H , respectively, and

$$d\tau_h = \frac{d^4 p_h}{(2\pi)^3} (2\pi)^4 \theta(p_h^0) \delta(p_h^2 - m_h^2), \quad (3.8)$$

is the Lorentz invariant phase-space. Here, p_h^μ is the four-momentum and m_h the mass of the hadron h . By inserting Eq. (3.7) into the correlation function (3.1) we obtain the hadronic sum

$$\Pi_{\mu\nu}^{(\text{had})}(q^2) = \frac{\langle 0 | \bar{q} \gamma_\mu Q | H^* \rangle \langle H^* | \bar{Q} \gamma_\nu q | 0 \rangle}{m_{H^*}^2 - q^2} + \int d\tau_h \frac{\langle 0 | \bar{q} \gamma_\mu Q | h(p_h) \rangle \langle h(p_h) | \bar{Q} \gamma_\nu q | 0 \rangle}{p_h^2 - q^2}. \quad (3.9)$$

This sum is separated into the H^* resonance and the continuum states $|h(p_h)\rangle$. Note that this relation also contains the imaginary offset $-i\varepsilon$ implicitly, but it is neglected for reasons of clarity. The right-hand side of Eq. (3.9) characterizes a spectrum of hadronic particles on their mass-shell. To this end, we use the spectral representation [70] as a function of the threshold energy $s = q^2$:

$$\rho_{\mu\nu}^h(s) \theta(q_0) = \sum_{h \neq H^*} (2\pi)^3 \delta(s - m_h^2) \delta^{(4)}(q - p_h) \langle 0 | j_\mu(0) | h(p_h) \rangle \langle h(p_h) | j_\nu(0)^\dagger | 0 \rangle \quad (3.10)$$

to rewrite Eq. (3.9) as

$$\Pi_{\mu\nu}^{(\text{had})}(q^2) = \frac{\langle 0 | \bar{q} \gamma_\mu Q | H^* \rangle \langle H^* | \bar{Q} \gamma_\nu q | 0 \rangle}{m_{H^*}^2 - q^2} + \int ds \frac{\rho_{\mu\nu}^h(s)}{s - q^2}. \quad (3.11)$$

One can also derive the result by using the optical theorem [69], which follows from the unitarity of the scattering matrix, see Fig. 3.1, in conjunction with dispersion

relations. In Eq. (3.11) the sum over all possible hadronic states also implies summing over all polarization states, i.e. $\sum_{\lambda} \varepsilon_{\mu}(\vec{q}, \lambda) \varepsilon_{\nu}^*(\vec{q}, \lambda) = -(g_{\mu\nu} - \frac{q_{\mu}q_{\nu}}{p_h^2})$. Hence, in case of vector particles with spin-parity 1^- , just the transverse component of $\Pi_{\mu\nu}$ is relevant. Inserting the hadronic matrix elements at the ground states, which are related to the decay constants as defined in Eqs. (3.5) and (3.6), we find the transverse (t) and pseudoscalar (5) component of the spectral density:

$$\rho_t(s) \equiv \frac{1}{\pi} \text{Im} \Pi_t(s) = m_{H^*}^2 f_{H^*}^2 \delta(s - m_{H^*}^2) + \rho_t^h(s) \theta(s - (m_H + m_P)^2), \quad (3.12)$$

$$\rho_5(s) \equiv \frac{1}{\pi} \text{Im} \Pi_5(s) = m_H^4 f_H^2 \delta(s - m_H^2) + \rho_5^h(s) \theta(s - (m_{H^*} + m_P)^2). \quad (3.13)$$

The ground state meson is approximated by a delta function, whereas excited and multiparticle states are absorbed into the continuum spectral density. The continuum spectrum starts with a two-particle configuration, a heavy ground-state meson and the lightest pseudoscalar meson (π or K) depending on the flavor content of $H^{(*)}$, e.g. the $B_{(s)}^*$ resonance is followed by the threshold of $B\pi$ (BK). Note that in the pseudoscalar meson channel, there is a energy gap between the ground state and the lowest threshold of the continuum state. This clean separation between H and the residual spectrum leads to an enhanced extraction quality of f_H . In the D^* channel the threshold of HP lies below and in the B^* case almost overlaps with the ground state resonance.

In the next section we will discuss dispersion relations that relate the imaginary part of the correlator to the spectral function in (3.10).

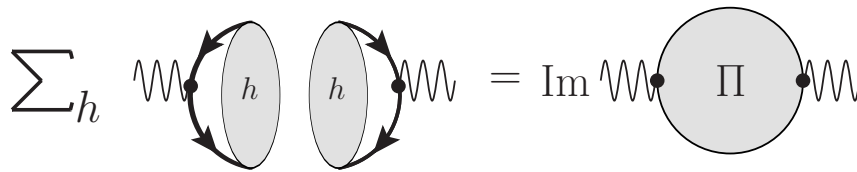


Figure 3.1: Schematic representation of the optical theorem.

3.3 Dispersion Relation

It has been proven by Källén and Lehmann [57, 58] that two-point functions obey dispersion relations, which follows from the analyticity properties of these functions. The given invariant amplitude $\Pi(q^2) \equiv \Pi_{t(5)}(q^2)$ is an analytic function in the perturbative

domain of $q^2 \ll m_Q^2$. To relate this domain to the hadronic one with physical poles beyond the threshold $s = q^2 \geq m_Q^2$, we introduce *Cauchy's integral formula*

$$\Pi(q^2) = \frac{1}{2\pi i} \oint_C ds \frac{\Pi(s)}{s - q^2}. \quad (3.14)$$

According to this formula, the function's value on the integration contour is related to values within the closed contour C , see Fig. 3.2. In this case, the chosen integration contour describes a closed loop with a branch cut starting at the threshold of the first hadronic state. In the last section we have pointed out that the branch point is determined by the ground-state meson mass $m_{H^{(*)}}^2$. The contour C (dashed line) is divided into four sections: $C_R + C_+ + C_\varepsilon + C_-$. In the limit $R \rightarrow \infty$ and $\varepsilon^+ \rightarrow 0$, integrals along C_ε and C_R vanish. Thus

$$\Pi(q^2) = \frac{1}{2\pi i} \int_{m_Q^2}^{\infty} ds \frac{\Pi(s + i\varepsilon^+) - \Pi(s - i\varepsilon^+)}{s - q^2}. \quad (3.15)$$

Using *Schwarz's reflection principle* [71], one obtains the spectral density

$$\rho(s) \equiv \frac{1}{\pi} \text{Im} \Pi(s) = \lim_{\varepsilon^+ \rightarrow 0} \frac{1}{2\pi i} [\Pi(s + i\varepsilon^+) - \Pi(s - i\varepsilon^+)]. \quad (3.16)$$

The dispersion relation of Eq. (3.15) thus takes the form

$$\Pi(q^2) = \int_{m_Q^2}^{\infty} ds \frac{\rho(s)}{s - q^2}. \quad (3.17)$$

A more detailed description of the dispersion relation in (3.17) is given in Appendix B.2. Note that Eq. (3.15) is valid only if the integrand of $\Pi(q^2)$ converges fast enough. In general, this is not the case. As a result, a subtraction polynomial of order n is required, which includes the value of the integral at an arbitrary point q_0^2 within the analytic region [72, 73]:

$$\Pi(q^2) = (q^2 - q_0^2)^n \int_{m_Q^2}^{\infty} ds \frac{\rho(s)}{(s - q_0^2)^n (s - q^2)} + \sum_{k=0}^{n-1} \frac{(q^2 - q_0^2)^k}{k!} \Pi^{(k)}(q_0^2). \quad (3.18)$$

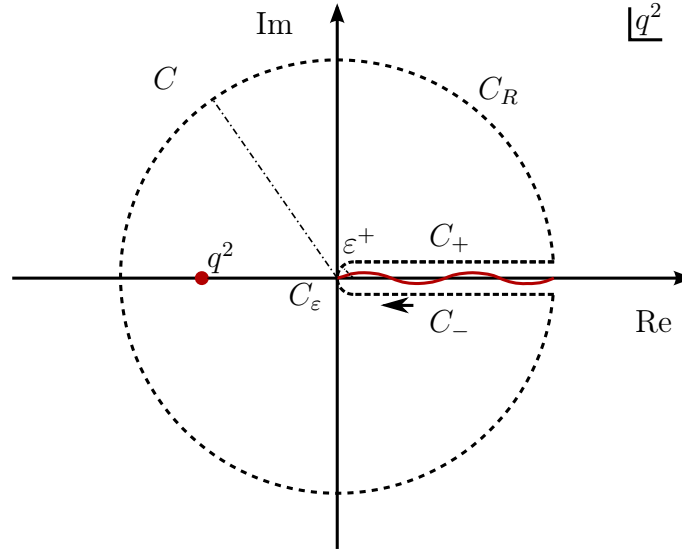


Figure 3.2: Complex continuation of $\Pi(q^2)$ by means of Cauchy's residue theorem. The chosen loop contour is given by the dashed line. Here the branch cut, starting at the threshold $s = m_{H^{(*)}}^2$, indicates the physical states.

The invariant amplitudes of Eqs. (3.3) and (3.4) require two subtraction terms. It follows the double-subtracted dispersion relation

$$\Pi_{t(5)}(q^2) - \Pi_{t(5)}(0) - q^2 \left(\frac{d\Pi_{t(5)}(q^2)}{dq^2} \right) \Big|_{q^2=0} = \frac{(q^2)^2}{\pi} \int_{m_Q^2}^{\infty} ds \frac{\text{Im} \Pi_{t(5)}(s)}{s^2(s - q^2)}. \quad (3.19)$$

We leave the discussion of how to treat the subtraction terms to Sec. 3.5.

3.4 Operator Product Expansion

Using dispersion relations we are able to link the hadronic representation of the correlation function to the domain for $q^2 \ll m_Q^2$, where short-distance quark-antiquark fluctuations dominate. In the latter domain the exponential phases in the integrals of Eqs. (3.1) and (3.4) are fast oscillating. This behavior allows a systematic treatment of the correlation functions $\Pi_t(q^2)$ and $\Pi_5(q^2)$ in terms of $1/(m_Q^2 - q^2)$ by using OPE. The OPE is a series of perturbative coefficient functions and local operators, which lead to non-perturbative matrix elements. At leading order only perturbative loop contributions arise. Local operators of higher dimension are suppressed by powers of $1/(m_Q^2 - q^2)$ and start with the dimension-3 operator $\bar{q}q$. The latter leads to the leading

condensate contribution, the quark condensate. As a physical picture, this condensate describes the interaction with background quarks and gluons of the QCD vacuum, interacting at typical scale of $\sim \Lambda_{\text{QCD}}$. Thus, the correlation functions can be expressed as

$$\Pi_{t(5)}^{(\text{OPE})}(q^2) = \sum_d C_d^{t(5)}(q^2, \mu_f) \langle 0 | \mathcal{O}_d | 0 \rangle (\mu_f) = C_0 + C_3 \langle \mathcal{O}_3 \rangle + C_4 \langle \mathcal{O}_4 \rangle + \dots \quad (3.20)$$

The coefficient functions $C_d^{t(5)}$ can be determined in perturbative calculations and, hence, enable the following perturbative series

$$C_d^{t(5)}(q^2, \mu_f) = \sum_{n=0}^{\infty} c_{d,n}^{t(5)}(q^2, \mu_f) \alpha_s^n(\mu_f), \quad (3.21)$$

where we order by the mass-dimension d . The operators $\mathcal{O}_d(\mu_f)$ are Lorentz and gauge-invariant local operators and are constructed from contracted quark and gluon fields in $\Pi_{t(5)}^{(\text{OPE})}(q^2)$. The coefficient functions are suppressed by powers of

$$(m_Q^2 - q^2)^{-n},$$

where $n \geq 1$ according to the mass-dimension of the local operators. Hence, we truncate the expansion at some order, but we keep in mind that contributions of higher dimensional operators are missing. Within the OPE the separation between the effective long- and short-distance region introduces the factorization scale μ_f . Interactions with momentum transfer of $q^2 > \mu_f^2$ are incorporated in $C_d(q^2)$ and $q^2 < \mu_f^2$ are included in the vacuum expectation values of local operators (vacuum condensates). The condensates cannot be calculated analytically. However, they are universal inputs, which can be determined from experimental measurements, see Ref. [74].

The complete set of operators for mesonic systems up to dimension six is given in Tab. 3.1. Other operators up to mass dimension six can be reduced to this set of operators via equation of motion. Note that we do not include the three gluon operator with $d = 6$ into consideration, since it typically leads to small contributions for the considered problems. The corresponding Feynman graphs to these operators are shown in Fig. 3.4. Other condensate contributions of $d \geq 6$ are neglected.

The unit operator is the operator of the lowest dimension, and it is associated with the perturbative contribution $C_0(q^2) = \Pi^{(\text{pert})}(q^2)$, which includes quark or quark-

Local Operator	Description
$\mathcal{O}_0 = \mathbf{1}$	Leading power operator
$\mathcal{O}_3 = \bar{q}q$	Quark condensate
$\mathcal{O}_4 = G_{\mu\nu}^a G^{a\mu\nu}$	Gluon condensate
$\mathcal{O}_5 = \bar{q}\sigma_{\mu\nu}\frac{\lambda^a}{2}G^{a\mu\nu}q$	Quark-gluon / Mixed condensate
$\mathcal{O}_6 = (\bar{q}\Gamma_r q)(\bar{q}\Gamma_s q)$	Four-quark condensate

Table 3.1: Table of local operators in the OPE. The operator $G_{\mu\nu}^a$ denotes a gluon field strength tensor with the color index a , the anti-symmetric tensor in \mathcal{O}_5 is $\sigma_{\mu\nu} = \frac{i}{2}[\gamma_\mu, \gamma_\nu]$ and λ^a are the Gell-Mann matrices. The local operator \mathcal{O}_6 includes combinations of Lorentz and color matrices, collectively expressed as Γ_r and Γ_s .

gluon loops. We refer to this contribution as the perturbation theory (PT) part. In the timelike momentum-transfer region, the correlation function (3.2) can be treated perturbatively due to the asymptotic freedom of quarks. In first approximation this implies contractions of quark fields to free-quark propagators (see Fig. 3.3 (a)). Radiative corrections at NLO in α_s to the PT part are two-loop diagrams with two different topologies. All contributing two-loop diagrams are shown in Figs. 3.3 (b)-(d). In this thesis, we compute the NLO corrections, whereas higher order corrections at NNLO were determined in [75], assuming one massive and one massless quark. We denote the spectral function of the PT contribution in the OPE as

$$\rho_{t(5)}^{(\text{pert})}(s) \equiv \frac{1}{\pi} \text{Im} \Pi_{t(5)}^{(\text{pert,LO})}(s) \quad (3.22)$$

$$= \rho_{t(5)}^{(\text{pert})}(s) + \left(\frac{\alpha_s}{\pi}\right) \rho_{t(5)}^{(\text{pert,NLO})}(s) + \left(\frac{\alpha_s}{\pi}\right)^2 \rho_{t(5)}^{(\text{pert,NNLO})}(s), \quad (3.23)$$

which includes the NLO and NNLO terms. This form of the PT part is now suited for the dispersion relation in Eq. (3.18). In case of vector and pseudoscalar mesons the leading order terms are

$$\rho_t^{(\text{pert,LO})}(s) = \frac{1}{8\pi^2} s \left(1 - \frac{m_Q^2}{s}\right)^2 \left(2 + \frac{m_Q^2}{s}\right), \quad (3.24)$$

$$\rho_5^{(\text{pert,LO})}(s) = \frac{3}{8\pi^2} m_Q^2 s \left(1 - \frac{m_Q^2}{s}\right)^2 \quad (3.25)$$

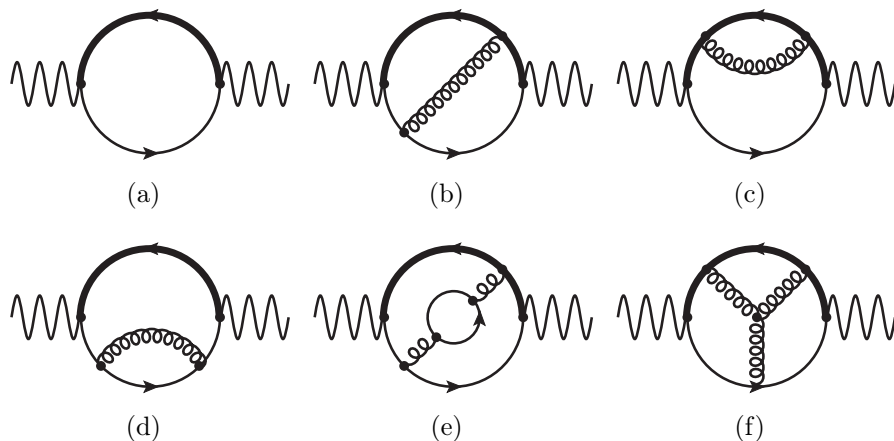


Figure 3.3: LO contribution (a), NLO corrections (b), (c) and (d), and a selection of NNLO corrections (e), (f) of the PT part C_0 . Wavy lines denote the external interpolating currents, thick (thin) solid lines are massive (light) quark propagators and curled lines are gluon propagators.

for $m_q = 0$. Taking the limit $s \rightarrow \infty$, one can easily see that two subtractions terms are necessary to ensure proper convergence of the dispersion integral in Eq. (3.17). Choosing the subtraction point $q_0^2 = 0$, the correlation function reads

$$\Pi_{t(5)}^{(\text{pert})}(q^2) = (q^2)^2 \int_{(m_Q+m_q)^2}^{\infty} ds \frac{\rho_{t(5)}^{(\text{pert})}(s)}{s^2(s-q^2)} + \Pi_{t(5)}^{(\text{pert})}(q^2) \Big|_{q_0^2=0} + q^2 \frac{d\Pi_{t(5)}^{(\text{pert})}(q^2)}{dq^2} \Big|_{q_0^2=0}.$$

The explicit computation of the LO and NLO corrections to $\rho_{t(5)}^{(\text{pert})}$ will be discussed in detail in Chap. 4. Furthermore, we explain the basics about the calculation of Feynman integrals.

The leading order process originates from a simple heavy-light quark loop, whereas higher order terms include additional gluon-exchange and quark-loop pair production. All corrections up to NLO are analytically known [65, 66]. The NNLO corrections stem from semi-numerical computations at the low and high energy region using conformal mapping and Padé approximation [75]. The authors of Ref. [75] made the Mathematica package `Rvs.m` available for public usage. Exemplary, we also calculate the tree-level quark condensate contribution below. More complicated contributions stemming from higher dimensional operators are elaborated in [69]. Note that

NLO corrections for the pseudoscalar-current have been known for a long time [62, 53], whereas the quark-condensate term in the vector-current correlator has been determined recently [A1]. In order to assess the coefficient functions of local operators with $d \geq 3$, we expand the external light background quark fields locally around $x = 0$ assuming the *Fock-Schwinger-gauge*, $x^\mu A_\mu = 0$, [76]:

$$q(x) = q(0) + x^\mu \overrightarrow{D}_\mu q(0) + \mathcal{O}(x^2). \quad (3.26)$$

To this end, the momenta of external vacuum fields are regarded as small compared to the momenta of propagating virtual quarks. We apply Wick's theorem in the correlation function to compute the quark condensate contribution. The contracted internal heavy quarks lead to the following tensorial condensate contribution in case of a interpolating vector current:

$$\begin{aligned} \Pi_{\mu\nu}^{(\bar{q}q)}(q^2) &= i \int d^4x e^{iqx} \langle 0 | \{ \dots + \bar{q}(x) \gamma_\mu \overline{Q}(x) \overline{Q}(0) \gamma_\nu q(0) + \dots \} | 0 \rangle \\ &= i \int d^4x e^{iqx} \langle 0 | \{ \bar{q}^\alpha(x) [\gamma_\mu S_Q^{(0)}(x, 0) \gamma_\nu]_{\alpha\beta} q^\beta(0) \} | 0 \rangle. \end{aligned} \quad (3.27)$$

In the second line of (3.27) we use

$$\begin{aligned} S_Q^{ij,(0)}(x, y) &= \overline{Q^i(x) Q^j(y)} = \langle 0 | \mathcal{T} \{ Q^i(x) \bar{Q}^j(y) \} | 0 \rangle \\ &= \delta^{ij} \int \frac{d^4k}{i(2\pi)^4} \frac{\not{k} + m_Q}{m_Q^2 - k^2} e^{-ik(x-y)}, \end{aligned} \quad (3.28)$$

which denotes the leading order heavy quark propagator with explicit imposed color indices. Due to the condition $m_Q \gg \Lambda_{\text{QCD}}$, the heavy quark fields do not form non-perturbative vacuum fluctuations. Thus, any contributions proportional to $\langle Q\bar{Q} \rangle$ will be neglected in our calculation. If we use the light-quark-field expansion in (3.26) as well as the matrix elements

$$\langle 0 | \bar{q}_i^\alpha(0) q_j^\beta(0) | 0 \rangle = \frac{1}{12} \delta^{\alpha\beta} \delta_{ij} \langle \bar{q}q \rangle, \quad (3.29)$$

$$\langle 0 | \bar{q}_i^\alpha(0) \overleftarrow{D}_\mu q_j^\beta(0) | 0 \rangle = \frac{im_q}{48} \delta_{ij} (\gamma_\mu)_{\beta\alpha} \langle \bar{q}q \rangle, \quad (3.30)$$

we obtain the leading quark condensate contribution

$$\Pi_{\mu\nu}^{\langle\bar{q}q\rangle}(q^2) = \frac{1}{4} \int d^4x \int \frac{d^4k}{(2\pi)^4} e^{i(q-k)x} \text{Tr} \left[\gamma_\mu \frac{\not{k} + m_Q}{m_Q^2 - k^2} \gamma_\nu \right] \langle q\bar{q} \rangle. \quad (3.31)$$

Eq. (3.30) drops out in case of vanishing light quark masses. Hence, the integrated result of (3.31) for massless light quarks is

$$\Pi_{\mu\nu}^{\langle\bar{q}q\rangle}(q^2) = \frac{m_Q}{m_Q^2 - q^2} g_{\mu\nu} \langle q\bar{q} \rangle \quad (3.32)$$

and the corresponding transverse mode reads

$$\Pi_t^{\langle\bar{q}q\rangle}(q^2) = \frac{-m_Q}{m_Q^2 - q^2} \langle q\bar{q} \rangle. \quad (3.33)$$

All relevant condensate contributions of dimension $d \leq 6$ are summed up in the condensate term

$$\Pi_{t(5)}^{(\text{cond})}(q^2) = \Pi_{t(5)}^{\langle\bar{q}q\rangle}(q^2) + \Pi_{t(5)}^{\langle GG\rangle}(q^2) + \Pi_{t(5)}^{\langle\bar{q}Gq\rangle}(q^2) + \Pi_{t(5)}^{\langle\bar{q}q\bar{q}q\rangle}(q^2). \quad (3.34)$$

Here, we introduce the notation $\{\langle\mathcal{O}_3\rangle, \langle\mathcal{O}_4\rangle, \langle\mathcal{O}_5\rangle, \langle\mathcal{O}_6\rangle\} = \{\langle\bar{q}q\rangle, \langle\bar{G}G\rangle, \langle\bar{q}Gq\rangle, \langle\bar{q}q\bar{q}q\rangle\}$. Explicit expressions of all terms in (3.34) are given in Appendix B.5. The LO coefficient functions of the gluon, quark-gluon (mixed) and four-quark condensates are known [45, 67, 77] and sufficient for the purpose of this thesis.

Light Quark Mass Corrections

In case of non-strange heavy-light mesons we neglect the masses of up and down-quarks. They are numerically small compared to all other relevant energy-momentum scales. However, for the description of strange mesons, we take the strange quark mass into account. We refrain from using the full mass-dependence, and instead keep only expansion terms of the light-quark mass. The corresponding quark currents are $j_\mu = \bar{s}\gamma_\mu Q$ and $j_5 = (m_Q + m_s)\bar{s}i\gamma_5 Q$. Both functions can be expanded in m_s according to

$$\begin{aligned} \Pi_{t(5)}^{(\text{OPE})}(q^2, m_Q, m_s) = & \Pi_{t(5)}(q^2, m_Q, 0) \\ & + m_s \Pi_{t(5)}^{(1)}(q^2, m_Q, 0) + m_s^2 \Pi_{t(5)}^{(2)}(q^2, m_Q, 0) + \mathcal{O}(m_s^3). \end{aligned} \quad (3.35)$$

Despite the violation of $SU(3)_F$ -symmetry due to massive light-quarks in the PT part, we also must change the quark condensate for strange quarks: $\langle \bar{q}q \rangle$ is replaced by $\langle \bar{s}s \rangle$, which is suppressed by $\sim 20\%$ in comparison to the massless case [78]. We truncate the mass expansion at $\mathcal{O}(m_s^2)$ and $\mathcal{O}(\alpha_s m_s)$ in the PT part. In the condensate contributions only the leading mass corrections $\mathcal{O}(m_s)$ are taken into account, which stem from the first order expansion term in the local expansion of Eq. (3.26), see also [69]. As a result, we keep just small mass contributions of the same magnitude, see Appendix B.4. The pseudoscalar correlator $\Pi_5(q^2)$ also has the prefactor $(m_Q + m_q)^2$, which arises from the RGE invariant quark-current j_5 as stated above. We retain this prefactor in our calculation.

Computational strategies about the calculation of $\Pi_{t(5)}^{(1)}$ and $\Pi_{t(5)}^{(2)}$ are discussed in Chap. 4.

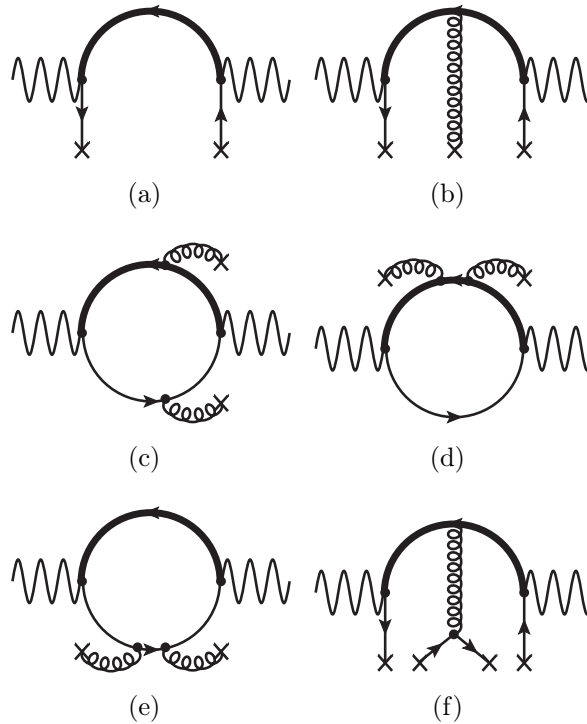


Figure 3.4: Leading order condensate contributions included in the coefficient functions C_d : (a) C_3 quark; (b) C_5 quark-gluon (mixed); (c), (d) and (e) C_4 gluon; (f) C_6 four-quark condensate. Wavy lines denote the external interpolating currents, thick (thin) solid lines are massive (light) quark propagators and curled lines are gluon propagators.

3.5 Quark-Hadron Duality and Borel Transformation

Before we obtain the sum rules for $f_{H^{(*)}}$, there are still two issues, which have not been discussed yet. At first, it is still unclear, how to interpret the hadronic representation, since the spectral densities in Eqs. (3.12) and (3.13) are mainly unknown. Secondly, the subtraction polynomial (3.18) are necessary to avoid divergent dispersion integrals, which should vanish or be more specified. These issues will be discussed in the following.

We describe the correlation function for two different domains, resulting in the following representations for $\Pi_{t(5)}(q^2)$:

$$\Pi_t^{(\text{had})}(q^2) = \frac{m_{H^*}^2 f_{H^*}^2}{m_{H^*}^2 - q^2} + \int_{s_0^h}^{\infty} ds \frac{\rho_t^h(s)}{s - q^2}, \quad (3.36)$$

$$\Pi_5^{(\text{had})}(q^2) = \frac{m_H^4 f_H^2}{m_H^2 - q^2} + \int_{s_0^h}^{\infty} ds \frac{\rho_5^h(s)}{s - q^2}, \quad (3.37)$$

$$\Pi_{t(5)}^{(\text{OPE})}(q^2) = (q^2)^2 \int_{(m_Q+m_q)^2}^{\infty} ds \frac{\rho_{t(5)}^{(\text{pert})}(s)}{s^2(s - q^2)} + \text{subtr. polynomial} + \Pi_{t(5)}^{(\text{cond})}(q^2), \quad (3.38)$$

where ρ_t^h and ρ_5^h are unknown quantities. Nevertheless, one can estimate the unknown spectral integrals by applying the so-called *quark-hadron duality*. An introduction to this concept and its phenomenology are discussed in Refs. [59, 60] as well as [43] in the context of inclusive, inelastic electron scattering. The quark-hadron duality allows to bridge a gap between theoretical predictions and experimental cross sections. It allows to equate certain inclusive particle interactions with perturbative calculations, if a reasonable energy average is used. This statement can be adapted to our problem as well. For deep Euclidean processes ($q^2 \rightarrow -\infty$) all condensates are suppressed. From this follows the global quark-hadron duality approximation

$$\Pi^{(\text{had})}(q^2) \approx \Pi^{(\text{pert})}(q^2). \quad (3.39)$$

Note that both spectral functions need to have the same power asymptotics in the limit $s \rightarrow \infty$ to ensure the approximation in (3.39) is valid, i.e.

$$\rho_{t(5)}^h(s) \rightarrow \rho_{t(5)}^{(\text{pert})}(s). \quad (3.40)$$

However, $\rho_{t(5)}^h(s)$ still could oscillate around this limit. A more stringent condition

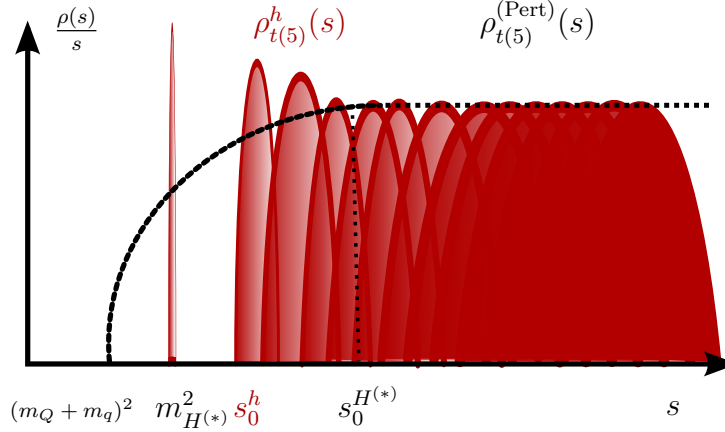


Figure 3.5: Illustration of the semi-local duality. The hadronic continuum spectrum is fitted by the perturbative correlation function.

$\rho_{t(5)}^h(s) \simeq \rho_{t(5)}^{(\text{pert})}(s)$ for threshold values larger than a specific effective threshold is the local quark-hadron duality. We use instead a combination of both conditions at sufficiently large $Q^2 = -q^2$, which postulates a weaker condition than the local approximation. It is the semi-local quark-hadron duality, which is defined as

$$\int_{s_0^h}^{\infty} ds \frac{\rho_{t(5)}^h(s)}{s - q^2} \simeq \int_{s_0^{H^{(*)}}}^{\infty} ds \frac{\rho_{t(5)}^{(\text{pert})}(s)}{s - q^2}. \quad (3.41)$$

Above, the duality-threshold parameter $s_0^{H^{(*)}}$ is introduced, which has to be externally determined. It does not necessarily coincide with s_0^h (see Fig. 3.5). Furthermore, it is useful to apply a Borel transformation to the correlation functions:

$$\Pi(M^2) \equiv \mathcal{B}_{M^2} \{ \Pi(q^2) \} = \lim_{\substack{-q^2, n \rightarrow \infty \\ -q^2/n = M^2}} \frac{(-q^2)^{n+1}}{n!} \left(\frac{d}{dq^2} \right)^n \Pi(q^2). \quad (3.42)$$

Two special cases are relevant to transform the complete sum rules in Eqs. (3.36)-(3.38):

$$\mathcal{B}_{M^2} \left\{ (-q^2)^k \ln \left(\frac{-q^2}{\mu^2} \right) \right\} = -k! \cdot M^{2k}, \quad (3.43)$$

$$\mathcal{B}_{M^2} \left\{ \frac{1}{(s - q^2)^k} \right\} = \begin{cases} \frac{1}{(k-1)!} \cdot \frac{1}{M^{2(k-1)}} e^{-s/M^2} & \text{if } k > 0, \\ 0 & \text{if } k < 0 \end{cases} \quad (3.44)$$

for integer values of k . This procedure has two advantages: The subtraction terms, which are still unknown are cancelled. In addition, this allows us to control the convergence of the OPE.

The final (Borel) sum rule of the vector-meson decay constant now yields in conjunction with the quark-hadron duality approximation to

$$f_{H^*}^2 = \frac{e^{m_{H^*}^2/M^2}}{m_{H^*}^2} \left\{ \Pi_t^{(\text{pert})}(M^2, s_0^{H^*}) + \Pi_t^{(\text{cond})}(M^2) \right\}, \quad (3.45)$$

and analogously for the pseudoscalar meson channel

$$f_H^2 = \frac{e^{m_H^2/M^2}}{m_H^4} \left\{ \Pi_5^{(\text{pert})}(M^2, s_0^H) + \Pi_5^{(\text{cond})}(M^2) \right\}. \quad (3.46)$$

In the above equations we use the shorthand notation

$$\Pi_{t(5)}^{(\text{pert})}(M^2, s_0^{H^{(*)}}) = \int_{(m_Q+m_q)^2}^{s_0^{H^{(*)}}} ds e^{-s/M^2} \rho_{t(5)}^{(\text{pert})}(s). \quad (3.47)$$

All results including perturbative as well as condensate contributions are given in Appendix B.5. Note that the Borel parameter M^2 must be chosen carefully because of two reasons. On one hand, the continuum states have to be sufficiently suppressed. On the other hand, the leading OPE expressions, especially the PT part, which is very accurately determined, should keep a great influence. An explicit discussion concerning a proper choice of M^2 is deferred to the numerical analysis of f_{B^*} in chapter 5.1.

The final sum rule for decay constants of vector mesons is

$$\begin{aligned} f_{H^*}^2 m_{H^*}^2 &= \frac{1}{8\pi^2} e^{m_{H^*}^2/M^2} \int_{m_Q^2}^{s_0^{H^*}} ds s (2+z)(1-z)^2 e^{-s/M^2} \\ &+ \left[-m_Q \langle \bar{q}q \rangle - \frac{1}{12} \langle GG \rangle + \frac{m_0^2 m_Q^3}{4M^4} \langle \bar{q}q \rangle \right. \\ &\quad \left. - \frac{32\pi\alpha_s r_{vac}}{81M^2} \left(1 + \frac{m_Q^2}{M^2} - \frac{m_Q^4}{8M^4} \right) \langle \bar{q}q \rangle \right] e^{-m_Q^2/M^2}, \end{aligned} \quad (3.48)$$

with only leading order expressions in α_s and neglected light quark mass. In case of

pseudoscalar mesons the sum rule is

$$\begin{aligned}
f_H^2 m_H^2 &= \frac{1}{8\pi^2} \left(\frac{m_Q^2}{m_H^2} \right) e^{m_{H^*}^2/M^2} \int_{m_Q^2}^{s_0^H} ds s (1-z)^2 e^{-s/M^2} \\
&+ \left[-m_Q \langle \bar{q}q \rangle + \frac{1}{12} \langle GG \rangle - \frac{m_0^2 m_Q^3}{2M^2} \left(1 - \frac{m_Q^2}{2M^2} \right) \langle \bar{q}q \rangle \right. \\
&\quad \left. - \frac{16\pi\alpha_s r_{vac} m_Q^2}{27M^2} \left(1 - \frac{m_Q^2}{4M^2} - \frac{m_Q^4}{12M^4} \right) \langle \bar{q}q \rangle \right] e^{-m_Q^2/M^2}.
\end{aligned} \tag{3.49}$$

3.6 Sum rules in the Infinite Heavy-Quark-Mass limit

Nonrelativistic versions of sum rules were investigated long time ago by Shuryak [61]. Later on the sum rules method was used in the framework of HQET to evaluate hadronic observables around the threshold region $\omega_0 = q^2 - m_Q^2 \ll m_Q^2$. Here, divergent terms arise, namely large logarithms $\sim \log\left(\frac{m_Q}{\mu}\right)$, when naively expanding with respect to inverse quark masses in the OPE. These logarithmic terms can be resummed systematically [62]. In the standard form, as presented in Eqs. (3.45) and (3.46), the Borel sum rules are not suited for an expansion around $1/m_Q$ since the free parameters s_0 and M^2 have no explicit m_Q -dependence. Therefore, we introduce a new set of mass dependent variables:

$$m_{H^{(*)}}^2 = (m_Q + \bar{\Lambda})^2, \quad M^2 = 2m_Q\tau, \tag{3.50}$$

$$s_0^{H^{(*)}} = (m_Q + \omega_0)^2 \simeq m_Q^2 + 2m_Q\omega_0. \tag{3.51}$$

Using this reparametrization, the sum rule for the heavy-light vector meson decay constant transforms to

$$\begin{aligned}
&f_{H^*}^2 m_{H^*} \left(\frac{m_{H^*}}{m_Q} \right) e^{-\frac{\bar{\Lambda}}{\tau} - \frac{\bar{\Lambda}^2}{2m_Q\tau}} \\
&= \frac{\tau^3}{\pi^2} \int_0^{\frac{\omega_0}{\tau}} dz e^{-z} \left(\frac{z^2}{1 + \frac{2z\tau}{m_Q}} \right) \left(2 + \frac{1}{1 + \frac{2z\tau}{m_Q}} \right) \times \left\{ 1 + \frac{2\alpha_s}{\pi} \left[\ln\left(\frac{m_Q}{2\tau}\right) + \frac{3}{2} + \frac{2\pi^2}{9} - \ln(z) \right. \right. \\
&\quad \left. \left. + \frac{2}{3} \mathcal{K}_T\left(\frac{2z\tau}{m_Q}\right) \right] \right\} - \langle q\bar{q} \rangle (m_Q) \left\{ 1 + \frac{2\alpha_s}{3\pi} \left(3 + \left(\frac{2\tau}{m_Q} \right) \int_0^\infty dz \frac{e^{-z}}{\left(1 + \frac{2z\tau}{m_Q} \right)^2} \right) \right\} - \frac{\langle GG \rangle}{12m_Q} \\
&+ \frac{m_0^2 \langle q\bar{q} \rangle}{16\tau^2} + \frac{\pi\alpha_s r_{vac} \langle q\bar{q} \rangle^2}{162\tau^3} \left\{ 1 - \frac{16\tau}{m_Q} - \frac{32\tau^2}{m_Q^2} \right\},
\end{aligned} \tag{3.52}$$

where radiative corrections of $\mathcal{O}(\alpha_s^2)$ are neglected. The function $\mathcal{K}_t(x)$ reads

$$\begin{aligned} \mathcal{K}_T(x) = & 2 \operatorname{Li}_2(-x) + \ln(x) \ln(1+x) + \frac{x}{(3+2x)} \ln(x) \\ & + \frac{(1+2x)(2+x)(1+x)}{(3+2x)x^2} \ln(1+x) + \frac{6x^2+3x-8}{4(3+2x)x} - \frac{9}{4}, \end{aligned} \quad (3.53)$$

which vanishes in the limit $m_Q \rightarrow \infty$ ($x \rightarrow 0$) according to

$$\mathcal{K}_T(x) \rightarrow \frac{4}{3}x \ln(x) - \frac{29}{18}x + \mathcal{O}(x^2). \quad (3.54)$$

For simplicity we use the renormalization-group-invariant heavy-quark pole mass to express the sum rule. It is also more convenient for the matching with HQET. In (3.52) the logarithmic enhancement has been singled out, whereas the quark condensate still has an intrinsic divergence. The corresponding HQ sum rule formula in the pseudoscalar channel is given in Appendix B.6. For neglected radiative corrections, we obtain the well-known asymptotic scaling law [79]:

$$f_H = f_{H^*} = \frac{\hat{f}}{\sqrt{m_H}}, \quad (3.55)$$

where the rescaled decay constant \hat{f} is introduced. The sum rule of the rescaled decay constant reads

$$\hat{f} = e^{\frac{\Lambda}{2\tau}} \left(\frac{3\tau^3}{\pi^2} \int_0^{\frac{\omega_0}{\tau}} dz z^2 e^{-z} - \langle q\bar{q} \rangle + \frac{m_0^2 \langle q\bar{q} \rangle}{16\tau^2} + \frac{\pi\alpha_s r_{\text{vac}} \langle q\bar{q} \rangle^2}{162\tau^3} \right)^{1/2}. \quad (3.56)$$

It includes all LO contributions of operators of dimension $d \leq 6$ except the gluon condensate terms, which enters the sum rule at $1/m_Q$ -level.

Effects of Heavy-Quark Spin Symmetry Violation

The ratio of Eqs. (3.52) and (B.57) at the heavy quark limit leads to the heavy-quark symmetry relation with NLO accuracy

$$\frac{f_{H^*}}{f_H} = 1 - \frac{2}{3} \left(\frac{\alpha_s}{\pi} \right). \quad (3.57)$$

It also follows from the matching calculation between HQET and full QCD heavy-light currents [79, 80]. The expression of finite-mass sum rules also allows us to estimate the first power suppression and to compare with the HQET relation in [62] according to

$$\frac{f_{H^*}}{f_H} = \left[1 - \frac{2}{3} \left(\frac{\alpha_s}{\pi} \right) \right] \left\{ 1 + \frac{\Delta}{m_Q} \right\}. \quad (3.58)$$

Setting the pole mass of the b -quark at $m_Q = 4.6$ GeV, this corresponds to $\Delta \sim 200$ MeV at the heavy-quark limit $f_{H^*}/f_H = 1$. In the next chapter we also estimate Δ from the results of our sum rules.

Effects of Heavy-Quark Flavor Symmetry Violation

Aside from ratios of mesons with the same flavor content, we determine ratios with mixed flavors as well. Concerning this matter, there also exist HQET estimates including two-loop radiative and no inverse heavy-mass corrections [79]:

$$\frac{f_B}{f_D} = \sqrt{\frac{m_D}{m_B}} \left(\frac{\alpha_s(m_c)}{\alpha_s(m_b)} \right)^{6/25} \left(1 + 0.894 \frac{\alpha_s(m_c) - \alpha_s(m_b)}{\pi} \right) \simeq 0.69. \quad (3.59)$$

In the final section of this chapter we compare this relation to our determined ratio value.

Perturbative Corrections to the Two-Point Correlation Functions

We analytically compute the absorptive part of the leading term in the OPE with NLO accuracy, see the correlation function in Eq. (3.20). From OPE we obtain the perturbative series

$$\rho_{t(5)}^{(\text{pert})}(s) = \frac{1}{\pi} \text{Im} \Pi_{t(5)}^{(\text{pert})}(s) = \rho_{t(5)}^{(\text{pert, LO})}(s) + \frac{\alpha_s}{\pi} \rho_{t(5)}^{(\text{pert, NLO})}(s). \quad (4.1)$$

Note that the above equation implicitly contains the Heaviside function $\theta(s - (m_Q + m_q)^2)$, which defines the physical cut in the perturbative regime. In the first step of our calculation the light quark is treated as massless, $m_q = 0$. Further, we will also perform a small mass expansion and include the leading contributions that arise from the light quark mass. From Wick's theorem all relevant Feynman diagrams are determined: a simple quark-loop contributes at LO and three two-loop diagrams contribute at NLO. For simplification we use the results from Π_5 to determine the transverse invariant amplitude Π_t . Solving Eq. (3.2) for Π_t , we find

$$\Pi_t = \frac{1}{(1-d)} \left[g^{\mu\nu} - \frac{q^\mu q^\nu}{q^2} \right] \Pi_{\mu\nu} \quad (4.2)$$

$$= \frac{1}{(1-d)} \left[\Pi_\mu^\mu - \frac{(m_Q + m_q)^2}{q^2} \Pi_5 \right]. \quad (4.3)$$

Here, we use the equation of motion $\partial^\mu j_\mu = (m_Q + m_q) j_5$ in tensorial correlation function $\Pi_{\mu\nu}$.

In order to compute the spectral function $\rho_{t(5)}^{(\text{pert})}$ it is necessary to determine the imaginary part of scalar Feynman integrals. For this purpose, we discuss definitions of such integrals within dimensional regularization and give explicit results of one-loop spectral functions, which are required in the following calculations. More details about the integration within dimensional regularization are also given in Appendix A.1 and A.2.

4.1 Essentials for Loop Computation

Feynman integrals can be analytically computed with various parametrization techniques such as Feynman parametrization [81, 82]. We present these integrals in “Euclidean” dependence, e.g. momenta in the denominator have a sign $-k^2$, to avoid complex-valued powers of (-1) , when shifting from Minkowskian to Euclidean coordinates. This convention also leads to positive spectral functions. We neglect the small offset ε^+ in the complex plane $-k^2 \rightarrow -k^2 - i\varepsilon^+$, but take it implicitly into account. For a better overview the shorthand notation for integrations over the momentum q is used:

$$\int_q \equiv \int \frac{d^4q}{(2\pi)^{4i}}. \quad (4.4)$$

We also redefine the integration measure into a $d(= 4-2\varepsilon)$ dimensional object according to dimensional regularization in the $\overline{\text{MS}}$ scheme notation

$$\int_q \rightarrow \int \bar{\mu}^2 \frac{d^d q}{(2\pi)^{di}},$$

where the scale parameter $\bar{\mu}^2 \equiv \left(\frac{\mu^2 e^{\gamma_E}}{4\pi}\right)^\varepsilon$ preserves the dimensionality of the integral. Furthermore, $\bar{\mu}^2$ prevents a proliferation of the *Euler’s constant* and 4π .

General One-Loop Master Formula

One-loop scalar integrals with two different masses m_1 and m_2 are

$$\begin{aligned} \int_k \frac{1}{[m_1^2 - (q-k)^2]^\alpha [m_2^2 - k^2]^\beta} &\equiv \frac{1}{(4\pi)^{\frac{d}{2}}} \times V(\alpha, \beta, q^2) \\ &= \frac{\Gamma(\alpha + \beta - d/2)}{\Gamma(\alpha)\Gamma(\beta)} \int_0^1 dx \frac{x^{\alpha-1} \bar{x}^{\beta-1}}{\Lambda^{\alpha+\beta-d/2}} \end{aligned} \quad (4.5)$$

using Feynman parametrization. Here, we introduce the abbreviation

$$\Lambda \equiv m_1^2 x + m_2^2 \bar{x} - q^2 x \bar{x}. \quad (4.6)$$

In this thesis we consider special cases such as the massless ($m_1 = m_2 = 0$) and the single-mass case ($m_1 = m, m_2 = 0$). If both masses are zero, Eq. (4.5) leads to

$$I(\alpha, \beta, q^2) \equiv V(\alpha, \beta, q^2) \Big|_{m_1=m_2=0} = G(\alpha, \beta) \times [-q^2]^{d/2-\alpha-\beta}. \quad (4.7)$$

The dimensionless function $G(\alpha, \beta)$ is a product of gamma functions and can be written as

$$G(\alpha, \beta) = \frac{\Gamma(-d/2 + \alpha + \beta)}{\Gamma(\alpha)\Gamma(\beta)} \int_0^1 dx x^{d/2-\beta-1} \bar{x}^{d/2-\beta-1} \quad (4.8)$$

$$= \frac{\Gamma(-d/2 + \alpha + \beta)\Gamma(d/2 - \alpha)\Gamma(d/2 - \beta)}{\Gamma(\alpha)\Gamma(\beta)\Gamma(d - \alpha - \beta)} \quad (4.9)$$

$$= g(\alpha, \beta) \times \frac{1}{\varepsilon}. \quad (4.10)$$

In the last line we separate the pole term, which yields to the finite function $g(\alpha, \beta)$. The common notation of $g(1, 1)$ is G . Another important case is the massive tadpole integral

$$T(\alpha; m^2) \equiv V(0, \beta, q^2) \Big|_{m_1=0, m_2=m} = \int \frac{d^d k}{i\pi^{d/2}} \frac{1}{[m^2 - k^2]^\alpha} = \frac{\Gamma(\alpha - d/2)}{\Gamma(\alpha)} \times [m^2]^{d/2-\alpha}. \quad (4.11)$$

Apart from the above results of one-loop integrals $V(\alpha, \beta, q^2)$, we also require their imaginary part. This issue will be discussed in the next section.

One-Loop Spectral Function with One Mass

The Feynman integral in (4.5) is a function of q^2 . We consider the case with one massive ($m_2 = m$) and one massless propagator ($m_1 = 0$). The integrand of (4.5) has a cut along the positive half-axis according to $[q^2 x - m^2] > 0$, starting with the branching point at the origin $q^2 x - m^2 = 0$. The analytic continuation leads from negative ($[q^2 x - m^2] < 0$) to positive values along the contour

$$t(\phi) \equiv -[sx - m^2]e^{-i\phi} \quad (s \equiv |q^2|). \quad (4.12)$$

We obtain the discontinuity relation from the difference $t(\pi + \pi i\varepsilon^+)$ and $t(-\pi - \pi i\varepsilon^+)$:

$$\begin{aligned}
 \text{Disc} \left[\frac{1}{[m^2 - q^2 x]^\gamma} \right] &= 2i \text{Im} \left[\frac{1}{[m^2 - q^2 x]^\gamma} \right] = \left[\frac{1}{t^\gamma(-\pi[1 + i\varepsilon^+])} - \frac{1}{t^\gamma(\pi[1 + i\varepsilon^+])} \right] \\
 &= \lim_{\varepsilon^+ \rightarrow 0} \left[\frac{1}{[sx - m^2]^\gamma} e^{i\gamma[\pi + \varepsilon^+]} - \frac{1}{[sx - m^2]^\gamma} e^{-i\gamma[\pi + \varepsilon^+]} \right] \theta(sx - m^2) \\
 &= 2\pi i \frac{\sin(\pi\gamma)}{\pi} \times \frac{\theta(sx - m^2)}{[sx - m^2]^\gamma} \\
 &= \frac{2\pi i}{[sx - m^2]^\gamma} \times \frac{\theta(sx - m^2)}{\Gamma(\gamma)\Gamma(1 - \gamma)}, \tag{4.13}
 \end{aligned}$$

where γ is a arbitrary exponent and the functional identity

$$\sin(\pi x) = \frac{\pi}{\Gamma(x)\Gamma(1 - x)}$$

is used. From Eq. (4.13) follows the spectral function ($z \equiv m_Q^2/s$)

$$\begin{aligned}
 \rho(\alpha, \beta, z) &\equiv \frac{1}{\pi} \text{Im} \left[V(\alpha, \beta, q^2) \right] \Big|_{m_1=0, m_2=m} \\
 &= \frac{1}{\Gamma(\alpha)\Gamma(\beta)\Gamma(1 + d/2 - \alpha - \beta)} \int_z^1 dx \bar{x}^{d/2 - \beta - 1} x^{\beta - 1} (sx - m^2)^{d/2 - \alpha - \beta} \\
 &= \frac{\Gamma(\frac{d}{2} - \beta)}{\Gamma(\alpha)\Gamma(\beta)\Gamma(1 + d - \alpha - 2\beta)} s^{\frac{d}{2} - \alpha - \beta} z^{\beta - 1} (1 - z)^{d - \alpha - 2\beta} \\
 &\quad \times {}_2F_1 \left(1 - \beta, \frac{d}{2} - (\alpha + \beta + 1); 1 + d - \alpha - 2\beta; \frac{z - 1}{z} \right). \tag{4.14}
 \end{aligned}$$

Here, we introduced the *ordinary hypergeometric function*:

$${}_2F_1(a, b; c; z) = \frac{\Gamma(c)}{\Gamma(b)\Gamma(c - b)} \int_0^1 dt t^{b-1} (1 - t)^{c-b-1} (1 - tz)^{-a} \tag{4.15}$$

and $\text{Re}(c) > \text{Re}(b) > 0$, $|\arg(1 - z)| < \pi$. In order to Laurent-expand the hypergeometric function in terms of ε , we use the Mathematica package `HypExp` [83]. This approach can easily be employed in the generic one-loop massless case ($m_1 = m_2 = 0$). The massless one-loop spectral function yields

$$\hat{\rho}(\alpha, \beta, s) \equiv \frac{1}{\pi} \text{Im}[I(\alpha, \beta, q^2)] = G(\alpha, \beta) \cdot s^{-\varepsilon} \cdot \frac{\sin(\pi\varepsilon)}{\pi} = g(\alpha, \beta) \cdot s^{-\varepsilon}. \tag{4.16}$$

For computations of diagrams beyond the one-loop level we define two-loop integrals with a single mass and arbitrary powers in the denominator as

$$\int_q \int_k \frac{1}{[m^2 - (p - q)^2]^\alpha [m^2 - (p - k)^2]^\beta [-k^2]^\delta [-q^2]^\rho [-(q - k)^2]^\sigma} \equiv \frac{1}{(4\pi)^d} V(\alpha, \beta, \delta, \rho, \sigma; p^2). \quad (4.17)$$

The corresponding two-loop spectral function shall be defined as

$$\rho_V(\alpha, \beta, \delta, \rho, \sigma; s) \equiv \frac{1}{\pi} \text{Im} \left[V(\alpha, \beta, \delta, \rho, \sigma; p^2) \right]. \quad (4.18)$$

Due to the complexity of two-loop integrations it is often useful to reexpress these integrals by simpler integrals if possible. We will discuss a strategy about how to obtain the simplest set of integrals for a specific topology of integrals in the next section.

Integration By Parts

If the number of different Feynman integrals is large, it is reasonable to derive some recurrence relations for a given topology of integrals to reduce the number of resulting integrals to a minimum. A common approach to obtain such relations is provided by the method of *integration by parts* (IBP) [84]. The minimal set of integrals are built up by irreducible *master integrals* or *masters*, which are simpler to compute than integrals of the original set. In order to demonstrate this method we consider a massless two-loop integral

$$V(n_1, n_2, n_3, n_4, n_5) = \int_k \int_q I(p, q, k) \quad I(p, q, k) \equiv \frac{1}{D_1^{n_1} D_2^{n_2} D_3^{n_3} D_4^{n_4} D_5^{n_5}}, \quad (4.19)$$

where $D_1 \equiv -(p - q)^2$, $D_2 \equiv -(p - k)^2$, $D_3 \equiv -k^2$, $D_4 \equiv -q^2$ and $D_5 \equiv -(q - k)^2$, see also Fig. 4.1. The basic idea of IBP includes the vanishing surface terms within dimensional regularization

$$\int_k \int_q \frac{\partial}{\partial q_\mu} I(p, q, k) = \int_k \int_q \frac{\partial}{\partial k_\mu} I(p, q, k) = 0, \quad (4.20)$$

if the integrand is derived with respect to the integration momenta. From differentiation with respect to q^μ in Eq. (4.20) we obtain

$$\frac{\partial}{\partial q_\mu} I(p, q, k) = \left[(-n_1) \frac{2(p - q)^\mu}{D_1} + (-n_4) \frac{-q^\mu}{D_4} + (-n_5) \frac{-2(q - k)^\mu}{D_5} \right] \times I(p, q, k). \quad (4.21)$$

For the purpose of (4.19), we evaluate three reduction relations, using the notation of increasing and lowering operators, e.g. $\mathbf{4}^+\mathbf{5}^- \times V(n_1, n_2, n_3, n_4, n_5) = V(n_1, n_2, n_3, n_4 + 1, n_5 - 1)$:

$$\begin{aligned} & \frac{\partial}{\partial q_\mu} (q - k)^\mu \times I(p, q, k) \\ &= \left[D - n_1 - n_4 - 2n_5 - n_1 \mathbf{1}^+ (\mathbf{5}^- - \mathbf{2}^-) - n_4 \mathbf{4}^+ (\mathbf{5}^- - \mathbf{3}^-) \right] \times I, \end{aligned} \quad (4.22)$$

$$\begin{aligned} & \frac{\partial}{\partial q_\mu} (p - q)^\mu \times I(p, q, k) \\ &= \left[2n_1 + n_4 - n_5 - D + n_4 \mathbf{4}^+ (p^2 + \mathbf{1}^-) + n_5 \mathbf{5}^+ (\mathbf{1}^- - \mathbf{2}^-) \right] \times I, \end{aligned} \quad (4.23)$$

$$\begin{aligned} & \frac{\partial}{\partial q_\mu} q^\mu \times I(p, q, k) \\ &= \left[D - n_1 - 2n_2 - n_5 - n_1 \mathbf{1}^- (p^2 + \mathbf{4}^+) + n_5 \mathbf{5}^- (\mathbf{3}^+ - \mathbf{4}^+) \right] \times I. \end{aligned} \quad (4.24)$$

Furthermore, it is useful to reexpress the scalar products into linear expressions of inverse propagators D_i :

$$\begin{aligned} 2(q - k)(p - q) &= D_1 - D_2 + D_5, & 2(q - k)q &= D_3 - D_4 - D_5, \\ 2(p - q)q &= D_1 + D_4 + p^2. \end{aligned} \quad (4.25)$$

If we successively use the relations (4.22) to (4.24), we find

$$\begin{aligned} & V(1, 1, 1, 1, 1) \\ &= \frac{1}{D - 4} \left[V(2, 1, 1, 1, 0) + V(1, 1, 1, 2, 0) - V(2, 0, 1, 1, 1) - V(1, 1, 0, 2, 1) \right], \\ &= \frac{2}{D - 4} \left[V(2, 1, 1, 1, 0) - V(2, 0, 1, 1, 1) \right], \\ &= \frac{1}{D - 4} \left[\frac{2(D - 3)}{p^2} V(1, 1, 1, 1, 0) + \frac{2(3D - 10)(3D - 8)}{(D - 4)p^4} V(0, 1, 0, 1, 1) \right] \end{aligned} \quad (4.26)$$

In the first and second line of the above equation the recurrence relation in Eq. (4.22) and some symmetry properties

$$V(2, 1, 1, 1, 0) = V(1, 1, 1, 2, 0), \quad V(2, 0, 1, 1, 1) = V(1, 1, 0, 2, 1)$$

allow us to express $V(1, 1, 1, 1, 1)$ with five propagators via two integrals with only four propagators. The other two relations in (4.23) and (4.24) provide a simplification of

the remaining integrals into terms of master integrals, which are given by $V(1, 1, 1, 1, 0)$ and $V(0, 1, 0, 1, 1)$. In general, one has to determine all possible IBP relations for a given topology of Feynman integrals to find the set of master integrals. In the massless two-loop case there are six relations corresponding to the derivatives

$$\frac{\partial}{\partial k_\mu} k_\mu, \quad q_\mu \frac{\partial}{\partial k_\mu}, \quad \frac{\partial}{\partial q_\mu} q_\mu, \quad k_\mu \frac{\partial}{\partial q_\mu}, \quad p_\mu \frac{\partial}{\partial k_\mu}, \quad p_\mu \frac{\partial}{\partial q_\mu}$$

that we apply on the integrand of Eq. (4.19). These relations lead to a linear combination in terms of master integrals for $V(n_1, n_2, n_3, n_4, n_5)$. Nowadays many programs are available for solving IBP reduction problems for various classes of integrals. In this thesis the Mathematica package `LiteRed` is used to build up the IBP reduction rules and obtain the master integrals. For a detailed description of `LiteRed` we refer to Refs. [85] and [86]. In order to obtain the reduction rules we define a specific two-loop diagram, which has the corresponding complexity and includes all integrals of the given problem. Based on Eq. (4.19) we choose a basis \mathcal{D}_S with 5 linear independent denominators D_α :

$$\mathcal{D}_S = \{D_1, D_2, D_3, D_4, D_5\}.$$

Having solved the reduction problem, the number of master integrals reduces to the formula stated above. The set of masters is

$$\text{MIS} = \{V(1, 1, 1, 1, 0), V(0, 1, 0, 1, 1)\} \quad (4.27)$$

for the given topology in (4.19).

The analytic computation of relevant master integrals for $\rho_{t(5)}^{(\text{pert})}(s)$ is performed and explained in the following sections and Appendix B.3.

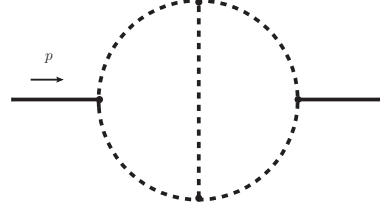
Cutkosky Rules

The discontinuity of a scalar propagator is related to the imaginary part by

$$\text{Im}\left\{\frac{1}{m^2 - p^2 - i\varepsilon^+}\right\} = \frac{1}{2i}\left(\frac{1}{m^2 - p^2 - i\varepsilon^+} - \frac{1}{m^2 - p^2 + i\varepsilon^+}\right) = \pi\delta(m^2 - p^2). \quad (4.28)$$

We explicitly write the small imaginary offset $i\varepsilon^+$ in the complex plane since it determines the sign of the delta distribution. In the same manner, one can also determine the imaginary part for a Feynman integral. As an example, we consider a one-loop

Basis of two-loop topology



(a) Two-loop basis for LiteRed

Feynman graphs of master integrals

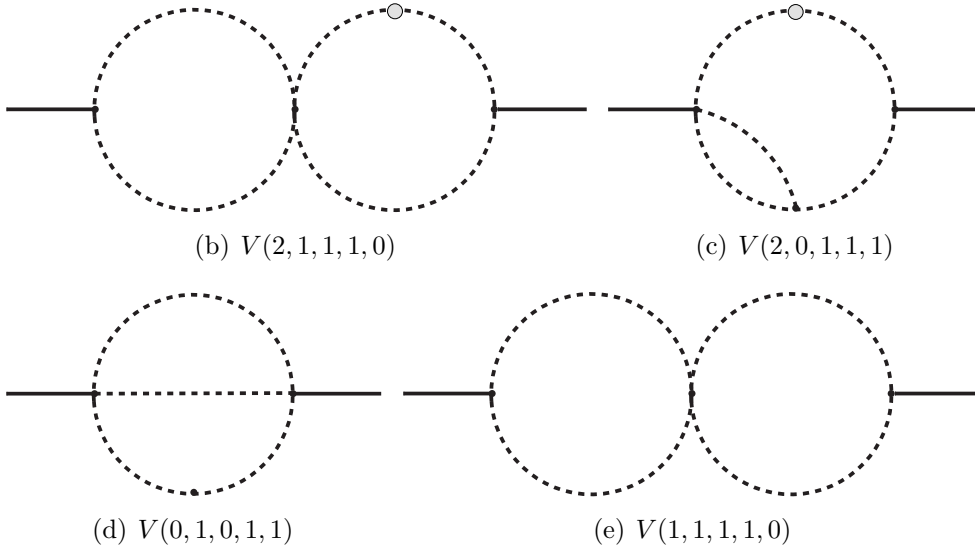


Figure 4.1: Basis to generate IBP identities for massless two-loop Feynman integrals is shown in (a). The reduced integrals (b), (c) and two master integrals after IBP reduction (d), (e). A dotted line denotes an additional power of the propagator.

integral with a single mass:

$$\begin{aligned}
 \Pi(p^2) &= \int_k \frac{1}{[m^2 - k^2 - i\varepsilon^+]} \frac{1}{[m^2 - (p - k)^2 - i\varepsilon^+]} \\
 &= \int_k \left(\hat{I}(k_0) - \frac{i\pi}{k_0} \delta(\omega_k - k_0) \right) \\
 &\quad \times \left(\hat{I}(k_0 - p_0) - \frac{i\pi}{k_0 - p_0} \delta(\omega_{k-p} - k_0 + p_0) \right) \theta(k_0) \theta(k_0 - p_0)
 \end{aligned}$$

$$= \int_k \left(\frac{1}{m^2 - k^2} \times \frac{i\pi}{k_0 - p_0} \delta(\omega_{k-p} - k_0 + p_0) + \frac{1}{m^2 - (k-p)^2} \times \frac{i\pi}{k_0} \delta(\omega_k - p_0) \right),$$

where $\hat{I}(k_0) \equiv \frac{1}{\omega_k - k_0 - i\varepsilon^+} - \frac{1}{\omega_k + k_0 - i\varepsilon^+}$ and $\omega_k \equiv \sqrt{\vec{k}^2 + m^2}$. Products of delta distributions vanish in the second line of the above equation. Moreover, the integrands $\hat{I}(k_0)$ and $\hat{I}(k_0 - p_0)$ have their poles on the lower half of the complex plane. The closed integration contour can go along the upper complex plane, which is singularity-free. As a result, the integral along this contour is zero. We now use the discontinuity relation in Eq. (4.28) to calculate the imaginary part of the Feynman integral:

$$\begin{aligned} & \text{Im } \Pi(p^2) \\ &= \int_k \left(\pi \delta(m^2 - k^2) \frac{i\pi}{k_0 - p_0} \delta(\omega_{k-p} - k_0 + p_0) + \pi \delta(m^2 - (k-p)^2) \frac{i\pi}{k_0} \delta(\omega_k - p_0) \right) \\ &= \frac{1}{2i} \int_k \left((2\pi i) \delta(m^2 - k^2) \times (2\pi i) \delta(m^2 - (k-p)^2) \right). \end{aligned} \quad (4.29)$$

Hence, the imaginary part of one-loop integrals can be instantly evaluated by replacing the propagators by on-shell delta distributions,

$$\frac{1}{m^2 - k^2} \rightarrow (2\pi i) \delta(m^2 - k^2) \theta(k_0 - m_0), \quad (4.30)$$

$$\frac{1}{m^2 - (k-p)^2} \rightarrow (2\pi i) \delta(m^2 - (k-p)^2) \theta((k_0 - p_0) - m_0) \quad (4.31)$$

and introduce the prefactor $\frac{1}{2i}$. Here, we also add the terms $\theta(k_0 - m_0)$ and $\theta((k_0 - p_0) - m_0)$ to guarantee positive energy components along the given propagating direction. Eq. (4.14) can easily be confirmed by these substitutions. In general they also work for any loop integrals, known as *Cutkosky (cutting) rules* [87]. For amplitudes with more than one loop it is necessary to perform all possible *cuts* and sum over them. Cutted lines indicate the transition from virtual to on-shell particles. We will use the cutting rules in this thesis in order to calculate the most complicated integrals.

4.2 Leading Order Contribution

The PT part of the two-point correlator with either tensor or pseudoscalar structure at LO is given by

$$\Pi_{\mu\nu(5)}^{(\text{pert, LO})}(p^2) = - \int_k \text{Tr} \{ \Gamma_{\nu(5)} S_{ij}(p-k, m_Q) \Gamma_{\mu(5)} S_{ji}(k, 0) \}, \quad (4.32)$$

where we introduced $\Gamma_\mu = \gamma_\mu$ and $\Gamma_5 = i\gamma_5$. This integral is a simple quark-antiquark loop with the massive $S_{ij}(p - k, m)$ and massless $S_{ij}(k, 0)$ bare fermion propagator. $SU(3)$ color indices are denoted by i, j . A minus sign arises because of the fermionic loop configuration. The resulting spectral functions are

$$\rho_t^{(\text{pert, LO})}(s) = \frac{2}{3}(1 - z)(2 + z)\rho(1, 1; z), \quad (4.33)$$

$$\rho_5^{(\text{pert, LO})}(s) = 2(1 - z)\rho(1, 1; z). \quad (4.34)$$

The strategy for computation is to substitute mixed scalar products of q and k in the numerator of (4.32) by inverse scalar propagators $[m^2 - k^2]$ and $[-(q - k)^2]$ and to then perform the discontinuity cuts. Note that both LO spectral functions include no poles because the preformed cuts reduce divergences of the form $1/\varepsilon^n$ to $1/\varepsilon^{n-1}$ and, hence, by one order.

4.3 Next-to-Leading Order Contribution

NLO corrections to the correlation functions result from three Feynman graphs. The most complicated topology at this level of complexity is the scalar “fish”-type diagram including 5 propagators, see Eq. (4.17). This topology is used to define the basis, which is necessary to obtain the IBP reduction rules with LiteRed. We end up with 5 masters, i.e. any (non-vanishing) integrals as defined in Eq. (4.17) can be reduced to these five integrals. One of the masters is a product of two massive tadpoles and therefore has a vanishing imaginary part. We start with radiative corrections on the massless and massive quark line. The full quark propagator is given by

$$\begin{aligned} \tilde{S}_{ij}(k, m) &= i \int d^d x e^{-ikx} \langle 0 | T \{ \psi_i(x) \bar{\psi}_j(0) e^{i \int d^d x \mathcal{L}_I(x)} \} | 0 \rangle \\ &= \frac{\delta_{ij}}{[S(k, m)]^{-1} - \Sigma(k, m) + \delta m} \\ &= \delta_{ij} \left(S(k, m) + S(k, m) \Sigma(k, m) S(k, m) + \mathcal{O}(\alpha_s^2) \right) \end{aligned} \quad (4.35)$$

where $[S(k, m)]^{-1} = \not{k} - m$ is the inverse bare propagator, $\Sigma(k, m)$ is the one-particle irreducible (1PI) self-energy and δm denotes the mass counterterm. From this follows

that the correlation functions at NLO level are:

$$\Pi_{\mu\nu(5)}^{(\text{pert, NLO})}(p^2)\Big|_{\text{SEmQ}} = - \int_k \text{Tr}\{\Gamma_{\nu(5)} S_{li}(p-k, m_Q) \Gamma_{\mu(5)} S_{ij}(k, 0) (i\Sigma_{jr}(k, 0)) S_{rl}(k, 0)\}, \quad (4.36)$$

$$\Pi_{\mu\nu(5)}^{(\text{pert, NLO})}(p^2)\Big|_{\text{SEmQ}} = - \int_k \text{Tr}\{\Gamma_{\nu(5)} S_{li}(p-k, m_Q) (i\Sigma_{ij}(p-k, m_Q)) S_{jr}(p-k, m_Q) \times \Gamma_{\mu(5)} S_{rl}(k, 0)\}. \quad (4.37)$$

The massive 1PI self-energy $\Sigma(p, m)$ reads

$$i\Sigma_{ij}(p, m) = (-i)g_s^2 C_F \delta_{ij} \times \int_q \frac{\gamma_\mu (\not{q} + m) \gamma^\mu}{[m^2 - q^2][-(p-q)^2]}. \quad (4.38)$$

Here, we introduce the coupling $g_s^2 = \alpha_s(4\pi)$. From Dirac and IBP reduction we find the absorptive part

$$\rho_t^{(\text{pert, NLO})}(s)\Big|_{\text{SEmQ}} = - \frac{4}{3\varepsilon} (1-z)(\rho_V(0, 1, 0, 1, 1) + sz\rho_V(0, 2, 0, 1, 1)) + \mathcal{O}(\varepsilon^0) \quad (4.39)$$

$$\rho_5^{(\text{pert, NLO})}(s)\Big|_{\text{SEmQ}} = - \frac{4}{\varepsilon} (\rho_V(0, 1, 0, 1, 1) + sz\rho_V(0, 2, 0, 1, 1)) + \mathcal{O}(\varepsilon^0) \quad (4.40)$$

$$\begin{aligned} \rho_t^{(\text{pert, NLO})}(s)\Big|_{\text{SEmQ}} &= \frac{8}{3\varepsilon} (1-z)(\rho_V(0, 1, 0, 1, 1) + sz\rho_V(0, 2, 0, 1, 1)) \\ &\quad + 2 \frac{(1-z)(1+3z)}{z} \rho_V(1, 1, 0, 1, 0) + \mathcal{O}(\varepsilon^0) \end{aligned} \quad (4.41)$$

$$\begin{aligned} \rho_5^{(\text{pert, NLO})}(s)\Big|_{\text{SEmQ}} &= \frac{8}{\varepsilon} (\rho_V(0, 1, 0, 1, 1) + sz\rho_V(0, 2, 0, 1, 1)) \\ &\quad + 6 \left(\frac{1}{z} - 3 \right) \rho_V(1, 1, 0, 1, 0) + \mathcal{O}(\varepsilon^0), \end{aligned} \quad (4.42)$$

where only the pole terms are presented. The self-energy contribution with correction on the massless (massive) line can be reduced to two (three) masters. The third contribution arises from the fish-type diagram, which has maximum complexity at NLO level. From IBP reduction we find 4 masters. The explicit two-point function formula reads

$$\begin{aligned} \Pi_{\mu\nu(5)}^{(\text{pert, NLO})}(p^2)\Big|_{\text{fish}} &= - \int_k \int_q \text{Tr}\{\Gamma_{\nu(5)} S_{ij}(p-q, m_Q) (ig_s T_{jl}^a \gamma_\alpha) S_{ln}(p-k, m_Q) \Gamma_{\mu(5)} S_{nr}(k, 0) \\ &\quad (ig_s T_{rs}^b \gamma_\beta) S_{rs}(q, 0) D_{ab}^{\alpha\beta}(q-k, 0)\}. \end{aligned} \quad (4.43)$$

As a result, we obtain the following spectral functions

$$\begin{aligned}
 \rho_t^{(\text{pert, NLO})}(s) \Big|_{\text{fish}} &= -\frac{4(z-1)}{9z\varepsilon} \left(sz(5z+3)\rho_V(0, 2, 0, 1, 1) + 3(sz\rho_V(1, 1, 1, 1, 0) \right. \\
 &\quad \left. + (z+1)\rho_V(1, 1, 0, 1, 0) \right) + 17z\rho_V(0, 1, 0, 1, 1) \\
 &\quad + \frac{4}{9z\varepsilon}(1-z)(5-z)\rho_V(1, 1, 0, 1, 0) + \mathcal{O}(\varepsilon^0), \\
 \rho_5^{(\text{pert, NLO})}(s) \Big|_{\text{fish}} &= -\frac{4}{z\varepsilon} \left(sz(3z+1)\rho_V(0, 2, 0, 1, 1) + sz\rho_V(1, 1, 1, 1, 0) \right. \\
 &\quad \left. + (1+z)\rho_V(1, 1, 0, 1, 0) + 7z\rho_V(0, 1, 0, 1, 1) \right) \\
 &\quad - \frac{4}{z\varepsilon}(1-z)\rho_V(1, 1, 0, 1, 0) + \mathcal{O}(\varepsilon^0).
 \end{aligned}$$

Adding up all three spectral functions of NLO level

$$\rho_{t(5)}^{(\text{pert, NLO})}(s) = \rho_{t(5)}^{(\text{pert, NLO})}(s) \Big|_{\text{SEmQ}} + \rho_{t(5)}^{(\text{pert, NLO})}(s) \Big|_{\text{SEmQ}} + \rho_{t(5)}^{(\text{pert, NLO})}(s) \Big|_{\text{fish}} \quad (4.44)$$

leads to a simple pole expression. It is sufficient to renormalize the bare quark mass within a suitable renormalization scheme, since we choose a renormalization-group-invariant current operator. In the pole mass scheme $m_Q^{\text{pole}} = Z_m^{\text{OS}} m_Q^{\text{bare}}$ we find

$$\begin{aligned}
 \rho_t^{(\text{pert, LO})}(s) &= \frac{2}{3}(1-z)^2(2+z) \\
 \rho_t^{(\text{pert, NLO})}(s) \Big|_{\text{mQ@pole}} &= \left(1 - \frac{5}{2}z + \frac{2}{3}z^2 + \frac{5}{6}z^3 + \frac{1}{3}z(-5 - 4z + 5z^2) \log(z) \right. \\
 &\quad \left. - \frac{1}{3}(1-z)^2(4+5z) \log(1-z) \right. \\
 &\quad \left. + \frac{2}{3}(1-z)^2(2+z) \left[\log\left(\frac{z}{1-z}\right) \log(1-z) - 2\text{Li}_2\left(-\frac{z}{1-z}\right) \right] \right). \quad (4.45)
 \end{aligned}$$

In the case of pseudoscalar current operators the corresponding spectral function reads

$$\begin{aligned}
 \rho_5^{(\text{pert, LO})}(s) &= 2(1-z)^2 \\
 \rho_5^{(\text{pert, NLO})}(s) \Big|_{\text{mQ@pole}} &= (1-z) \left(\frac{9}{2}(1-z) + (3-z)(1-2z) \log(z) \right. \\
 &\quad \left. - (1-z)(5-2z) \log(1-z) \right. \\
 &\quad \left. + 2(1-z) \log(z) \log(1-z) + 4(1-z)\text{Li}_2(z) \right), \quad (4.46)
 \end{aligned}$$

which is in agreement with [75] and [88]. In the $\overline{\text{MS}}$ scheme of the quark mass m_Q the spectral functions $\rho_{t(5)}$ obtain additional terms from the pole-to- $\overline{\text{MS}}$ -mass conversion formula, see Eq. (A.33). Note that PT contributions at NNLO level are also computed in the pole mass scheme of the heavy quark [75]. Therefore additional terms $\Delta\rho_{t(5)}^{(\text{pert})}(s)$ are required that stems from the pole-to- $\overline{\text{MS}}$ -mass expansion in Eq. (A.44). The LO and NLO terms contribute to $\Delta\rho_{t(5)}^{(\text{pert})}(s)$ up to $\mathcal{O}(\alpha_s^2)$. We present the additional terms in Appendix B.4, where both contributions are denoted by $\Delta_{1,2}\rho_{t(5)}^{(\text{pert, NNLO})}(s)$. The overall spectral function in the $\overline{\text{MS}}$ scheme reads

$$\rho_{t(5)}^{(\text{pert})}(s) = \rho_{t(5)}^{(\text{pert})}(s) \Big|_{m_Q @ \text{pole}} + \Delta\rho_{t(5)}^{(\text{pert})}(s) \quad (4.47)$$

$$\begin{aligned} &= \rho_{t(5)}^{(\text{pert})}(s) \Big|_{m_Q @ \text{pole}} + \left(\frac{\alpha_s}{\pi}\right) \Delta\rho_{t(5)}^{(\text{pert, NLO})}(s) \\ &\quad + \left(\frac{\alpha_s}{\pi}\right)^2 \Delta_1\rho_{t(5)}^{(\text{pert, NNLO})}(s) + \left(\frac{\alpha_s}{\pi}\right)^2 \Delta_2\rho_{t(5)}^{(\text{pert, NNLO})}(s). \end{aligned} \quad (4.48)$$

At NLO level we find

$$\Delta\rho_t^{(\text{pert, NLO})}(s) = -z(1-z^2) \left(3 \log\left(\frac{\mu^2}{m_Q^2}\right) + 4 \right), \quad (4.49)$$

$$\Delta\rho_5^{(\text{pert, NLO})}(s) = (1-3z) \left(3 \log\left(\frac{\mu^2}{m_Q^2}\right) + 4 \right). \quad (4.50)$$

4.4 Light-Quark Mass Corrections

In the previous sections of this chapter all calculations were performed with vanishing light-quark mass. If we consider the strange quark as the light partner in the heavy-light meson system, the light-quark mass contributions must be included since radiative corrections of $\mathcal{O}(\alpha_s^2)$ are of the same magnitude as the strange quark mass (m_s) contributions of $\mathcal{O}(m_s\alpha_s)$. The light-quark mass corrections to the spectral function can be assessed with preceding methods and results of Sects. 4.2 and 4.3. We start with Eq. (4.32) and replace the massless propagator by the mass-expanded one:

$$S_{ji}(k, 0) \rightarrow S_{ji}(k, m_s) = (-i) \frac{\not{k} + m_s}{m_s^2 - k^2} = (-i) \left[\frac{\not{k}}{-k^2} + m_s \frac{1}{-k^2} - m_s^2 \frac{\not{k}}{[-k^2]^2} \right] + \mathcal{O}(m_s^3). \quad (4.51)$$

Expansion terms of order m_s^3 and higher are neglected at LO in α_s . From Eq. (4.51) we promote the PT part by two additional terms with one additional power in the massless propagator. At NLO level we retain only the linear term in m_s . Note that all contributions from mass corrections are determined by the set of masters as in the massless light-quark computation. We denote the mass corrections by $\delta\rho_{t(5)}(s)$, which should be added to the yet known results:

$$\rho_{t(5)}^{(\text{pert})}(s) = \rho_{t(5)}^{(\text{pert})}(s) \Big|_{m_s=0} + \delta\rho_{t(5)}^{(\text{pert},m_s)}(s). \quad (4.52)$$

The explicit expressions to the LO contributions are

$$\begin{aligned} \delta\rho_t^{(\text{pert},\text{LO},m_s)}(s) &= -\frac{2}{3} \left[2m_s m_Q (4-z) \rho(1,1) + m_s^2 (2+z) (\rho(1,1) + s(1-z) \rho(1,2)) \right] \\ &= -\frac{2}{3} \left[2m_s m_Q (4-z)(1-z) + 2m_s^2 (2+z) \right], \end{aligned} \quad (4.53)$$

$$\begin{aligned} \delta\rho_5^{(\text{pert},\text{LO},m_s)}(s) &= 4m_s m_Q \rho(1,1) - 2m_s^2 (s(1-z) \rho(1,2) + \rho(1,1)) \\ &= 4(m_s m_Q (1-z) - m_s^2). \end{aligned} \quad (4.54)$$

Mass correction terms to the NLO contribution $\delta\rho_{t(5)}^{(\text{pert},\text{NLO},m_s)}$ are given in Appendix B.4. The strange quark mass is renormalized in the $\overline{\text{MS}}$ scheme to remove the extra mass pole $m_s = Z_m^{\overline{\text{MS}}} m_s^{\text{bare}}$.

Decay Constants of B and D Mesons from QCD Sum Rules

In this chapter we perform the numerical evaluation of decay constants for heavy-light bottom and charmed vector mesons $H^* = \{B^*, B_s^*, D^*, D_s^*\}$ and, analogously, for the corresponding pseudoscalar meson channel $H = \{B, B_s, D, D_s\}$. As an example, a detailed discussion of f_{B^*} will be presented. We also determine the HQ and $SU(3)_F$ -violation by means of various ratios of decay constants. In the end, we perform estimations with alternative versions of sum rules to test the consistency of the given sum rules framework.

Before we start the analysis, some prerequisites need to be discussed concerning the adopted QCD parameters, see Tab. 5.1, and method-based variables, i.e. the Borel parameter, the renormalization scale and the duality-threshold.

5.1 Numerical analysis of Borel sum rules

Setup and Input Parameters

For correlation functions of highly virtual quarks, which are involved in our computation, we use quark masses in the $\overline{\text{MS}}$ scheme. Note that the integrated spectral function shows an improved convergence behavior if $\overline{\text{MS}}$ masses are used instead of pole masses. This issue has already been pointed out in [53]. Currently, there is a good agreement between various lattice and continuum-QCD determinations of b and c quark masses. Hence, we use the averaged $\overline{\text{MS}}$ masses from PDG [36]. In particular, the heavy quark mass extractions from QCD quarkonium sum rules [89, 90] are in good agreement with our selected value. Regarding the strange quark mass, we double the theoretical uncertainty to retain conservative uncertainties for the sum rule predictions [91, 92, 93]. However, one needs to have in mind that recent lattice determinations state higher accuracy.

The quark condensate density is determined according to the Gell-Mann-Oakes-Renner (GMOR) relation that relates $\langle \bar{q}q \rangle$ via chiral symmetry breaking in QCD to physical quantities of the π -meson:

$$\langle \bar{q}q \rangle(2 \text{ GeV}) = \frac{m_\pi^2 f_\pi^2}{2(m_u + m_d)}. \quad (5.1)$$

In Ref. [94] there is a discussion of how to determine $\langle \bar{q}q \rangle$ in a precise manner. The authors also use the strange quark mass as a further input [95]. Besides $SU(3)_f$ symmetry violation in the OPE, which originates from the quark mass difference $m_s - m_{u,d}$, it also arises from the difference between strange and non-strange quark-condensate densities. Regarding the condensate ratio we adopt a rather broad interval from Ref. [78]. All condensate densities of higher dimensionality $d = 4, 5, 6$ are also provided in [78], where we follow the standard notation: The quark-gluon and gluon-gluon condensate are parametrized as

$$\langle GG \rangle \equiv \frac{\alpha_s}{\pi} \langle 0 | G_{\mu\nu}^a G^{a\mu\nu} | 0 \rangle \quad \text{and} \quad \langle \bar{q}Gq \rangle \equiv \langle 0 | g_s \bar{q} \sigma_{\mu\nu} t^a G_{\mu\nu}^a q | 0 \rangle = m_0^2 \langle \bar{q}q \rangle, \quad (5.2)$$

respectively. We introduced the mass parameter m_0 in the quark-gluon condensate term. It is numerically accessible via sum rule techniques at baryonic resonances. Furthermore, following [45], the four-quark condensate density is factorized with an intermediate vacuum insertion into the square of the ordinary quark condensate:

$$\langle \bar{q} \Gamma_\alpha q \bar{q} \Gamma_\beta q \rangle = r_{\text{vac}} \langle \bar{q}q \rangle^2, \quad (5.3)$$

where Γ_α and Γ_β are Dirac matrices. Here, the additional coefficient r_{vac} denotes the deviation from the original expression due to the factorization procedure.

Note that all parameters, which were introduced, have a specific renormalization scale dependence. Quark masses, OPE coefficient functions and vacuum expectation values of local operators are multiplicably renormalizable by means of

$$m(\mu_m) = \left(\frac{\alpha_s(\mu_m)}{\alpha_s(\mu'_m)} \right)^{\gamma_m} m(\mu'_m), \quad (5.4)$$

$$\langle \mathcal{O}_d \rangle(\mu_f) = \left(\frac{\alpha_s(\mu_f)}{\alpha_s(\mu'_f)} \right)^{\gamma_{\mathcal{O}_d}} C_d(\mu_f, \mu'_f) \langle \mathcal{O}_d \rangle(\mu'_f). \quad (5.5)$$

At leading order the strong coupling satisfies the scaling behavior as described in Eq.

(A.38). It is also related to the beta-function by the renormalization-group equation, see Eq. (A.19). The anomalous dimension of the running quark mass (see Eq. (A.36)) is known up to the four-loop order [96], where the first coefficient is $\gamma_m^{(0)} = 4$ as discussed in Sect. A.3. From Eq. (5.1) follows $\gamma_{\bar{q}q} = -4$ for the quark condensate. The anomalous dimension of the gluon condensate and the parameter m_0^2 are $\gamma_{GG}^{(0)} = 0$ and $\gamma_{m_0}^{(0)} = 4$, respectively. In case of the quark-gluon and four-quark condensate we neglect any scale dependence and take their densities $m_0^2 \langle \bar{q}q \rangle$ and $\alpha_s r_{\text{vac}} \langle \bar{q}q \rangle^2$ at a low scale ($\mu = 1$ GeV). The strong coupling is perturbatively expanded up to $\mathcal{O}(\alpha_s^3)$, starting at the Z -boson mass [36]. We employ the Mathematica package RunDec [68] to perform the running of the strong coupling and the quark masses with four-loop accuracy. For simplification we adopt a uniform scale dependence, $\mu = \mu_m = \mu_f$ for all scale-dependent expressions. Moderate adjustments of individual scales do not affect the numerical results significantly.

In order to evaluate the decay constants f_{H^*} and f_H in Eqs. (3.45) and (3.46), we still require a more elaborate discussion regarding the method-based parameters. These parameters are, to wit the renormalization scale μ , the Borel parameter M^2 and the effective thresholds $s_0^{H^*}$. The latter is an intrinsic method-inherent quantity, the other two appear either due to truncation of the perturbative series or after the Borel transformation. To provide reliable predictions it is reasonable to choose specific restrictions, for which the sum rules show apparent stability under variations of input parameters. First, we should select the renormalization scale μ in the vicinity of typical momentum transfers of a given process to prevent large logarithmic terms. From other studies [97] it is reasonable to choose the following scaling relation as a directive:

$$\mu \sim \sqrt{m_{H^*}^2 - m_Q^2} \sim \sqrt{2m_Q \Lambda_{QCD}}. \quad (5.6)$$

As a result, we find that μ is close to the scales m_Q and M , which defines the typical virtualities of the correlation function. Hence, the default scale is fixed at $\mu = 3$ GeV ($\mu = 1.5$ GeV) in case of b (c)-quark systems: This scale configuration also retains a reasonable hierarchy of LO, NLO and NNLO contributions in the PT part of the OPE. The scale dependence of our sum rules is estimated by varying μ within distinct intervals as shown in Tab. 5.2 and 5.3.

Another free parameter is the duality-threshold $s_0^{H^*}$. It can be fixed to the experimental ground-state meson mass through the ratios of Eqs. (3.45) and (3.46). The vector and pseudoscalar sum rules have the form

$$\Pi_t(M^2, s_0^{H^*}) = m_{H^*}^2 f_{H^*}^2 e^{-\frac{m_{H^*}^2}{M^2}}, \quad (5.7)$$

$$\Pi_5(M^2, s_0^H) = \frac{m_H^4}{m_Q^2} f_H^2 e^{-\frac{m_H^2}{M^2}}, \quad (5.8)$$

where $\Pi_{t(5)}(M^2, s_0^{H(*)})$ denotes the Borel-transformed OPE of the correlation functions. Derivatives with respect to the inverse Borel parameter yield

$$-\frac{d}{d(1/M^2)} \Pi_t(M^2, s_0^{H*}) = m_{H*}^4 f_{H*}^2 e^{-\frac{m_{H*}^2}{M^2}}, \quad (5.9)$$

$$-\frac{d}{d(1/M^2)} \Pi_5(M^2, s_0^H) = \frac{m_H^6}{m_Q^2} f_H^2 e^{-\frac{m_H^2}{M^2}}. \quad (5.10)$$

Finally, we find the meson-mass relation from our sum rules:

$$m_{H(*)}^{\text{SR}} = \sqrt{\frac{-\frac{d}{d(1/M^2)} \Pi_{t(5)}(M^2, s_0^{H(*)})}{\Pi_{t(5)}(M^2, s_0^{H(*)})}}. \quad (5.11)$$

At first, we set up M^2 and then use the experimental meson mass as reference value to fix $s_0^{H(*)}$. We obtained a reproduction accuracy of less than 0.5% on the fitted meson mass $m_{H(*)}^{\text{SR}}$.

Finally, we have to choose a proper Borel parameter. The actual size of our selected ‘‘Borel window’’ ($M_{\min}^2 < M_{\text{default}}^2 < M_{\max}^2$) depends on quantum numbers of the considered particle and its flavor. If the Borel parameter M^2 is too small, higher dimensional operators prevail and the OPE is heavily biased to the condensate sector. On the other side, if M^2 is set too large, contributions of continuum states are not sufficiently suppressed compared to the ground state. Thus, a balanced range should be chosen to guarantee reliable sum rule predictions. As a general rule, this requirement can also be achieved if the continuum states stay below 50% of the total correlation function, i.e.

$$\Omega_{t(5)}^{(\text{cont})} = 1 - \frac{\Pi_{t(5)}^{(\text{pert})}(M^2, s_0)}{\Pi_{t(5)}^{(\text{pert})}(M^2, \infty)} < 0.5. \quad (5.12)$$

According to this statement, we constrain the Borel parameter at $M_{\max} = 6.5$ GeV and 2.5 GeV in case of b and c -quark system, respectively. A reasonable adjustment of the default value is located around $M_{\text{default}} \sim \sqrt{2m_Q\tau}$ based on the heavy-quark limit, where $\tau \sim 1$ GeV $\gg \Lambda_{\text{QCD}}$. The lower bound is aligned at $M_{\min} = 4.5$ GeV and

1.5 GeV, so that the contribution of $d = 4, 5, 6$ condensates in total do not exceed $\pm 5\%$ of the perturbative part.

From the dispersion relation of the invariant amplitude $\Pi_{t(5)}$ we can also determine a systematic upper bound. This bound follows from the positivity of the hadronic spectral density at which the quark-hadron duality approximation diminishes. In principle, the integrated hadronic spectrum vanishes, i.e. the ground-state resonance is saturated by the OPE of the correlation function. Earlier uses of upper bounds are elaborated in Refs. [98] and [99]. Formally, we obtain the upper bounds for f_{H^*} by taking the limit $s_0^{H^*} \rightarrow \infty$:

$$f_{H^*} < \sqrt{\frac{e^{m_{H^*}^2/M^2}}{m_{H^*}^2} \Pi_t^{(\text{pert+cond})}(M^2, \infty)}. \quad (5.13)$$

In the pseudoscalar channel the limit of $s_0^H \rightarrow \infty$ provides the upper bounds for f_H .

In order to estimate the uncertainties of our decay constant estimations, we vary each physical parameter separately and add them in quadrature. Correlations between these parameters are not taken into account. As a result, the total uncertainty is considered to be more conservative. However, the meson-mass-fixed threshold parameter shows some correlation to the Borel parameter. We adjust $s_0^{H^{(*)}}$ after varying M^2 , but we refrain from a separate uncertainty estimation related to the choice of $s_0^{H^{(*)}}$. In addition, we add the total $d = 4, 5, 6$ condensate contribution symmetrically as an estimate to missing operator contributions of dimension $d \leq 7$. Uncertainties regarding the strong coupling (because of inaccuracies of the boson mass M_Z and higher order μ -dependence) have been evaluated but show no numerical significance.

Results of the B^* Meson Decay Constants

In the first part of the numerical analysis, we discuss the Borel parameter M^2 , the scale μ and the effective threshold $s_0^{H^{(*)}}$ in greater detail. We emphasize their influence on the values of $f_{H^{(*)}}$. Other aspects of this analysis are the behavior of the PT part in the OPE and the hierarchy structure of the LO, NLO and NNLO contribution. Note that the calculations lead to unreliable numerical results in the pole mass scheme due to slow convergence of the expansion, which is discussed in [53]. This encourages an analysis based on quark masses in the $\overline{\text{MS}}$ scheme.

Parameters	Values (comments)	Reference
Quark masses	$\bar{m}_b(\bar{m}_b) = 4.18 \pm 0.03 \text{ GeV}$	[36]
	$\bar{m}_c(\bar{m}_c) = 1.275 \pm 0.025 \text{ GeV}$	
	$\bar{m}_s(2 \text{ GeV}) = 95 \pm 10 \text{ MeV}$ (error doubled)	
Strong coupling	$\alpha_s(M_Z) = 0.1184 \pm 0.0007$	[36]
	$\alpha_s(3 \text{ GeV}) = 0.255 \pm 0.003$	
	$\alpha_s(1.5 \text{ GeV}) = 0.353 \pm 0.006$	
Quark condensate	$\langle \bar{q}q \rangle(2 \text{ GeV}) = -(277_{-10}^{+12} \text{ MeV})^3$ (ChPT $\oplus m_s$)	[36], [95]
Condensates $d = 4, 5, 6$	$\langle \bar{s}s \rangle / \langle \bar{q}q \rangle = 0.8 \pm 0.3$	[78]
	$\langle GG \rangle = 0.012_{-0.012}^{+0.006} \text{ GeV}^4$	
	$m_0^2 = 0.8 \pm 0.2 \text{ GeV}^2$	
	$\langle \bar{s}Gs \rangle / \langle \bar{q}Gq \rangle = \langle \bar{s}s \rangle / \langle \bar{q}q \rangle$	
	$r_{\text{vac}} = 0.1 - 1.0$	
Meson mass [GeV]	$m_{B^*} = 5.325 \quad m_{B_s^*} = 5.415$	[36]
	$m_B = 5.280 \quad m_{B_s} = 5.367$	
	$m_{D^*} = 2.010 \quad m_{D_s^*} = 2.112$	
	$m_D = 1.870 \quad m_{D_s} = 1.968$	

Table 5.1: Input parameters as used in the numerical analysis.

We present an explicit estimation of f_{B^*} with the choice of all required input parameters as described in the previous section. Note that it is unnecessary to restate detailed discussions about each decay constant because of similar characteristics for all bottom mesons. The numerical evaluation is performed with up-to-date accuracy for all used coefficient functions. The renormalization scale is set to

$$\mu \in [3, 5] \text{ GeV}, \quad (5.14)$$

whereas the ‘‘Borel window’’ extends

$$M^2 \in [4.5, 6.5] \text{ GeV}^2. \quad (5.15)$$

The continuum threshold parameter $s_0^{B^*}$ is fixed to the experimental meson mass, see Eq. (5.11), with a deviation of less than one per mille. Hence, we find the effective threshold $s_0^{B^*} = 34.1 \text{ GeV}^2$. Adding all individual uncertainties, which are collected in

Tab. 5.2, we obtain the following B^* meson decay constant

$$f_{B^*} = (210_{-12}^{+10}) \text{ MeV} . \quad (5.16)$$

Figs. 5.2 and 5.3 show plots of the decay constant regarding the individual OPE contributions and each piece of the PT part, respectively. In total, the sum rule presents a rather insensitive renormalization scale dependence and a good stability in the variation of M^2 within the selected parameter window. These facts additionally confirm our choice of method-based parameters, which we use for extracting f_{B^*} . Moreover, every condition that we impose in the previous section is fulfilled.

The most significant details about this analysis are:

- The suppression of the continuum states satisfies $\Omega_{t(5)}^{(\text{cont})} = 40\%$ and so our determination of f_{B^*} is based predominantly on the low threshold region.
- We find a reasonable convergence of the OPE due to the fact that the condensate terms contribute by about 25 % to the total correlation function, and radiative corrections converge with increasing order in α_s (see Fig. 5.2). The perturbative coefficient function amounts to 14% (NLO) and -4% (NNLO) in comparison to the LO term.
- If we choose the b quark mass in the pole mass scheme, we fail to present a series, which decays sufficiently fast. Numerically the hierarchy is 71% for (NLO/LO) and 78% for (NNLO/LO) with no sign of convergence.
- The recently evaluated NLO correction to the quark condensate [A1, 69] generates a shift of more than -30% compared to the LO condensate contribution. This is the reason why our predicted decay constant has a smaller value than former determinations.
- The total error budget is dominated by the variation of a few parameters, see Tab. 5.2. An essential source of uncertainty is the b quark mass error. It moves the central value of f_{B^*} by $\pm 5\%$. The variation of $\langle \bar{q}q \rangle$ within the selected error limits has a mild impact of a few percent. This is comparable to variations of the combined $d = 4, 5, 6$ condensate contribution.
- We choose $\mu = 3 \text{ GeV}$ as the default scale value. Note that the given sum rule fails, if the traditional scale region around $\mu = 4 \text{ GeV}$ is used. This behavior of instability is imposed by the quark-gluon condensate $\langle \bar{q}Gq \rangle$, which shifts the

OPE into a negative direction. We see a significant sensitivity regarding the choice of μ due to the factor m_Q^3 in $\Pi_t^{(\bar{q}Gq)}$, see Eq. (B.51). Radiative corrections to the quark-gluon condensate would cancel the leading logarithmic enhancement. However, without these corrections the interplay of fixing $s_0^{B^*}$ and satisfying the selected constraints of the Borel parameter cannot be fulfilled.

We also give an upper bound of the decay constant by integrating the sum rule over the full range of the threshold ($s_0^{B^*} \rightarrow \infty$). In order to determine the bound, we choose some specific requirements, which are also discussed in Ref. [99]: Upper bounds become the more restrictive for small Borel parameters and large renormalization scales as shown in Fig. 5.1. Our aim is to predict the most restrictive bound within the selected parameter constraints. At $M^2 = 4.5 \text{ GeV}^2$ the condensate contributions are more suppressed than for the default parameter value. Therefore, the OPE converges sufficiently fast. The renormalization scale is set to the default value $\mu = 3 \text{ GeV}$, where we encounter good convergence of the perturbative series. NLO and NNLO terms contribute by 17% and -2% compared to the leading order term. The total theoretical error reads $\Delta f_{B^*} = {}^{+12}_{-24}$, which is determined by parameter variation as before. We finally add the upper uncertainty value to the bound estimation of Eq. (5.17). Hence, the final upper bound is given by

$$f_{B^*} < 261 \text{ MeV}. \quad (5.17)$$

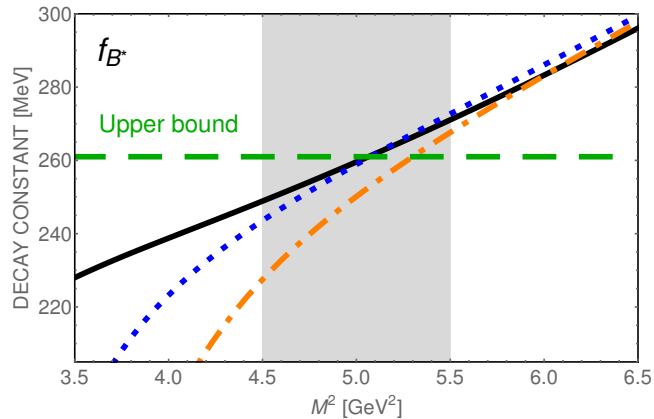


Figure 5.1: Upper bound scaling with respect to the Borel parameter M^2 at $\mu = 3, 4, 5 \text{ GeV}$ (black solid, blue dashed, orange dash-dotted line). The green dashed line indicates the final upper bound including the total theoretical error. The gray box shows the selected Borel window.

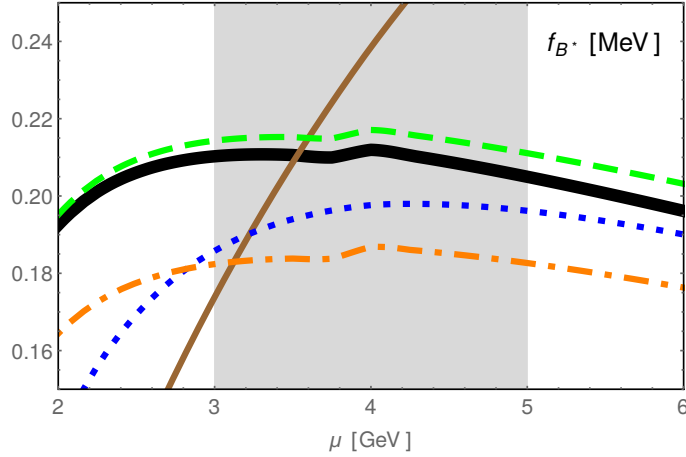


Figure 5.2: Scale dependence of the B^* meson decay constant: The black solid-thick line includes all contributions, the brown solid line includes the PT part at LO, the blue dashed line includes the PT part up to NLO contribution, the orange dash-dotted line includes the PT part up to NNLO contribution and the green dashed line includes the PT part up to NNLO and quark condensate contribution. The gray box shows the selected Borel window.

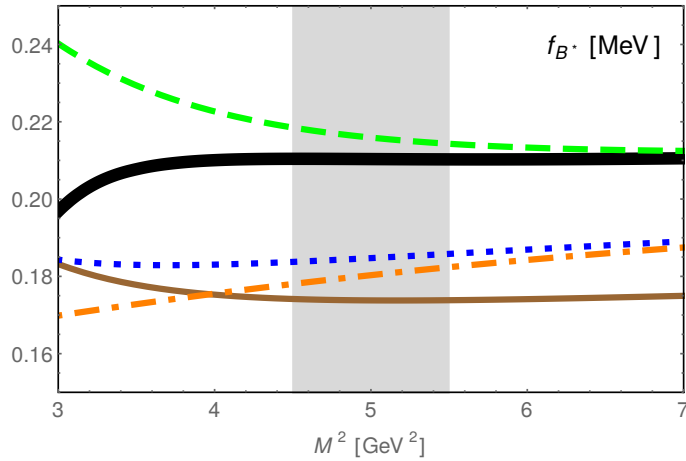


Figure 5.3: B^* meson decay constant against the Borel parameter M^2 : The black solid-thick line includes all contributions, the brown solid line includes the PT part at LO, the blue dashed line includes the PT part up to NLO contribution, the orange dash-dotted line includes the PT part up to NNLO contribution and the green dashed line includes the PT part up to NNLO and quark condensate contribution. The gray box shows the selected Borel window.

5.2 Numerical Results of Borel Sum Rules

In the following, we present the results of heavy-light meson decay constants with bottom and charmed flavor content. The individual uncertainties, except small ones with a magnitude of ≤ 0.1 MeV, are listed in Tab. 5.2 and 5.3. For the total error we add the individual uncertainties in quadrature. Our final results read

$$f_{B^*} = (210_{-12}^{+10}) [261] \text{ MeV}, \quad f_B = (207_{-09}^{+17}) [258] \text{ MeV}, \quad (5.18)$$

$$f_{B_s^*} = (251_{-16}^{+14}) [296] \text{ MeV}, \quad f_{B_s} = (242_{-12}^{+17}) [285] \text{ MeV}, \quad (5.19)$$

$$f_{D^*} = (242_{-12}^{+20}) [297] \text{ MeV}, \quad f_D = (201_{-13}^{+12}) [237] \text{ MeV}, \quad (5.20)$$

$$f_{D_s^*} = (293_{-14}^{+19}) [347] \text{ MeV}, \quad f_{D_s} = (238_{-23}^{+13}) [266] \text{ MeV}, \quad (5.21)$$

where the upper bounds are given in brackets. We also evaluate the ratios of vector to pseudoscalar meson decay constants to determine the heavy-spin-symmetry violation. These ratios are determined by dividing both sum rules and performing the analogous uncertainty analysis as stated above:

$$f_{B^*}/f_B = 1.02_{-0.09}^{+0.02}, \quad f_{B_s^*}/f_{B_s} = 1.04_{-0.08}^{+0.01}, \quad (5.22)$$

$$f_{D^*}/f_D = 1.20_{-0.07}^{+0.13}, \quad f_{D_s^*}/f_{D_s} = 1.24_{-0.05}^{+0.13}. \quad (5.23)$$

Due to arising correlations of both sum rules, the ratios result in somewhat smaller total uncertainties. Finally, we also obtain the ratios of strange to non-strange meson decay constants

$$f_{B_s}/f_B = 1.17_{-0.04}^{+0.03}, \quad f_{B_s^*}/f_{B^*} = 1.20 \pm 0.04, \quad (5.24)$$

$$f_{D_s}/f_D = 1.18_{-0.05}^{+0.04}, \quad f_{D_s^*}/f_{D^*} = 1.21 \pm 0.05, \quad (5.25)$$

to give a measure of the $SU(3)_{\text{fl}}$ -breaking effects.

Note that all presented results do not include any uncertainty bounds on the quark-hadron duality approximation. In the next section we will give a qualitative statement by using a modified version of sum rules and by testing the consistency of the method.

		Default M^2 [GeV 2]				Default μ [GeV]					
		Range ($M_{min}^2 \div M_{max}^2$)				Range ($\mu_{min} \div \mu_{max}$)					
		5.5				3.0					
		(4.5 \div 6.5)				(3.0 \div 5.0)					
Meson	$\bar{f}_{H^{(*)}}$ [MeV]	s_0 [GeV 2]	ΔM^2	$\Delta\mu$	Δm_Q	Δm_s	$\Delta\langle\bar{q}q\rangle$	$\Delta\langle\frac{\bar{s}s}{\bar{q}q}\rangle$	$\Delta\langle GG\rangle$	Δm_0^2	Δd_{456}
B^*	210.3	34.1	-1.8 +0.1	-5.3 +0.0	-8.7 +9.0	—	∓ 3.2	—	-0.2 +0.4	∓ 0.9	± 4.0
B_s^*	251.4	36.3	-5.4 +3.8	-8.6 +0.0	-9.7 +9.9	± 1.5	-2.4 +2.3	+7.1 -7.3	-0.2 +0.4	∓ 0.7	± 3.2
B	206.7	33.9	-4.5 +6.1	+13.0 -0.0	-7.5 +7.6	—	-2.9 +2.8	—	+0.1 -0.3	∓ 0.3	± 0.9
B_s	241.7	35.6	-5.8 +8.1	+10.3 -0.0	∓ 8.2	± 1.6	-2.2 +2.1	+6.5 -6.7	∓ 0.2	∓ 0.2	± 0.6

Table 5.2: Detailed results of the numerical analysis for bottom meson decay constants. Individual uncertainty intervals ΔM^2 , $\Delta\mu$ etc. were obtained by parameter variation. All numbers are given in units of MeV.

		Default M^2 [GeV 2]				Default μ [GeV]					
		Range ($M_{min}^2 \div M_{max}^2$)				Range ($\mu_{min} \div \mu_{max}$)					
		2.0				1.5					
		(1.5 \div 2.5)				(1.3 \div 3.0)					
Meson	$\bar{f}_{H^{(*)}}$ [MeV]	s_0 [GeV 2]	ΔM^2	$\Delta\mu$	Δm_Q	Δm_s	$\Delta\langle\bar{q}q\rangle$	$\Delta\langle\frac{\bar{s}s}{\bar{q}q}\rangle$	$\Delta\langle GG\rangle$	Δm_0^2	Δd_{456}
D^*	241.9	6.2	-5.0 +3.6	+17.3 -3.9	∓ 7.5	—	∓ 4.0	—	-0.9 +1.9	∓ 0.7	± 4.6
D_s^*	293.3	7.4	-9.5 +10.1	+12.3 -2.3	∓ 8.0	± 2.2	-2.9 +2.8	+8.6 -8.9	-0.9 +1.7	∓ 0.5	± 3.8
D	201.0	5.6	-12.1 +10.7	-3.5 +1.3	-1.9 +1.6	—	∓ 3.0	—	+0.4 -0.8	± 0.5	± 2.8
D_s	237.4	6.3	-19.3 +8.6	-9.3 +3.5	-2.1 +1.7	± 3.1	∓ 2.2	+6.6 -6.9	+0.4 -0.8	± 0.4	± 2.5

Table 5.3: Detailed results of the numerical analysis for charmed meson decay constants. Individual uncertainty intervals ΔM^2 , $\Delta\mu$ etc. were obtained by parameter variation. All numbers are given in units of MeV.

5.3 Alternative Versions of Sum Rules

Besides the uncertainty estimates from individual shifts of the input parameters, one should keep in mind that the quark-hadron duality approximation has not been addressed yet, which also represents a source of uncertainty. The connection to the experiment is set since we fixed our sum rules to the experimental meson mass with a high precision. One can also argue that the “semi-local” duality that we use here is reasonable due to the positivity of the spectral function and its asymptotics for large threshold values. A model-independent study of this approximation is not at hand, and so we have to find a handle to assess the “systematic” uncertainty of the adopted procedure. One way to check the given calculational framework is to employ an alternative version of QCD sum rules, which is based on the same correlation function. The alternative versions include additional weight functions $\omega(s)$ in the spectral integral:

$$\Pi^\omega(M^2) = \int ds \omega(s) \rho(s) e^{-s/M^2}. \quad (5.26)$$

Further, we use power moments to control the suppression of OPE expressions and remove subtraction terms associated to the dispersion integrals. All results of modified QCD sum rules are listed in Tab. 5.4.

Weighted Borel Sum Rules

At first, we vary the original invariant amplitudes from Sect. 3.1 and take the combination

$$\Pi_{t(5)}^{1/s}(q^2) \equiv \frac{\Pi_{t(5)}(q^2) - \Pi_{t(5)}(0)}{q^2}, \quad (5.27)$$

which is finite at the zero-recoil point ($q^2 = 0$). Following the procedure of the preceding Borel sum rules, the modified correlation functions read

$$\Pi_{t(5)}^{1/s,(\text{had})}(q^2) = f_{H^*}^2 e^{-m_{H^*}^2/M^2} + \int_{(m_H+m_P)^2}^{\infty} ds \frac{\rho_t^h(s)}{s} e^{-s/M^2}. \quad (5.28)$$

The spectral integration includes an additional suppression factor of $1/s$. It enhances the low threshold region and therefore the ground-state meson resonance. We divide the modified sum rules with the original one to obtain the meson-mass formula. In general, the new threshold $s_0^{H^*}$, which is fitted to the measured meson mass, is larger than before.

We obtain another modification of our sum rules by differentiating the invariant amplitude (see Eq. (3.3) and (3.4)) with respect to $(-1/M^2)$:

$$\Pi_{t(5)}^{s,(\text{had})}(q^2) = m_{H^*}^4 f_{H^*}^2 e^{-m_{H^*}^2/M^2} + \int_{(m_H+m_P)^2}^{\infty} ds s \rho_t^h(s) e^{-s/M^2}. \quad (5.29)$$

It follows an extra power of s in the spectral integral that shifts the sensitivity to the continuum region. Once again, the duality-threshold is estimated by dividing the modified sum rules with the original one, which tends to lower values compared to the default threshold.

Excluding the First Radial Excitation

Radial excitations of heavy-light mesons could also be included as a second resonance in the sum rule formalism. In the previous analysis we implicitly incorporated their contributions by averaging over them as a part of the hadronic continuum, see Eqs. (3.12) and (3.13). Formally, we separate the first radially excited state $H^{*'}$ from the rest of the continuum spectrum as follows:

$$\rho_t^h(s)\theta(s - (m_H + m_P)^2) = m_{H^{*'}}^2 f_{H^{*'}}^2 \delta(s - m_{H^{*'}}^2) + \rho_t^{(\text{pert})}(s)\theta(s - s_0^{H^{*'}}). \quad (5.30)$$

The shape of the excited state has been reduced to a delta distribution. However, one can also assume a Breit-Wigner ansatz to reconstruct the decay width distribution. The corresponding spectral density in the pseudoscalar channel is given by

$$\rho_5^h(s)\theta(s - (m_{H^*} + m_P)^2) = m_{H'}^4 f_{H'}^2 \delta(s - m_{H'}^2) + \rho_5^{(\text{pert})}(s)\theta(s - s_0^{H'}). \quad (5.31)$$

At the moment, only limited experimental data on radially excited charmed mesons are available [36, 100]. Therefore, we rely on estimations of the mass of the excited states in order to localize the duality-threshold. The mass difference between charmed meson ground states and their excited resonances are about the same as for light unflavored mesons, cf. the mass difference between the first radial excitation $\rho' = \rho(1450)$ and the ground-state ρ meson. We generalize these relations for all heavy-light mesons:

$$m_{B'} - m_B \simeq m_{D'} - m_D \simeq m_{D'_s} - m_{D_s}, \quad (5.32)$$

$$m_{B^{*'}} - m_{B^*} \simeq m_{D^{*'}} - m_{D^*} \simeq m_{D_s^{*'}} - m_{D_s^*}. \quad (5.33)$$

But instead of introducing the decay constants for excited states, we remove these states from the spectral density. To this end, a linear suppression factor $(m_{H^{(*)'}} - s)$ is

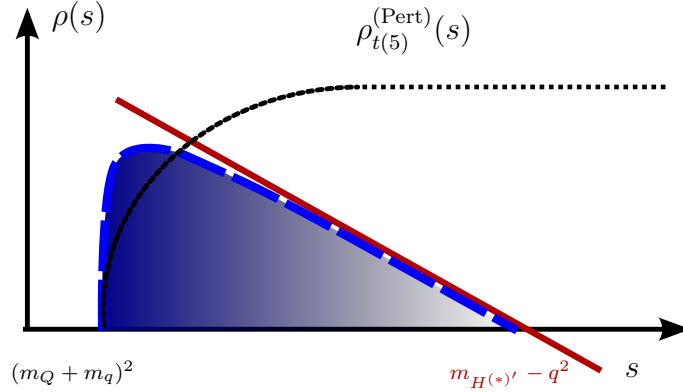


Figure 5.4: *Duality-improved spectral function (with suppressed first radial excitation) normalized to s .*

used. From this follows a strong diminishment in the vicinity of the excited state and a full cancellation of the continuum spectrum, see Fig. 5.4. We multiply the invariant amplitude $\Pi_{t(5)}$ by $(m_{H^{(*)}'} - q^2)$ to build up the corresponding sum rule. The final Borel-transformed sum rules read

$$f_{H^*}^2 = \frac{e^{m_{H^*}^2/M^2}}{m_{H^*}^2(m_{H^{*'} }^2 - m_{H^*}^2)} \left[\int_{(m_Q+m_q)^2}^{s_0^{H^{*'}}} ds (m_{H^{*'}} - s) \rho_t^{(\text{pert})}(s) + \left(m_{H^{*'}}^2 - \frac{d}{d(-1/M^2)} \right) \Pi_t^{(\text{cond})}(M^2) \right], \quad (5.34)$$

$$f_H^2 = \frac{m_Q^2 e^{m_H^2/M^2}}{m_H^4(m_{H'}^2 - m_H^2)} \left[\int_{(m_Q+m_q)^2}^{s_0^{H'}} ds (m_{H'} - s) \rho_5^{(\text{pert})}(s) + \left(m_{H'}^2 - \frac{d}{d(-1/M^2)} \right) \Pi_5^{(\text{cond})}(M^2) \right]. \quad (5.35)$$

For the estimations of missing meson masses we consider the measured values $m_{D'} = 2.55$ GeV and $m_{D^{*'}} = 2.60$ GeV [100]. All other masses can be deduced from the heavy-quark mass limit relation as given in Eqs. (5.32) and (5.33). Due to this large suppression at $s = m_{H^{(*)}'}^2$, we are not committed to accurate experimental mass input. The modified sum rule show less sensitivity to the quark-hadron duality ansatz than before and, hence, it is reasonable to adjust the effective threshold parameter at $s_0^{H^{(*)}'} = m_{H^{(*)}'}^2$. Small variations of $s_0^{H^{(*)}'}$ lead to minor changes in $f_{H^{(*)}}$ and, more importantly, it reconstructs the meson mass to a high precision.

A more detailed discussion of radially excited states and the possibility to estimate their decay constants will be given in the next chapter.

Power Moments

In the previous section we discussed modification of Borel sum rules. Now we step aside from Borel transformations and apply the power moments (*Hilbert moments*) instead, which are well-proven in *finite-energy sum rules* (FESR). The dispersion relations to the invariant amplitudes are differentiated with respect to q^2 at timelike momenta $q_0^2 \leq 0$ within this method. At least two differentiations are necessary to remove two subtraction terms, which are required to validate the dispersion integral formalism in Eq. (3.38). In this manner, the decay constants are determined as follows

$$f_{H^*}^2 = \frac{(m_{H^*}^2 - q_0^2)^{n+1}}{m_{H^*}^2} \Pi_t^{(n)}(s_0^{H^*}, q_0^2), \quad (5.36)$$

$$f_H^2 = \frac{(m_H^2 - q_0^2)^{n+1}}{m_H^4} \Pi_5^{(n)}(s_0^H, q_0^2). \quad (5.37)$$

In the above equations the n -th moment of the invariant amplitudes is

$$\Pi_{t(5)}^{(n)}(s_0^{H^{(*)}}, q_0^2) \equiv \int_{(m_Q+m_q)^2}^{s_0^{H^{(*)}}} ds \frac{\rho_t^{(\text{pert})}(s)}{(s - q_0^2)^{n+1}} + \left(\frac{d}{dq^2}\right)^n \Pi_{t(5)}^{(\text{cond})}(q^2) \Big|_{q^2=q_0^2}.$$

One can see that the weight function is a power suppression in the dispersion integral. Our analysis includes a minimal number of derivatives ($n = 2, 3$), which guarantee a sufficient suppression of condensate contributions. The duality-threshold is fixed to the ground-state meson mass. We find the meson mass by taking the ratio of the 2nd and 3rd power of the invariant amplitude. In case of bottom mesons it is sufficient to refrain from any additional shifts ($q_0^2 = 0$) for reasonable convergence in the perturbative series and small condensate terms of dimension $d \geq 4$. The sum rules for charmed mesons require negative q_0^2 to provide an adequate OPE hierarchy.

Numerical Results and Comments on Alternative Sum Rules

In Tab. 5.4 we present the results from modified sum rules. Note that we do not give any uncertainties since this is a basic study. Our aim was to determine a “systematic” error to the standard Borel sum rules by testing the consistency for other weights in the spectral integral and by employing power moments. Using the weights $\omega(s) = 1/s$

or s , we find either an enhanced or reduced contribution of the hadronic continuum within the defined acceptance criteria as discussed in Sect.5.1. We also removed the first radial excitation by a linear suppression function $\omega(q^2) = m_{H^{(*)}}^2 - q^2$. As a result, the complete spectral density fades out except the region close to the ground-state meson. Furthermore, we strongly loose sensitivity to the quark-hadron duality approach. The meson mass reproduction for all mesons is of a high quality (less than 1% deviation from experimental input). Due to the selected input parameters for all decay constants, we determine almost identical values compared to the default sum rules estimations. In most cases the power moments method leads to slightly smaller values (~ 10 MeV). The estimations in the pseudoscalar meson channel are reliable, i.e. alternative methods shift the central values of f_H by ± 20 MeV, which is compatible within the typical sum rules uncertainty bounds. For vector mesons we approach the limits of reasonable sum rule predictions with the given setup. In this case the default Borel parameter should be readjusted to larger values.

Method	Decay constant [MeV]							
	f_{B^*}	$f_{B_s^*}$	f_B	f_{B_s}	f_{D^*}	$f_{D_s^*}$	f_D	f_{D_s}
Standard Borel SR	210	251	207	242	242	293	201	238
Borel SR with $\omega(s) = 1/s$	211	248	220	260
Borel SR with $\omega(s) = s$	208	245	201	233	232	271	175	207
Borel SR excl. 1st radial excit.	208	249	208	242	243	290	204	239
SR with power moments	196	236	198	231	228	281	203	238

Table 5.4: Alternative versions of Borel sum rule and power moments with momentum shift $q_0^2 = 0$ ($q_0^2 = -4$) GeV^2 for bottom (charmed) mesons. Three dots mark a missing prediction.

5.4 Discussion of Results

We estimated the decay constants of heavy-light vector and pseudoscalar mesons including bottom and charmed flavor with the method of QCD sum rules. In the vector meson channel the QCD NLO corrections to the quark condensate were included for the first time, which drive the theoretical uncertainties to smaller values as compared to former estimates, see LO study in [88]. Moreover, the PT contribution with NNLO accuracy were taken into account [90]. NLO PT corrections were confirmed and technical strategies as well as relevant tools for their computations were discussed in Chap. 4. Other condensate contributions, which arise from $d \leq 6$ local operators are included at LO level. We also determined the upper bound values and various ratios. The latter reflect mutual QCD differences and give a measure for symmetry-violating effects. In the following, we summarize important facts of our sum rule analysis:

- The considered heavy-light B and D meson decay constants have three key values. f_B and f_{B^*} are about 210 MeV, whereas their strange meson partners are centered around 240 and 250 MeV, see Fig. 5.5. The typical relative uncertainties are estimated at 6 – 8%. In the charmed sector the smallest decay constant is f_D at 200 MeV, f_{D_s} and f_{D^*} are about 240 MeV. And finally, $f_{D_s^*}$ ranges around 290 MeV. The relative uncertainties are about 6 – 10%. Ratios of vector to pseudoscalar meson decay constants give a measure of the HQ spin-violating effects. With included uncertainties the B meson ratios deviate by less than 10% from the infinite heavy-quark mass limit. D meson ratios break the HQ spin symmetry by less than 40%. The $SU(3)_F$ -breaking contributions from strange to non-strange meson decay constants is about 20%.
- Theoretical errors are mainly driven by uncertainties of two sources:
 1. External parameters such as the quark mass and quark condensate have an impact on each decay constant of 8 – 10 MeV and 3 – 10 MeV, respectively, where in the latter the conversion from massless to massive light-quark condensate ($\langle q\bar{q} \rangle \rightarrow \langle s\bar{s} \rangle$) inflates the total error.
 2. We chose rather large intervals, in which the renormalization scale μ and the Borel parameter M^2 vary. As a result of this conservative treatment, the central values from alternative versions of QCD sum rules mostly lie within the uncertainty intervals.

However, there is space for improvement: NLO corrections to the quark-gluon condensate are desirable since the LO contribution leads to instabilities in the

meson-mass reproduction, especially in the vector current channel. Improved precision of external parameters would also decrease the total error budget. Besides, it is desirable to have the full analytic expression of NNLO PT corrections, which would provide a better stability regarding the renormalization scale dependence.

- Modified Borel sum rules including various weight functions in the spectral integrals are in good agreement with the standard form. We also evaluated the decay constants using power moments. The resulting predictions are consistent to the others, which indicates a good reliability of the given sum rules. Note that excluding the first radial excitation from the hadronic continuum pins down the effective duality-threshold to the mass of the first radially excited state. We also find that the sum rules are less sensitive with respect to the threshold.
- By proper reparametrization we could expand the Borel sum rules of single decay constants and the vector to pseudoscalar ratio in terms of the inverse heavy-quark mass. Radiative PT corrections pulled down the ratios below unity, whereas inverse mass corrections led to ratios above unity. We determined the leading mass corrections Δ/m_b for the B^* to B meson decay constant ratio and evaluated the interval $\Delta \in [-110, 420]$ MeV using the b -quark pole mass. The same shift Δ in the charmed meson channel leads to $f_{D^*}/f_D = 0.86 - 1.21$. Our predicted central value hits the border of this range, which signals a deterioration of heavy quark expansion based on the charm quark mass. Sum rule estimations in the framework of HQET including the leading mass corrections yield to larger ratios and a better agreement: $f_{B^*}/f_B = 1.07 \pm 0.02$ and $f_{D^*}/f_D = 1.35 \pm 0.05$ [79]. Numerically, the heavy-quark spin symmetry from f_{H^*}/f_H is violated by about 4-14% (12-43%) for bottom (charmed) mesons. In addition, we can also give a measure for heavy-quark flavor violating effects by taking the ratio f_B/f_D . Compared to the ratio $f_B/f_D \simeq 0.69$, which is determined by Neubert [79], our value ranges to larger values, i.e. $f_B/f_D \simeq 0.93 \div 1.19$. We assumed no error correlation between the individual parameter uncertainties. The discrepancy could arise due to missing heavy quark corrections in the prediction of Ref. [79].
- A rich resource of determinations of decay constants has been established by mainly two research communities that either uses the method of sum rules or lattice gauge theory. In Fig. 5.5 a selection of recent (state-of-the-art) or well-known, reliable predictions are shown. Decay constants of pseudoscalar mesons are well studied due to the phenomenological access. However, since the computation of the missing NLO correction of the quark condensate in [A1], several subsequent studies have been published with dedication to decay constants of

the vector meson channel [101, 102, 103], see Fig 5.6. Estimations from lattice QCD for vector heavy-light mesons also became topical in the last years. At first, we compare our values with other QCD sum rules determinations: In general f_B and f_D are center around 200 MeV, whereas f_{B_s} is slightly larger at 240 MeV with typical errors of about ± 20 MeV [53, 104]. Due to higher precision of external parameters and in particular smaller uncertainties of the $\overline{\text{MS}}$ quark masses, we could reduce the error interval by up to 40%. Determinations of $f_{B_{(s)}}$ and $f_{D_{(s)}}$ from FESR [105, 106] are usually smaller than our prediction. A comparison to recent lattice results reveals a good agreement within the uncertainty bounds, see Fig. 5.5, 5.6 and 5.7. However, our bottom (charmed) meson decay constants are somewhat smaller (larger) in their the central value. Vector to pseudoscalar decay constant ratios of bottom and charmed mesons, respectively, are close to unity and 1.20. $SU(3)_F$ -violating effects are reflected by about 20% shifts from unity. Our predicted ratio are in good agreement with estimations within lattice QCD, where $f_{B_q^*}/f_B$ in [107] has a strong tendency to values below 1. Ratios from sum rules within HQET tend to ratios above 1 [79]. Finally, one can also give predictions of f_B , f_D and f_{D_s} from leptonic decay measurements. The measured decay widths of $D_{(s)} \rightarrow \ell \bar{\nu}_\ell$ [36] lead in average to $f_D^{\text{exp.av.}} = 206.7 \pm 8.5 \pm 2.5$ MeV and $f_{D_s}^{\text{exp.av.}} = 260.0 \pm 5.4$ MeV, which in the latter signals some tension to our prediction and others. A measurement of $B \rightarrow \tau \bar{\nu}_\tau$ [108] yields $f_B^{\text{exp.}} = (211 \pm 22 \pm 14)$ MeV/ $(|V_{ub}|/0.0035)$ including the typical CKM coefficient from exclusive semileptonic decays. High experimental precision could also open a possibility for an independent $|V_{ub}|$ determination. Moreover, one could use CKM independent observables such as the ratio of $B \rightarrow \pi \ell \bar{\nu}_\ell$ and $B \rightarrow \tau \bar{\nu}_\tau$ [109] to check QCD calculations of form factors and decay constants.

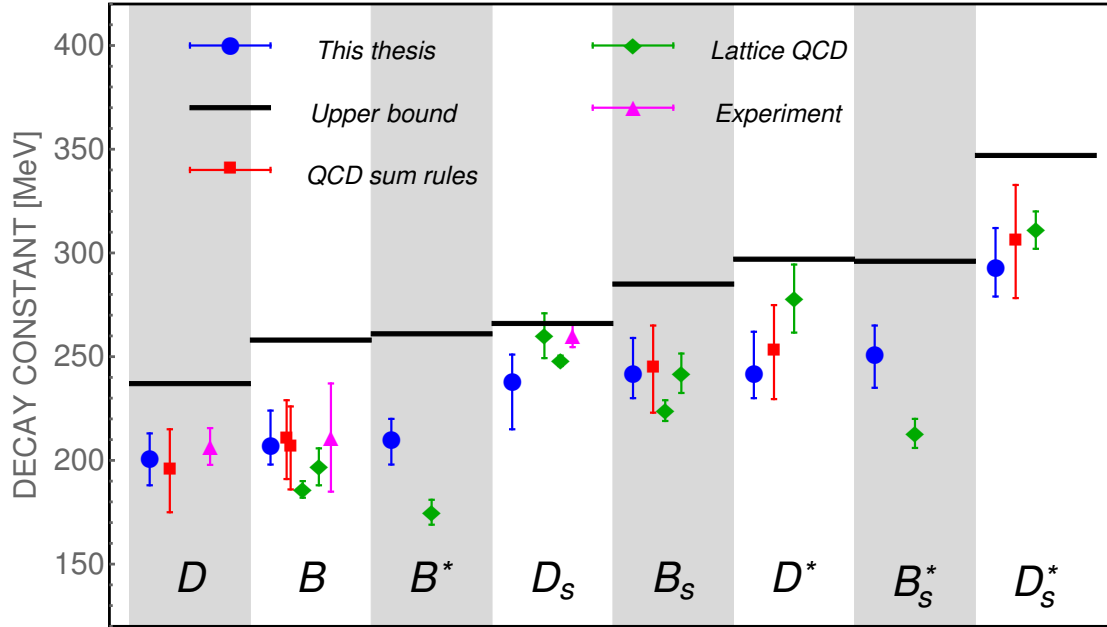


Figure 5.5: An overview of decay constants, which were determined in this work (blue dot on the left) compared to selected literature values based on QCD sum rules (magenta squares at center-left), Lattice QCD computation (yellow checks at center-right) and measurements with averaged CKM values (green triangle on the right). Upper bounds are marked by horizontal bars. The references are from left to right: [104, 53, 104] from QCD sum rules, [51, 49, 107, 49, 50, 51, 49, 110, 107, 110] from lattice QCD and [111] from measurements.

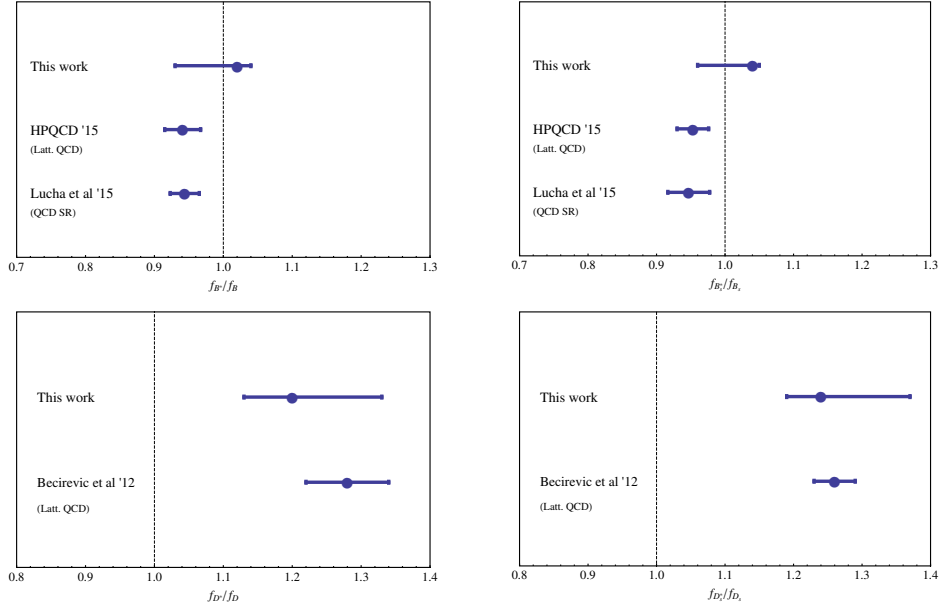


Figure 5.6: A comparison of topical results for ratios of vector to pseudoscalar heavy-light meson decay constants. The ratios were evaluated in Ref. [103] based on QCD sum rules and in [107, 110] based on lattice QCD.

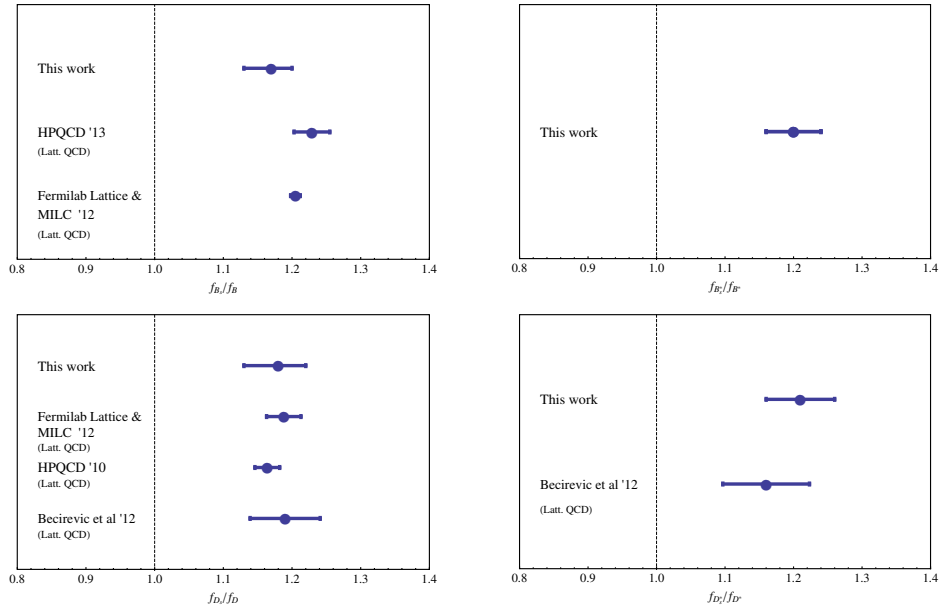


Figure 5.7: A comparison of topical results for ratios of strange to non-strange heavy-light meson decay constants. The ratios were evaluated in Refs. [51, 49, 50, 110] based on lattice QCD.

Decay Constants of Radially Excited B and D Mesons from QCD Sum Rules

Apart from ground-state mesons, the mesonic spectrum also includes a variety of excited states with equal flavor content but different masses. We refer to radial excitations as resonances with the same spin-parity (J^P) as their ground-state. At the moment radial excitations have been studied for compact bound meson states consisting of a quark and anti-quark pair. In particular, charmonium states $c\bar{c}$ were observed such as excitations of $J/\Psi(1S)$ or light unflavored mesons, $\rho(1450)$ and $\rho(1700)$, based on $\rho(770)$ [36]. In case of heavy-light mesons just a few observations of charmed resonances are established, to wit excited states of D , D^* and D_s^* [36, 100, 112, 113]. In the bottom sector many excitations of bottomonia states with total (orbital) angular momentum $J = 1$ ($L = 0$), so-called $\Upsilon(nS)$, were produced and studied at electron-positron colliders [114]. Evidence of heavy-light bottom mesons with $J^P = 1^-$ beyond the ground-state are not yet available. However, there are hints based on recent results of the LHCb [113] and CDF [115] collaborations. Currently, many studies of excited heavy-light resonances are based on the constituent quark model [116, 117]. Alternatively, some lattice QCD computations were performed regarding the properties of excited open-charmed mesons with $J^P = 0^-, 1^-$ [118, 119, 120]. A topical discussion of excitations of charmed mesons was published in connection with the semileptonic decay $B \rightarrow D'\ell\nu_\ell$ [121]. Future precision measurements for decays of these kind will require detailed characteristics of radial excitations as well.

In this chapter we present a possibility to extract the properties of radially excited mesons by extending the method of QCD sum rules, which was used to determine the decay constants of ground-state mesons. We consider as a study case the sum rules for heavy-light pseudoscalar and vector mesons of charmed and bottom flavor in their first radially excited state.

The main results of this chapter have been published in Ref. [A2].

6.1 Including Radial Excitations in QCD Sum Rules

In the following, we adopt the same definitions of the sum rule formulas as discussed in Chap. 3-5. The decay constant $f_{H^{(*)}}$ is defined as a transition of a one-meson state to the QCD vacuum, which is mediated by a local quark-flavor current, see Eqs. (3.6) and (3.5). We use an analogous definition for $f_{H'}$, $f_{H^{*}'}$ of the radially excited states H' and $H^{*'}$. Their masses are $m_{H'}$ and $m_{H^{*'}}$, respectively. The sum rules method is based on the evaluation of two-point correlation functions $\Pi_{t(5)}(q^2)$, see Eqs. (3.4) and (3.3). At first, we modify the hadronic representation of the correlation functions by separating the first radial excited state in addition to the ground-state meson of the hadronic spectral densities. In the vector and pseudoscalar meson channel these are

$$\rho_5(s) \equiv \frac{1}{\pi} \text{Im} \Pi_5(s) = m_H^4 f_H^2 \delta(s - m_H^2) + m_{H'}^4 f_{H'}^2 \frac{\Gamma_{H'} m_{H'}}{\pi[(m_{H'}^2 - s)^2 + \Gamma_{H'}^2 m_{H'}^2]} + \tilde{\rho}_5^h(s) \theta(s - (m_{H^*} + m_P)^2), \quad (6.1)$$

$$\rho_t(s) \equiv \frac{1}{\pi} \text{Im} \Pi_t(s) = m_{H^*}^2 f_{H^*}^2 \delta(s - m_{H^*}^2) + m_{H^{*'}}^2 f_{H^{*'}}^2 \frac{\Gamma_{H^{*'}} m_{H^{*'}}}{\pi[(m_{H^{*'}}^2 - s)^2 + \Gamma_{H^{*'}}^2 m_{H^{*'}}^2]} + \tilde{\rho}_t^h(s) \theta(s - (m_H + m_P)^2). \quad (6.2)$$

Here, P is the lightest pseudoscalar meson, which is kinematically allowed, i.e. either a pion or kaon, depending on the quark content of the initial meson $H^{(*)}'$. We implement ground-state mesons as delta-resonances into the spectral densities, which is a good approximation due to their small total width from measurements. However, for the spectral function of radially excited states a Breit-Wigner ansatz is used, including a constant total width $\Gamma_{H^{(*)}'}$. Note that the widths of the excited resonances are generated by their strong couplings to the continuum states. Hence, a part of the continuum contribution is effectively included in the radially excited resonance terms in the above spectral densities. We also investigate a energy-dependent width as a consistency check for the constant width approximation. Both continuum spectra $\rho_{5(t)}^h$ start at a two-hadron threshold that locate above the mass of the ground-state meson: the decay $H \rightarrow H^* P$ ($H^* \rightarrow H P$) is taken as the physical process at the threshold in the pseudoscalar (vector) channel. In order to model the unknown hadronic sum, we assume the semilocal quark-hadron duality approximation

$$\tilde{\rho}_5^h(s) \theta(s - (m_{H^*} + m_P)^2) = \rho_5^{(\text{pert})}(s) \theta(s - \tilde{s}_0^H), \quad (6.3)$$

$$\tilde{\rho}_t^h(s) \theta(s - (m_H + m_P)^2) = \rho_t^{(\text{pert})}(s) \theta(s - \tilde{s}_0^{H^*}). \quad (6.4)$$

In the equations above, $\rho_{5(t)}^{(\text{pert})}(s)$ is the absorptive part of the leading order contribution in the OPE and $\tilde{s}_0^{H^{(*)}}$ denotes the effective threshold. In addition to the duality ansatz we use Borel transformations to control the hierarchy of the OPE. The final form of the Borel sum rules is

$$\begin{aligned} f_H^2 m_H^4 e^{-\frac{m_H^2}{M^2}} + f_{H'}^2 m_{H'}^4 \int_{(m_{H^*} + m_P)^2}^{\infty} ds \frac{\Gamma_{H'} m_{H'}}{\pi[(m_{H'}^2 - s)^2 + \Gamma_{H'}^2 m_{H'}^2]} e^{-\frac{s}{M^2}} \\ = \Pi_5^{(\text{pert})}(M^2, \tilde{s}_0^H) + \Pi_5^{(\bar{q}q)}(M^2) + \Pi_5^{(d456)}(M^2) \end{aligned} \quad (6.5)$$

and

$$\begin{aligned} f_{H^*}^2 m_{H^*}^2 e^{-\frac{m_{H^*}^2}{M^2}} + f_{H^{*'}}^2 m_{H^{*'}}^2 \int_{(m_H + m_P)^2}^{\infty} ds \frac{\Gamma_{H^{*'}} m_{H^{*'}}}{\pi[(m_{H^{*'}}^2 - s)^2 + \Gamma_{H^{*'}}^2 m_{H^{*'}}^2]} e^{-\frac{s}{M^2}} \\ = \Pi_t^{(\text{pert})}(M^2, \tilde{s}_0^{H^*}) + \Pi_t^{(\bar{q}q)}(M^2) + \Pi_t^{(d456)}(M^2). \end{aligned} \quad (6.6)$$

Eqs. (6.5) and (6.6) include the same shorthand notation for OPE expressions as we use in Chap. 3. In the ground-state sum rules we perform the meson mass-fixing procedure to adjust the effective threshold. This procedure is not adequate for a two state ansatz because of two aspects: To differentiate the correlation function over $(-1/M^2)$ and divide with the original sum rules does not result in the mass of the resonance since a Breit-Wigner form for the first radial excitation is used. It only works if we assume the zero-width approximation for resonances in the spectral densities $\rho_{t(5)}$. Moreover, the experimental mass input of radially excited mesons is very limited compared to the ground-state resonance. Currently, only the masses of D' , $D^{*'}$ and $D_s^{*'}$ are known. All other particles can only be estimated via symmetry relations based on the known masses, which will be explained later on. For these estimates we are obliged to assume conservative error intervals. Besides, despite the known masses of charmed mesons, which are measured with 0.1% accuracy, the mass-fixing procedure does not work due to the strong dependence of $\tilde{s}_0^{H^{(*)}}$ on the meson mass. This leads to inaccurate $f_{H^{(*)}'}$ determinations. To this end, we present a method that allows us to fit the first two resonances of a meson to the corresponding correlation function and extract their decay constants.

6.2 Strategies and Prerequisites for the Numerical Analysis

As an alternative to the standard meson-mass fixing approach, we introduce two more promising procedures:

- Procedure (I): At a given Borel interval I_{M^2} all free parameters, i.e. the decay constants $f_{H^{(*)}}$ and $f_{H^{(*)}'}$ and the effective threshold $\tilde{s}_0^{H^{(*)}}$, are fitted simultaneously. In particular, we minimize the squared difference (χ^2 -fit) between the first two hadron states (ground- and radial-excited state) and the OPE of the correlation functions for various points within I_{M^2} . In the vector heavy-light meson channel the minimization procedure takes the following form:

$$\sum_{i=1}^N \frac{1}{N} \left| f_{H^*}^2 m_{H^*}^2 e^{-\frac{m_{H^*}^2}{M_i^2}} + f_{H^{*'}}^2 m_{H^{*'}}^2 e^{-\frac{m_{H^{*'}}^2}{M_i^2}} - [\Pi_t^{(\text{pert})}(M_i^2, \tilde{s}_0^{H^*}) + \Pi_t^{(\bar{q}q)}(M_i^2) + \Pi_t^{(d456)}(M_i^2)] \right|^2 = \chi_{\min}. \quad (6.7)$$

In the equation above the Breit-Wigner width approximation is neglected for reasons of simplicity, but included in the numerical analysis. An analogous procedure is used for the pseudoscalar meson channel:

$$\sum_{i=1}^N \frac{1}{N} \left| f_H^2 m_H^4 e^{-\frac{m_H^2}{M_i^2}} + f_{H'}^2 m_{H'}^4 e^{-\frac{m_{H'}^2}{M_i^2}} - [\Pi_5^{(\text{pert})}(M_i^2, \tilde{s}_0^H) + \Pi_5^{(\bar{q}q)}(M_i^2) + \Pi_5^{(d456)}(M_i^2)] \right|^2 = \chi_{\min}. \quad (6.8)$$

- Procedure (II): In the ground-state analysis we figured out that the isolation of the first resonance of the residual spectrum, introducing a linear suppression factor $(m_{H^{(*)}'}^2 - q^2)$ at the mass of $H^{(*)}'$, leads to a stabilization of the sum rule and a good extraction quality of $f_{H^{(*)}}$. This behavior indicates a good separation between the first two meson resonances $H^{(*)}$ and $H^{(*)}'$. We can also turn this idea around and cancel the ground-state in order to simplify the problem to a single decay constant fit of $f_{H^{(*)}'}$. For this purpose the differential operator $[d/d(1/M^2) + m_{H^{(*)}}^2]$ is employed in Eqs. (6.5) and (6.6), respectively.

We emphasize that both procedures have distinct differences in comparison with the standard sum rules method due to the multi-parameter fit ansatz. Therefore, we cannot

assume that the quark-hadron duality approximation has the same reliability as before. Radial excitations also tend to mix with strong-coupled interactions ($B' \rightarrow B^*\pi$) and, hence, less control to systematic uncertainties is expected. However, due to the positivity of the hadronic spectral function a cancellation between the ground- and excited states can be excluded. We will also compare predictions of the procedures (I) and (II). A good agreement of both procedure is an indication of reliability.

We choose the same input values for the external parameters such as the quark mass and condensate as discussed in Chap. 5. The Borel interval is selected in such a way that the central values are close to the default values in Sect. 5.1, but it is also located to slightly larger values of M^2 for enhanced contributions of the excited states. In this manner, we guarantee to satisfy the reliability criteria as discussed in the last chapter. The default Borel window is $I_{M^2} = 2.5 - 3.5 \text{ GeV}^2$ ($6 - 8 \text{ GeV}^2$) with variations to $I_{M^2}^{\min} = 2 - 3 \text{ GeV}^2$ ($5.5 - 7.5 \text{ GeV}^2$) and $I_{M^2}^{\max} = 3 - 4 \text{ GeV}^2$ ($6.5 - 8.5 \text{ GeV}^2$) for error estimation in the charmed (bottom) meson channel. In the hadronic part of the sum rules we use as much input from experiments as currently available, i.e. the meson masses of D' , $D^{*'}$ and $D_s^{*'}$ as well as the corresponding total width measurements. The BaBar collaboration observed two candidates for radially excited charmed mesons, to wit $D(2550)$ ($J^P = 0^-$) and $D^*(2600)$ ($J^P = 1^-$). $D_s^{*'}(2700)$ ($J^P = 1^-$) was observed in several experiments [100]. The residual meson masses can either be estimated by $SU(3)_\text{fl}$ -symmetry relations

$$\Delta_{SU(3)_\text{fl}} \equiv m_{D'_s} - m_{D_s} \simeq m_{D'} - m_D \quad (6.9)$$

or the heavy quark symmetry at the infinite mass limit

$$\Delta_{\text{HQL}} \equiv m_{B_{(s)}^{(*)'}} - m_{B_{(s)}^{(*)}} \simeq m_{D_{(s)}^{(*)'}} - m_{D_{(s)}^{(*)}}. \quad (6.10)$$

The accuracy of Δ_{HQL} for bottom mesons is expected to be higher since corrections are of $\mathcal{O}(1/m_Q)$. The resulting meson masses from symmetry consideration in Eqs. (6.9), (6.10) with experimental input are

$$\Delta_{SU(3)_\text{fl}} = \{669 \pm 8, 601 \pm 6, 597 \pm 4\} \text{ MeV} \quad (6.11)$$

for the $D' - D$, $D^{*'} - D^*$ and $D_s^{*'} - D_s^*$ mass shift. Based on these values we set a averaged shift of

$$\Delta_{SU(3)_\text{fl}} = 650 \pm 50 \quad (6.12)$$

for all remaining unknown resonances, which includes a conservative uncertainty. The estimated masses of excited hadrons are shown in Tab. 6.1 and compared to quark-model estimates from Ref. [116]. Note that the recently observed $B(5970)$ state [113] is interpreted as an excitation of the bottom channel with spin-parity $J^P = 1^-$. Its mass coincides with our estimate of $m_{B^{*}}$ as shown in Tab. 6.1. This confirms the reliability of the heavy-quark symmetry relations. Since we assume Breit-Wigner shaped resonances, all measured total width information is included, whereas the unknown widths are determined by 100 ± 50 MeV that is in the ballpark of charmed meson measurements. In case of excited states it is rather difficult to estimate the corresponding width due to the fact that strong flavor-conserving decays contribute and smear over the considered resonance. It is clear that upcoming measurements of branching fractions and total widths of all radially excited heavy-light mesons will substantially refine the used input.

6.3 Numerical Results of Borel Sum Rules for Radial Excitations

In Tab. 6.2 the decay constants of ground-state mesons and first radial excitations are presented, using the methods as described above. In the first column we repeat the results from Chap. 3 as reference values. Besides, these values are also used as input to determine the upper bounds. These bounds are calculated in the limit $\tilde{s}_0^{H^{(*)}} \rightarrow \infty$ within the default Borel window and default values for all other free parameters. We add the uncertainties from parameter variations to the upper bound and present the final value in the last column of Tab. 6.2. Our main results are computed according to procedures (I) and (II). They are also presented with corresponding fitted thresholds, which satisfy the defined criteria of reliability. The total error budget is examined in more detail in Tab. 6.3. At first, we give the combined error from external parameters ($m_Q, \langle q\bar{q} \rangle, \dots$) and scale variation. Secondly, the Borel window is shifted by ± 0.5 GeV². Meson mass uncertainties of excited states and variations of the Breit-Wigner width are shown in the last two columns. The mean squared fit error $\Delta\chi^2$, which arises due to the minimization of the first two resonances against the OPE expressions is a novelty compared to the ground-state analysis. This error reflects the inaccuracy of the duality threshold $\tilde{s}_0^{H^{(*)}}$. Note that we consider a conservative estimation and neglect correlations between individual parameters by adding them in quadrature. As an alternative to a constant total width for the resonance shape, we also adopt an energy-dependent width. Technically, we investigate this effect by inserting $\sqrt{s} \Gamma_{H^{(*)}'}(s)$ instead of $m_{H^{(*)}'} \Gamma_{H^{(*)}'}$ in the Breit-Wigner ansatz of the hadronic spectral densities.

From Refs. [122] and [123] we introduce the s -dependent width function of vector mesons, which is given by

$$\Gamma_{H^{*'}}(s) = \frac{\Gamma_{H^{*'}} m_{H^{*'}}^2}{s} \left(\frac{\lambda(s, m_H^2, m_P^2)}{\lambda(m_{H^{*'}}^2, m_H^2, m_P^2)} \right)^{3/2}, \quad (6.13)$$

where $\lambda(a, b, c) = a^2 + b^2 + c^2 - 2(ab + bc + ac)$. The kinematical factor originates from the p-wave phase space of the decay $H^{*'} \rightarrow HP$. In the pseudoscalar meson channel the analogous formula holds. Here, the width is dominated by the $H' \rightarrow H^*P$ decay. As an example we evaluate the D'_s decay constant to give an impression on the sensitivity of the sum rules with a threshold-dependent width. Procedure (I) leads to

$$f_{D'_s} = 143(\pm 8)|_{\Delta\Gamma} \text{ MeV} \quad (6.14)$$

with default input values and variations of the constant width according to 100 ± 50 MeV. Assuming a delta resonance for the excited state in the spectral density, we find

$$f_{D'_s} = 128|_{\Gamma=0} \text{ MeV}. \quad (6.15)$$

In case of a energy-dependent width we obtain

$$f_{D'_s} = 148(\pm 16)|_{\Delta\Gamma(s)} \text{ MeV}. \quad (6.16)$$

Altogether this is a relative shift to the central value of about 10% with the zero width approximation and a shift of 3% if a s -independent width is used. Finally, one can also investigate the impact of individual OPE contributions to find the source for differences between ground and excited states decay constants as shown in Tab. 6.4. If only the PT part is included, the decay constants f_D and $f_{D'}$ show increasing values for every additional correction terms in the PT part. However, the condensate terms lead to a suppression of $f_{D'}$, which opens up the discrepancy between the radially excited and ground-state meson decay constant.

$H^{(*)'}$	$m_{H^{(*)'}}$ [MeV]	$m_{H^{(*)'}}^{\text{QM}}$ [MeV]	$\Gamma_{H^{(*)'}}$ [MeV]	Ref.
D'	2539 ± 8	2581	130 ± 18	[36, 100]
$D^{*'}$	2612 ± 6	2632	93 ± 14	[36, 100]
D'_s	2618 ± 50	2688	100 ± 50	
$D_s^{*'}$	2709 ± 4	2731	117 ± 13	[36]
B'	5929 ± 50	5890	100 ± 50	
$B^{*'}$	5975 ± 50	5906	100 ± 50	
B'_s	6017 ± 50	5976	100 ± 50	
$B_s^{*'}$	6065 ± 50	5992	100 ± 50	

Table 6.1: Masses and corresponding quark model predictions [116] are shown in the first two columns. The total width and mass shifts with respect to the ground-state meson mass are given in the last two rows. Boxed values are taken from experiment, whereas others are estimations for yet unobserved resonances.

Meson	From Chap. 3	Procedure (I)			Procedure (II)		Upper bound
	$f_{H^{(*)}}$ [MeV]	$f_{H^{(*)}}$ [MeV]	$f_{H^{(*)}'}$ [MeV]	$\tilde{s}_0^{H^{(*)}}$ [GeV ²]	$f_{H^{(*)}'}$ [MeV]	$\tilde{s}_0^{H^{(*)}}$ [GeV ²]	$f_{H^{(*)}'}$ [MeV]
$D^{(\prime)}$	201^{+12}_{-13}	194^{+6}_{-6}	137^{+10}_{-23}	7.24	138^{+10}_{-22}	7.24	189
$D_s^{(\prime)}$	238^{+13}_{-23}	230^{+7}_{-9}	143^{+19}_{-31}	7.48	146^{+12}_{-36}	7.49	219
$D^{*(\prime)}$	242^{+20}_{-12}	235^{+25}_{-12}	182^{+12}_{-27}	7.43	183^{+13}_{-24}	7.44	275
$D_s^{*(\prime)}$	293^{+19}_{-14}	279^{+21}_{-12}	174^{+22}_{-45}	7.87	178^{+20}_{-39}	7.88	265
$B^{(\prime)}$	207^{+17}_{-9}	200^{+18}_{-10}	163^{+10}_{-11}	36.75	166^{+9}_{-10}	36.78	279
$B_s^{(\prime)}$	242^{+17}_{-12}	234^{+15}_{-11}	174^{+19}_{-19}	37.72	178^{+19}_{-17}	37.75	320
$B^{*(\prime)}$	210^{+10}_{-12}	208^{+12}_{-21}	163^{+54}_{-13}	36.70	165^{+46}_{-12}	36.71	314
$B_s^{*(\prime)}$	251^{+14}_{-16}	244^{+13}_{-26}	190^{+67}_{-20}	38.58	194^{+57}_{-18}	38.61	325

Table 6.2: Decay constants of charmed and bottom mesons obtained from QCD sum rules and the corresponding effective thresholds using two fit procedures. The last column shows the duality-independent upper bounds.

Meson	ΔP_{tr}	ΔM^2	$\Delta \chi^2$	$\Delta \Gamma$	$\Delta m_{H^{(*)'}}$
D'	+9 (+9) -21 (-20)	+5 (+5) -10 (-8)	+1 (+1) -1 (-1)	+1 (+1) -1 (-1)	< ± 1 (< ± 1)
D'_s	+12 (+7) -27 (-29)	+7 (+6) -14 (-16)	+1 (+2) -1 (-2)	+8 (+4) -8 (-14)	+9 (+7) -4 (-4)
$D^{*'}$	+11 (+10) -24 (-22)	+8 (+7) -12 (-10)	+2 (+3) -2 (-3)	+1 (+1) -1 (-1)	< ± 1 (< ± 1)
$D_s^{*'}$	+14 (+13) -34 (-31)	+15 (+13) -29 (-23)	+5 (+7) -5 (-7)	+2 (+2) -2 (-2)	< ± 1 (< ± 1)
B'	+7 (+7) -8 (-7)	+5 (+5) -7 (-6)	+1 (+2) -1 (-2)	+4 (+4) -4 (-4)	+2 (+1) -1 (-1)
B'_s	+11 (+9) -11 (-10)	+8 (+7) -10 (-8)	+2 (+3) -2 (-3)	+11 (+11) -10 (-10)	+9 (+10) -1 (-1)
$B^{*'}$	+53 (+46) -12 (-10)	+4 (+3) -4 (-3)	+1 (+2) -1 (-2)	+4 (+4) -4 (-4)	+5 (+4) -3 (-3)
$B_s^{*'}$	+66 (+56) -15 (-13)	+8 (+7) -11 (-9)	+2 (+3) -2 (-3)	+7 (+7) -7 (-7)	+4 (+3) -1 (-1)

Table 6.3: Individual uncertainties for decay constants of heavy-light excited mesons from QCD sum rules using procedure (I) ((II)). All numbers are presented in units of MeV.

f_D [MeV]	$f_{D'}$ [MeV]	Included OPE contributions
120	123	PT (LO)
150	177	PT (LO + NLO + NNLO)
190	142	PT + $\langle q\bar{q} \rangle$ (LO + NLO)
194	137	full precision

Table 6.4: Decay constants of D and D' are determined according to procedure (I) with varied OPE approximation. The parameter input is set to default values.

6.4 Summary and Concluding Remarks

This project was dedicated to the determination of decay constants of first radially excited bottom and charmed heavy-light mesons with spin-parity $J^P = 0^-$ and 1^- . To this end, we constructed two procedures based on the method of QCD sum rules. In the first procedure the ground- and radial-excited state resonances were fitted to the OPE expressions of the corresponding two-point correlation functions. For additional validation a single fit of the radial-excited state was performed. In this procedure the ground-state was removed in the spectral function by a linear weight.

- Both fit approaches lead to almost identical results for decay constants of $\{B', B'_s, B^{*'}, B_s^{*'}\}$ and $\{D', D'_s, D^{*'}, D_s^{*'}\}$, which are centered around 160 – 190 MeV with 15–26 % relative uncertainty and 140–180 MeV with 7–35 % relative uncertainty, respectively, see also Fig. 6.1. The results of the double-fit procedure confirm the ones from the ground-state analysis, which shows consistency of the sum rules method. The central values and associated total errors from the fit method are comparable to the results in Section 5.2. Note that the uncertainties for pseudoscalar mesons tend to be smaller due to the choice of the Borel parameter window I_{M^2} : In the standard one-resonance sum rules of Chap. 3 we optimized the free parameters to the vector channel. In this case, however, the focus is set on pseudoscalar mesons and, hence, it is “natural” that the vector channel predictions are less precise. Further, M^2 is readjusted to larger values to enhance the effects of excited states.
- In general, our predictions to radial excitations are smaller (up to 120 MeV) than their ground-state partners. They also have larger uncertainties, predominantly due to the variations of external parameters such as the quark mass and the quark condensate. Another significant source of uncertainty is the renormalization scale-dependence μ , which contributes to ΔP_{tr} . The Borel parameter uncertainty ΔM^2 as well as changes in the width of the excited resonances also have significant influence on the total error budget, whereas the fit procedure $\Delta \chi^2$ and uncertain meson masses $\Delta m_{H'}$ are comparably small.
- Our results show a suppression regarding the decay constants of excited mesons compared to their ground-state partners. The reason is the negative contribution of condensate terms in the OPE.
- There is still room for improvement since some meson masses are determined from heavy quark symmetry relations with conservative uncertainty estimates. Hence,

upcoming measurement should substantially refine our method by reducing the uncertainty $\Delta m_{H^{(*)'}}$.

- Predictions to decay constants of radial excitations are rare. A recent determination in Ref. [118] is based on the lattice QCD. The authors of [118] find $f_{D'} = 117 \pm 25$ MeV, which is in good agreement with our estimation. The estimate $f_{D^{*'}} \sim 300$ MeV from Ref. [121] is inconsistent with the uncertainty bounds of our predicted value.

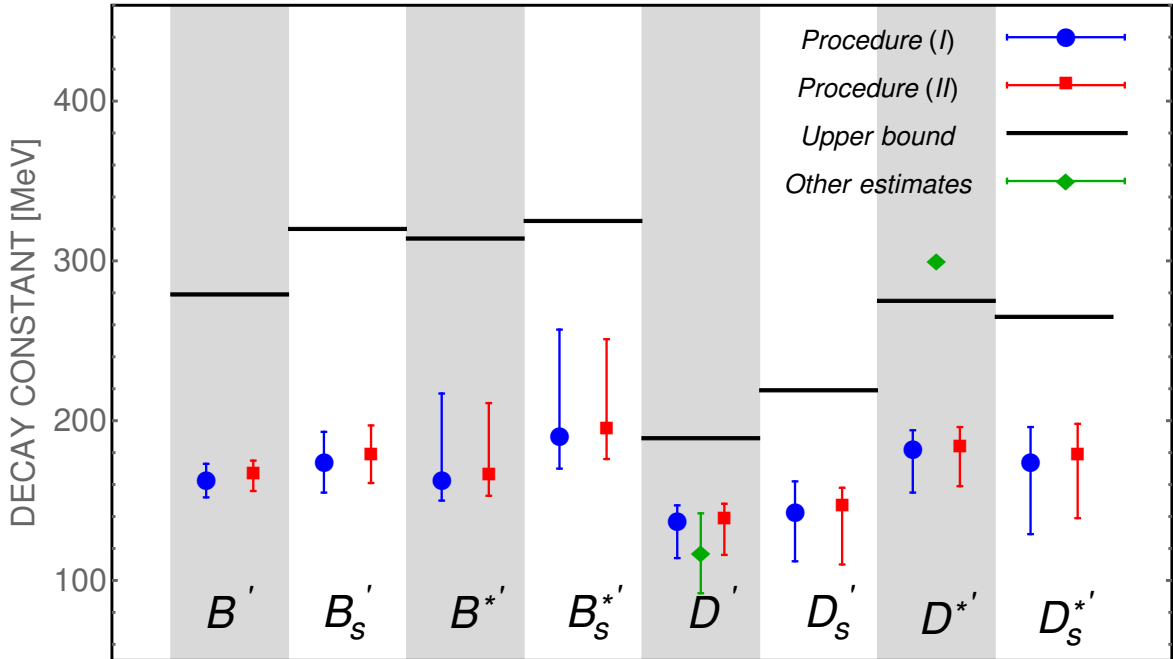


Figure 6.1: An overview of decay constants of the first radial excitation. Central values and uncertainties based on procedure (I) and (II), respectively, are presented by blue dots and magenta squares, respectively. Upper bound determinations are marked by horizontal bars. Green checks denote predictions of $f_{D'}$ and $f_{D^{*'}}$ from lattice QCD and QCD sum rules in Ref. [118] and [121].

Decay Rate of Inclusive Semileptonic B Decays from QCD

In the search for New Physics phenomena the quark sector of the Standard Model shows distinct potential for finding signs that go beyond the common framework. As an example, one can consider flavor-changing $s \rightarrow u$ transitions in correspondence to $K \rightarrow \pi e \bar{\nu}_e$ at hadron level. This kind of decay is experimentally well measured, but the treatment on the theoretical side is rather problematic due to arising infrared (IR) divergences in the description of light hadrons. Decays of heavy mesons, however, reveal a different picture. The advantage of hadronic systems with heavy quark content is the well-separated hierarchy between typical energy scales. Typical scales are the large mass m_Q of the heavy quark and the hadronic scale Λ_{QCD} , which marks the IR regime of QCD. If we consider the physical system at a scale around m_Q , perturbative calculation in the regime of asymptotic freedom can be performed. Such properties allow for an efficient decomposition of certain hadronic observables via OPE into a finite number of factorized terms, separated into coefficient functions that are well-defined in perturbative QCD, and parameters of non-perturbative nature. The latter can either be extracted from data or assessed with non-perturbative methods. One prominent non-perturbative method is the technique of QCD sum rules which was used in the previous chapters. For maximum separation of scales one should consider the heaviest quark there is, that is the top-quark. However, top quarks do not form hadrons due to their short lifetime and, hence, they are not suitable for our considerations. On the other hand, the charm quark mass is probably not large enough compared to Λ_{QCD} . Therefore B -meson decays have just suitable properties for a proper theoretical treatment. Such decays have been studied intensively in the last decades. The OPE technology is applicable to $b \rightarrow u$ and $b \rightarrow c$ transitions with semileptonic or purely hadronic final states. For definiteness, we stick to semileptonic $b \rightarrow c$ transitions, more specifically, to inclusive decays of the form $B \rightarrow X_c \ell \bar{\nu}_\ell$, where X_c refers to every charmed hadron state which is kinematically allowed and corresponds to the quantum numbers of the initial state. The following considerations can immediately be applied to heavy-to-light transitions where the mass of the light quark is usually neglected.

Model-independent studies of inclusive semileptonic B -meson decays were started 20 years ago [124, 125, 126, 127]. Such studies are based on the OPE in the realm of *heavy quark effective theory* (HQET). The main goal is to give accurate determinations of the CKM matrix element $|V_{cb}|$ (and $|V_{ub}|$) from precisely measured partial decay rates at the B factories in conjunction with a detailed theoretical description of the same observable. Since $|V_{cb}|$ also influences many rare FCNC decays such as $B_s \rightarrow \mu^+ \mu^-$ or $K \rightarrow \pi \nu \bar{\nu}$, there is a strong interest to have a comprehensive understanding of this CKM entry in order to sharpen the sensitivity to effects beyond the Standard Model. The key observable is the total inclusive rate of $B \rightarrow X_c \ell \bar{\nu}_\ell$, from which the OPE allows extraction of $|V_{cb}|$. The resulting structure of the OPE is a double expansion in the strong coupling α_s and Λ_{QCD}/m_b [128]:

$$\Gamma(B \rightarrow X_c \ell \bar{\nu}_\ell) = \Gamma_0 |V_{cb}|^2 \left[a_0 \left(1 - \frac{\mu_\pi^2}{2m_b^2} \right) + a_2 \frac{\mu_G^2}{2m_b^2} + a_3^{\text{D}} \frac{\rho_{\text{D}}}{m_b^3} + a_3^{\text{LS}} \frac{\rho_{\text{LS}}}{m_b^3} + \mathcal{O}\left(\frac{\Lambda_{\text{QCD}}^4}{m_b^4}\right) \right] \quad (7.1)$$

where the normalization factor is given by $\Gamma_0 \equiv G_F^2 m_b^5 / (192\pi^3)$. In general, the coefficients a_0 to a_4 are functions of α_s and the quark masses m_c , m_b . The parameters μ_π^2 , μ_G^2 , ρ_{D} and ρ_{LS} are B -meson expectation values of local operators with growing dimensionality within HQET. The numerical values of those hadronic parameters are usually fitted from the moments of the differential decay rates with additional information from $B \rightarrow X_s \gamma$ [129]. The leading power coefficient a_0 is known with NNLO accuracy in α_s [130, 131]. Due to reparametrization invariance a_0 equates to the coefficient of μ_π^2 . Power corrections of $\mathcal{O}(\Lambda_{\text{QCD}}^{2,3}/m_b^{2,3})$ were first studied in [126, 127], whereas NLO corrections to μ_π^2 were confirmed in [132, 133]. Recently, the corrections to μ_G^2 were computed in [134]. Note that the computation of differential decay rates only allows numerical values for the total rate. To this end, in [134] the authors performed the phase space integration of the triple differential rate. As for higher order power-suppressed terms, a first study is given in [135]. At this level, the main problem is a proliferation of non-perturbative parameters. Mass corrections of $\mathcal{O}(\Lambda_{\text{QCD}}^{4,5}/m_b^{4,5})$ contain 9 and 18 new B -meson expectation values, respectively. This large number of free parameters cannot be extracted from experiment altogether. Thus, in Ref. [135] a special method is used to estimate these unknown parameters through combinations of known ones of $\mathcal{O}(\Lambda_{\text{QCD}}^{2,3}/m_b^{2,3})$. Current determinations of V_{cb} have total uncertainties at the level of 2% and less (including 1% theoretical uncertainty). The most precise result reads explicitly [129]

$$|V_{cb}|_{\text{incl.}} = (42.21 \pm 0.78) \times 10^{-3}. \quad (7.2)$$

Thanks to the large data set from BaBar and Belle the experimental precision has outpaced the theoretical one. The current global fit including the total rate and various moments for the extraction of V_{cb} with all available data does not include analytical NLO corrections to μ_G^2 yet, which are parametrically the largest missing pieces in the analysis [129]. Aside from studies of inclusive decays, one can also choose specific (exclusive) weak decays to determine V_{cb} . Prominent decay channels for this purpose are $B \rightarrow D^* \ell \bar{\nu}_\ell$ and $B \rightarrow D \ell \bar{\nu}_\ell$, which require knowledge of hadronic form factors, determined within either lattice QCD or light-cone sum rules. The most accurate value from exclusive decays is [136]

$$|V_{cb}|_{\text{excl.}} = (39.04 \pm 0.49_{\text{exp}} \pm 0.53_{\text{lat}} \pm 0.19_{\text{QED}}) \times 10^{-3}. \quad (7.3)$$

The direct comparison between the inclusive and exclusive determination of V_{cb} shows a long-standing tension of about 3σ . In this context, New Physics effects were studied in Ref. [137] and ruled out. The remaining (obvious) way to solve the V_{cb} tension is higher accuracy in measurements and theory.

To this end, we consider the NLO correction to the short-distance coefficient of the parameter μ_G^2 , encoded in a_2 , with the full mass dependence, i.e. we consider the final charm quark as massive. Concerning this issue, we will present the following aspects:

- Our calculation of a_2 is a matching computation between QCD and HQET. Thus, we discuss some relevant basics of HQET and show how to expand the total decay rate in terms of $1/m_Q$ within the effective theory (Section 7.1 & 7.2).
- We give results of all contributions relevant for a_2 including their mass dependence with respect to the ratio m_c^2/m_b^2 in Section 7.3.
- The Sections 7.4 and 7.5 present the numerical results for the total decay width and some moments with typical results as well as their influence on V_{cb} , when the new correction is included.
- In the final section we summarize our findings.
- Analytical results and computational strategies which lead to the final coefficient function a_2 are discussed in the next chapter and Appendix C.

The main results of Chap. 7 and 8 have also been published in Refs. [A3, A4].

7.1 Basics of Heavy Quark Effective Theory

A heavy hadronic system, e.g. a meson with valence quarks Q and q denoting a heavy and light quark, contains the mass of the heavy quark m_Q which is by definition much larger than Λ_{QCD} . The momentum transfer exchanged between the heavy quark and other light constituents in this system (sometimes also referred to as the "brown muck") is typically of the order Λ_{QCD} . Due to this large separation of scales the light degrees of freedom are blind to the properties of the heavy quark. In terms of Compton wavelengths, the wavelength of the heavy particle is $\sim 1/m_Q$ and, hence, much smaller than the wavelength of the light partner. In this configuration light quarks and gluons, the light degrees of freedom, that couple to the brown muck, cannot resolve the heavy quark. In the limit $m_Q \rightarrow \infty$ this leads to symmetries, namely the heavy quark spin and flavor symmetry. When taking this limit, the light degrees of freedom do not change if we modify the heavy quarks spin or flavor. Finite quark masses break these symmetries and corrections arise at the order Λ_{QCD}/m_Q . Formally, the QCD Lagrangian does not show a manifest spin-flavor symmetry as $m_Q \rightarrow \infty$. At first, we have to formalize the Lagrangian in terms of an effective field theory also known as heavy quark effective theory [138, 139, 140, 141]. We consider a heavy hadron with momentum p_H and mass m_H . The main contribution to p_H is given by the heavy quark kinematics, i.e. $p_H = m_Q v + \Delta p$, where we introduced the velocity of the hadron $v = p_H/m_H$. The small residual momentum Δp is related to the light degrees of freedom and to interactions of the brown muck particles with the heavy quark. The momentum Δp scales as Λ_{QCD} and therefore interactions are typically soft. One can now relate the large part of the momentum p_H on the level of quark field operators within matrix elements over a heavy hadron. We rewrite the original field operators $Q(x)$ to a set of effective fields

$$Q(x) = e^{-i(m_Q v)x} (h_v(x) + H_v(x)) . \quad (7.4)$$

The fast oscillating phase arising from the heavy quarks momentum is explicitly separated from the slowly (quickly) changing effective field h_v (H_v). Here, h_v and H_v are the upper and lower field components of Q , which can be projected out by the projection operators $P_{\pm} = (1 \pm \not{v})/2$ according to

$$h_v(x) = e^{i(m_Q v)x} P_+ Q(x) , \quad (7.5)$$

$$H_v(x) = e^{i(m_Q v)x} P_- Q(x) . \quad (7.6)$$

Using the Dirac basis one can immediately see that h_v corresponds to the upper two (quark) components of Q in the rest frame of the hadron, whereas H_v characterizes the lower two (antiquark) components for. In terms of the new field operators the QCD Lagrangian reads

$$\begin{aligned} \mathcal{L}_{\text{QCD}} &\supset \bar{Q}(i\not{D} - m_Q)Q \\ &= \bar{h}_v(ivD)h_v - \bar{H}_v(ivD + 2m_Q)H_v + \bar{h}_v(i\not{D}_\perp)H_v + \bar{H}_v(i\not{D}_\perp)h_v. \end{aligned} \quad (7.7)$$

For convenience, we split up the covariant derivative $D_\mu = \partial_\mu - ig_s A_\mu^a T^a$ into its longitudinal and transverse piece, i.e. $D^\mu = (vD)v^\mu + D_\perp^\mu$. Since the fields satisfy the conditions $\not{v}h_v = h_v$ and $\not{v}H_v = -H_v$ all mixed terms of the sort $\bar{h}_v i\not{D}H_v$ in Eq. (7.7) reduce to the transverse component $i\not{D}_\perp$, whereas even terms, e.g. $\bar{h}_v i\not{D}h_v$, reduce to the longitudinal derivative $i(vD)$. At tree level one can now easily integrate out the heavy degrees of freedom represented by H_v if the equation of motion (EOM)

$$(ivD + 2m_Q)H_v - i\not{D}_\perp h_v = 0 \quad (7.8)$$

is used. The effective Lagrangian now reads

$$\mathcal{L}_{\text{HQET}} = \bar{h}_v(ivD)h_v + \bar{h}_v i\not{D}_\perp \frac{1}{ivD + 2m_Q} i\not{D}_\perp h_v, \quad (7.9)$$

see also Ref. [142, 143] The first term describes the residual energy of the quark while the second (non-local) term is the remnant of the removed antiquark. The physical system, which satisfies the condition $m_Q \gg ivD$, can now be expanded in terms of ivD/m_Q . Due to the fact that the new fields carry only the small residual momentum Δp , we know that derivatives acting on the h_v lead to powers of Δp , which are chosen to be much smaller than m_Q . The expansion of the final HQET Lagrangian at the second order in the heavy quark mass results in

$$\mathcal{L}_{\text{HQET}} = \mathcal{O}_V + \frac{\mathcal{O}_\pi}{2m_Q} + C_{\text{mag}}(\mu) \frac{\mathcal{O}_G(\mu)}{2m_Q} + \frac{C_D \mathcal{O}_D + C_{SL} \mathcal{O}_{SL}}{2m_Q^2} + \mathcal{O}\left(\frac{\Lambda_{\text{QCD}}^3}{m_Q^3}\right).$$

In the equation above, we abbreviated various operators: $\mathcal{O}_V = \bar{h}_v(ivD)h_v$ is the leading power operator. It is spin and flavor invariant and represents the only term in the infinite quark mass limit. The two power-suppressed terms correspond to the kinetic energy of the heavy quark $\mathcal{O}_\pi = \bar{h}_v(iD_\perp)^2 h_v$ and its chromomagnetic interaction $\mathcal{O}_G = (g_s/2)\bar{h}_v\sigma_{\mu\nu}G^{\mu\nu}h_v$, where $ig_s G^{\mu\nu} = [iD^\mu, iD^\nu]$. The coefficient of \mathcal{O}_π is fixed by reparametrization (Lorentz) invariance to the leading power term, whereas \mathcal{O}_G requires

an additional short-distance coefficient C_{mag} from QCD-to-HQET matching, which compensates the scale dependence. The latter coefficient reads

$$C_{\text{mag}}(\mu) = 1 + \frac{\alpha_s}{2\pi} \left\{ C_F + C_A \left(1 + \log \left(\frac{\mu}{m_Q} \right) \right) \right\}, \quad (7.10)$$

which includes the radiative QCD corrections of the first order in α_s [144, 145]. Higher order terms are given by the Darwin term $\mathcal{O}_D = \bar{h}_v g_{\mu\nu} [[ivD, iD_\perp^\mu], iD_\perp^\nu] h_v$ and spin-orbit term $\mathcal{O}_{\text{SL}} = \bar{h}_v \sigma_{\mu\nu} [[ivD, iD_\perp^\mu], iD_\perp^\nu] h_v$. The corresponding coefficient functions C_D and C_{SL} are known up to NLO in α_s [143].

7.2 Heavy Quark Expansion for the Total Decay Rate

Experimental observable of inclusive hadronic decays are basically limited to the total decay rate and corresponding differential distributions. In case of an inclusive decay $B \rightarrow X_c \ell \bar{\nu}_\ell$ the total rate is defined as

$$\Gamma(B \rightarrow X_c \ell \bar{\nu}_\ell) = \frac{1}{2m_B} \int d\Phi(p_B; p_{X_c}, p_\ell, p_{\bar{\nu}}) \times |\mathcal{M}|^2. \quad (7.11)$$

The integrand is given by the amplitude $\mathcal{M} = \langle X_c \ell \bar{\nu} | \mathcal{L}_{\text{int}} | \bar{B} \rangle$ which describes the interaction process. One also integrates over the phase space Φ of all final state particles, namely any charmed meson X_c and the dilepton pair $\ell, \bar{\nu}$. We introduced the prefactor that stems from the normalization of the heavy meson states. In order to embed the considered interaction, we choose the (low-energy) effective Lagrangian

$$\mathcal{L}_{\text{eff}} = -\mathcal{H}_{\text{eff}} = -2\sqrt{2}G_F V_{cb} [\bar{c}\gamma^\mu P_L b] \times [\bar{\ell}\gamma_\mu P_L \nu_\ell] + h.c. \quad (7.12)$$

with $P_L = (1 - \gamma_5)/2$. The Fermi constant G_F is known with high precision from pure leptonic weak decays. Using the unitarity property of the scattering operator

$$\hat{S} = \mathbf{1} + i\hat{T} = \mathcal{T} \exp \left\{ i \int dx \mathcal{L}_{\text{eff}}(x) \right\}, \quad (7.13)$$

we find the relation

$$\hat{T}^\dagger \hat{T} = i(\hat{T}^\dagger - \hat{T}) = 2\text{Im} \hat{T}, \quad (7.14)$$

where \hat{T} is the transition operator. This is the optical theorem of scattering processes. One can now expand the exponential function in (7.13) to extract the leading contri-

butions. Since the Lagrangian is hermitian, only higher order expressions can have an imaginary part, starting with the second order expansion term. The leading term reads

$$\hat{T} = i \int dx \mathcal{T} \{ \mathcal{L}_{\text{eff}}(x) \mathcal{L}_{\text{eff}}(0) \}. \quad (7.15)$$

The amplitude in the definition of Γ can be identified as the matrix element of \hat{T} and therefore

$$\begin{aligned} \Gamma(H \rightarrow X) &= \frac{1}{2m_H} \sum_X d\Phi_X |\mathcal{M}(H \rightarrow X)|^2 \\ &= \frac{1}{2m_H} \sum_X d\Phi_X \langle H | \hat{T}^\dagger | X \rangle \langle X | \hat{T} | H \rangle \quad \left(\sum_X d\Phi_X |X\rangle \langle X| = \mathbf{1} \right) \\ &= \frac{1}{m_H} \langle H | \text{Im} \hat{T} (H \rightarrow X \rightarrow H) | H \rangle \end{aligned} \quad (7.16)$$

where a heavy hadron H decays inclusively. Inclusive decays describe the sum over all possible final states which are kinematically allowed and have the quantum numbers of the initial state. For convenience, we define a normalized transition operator \hat{T}_0 by separating the global tree-level phase space factor and the CKM coefficient

$$\text{Im} \hat{T} = \frac{G_F^2 m_b^5}{192\pi^3} \times |V_{qQ}|^2 \times \text{Im} \hat{T}_0. \quad (7.17)$$

Note that the transition operator is a non-local operator of the particle fields. It is further integrated over the whole phase space. Since all scales are involved in this object, it is not tractable in perturbative QCD. However, rewriting the original heavy-quark fields to effective fields within HQET singles out a large phase factor (as discussed in the previous section). It allows us to perform an OPE in terms of the inverse quark mass m_Q with factorized short-distance effects, which are treatable in perturbation theory, and non-perturbative properties, encoded in local operators. This expansion in the heavy quark is a matching from QCD to HQET according to

$$\text{Im} \hat{T}_0 = \int dx e^{-i(m_Q v)x} \bar{h}_v(\dots \text{“brown muck”} \dots) h_v, \quad (7.18)$$

$$\Rightarrow \text{Im} \hat{T}_0 = C_0 \mathcal{O}_0 + C_V \frac{\mathcal{O}_V}{m_Q} + C_\pi \frac{\mathcal{O}_\pi}{2m_Q^2} + C_G \frac{\mathcal{O}_G}{2m_Q^2} + \mathcal{O}\left(\frac{\Lambda_{\text{QCD}}^3}{m_Q^3}\right). \quad (7.19)$$

The operators are ordered by their dimension starting with $\mathcal{O}_0 = \bar{h}_v h_v$ ($d = 3$) and mass suppressed operators (see also in the previous section). One can determine the coefficients C_i by matching the corresponding matrix elements between QCD and HQET. Later on we will describe which states should be used to single out individual coefficients. Note that after taking the hadronic matrix element, such as the heavy meson state $|H\rangle$, the operator \mathcal{O}_V contributes to higher dimensional operators with the equation of motion. Eq. (7.19) is universal and coefficients are independent of the choice of external states. We choose on-shell quarks and external gluons for matching to QCD. For convenience, we also consider the local operator $\bar{Q}\psi Q$ that is defined in full QCD and the leading expression in HQE. This choice can be attributed to the current $\bar{Q}\gamma_\mu Q$ being conserved from which follows the forward hadronic matrix element

$$\langle H(p) | \bar{Q}\psi Q | H(p) \rangle = 2m_H \quad (7.20)$$

and our HQE is normalized. To perform the substitution of the local operator in (7.19), we also require the local expansion:

$$\bar{Q}\psi Q = \mathcal{O}_0 + \frac{\mathcal{O}_\pi}{2m_Q^2} + \tilde{C}_G \frac{\mathcal{O}_G}{2m_Q^2} + O\left(\frac{\Lambda_{\text{QCD}}^3}{m_Q^3}\right). \quad (7.21)$$

The leading power expression has no radiative corrections. Substituting Eq. (7.21) into (7.19) results in the final expansion for the transition operator

$$\text{Im } \hat{T}_0 = C_0 \left[\bar{Q}\psi Q - \frac{\mathcal{O}_\pi}{2m_Q^2} \right] + \left[-C_V C_{\text{mag}}(\mu) + C_G - \tilde{C}_G C_0 \right] \frac{\mathcal{O}_G}{2m_Q^2}, \quad (7.22)$$

where we used the equation of motion. In terms of B meson states we recover the total decay rate with nonperturbative hadronic matrix elements. The forward B meson matrix element of \mathcal{O}_G is commonly related to the mass splitting between the vector and pseudoscalar meson masses. For bottom mesons the mass splitting is approximately

$$\bar{\mu}_G^2 = -\frac{1}{2m_B} C_{\text{mag}}(\mu) \langle B(p_B) | \mathcal{O}_G(\mu) | B(p_B) \rangle = \frac{3}{4} (m_{B^*}^2 - m_B^2) \simeq 0.37 \text{ GeV}^2 \quad (7.23)$$

with state normalization $\langle B(p'_B) | B(p_B) \rangle = 2p_B^0 (2\pi)^3 \delta^3(\vec{p}_B - \vec{p}'_B)$. Higher order $1/m_Q$ corrections in the mass splitting formula were neglected. Correspondingly, the matrix element of the kinetic operator has the abbreviation $\mu_\pi^2 = -\frac{1}{2m_B} \langle B | \mathcal{O}_\pi | B \rangle$. With all

definitions stated above the total rate for semileptonic B decays now reads

$$\Gamma(B \rightarrow X_c \bar{\nu}_\ell \ell) = \frac{G_F^2 m_b^5}{192\pi^3} \times |V_{cb}|^2 \times \left[C_0 \left(1 - \frac{\mu_\pi^2}{2m_b^2} \right) + \left(-C_V + \frac{C_G - \tilde{C}_G C_0}{C_{\text{mag}}} \right) \frac{\tilde{\mu}_G^2}{2m_b^2} \right]. \quad (7.24)$$

7.3 Coefficient Functions of HQE

The matching procedure is based on the computation of matrix elements with partonic states (b -quarks and gluons) on the QCD and HQET side in Eq. (7.19). At NLO level three-loop Feynman diagrams with a massive c - and b -quark arise from the matrix element of the transition operator. In Fig. 7.1 we show typical NLO Feynman diagrams from the leading power and power suppressed contributions of the total decay rate. A detailed description concerning the HQE coefficients is given in the next chapter.

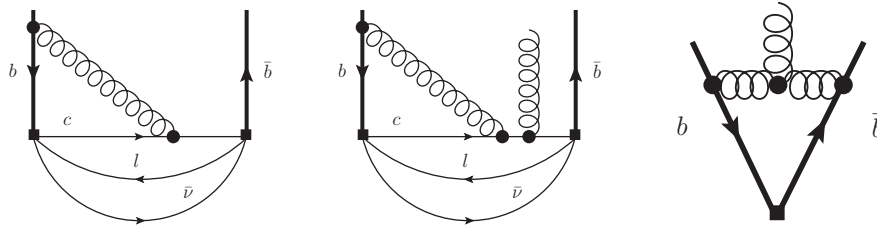


Figure 7.1: Perturbation theory diagrams for the matching computation at NLO level. Left diagram shows a contribution to the partonic rate, centered and right diagram contributes to power corrections (insertion of a background gluon).

Leading Power Coefficient (Partonic Width)

The coefficient C_0 up to NLO in α_s reads

$$C_0(r) = C_0^{\text{LO}}(r) + \left(\frac{\alpha_s}{\pi} \right) C_F C_0^{\text{NLO}}(r) + \mathcal{O}(\alpha_s^2) \quad (7.25)$$

as a function of the mass ratio $r \equiv m_c^2/m_b^2$. As an example, we explicitly show the computation of the leading order contribution

$$C_0^{\text{LO}}(r) = \frac{192\pi^3}{m_b^5} \text{Im} \int dx e^{ipx} \bar{u}(p) \gamma_\mu P_L S(x; m_c) \gamma_\nu P_L u(p) \times \Pi_{\mu\nu}^{\text{lep}}(x) \quad (7.26)$$

$$= \frac{192\pi^3}{m_b^5} \text{Im} \int_q \text{Tr} \left[P_+ \gamma_\mu P_L S(p - q; m_c) \gamma_\nu P_L \right] \times \Pi_{\mu\nu}^{\text{lep}}(q), \quad (7.27)$$

where the external momentum fulfills the on-shell condition $p = m_b v$. In the equation above we introduced the bare quark propagator $S(x; m_c)$ in configuration and $S(q; m_c)$ in momentum space. The function $\Pi_{\mu\nu}^{\text{lep}}(q)$ is the Fourier transform of the leptonic tensor

$$\Pi_{\mu\nu}^{\text{lep}}(q) = - \int_l \text{Tr} \left[\gamma_\mu P_L S(l - q; 0) \gamma_\nu P_L S(l; 0) \right] = (q_\mu q_\nu - q^2 g_{\mu\nu}) \Pi(q^2). \quad (7.28)$$

It is transverse in the massless lepton limit. The invariant amplitude $\Pi(q^2)$ has a single pole according to

$$\Pi(q^2) = \frac{G}{\varepsilon} \times \left(\frac{2}{3} - \frac{2}{9} \varepsilon \right) \times \frac{1}{[-q^2]^\varepsilon}. \quad (7.29)$$

The LO coefficient of the partonic width stems from a single diagram (with two-loops from the c -quark and both leptons), which is given by

$$C_0^{\text{LO}} = 1 - 8r - 12r^2 \log(r) + 8r^3 - r^4. \quad (7.30)$$

Including radiative QCD corrections to the leading order diagram, the NLO coefficient reads

$$\begin{aligned} C_0^{\text{NLO}}(r) = & \frac{1}{2}(1 - r^2) \times \left\{ \left(\frac{25}{4} - \frac{239}{3}r + \frac{25}{4}r^2 \right) + \left(-\frac{17}{3} + \frac{64}{3}r - \frac{17}{3}r^2 \right) \log(1 - r^2) \right\} \\ & \left(-20 - 90r + \frac{4}{3}r^2 - \frac{17}{3}r^3 \right) r \log(r) + \left(-36 - r^2 \right) r^2 \log^2(r) \\ & 4(1 + 30r^2 + r^4) \log(1 - r) \log(r) + (1 + 16r^2 + r^4) \left(3 \text{Li}_2(r) - \frac{1}{2} \pi^2 \right) \\ & + 32r^{3/2}(1 + r) \left(\pi^2 - 4 \text{Li}_2^- + 2 \log(r) \log \left(\frac{1 + \sqrt{r}}{1 - \sqrt{r}} \right) \right) \end{aligned} \quad (7.31)$$

where $r \equiv m_c^2/m_b^2$. Here, we also defined the function $\text{Li}_2^- \equiv \text{Li}_2(\sqrt{r}) - \text{Li}_2(-\sqrt{r})$. Our result is an independent confirmation of the stated formulas in [146], which have been determined from the differential cross-section of inclusive weak decays. In Fig. 7.2 the normalized coefficients C_0^{LO} and C_0^{NLO} are plotted against the quark mass ratio r . A detailed discussion of its computation is given in Ch. 8. The behavior of C_0 for small

charm-quark masses ($r \ll 1$) is

$$C_0(r) \rightarrow 1 - 8r + \left(\frac{\alpha_s}{\pi}\right) C_F \left[\frac{25}{8} - \frac{\pi^2}{2} - 34r - 12r \log(r) \right]. \quad (7.32)$$

Near the phase-space border ($r \approx 1$) reads

$$C_0(r) \rightarrow \frac{2}{5}(1-r)^5 - \left(\frac{\alpha_s}{\pi}\right) C_F \frac{3}{10}(1-r)^5. \quad (7.33)$$

For the computation of C_0 we used on-shell charm quarks. With Eq. (A.33) one can easily convert quark masses in the pole scheme to $\overline{\text{MS}}$ masses. Note that $C_0(r)$ changes its dependence on r significantly, see Fig. 7.3. The relative magnitude of the NLO contribution at a typical value of the mass ratio ($r = 0.07$) is

$$C_0(0.07) = 0.6 \left(1 - C_F \frac{\alpha_s}{\pi} 1.31 \right), \quad (7.34)$$

whereas the massless limit has the following value

$$C_0(0) = 1 - C_F \frac{\alpha_s}{\pi} 1.8. \quad (7.35)$$

Both values of C_0 (and Fig. 7.2) show a similar LO and NLO contribution behavior when normalized to their massless limit.

EOM Operator Coefficient

The coefficient of the operator \mathcal{O}_V is singled out by taking the matrix element between on-shell b -quarks and one gluon with vanishing momentum and longitudinal polarization, i.e. $A_\mu = v_\mu(vA)$. Due to the structure of the covariant derivative vD , one can also introduce an additional small momentum k , which shifts $p \rightarrow p+k$. By expanding the Feynman graphs in k that are associated to the leading power coefficient, we gain identical results if just expressions linear in kv are considered. The following form in terms of α_s is used:

$$C_V(r) = C_V^{\text{LO}}(r) + \left(\frac{\alpha_s}{\pi}\right) C_F C_V^{\text{NLO}}(r) + \mathcal{O}(\alpha_s^2), \quad (7.36)$$

where the color factor at NLO is C_F . The LO coefficient of the EOM operator reads

$$C_V^{\text{LO}}(r) = 5 - 24r - 12r^2 \log(r) + 24r^2 - 8r^3 + 3r^4$$

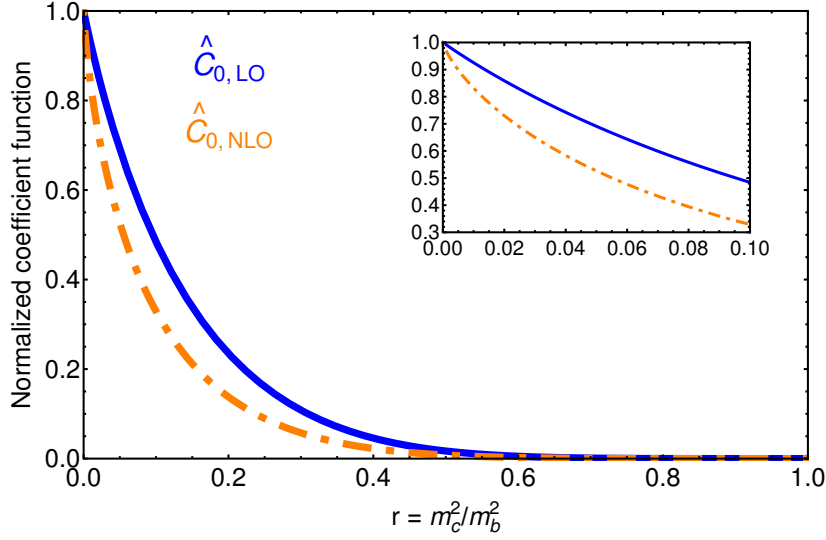


Figure 7.2: Plot of the normalized leading power coefficient ($\hat{C}_0 \equiv C_0(r)/C_0(0)$) against the quark mass ratio $r = m_c^2/m_b^2$. The blue solid (orange dashed-dotted) line denotes the LO (NLO) contribution in the pole mass scheme.

$$= \frac{1}{m_b^4} \frac{d}{dm_b} \left[m_b^5 \times C_0^{\text{LO}}(r) \right]. \quad (7.37)$$

We also calculate the NLO coefficient:

$$\begin{aligned} C_V^{\text{NLO}}(r) = & \left(3\text{Li}_2(r) - \frac{1}{2}\pi^2 \right) (1 - 16r^2 - 3r^4) - \frac{1}{24}(1-r)(25 - 1011r - 1487r^2 + 189r^3) \\ & + \frac{1}{6}r(12 + 450r + 4r^2 + 45r^3) \ln(r) - \frac{1}{6}(1-r)(11 + 11r + 83r^2 - 45r^3) \ln(1-r) \\ & + \frac{3}{2}r^2(4 + r^2) \ln^2(r) + 2(1 - 30r^2 - 3r^4) \ln(1-r) \ln(r) \\ & + 8r^{3/2}(1 + 3r) \left(4\text{Li}_2^- - \pi^2 - 2 \ln \left(\frac{1 + \sqrt{r}}{1 - \sqrt{r}} \right) \ln(r) \right). \end{aligned} \quad (7.38)$$

Around the massless charm quark limit C_V reads

$$C_V(r) \rightarrow 5 - 24r + \left(\frac{\alpha_s}{\pi} \right) C_F \left[-\frac{25}{24} - \frac{\pi^2}{2} + 36r \log(r) - 8\pi^2 r^{3/2} \right]. \quad (7.39)$$

On the border of the phase space ($r \approx 1$) the EOM coefficient function approaches asymptotically

$$C_V(r) \rightarrow 4(1-r)^4 - \left(\frac{\alpha_s}{\pi}\right) C_F 3(1-r)^4. \quad (7.40)$$

For a typical quark mass ratio $r = 0.07$ we obtain

$$C_V(0.07) = 3.6\left(1 - C_F \frac{\alpha_s}{\pi} 1.1\right), \quad (7.41)$$

while the massless limit is

$$C_V(0) = 5\left(1 - C_F \frac{\alpha_s}{\pi} 1.2\right). \quad (7.42)$$

One can see that the r -dependence of C_V is similar to C_0 . Therefore a reasonable NLO two-mass extrapolation based on the partonic width behavior is possible.

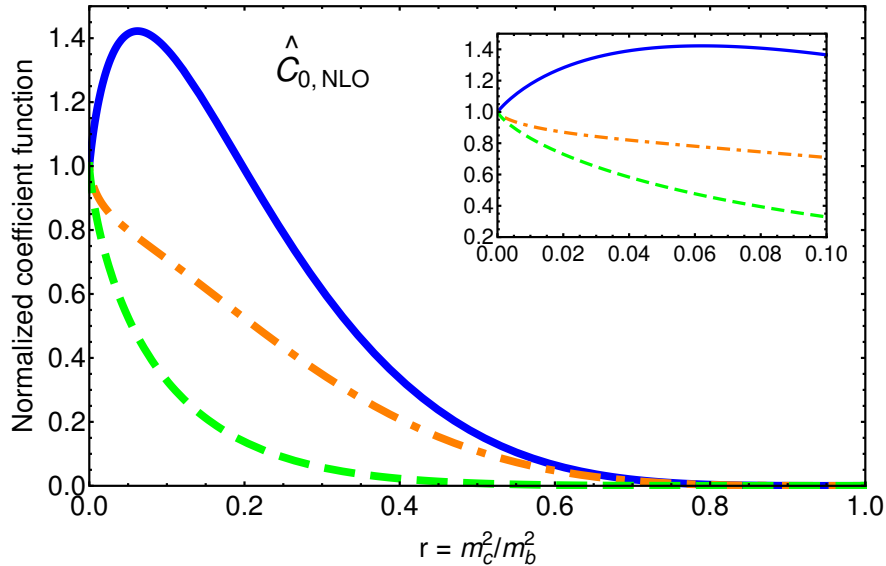


Figure 7.3: Plots of the normalized leading power coefficient ($\hat{C}_0 \equiv C_0(r)/C_0(0)$) against the quark mass ratio $r = m_c^2/m_b^2$. The blue solid (orange dash-dotted) line denotes the NLO contribution in the $\overline{\text{MS}}$ scheme at $\mu = m_b$ (m_c). The green dashed line shows the NLO contribution in the pole mass scheme.

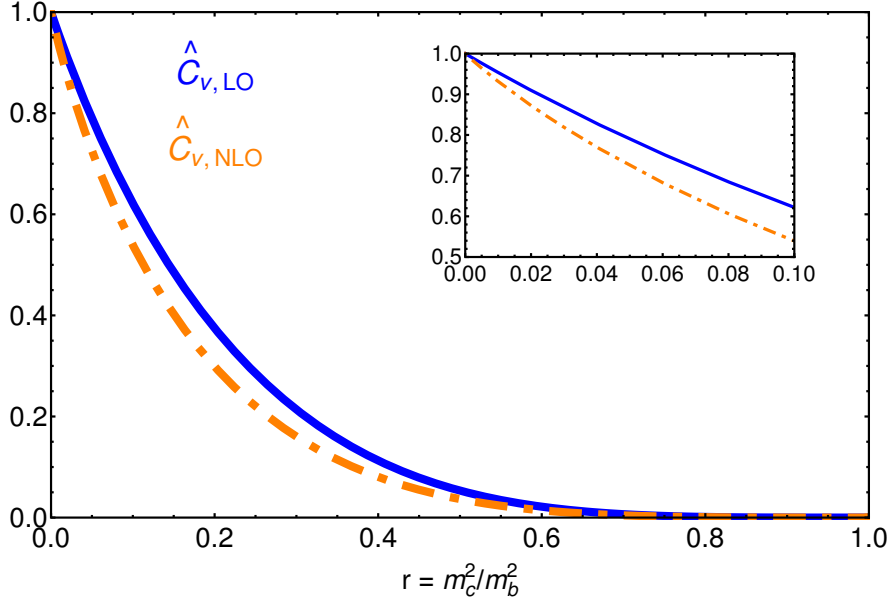


Figure 7.4: Plot of the normalized EOM coefficient ($\hat{C}_V \equiv C_V(r)/C_V(0)$) against the quark mass ratio $r = m_c^2/m_b^2$. The blue solid (orange dashed-dotted) line denotes the LO (NLO) contribution in the pole mass scheme.

Chromomagnetic Operator Coefficient

Due to the structure of the operator $\mathcal{O}_G = \frac{g_s}{2} \bar{h}_v \sigma_{\mu\nu} G^{\mu\nu} h_v$, the resulting coefficient function has two color factors, namely the invariants C_F and C_A . The coefficient function up to NLO is

$$C_G(r) = C_G^{\text{LO}}(r) + \frac{\alpha_s}{\pi} \left[C_F C_G^{\text{NLO,F}}(r) + C_A C_G^{\text{NLO,A}}(r) \right] + \mathcal{O}(\alpha_s^2). \quad (7.43)$$

The LO coefficient of the chromomagnetic operator reads

$$C_G^{\text{LO}}(r) = 2 \times C_0^{\text{LO}}(r) = 2(1 - 8r - 12r^2 \log(r) + 8r^3 - r^4). \quad (7.44)$$

We also calculate the NLO coefficient with full mass dependence. For brevity, only the massless limit $r \rightarrow 0$ results are given at this point. The fully renormalized coefficient $C_G^r = C_G - \tilde{C}_G C_0$ in this limit reads

$$C_G^r(r) \rightarrow 2 + \frac{\alpha_s}{\pi} \left[C_F \left(-\frac{47}{36} - \frac{7\pi^2}{9} \right) + C_A \left(\frac{49}{18} - \frac{\pi^2}{9} \right) \right]. \quad (7.45)$$

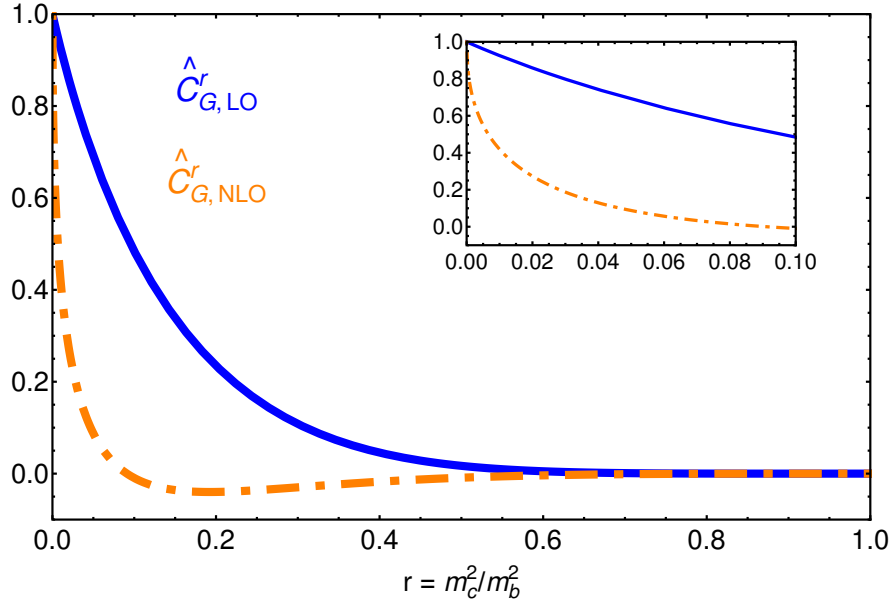


Figure 7.5: Plot of the normalized chromomagnetic operator coefficient ($\hat{C}_G^r \equiv C_G^r(r)/C_G^r(0)$) against the quark mass ratio $r = m_c^2/m_b^2$. The blue solid (orange dashed-dotted) line denotes the LO (NLO) contribution in the pole mass scheme.

The coefficient C_G^r has the asymptotics

$$C_G^r(r) \rightarrow \frac{4}{5}(1-r)^5 + \left(\frac{\alpha_s}{\pi}\right) C_F (1-r)^4 \quad (7.46)$$

near the border of phase-space ($r \approx 1$).

Renormalization Group Invariant Chromomagnetic Operator Coefficient

To present the final result of the chromomagnetic operator coefficient we prefer the renormalization group (RG) invariant expression entering the HQET Lagrangian after the use of equation of motion. This combination also determines the mass splitting in the ground state multiplets due to spin orientation. Hence, the final coefficient is given by

$$C_{\bar{\mu}_G^2}(r) = -C_V(r) + \frac{C_G^r(r)}{C_{\text{mag}}(\mu)} \quad (7.47)$$

after taking the heavy meson matrix element. With this combination the invariant hadronic matrix element in the HQE reads $\bar{\mu}_G^2 \equiv -1/(2m_B)C_{\text{mag}}(\mu)\langle\mathcal{O}_G(\mu)\rangle$. If we write the full coefficient, which is decomposed into the color structure with NLO accuracy, the final expression $C_{\bar{\mu}_G^2}$ to the invariant chromomagnetic moment reads

$$C_{\bar{\mu}_G^2}(r) = C_{\bar{\mu}_G^2}^{\text{LO}}(r) + \frac{\alpha_s}{\pi} \left[C_F C_{\bar{\mu}_G^2}^{\text{NLO,A}}(r) + C_A C_{\bar{\mu}_G^2}^{\text{NLO,F}}(r) \right] + \mathcal{O}(\alpha_s^2). \quad (7.48)$$

At the leading order we obtain the well known result

$$C_{\bar{\mu}_G^2}^{\text{LO}} = -3 + 8r - 24r^2 - 12r^2 \ln(r) + 24r^3 - 5r^4. \quad (7.49)$$

The C_A color structure coefficient at NLO reads

$$\begin{aligned} C_{\bar{\mu}_G^2}^{\text{NLO,A}} &= \frac{1}{108}(1-r)(156 - 4081r - 354r^2 - 405r^3) \\ &+ \frac{1}{9}(6\text{Li}_2(r) - \pi^2)(1 - 6r + 24r^2 - 11r^3) \\ &- \frac{(1-r)}{54r}(15 + 20r - 196r^2 - 292r^3 - 27r^4) \ln(1-r) \\ &- \frac{1}{54}r(786 + 972r + 131r^2 - 27r^3) \ln(r) - \frac{2}{9}(1 + 9r - 93r^2 + 19r^3) \ln(1-r) \ln(r) \\ &+ \frac{1}{9}r(9 - 33r + 5r^2) \ln(r)^2 \\ &+ \frac{8}{3}r^{1/2}\left(1 - \frac{11}{3}r\right) \left(4\text{Li}_2^- - \pi^2 - 2\ln(r) \ln\left(\frac{1+\sqrt{r}}{1-\sqrt{r}}\right)\right), \end{aligned} \quad (7.50)$$

whereas the C_F color structure is

$$\begin{aligned} C_{\bar{\mu}_G^2}^{\text{NLO,F}} &= -\frac{1}{216}(1-r)(321 - 13747r + 5421r^2 - 3807r^3) \\ &+ \frac{1}{18}(6\text{Li}_2(r) - \pi^2)(5 + 72r - 72r^2 - 88r^3 + 45r^4) \\ &- \frac{(1-r)}{54r}(12 - 19r + 917r^2 - 1795r^3 + 585r^4) \ln(1-r) \\ &+ \frac{1}{54}r(1500 - 330r + 2668r^2 - 585r^3) \ln(r) \\ &+ \frac{2}{9}(11 + 54r - 48r^2 - 94r^3 + 45r^4) \ln(1-r) \ln(r) \\ &- \frac{1}{18}r(72 + 60r - 112r^2 + 45r^3) \ln(r)^2 \\ &+ \frac{32}{3}\left(1 - \frac{4}{3}r\right)r^{1/2} \left(4\text{Li}_2^- - \pi^2 - 2\ln(r) \ln\left(\frac{1+\sqrt{r}}{1-\sqrt{r}}\right)\right). \end{aligned} \quad (7.51)$$

In order to get an impression of the mass ratio dependence we state the massless charm quark limit with inserted color factors $C_F = 4/3$ and $C_A = 3$ here, i.e.

$$C_{\bar{\mu}_G^2}(0) = -3 + \frac{\alpha_s}{\pi} \left(\frac{94}{27} - \frac{19\pi^2}{27} \right). \quad (7.52)$$

The behavior near the phase-space border is for the NLO contributions

$$C_{\bar{\mu}_G^2}^{\text{NLO}}(r) \rightarrow 4C_F(1-r)^4 \quad (7.53)$$

and at LO

$$C_{\bar{\mu}_G^2}^{\text{LO}}(r) \rightarrow -4(1-r)^4. \quad (7.54)$$

For a typical quark mass ratio $r = 0.07$, we obtain for the $C_{\bar{\mu}_G^2}$:

$$C_{\bar{\mu}_G^2}(0.07) = -2.4 \left(1 + \frac{\alpha_s}{\pi} [-1.53 C_F + 0.36 C_A] \right) = -2.4 \left(1 - 0.96 \frac{\alpha_s}{\pi} \right) \quad (7.55)$$

while the massless limit reads

$$C_{\bar{\mu}_G^2}(0) = -3 \left(1 + \frac{\alpha_s}{\pi} [1.33 C_F - 0.21 C_A] \right) = -3 \left(1 + 1.15 \frac{\alpha_s}{\pi} \right). \quad (7.56)$$

In the previous sections we have shown that the coefficient functions C_0 and C_V have a similar behavior of the LO and NLO contributions when changing r . The normalized function $C_{\bar{\mu}_G^2}^{\text{LO}}$ also has the common decay towards $r = 1$, whereas $C_{\bar{\mu}_G^2}^{\text{NLO}}$ is negative in the massless limit and decays very rapidly to positive values (see also Fig. 7.6).

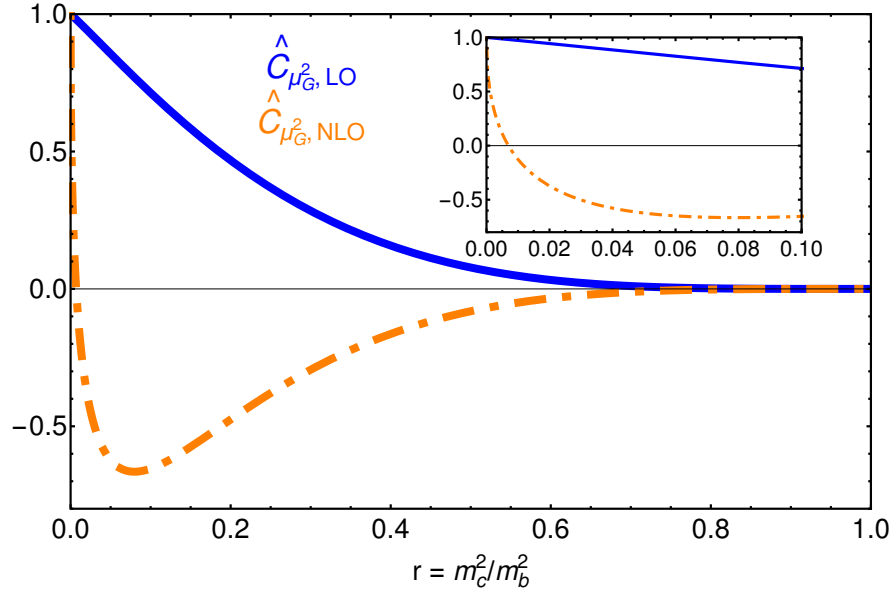


Figure 7.6: Plot of the normalized RG-invariant chromomagnetic operator coefficient ($\hat{C}_{\bar{\mu}_G^2} \equiv C_{\bar{\mu}_G^2}(r)/C_{\bar{\mu}_G^2}(0)$) against the quark mass ratio $r = m_c^2/m_b^2$. The blue solid (orange dashed-dotted) line denotes the LO (NLO) contribution in the pole mass scheme.

7.4 The Total Width and Moments of the Differential Distribution

The final result for the total width with power suppressed terms and NLO accuracy is

$$\Gamma/\tilde{\Gamma}_0 = \left(1 - 1.78 \frac{\alpha_s}{\pi}\right) \left[1 - \frac{\mu_\pi^2}{2m_b^2}\right] - 3.89 \left(1 - 0.92 \frac{\alpha_s}{\pi}\right) \frac{\bar{\mu}_G^2}{2m_b^2}. \quad (7.57)$$

Here, we introduce the common normalization $\tilde{\Gamma}_0 = \Gamma_0 |V_{cb}|^2 \times C_0^{\text{LO}}(r)$. We also compute some relevant moments in the lepton pair invariant mass q^2 analytically with full mass dependence. The moments are defined through the relation

$$\hat{M}_{q^2}^{(n)} = \frac{1}{M_{\text{parton}, q^2}^{(n)}} \int d\Gamma \left(\frac{q^2}{m_b^2}\right)^n. \quad (7.58)$$

We choose the n -th moment in q^2 of the partonic rate at LO

$$M_{\text{parton}, q^2}^{(n)} = \int d\Gamma_{\text{parton}} \times \left(\frac{q^2}{m_b^2}\right)^n \quad (7.59)$$

as normalization, i.e. all coefficient functions are zero except C_0^{LO} and higher moments of C_0^{LO} . For the q^2 moments up to third order we obtain with $r = 0.0625$:

$$\begin{aligned} \hat{M}_{q^2}^{(1)} &= \left(1 - 1.65 \frac{\alpha_s}{\pi}\right) \left\{1 - \frac{\mu_\pi^2}{2m_b^2}\right\} - 8.99 \left(1 - 0.68 \frac{\alpha_s}{\pi}\right) \frac{\bar{\mu}_G^2}{2m_b^2}, \\ \hat{M}_{q^2}^{(2)} &= \left(1 - 1.56 \frac{\alpha_s}{\pi}\right) \left\{1 - \frac{\mu_\pi^2}{2m_b^2}\right\} - 14.39 \left(1 - 0.56 \frac{\alpha_s}{\pi}\right) \frac{\bar{\mu}_G^2}{2m_b^2}, \\ \hat{M}_{q^2}^{(3)} &= \left(1 - 1.48 \frac{\alpha_s}{\pi}\right) \left\{1 - \frac{\mu_\pi^2}{2m_b^2}\right\} - 20.00 \left(1 - 0.47 \frac{\alpha_s}{\pi}\right) \frac{\bar{\mu}_G^2}{2m_b^2}. \end{aligned}$$

Moments in the variable $H = (p - q)^2 - m_c^2$ are defined as

$$\hat{M}_H^{(n)} = \int \frac{d\Gamma}{\Gamma_0} \times \left(\frac{(p - q)^2 - m_c^2}{m_b^2}\right)^n. \quad (7.60)$$

We obtain the following results for moments in H up to third order using $r = 0.0625$:

$$\begin{aligned} M_H^{(1)} &= 0.057 \frac{\alpha_s}{\pi} \left\{1 - \frac{\mu_\pi^2}{2m_b^2}\right\} + 0.397 \left(1 - 2.304 \frac{\alpha_s}{\pi}\right) \frac{\bar{\mu}_G^2}{2m_b^2}, \\ M_H^{(2)} &= 0.0058 \frac{\alpha_s}{\pi} \left\{1 - \frac{\mu_\pi^2}{2m_b^2}\right\} + 0.0554 \frac{\alpha_s}{\pi} \frac{\bar{\mu}_G^2}{2m_b^2}, \\ M_H^{(3)} &= 0.0011 \frac{\alpha_s}{\pi} \left\{1 - \frac{\mu_\pi^2}{2m_b^2}\right\} + 0.0069 \frac{\alpha_s}{\pi} \frac{\bar{\mu}_G^2}{2m_b^2}. \end{aligned}$$

7.5 Impact on CKM Matrix Element $|V_{cb}|$

An important implication of the calculations, as presented above, is the precision improvement of the inclusive B decay into charmed meson states and the accompanied CKM element V_{cb} . Since we have the analytical result at hand, we can immediately estimate its influence on $|V_{cb}|$ in a simple manner. Assuming the shift is solely driven by the NLO correction in the coefficient of the chromomagnetic moment we find

$$\frac{\Delta|V_{cb}|}{|V_{cb}|} \simeq -C_{\bar{\mu}_G^2}^{\text{NLO}} \left(\frac{\alpha_s}{\pi}\right) \times \frac{\bar{\mu}_G^2}{2m_b^2} \times \frac{1}{2C_0(r)}. \quad (7.61)$$

Here, we neglect power-suppressed terms in the denominator due to their small contribution. Furthermore, we assume $r = 0.0625$, $\alpha_s/\pi = 0.1$ and use the mass splitting approximation in (7.23) for $\bar{\mu}_G^2$. With this input the relative shift is

$$\frac{\Delta|V_{cb}|}{|V_{cb}|} = -0.14\% \quad (7.62)$$

in the value of $|V_{cb}|$. In the massless limit the new correction leads to a change of

$$\left. \frac{\Delta|V_{cb}|}{|V_{cb}|} \right|_{m_c=0} = +0.14\%. \quad (7.63)$$

7.6 Discussion of Results

We apply the heavy quark expansion method to heavy hadron decays (with one heavy quark), in order to compute analytically the leading power coefficient function and the coefficient of the power-suppressed chromomagnetic operator. The former can be related to the partonic decay rate, whereas the latter describes a breaking term of spin and flavor symmetry in the realm of HQET. A prominent application of the computed results is the precision determination of the CKM matrix element $|V_{cb}|$ from inclusive semileptonic $b \rightarrow c$ transitions. Corrections to the chromomagnetic moment are parametrically the largest missing piece in the analysis of inclusive weak decays.

An outline of the main results is:

- The short-distance coefficients for HQE operators of dimension 3 to 5 are computed up to next-to-leading order in QCD perturbation theory where the charm quark mass was taken into account. Leptons were considered as massless. The leading power coefficient C_0 (from $\bar{h}_v h_v$) was computed by taking on-shell b -quark states. In order to renormalize this expression it is sufficient to multiply the bare results (directly from diagram computation) with the on-shell renormalization constant Z_2^{OS} . For convenience, we chose a specific basis to determine the coefficient of the chromomagnetic operator C_G in the HQE. By substituting the leading power operator for the local operator $\bar{b}\psi b$ we ended up with the difference of the chromomagnetic and the local operator coefficient \tilde{C}_G . This combination is easier to compute since some of the emerging divergences cancel. For the final coefficient of the scale invariant chromomagnetic moment we also computed the coefficient C_V to the dimension-4 operator $\bar{h}_v v D h_v$. Each coefficient was extracted with suitable projectors reflecting the relevant structure of the corre-

sponding operator. As a first step, we calculated the massless charm quark case, which also provides an additional cross-check to the computation with a massive charm quark. Both calculations yield identical results when taking the massless limit of the result with full mass dependence.

- All necessary tools and computational environments were built up in `Mathematica`. In the analytical calculation we used the integration-by-parts method to reduce diagram expressions into a minimal set of master integrals. In case of full mass dependence the absorptive part of one master integral at two-loop level and four integrals at three-loop level are computed. In the case of a massless charm quark just one two-loop master and three three-loop masters, respectively, were computed.
- We give explicit expressions for the total width of semileptonic B decays into charmed mesons and a dilepton pair. For a specific value of the mass ratio $r = m_c^2/m_b^2 = 0.0625$ our result matches the numerical calculation as stated in Ref. [134]. This is a powerful cross-check, since both studies were performed independently with two different approaches. The NLO contribution of the chromomagnetic moment (leading power) coefficient reduces the LO one by about 9% (18%), assuming $\alpha_s/\pi = 0.1$. It turned out that the mass dependence is strongly affected by the charm-quark-mass scheme. If we use the charm quark mass in the pole scheme, each coefficient shows an improved convergence behavior as a function of r at small r .
- With analytical expressions for each coefficient function at hand, we also determine certain moments of differential distributions, which is of experimental interest. In addition to the total width we compute the moments over the invariant mass-squared of the leptonic pair q^2 and the partonic invariant mass-squared $(p - q)^2 - m_c^2$. We see that higher moments in q^2 decrease the influence of radiative corrections, whereas the power-suppressed coefficient of the chromomagnetic moment has an overall increasing impact. Numerically the partonic moments decrease very quickly with higher order.
- The shift of the CKM matrix element $|V_{cb}|$ due to the new correction is roughly -0.14% assuming pole masses for charm and bottom quark. The massless limit shifts $|V_{cb}|$ to positive direction by the same amount. One can compare this shift to corrections of higher order in Λ_{QCD}/m_b . The tree-level $(\Lambda_{\text{QCD}}/m_b)^3$ contribution induces a relative shift of $|V_{cb}|$ of $\sim -1.4\%$, whereas the terms of order

$(\Lambda_{\text{QCD}}/m_b)^4$ generate a shift of about 0.3% [135]. This means that our correction has roughly the same impact as the dimension-7 operator contribution at tree-level. For the first time, the impact on $|V_{cb}|$ is estimated due to the NLO corrections to the chromomagnetic operator by knowing the analytical expression with and without the charm quark mass.

Technical Aspects of Perturbative Corrections to Inclusive B-Decays

In the following, we give a detailed description of the technical aspects that pertain to our calculation. We remind the reader on the structure of the expansion in $1/m_b$ and the simultaneous expansion of the coefficient functions in α_s . The HQE of the transition operator to the relevant order is given by

$$\text{Im } \hat{T}_0 = C_0 \left(\mathcal{O}_0 - \frac{\mathcal{O}_\pi}{2m_b^2} \right) + C_V \frac{\mathcal{O}_V}{m_b} + C_G \frac{\mathcal{O}_G}{2m_b^2}. \quad (8.1)$$

For convenience we also consider the local operator

$$\bar{b}\psi b = \mathcal{O}_0 + \frac{\mathcal{O}_\pi}{2m_b^2} + \tilde{C}_G \frac{\mathcal{O}_G}{2m_b^2}. \quad (8.2)$$

Our calculation addresses all of the above-mentioned coefficients up to NLO in α_s . These are:

1. Leading power coefficient C_0 ,
2. Equation of motion (EOM) coefficient C_V ,
3. Chromomagnetic coefficient C_G ,
4. Chromomagnetic coefficient of the $\bar{b}\psi b$ operator \tilde{C}_G .

We will discuss the respective details in Sects. 8.1 to 8.4.

8.1 Leading Power Coefficient (Partonic Width)

A convenient way to compute the leading power coefficient C_0 is to take the imaginary part of the transition operator \hat{T}_0 between on-shell ($p = m_b v$) heavy quark states. These states are unphysical since quarks are confined in hadrons, but the expansion in

(8.1) holds on the operator level. As a consequence of this choice, the matrix elements of all operators that emerge in the HQE vanish, except for the leading-power operator:

$$\text{Im} \langle b(p) | \hat{T}_0 | b(p) \rangle = C_0 \langle b(p) | \bar{h}_v h_v | b(p) \rangle. \quad (8.3)$$

The on-shell wave-function renormalization constant of the effective quark field operator is $\tilde{Z}_2^{\text{OS}} = 1$, due to scale-free correction terms. That is

$$\langle 0 | h_v | b(mv + \Delta p) \rangle = \sqrt{\tilde{Z}_2^{\text{OS}}} u_v(\Delta p) = u_v(\Delta p), \quad (8.4)$$

where $u_v(\Delta p)$ is the HQET spinor [147]. The non-vanishing matrix element is

$$\langle b(p) | \bar{h}_v h_v | b(p) \rangle = 2m_b \quad (8.5)$$

to NLO in α_s . Therefore the matching formula to determine the leading power coefficient is

$$C_0 = \frac{1}{2m_b} \text{Im} \langle b(p) | \hat{T}_0 | b(p) \rangle. \quad (8.6)$$

The perturbative series with NLO accuracy reads

$$C_0(r) = C_0^{\text{LO}}(r) + \left(\frac{\alpha_s}{\pi} \right) C_F C_0^{\text{NLO}}(r), \quad (8.7)$$

which depends on the quark mass ratio $r \equiv m_c^2/m_b^2$. To leading order the coefficient C_0 can be extracted from one Feynman graph (see Fig. 8.1 (a)), which is given by

$$C_0^{\text{LO}}(r) = \frac{1}{2m_b} \text{Im} \langle b(p) | \hat{T}_0 | b(p) \rangle \Big|_{\text{LO}} = \frac{1}{\hat{\Gamma}_b} \text{Im} \int_q \text{Tr} \left[P_+ \times \Gamma_{\text{lo}}^{\mu\nu}(p, q; m_c) \right] \times \Pi_{\mu\nu}^{\text{lep}}(q), \quad (8.8)$$

where $\hat{\Gamma}_b \equiv m_b^2/(192\pi^3)$. We explicitly separate the parton kernel function from the leptonic part $\Pi_{\mu\nu}^{\text{lep}}$, see Eq. (7.28), in the integration. The parton kernel reads

$$\Gamma_{\text{lo}}^{\mu\nu} = \gamma^\nu P_L S(p - q; m_c) \gamma^\mu P_L \quad (8.9)$$

and, hence, the integration in (8.8) leads to two-loop master integrals of the sunset type.

The NLO QCD corrections to C_0 stem from four Feynman graphs as shown in Fig. 8.1 (b)-(e). These include

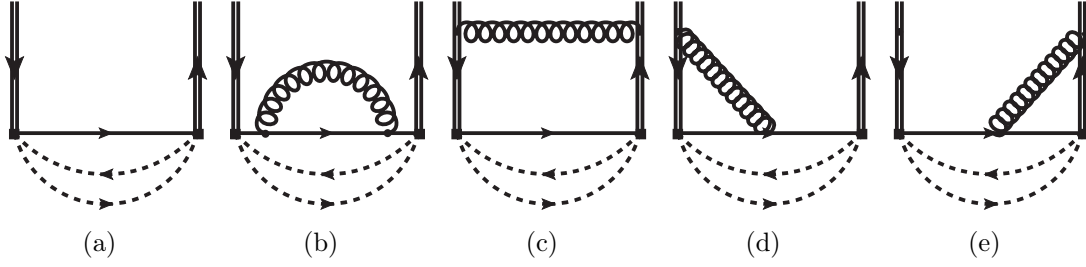


Figure 8.1: Leading order Feynman graph in (a) and next-to-leading order Feynman graphs in (b)-(e) for the leading power coefficient C_0 .

1. the self-energy correction to the charm-quark propagator (se),
2. the box-type correction, where a gluon line connects both heavy b -quarks (bx),
3. two radiative corrections to the b -to- c current (vx).

Note that both vertex contributions are equal. Altogether we obtain the following NLO contribution for the leading power coefficient:

$$C_0^{\text{NLO}}(r) = \sum_j C_0^{\text{NLO};j} = C_0^{\text{NLO};\text{se}} + C_0^{\text{NLO};\text{bx}} + 2 \times C_0^{\text{NLO};\text{vx}}. \quad (8.10)$$

The bare contributions have the general form:

$$C_0^{\text{bare},\text{NLO};j}(r) = \frac{1}{\hat{\Gamma}_b} \text{Im} \int_q \int_k \text{Tr} \left[P_+ \times \Gamma_j^{\mu\nu}(p, q, k; m_c) \right] \times \Pi_{\mu\nu}^{\text{lep}}(q), \quad (8.11)$$

where the parton kernels are

$$\Gamma_{se}^{\mu\nu} = \gamma^\nu P_L S(p - q; m_c) \gamma^\beta S(k - q; m_c) \gamma^\alpha D_{\alpha\beta}(p - k) S(p - q; m_c) \gamma^\mu P_L, \quad (8.12)$$

$$\Gamma_{bx}^{\mu\nu} = \gamma^\beta S(k; m_b) \gamma^\nu P_L S(k - q; m_c) \gamma^\mu P_L S(k; m_b) \gamma^\alpha D_{\alpha\beta}(p - k), \quad (8.13)$$

$$\Gamma_{vx}^{\mu\nu} = \gamma^\nu P_L S(p - q; m_c) \gamma^\alpha S(k - q; m_c) \gamma^\mu P_L S(k; m_b) \gamma^\alpha D_{\alpha\beta}(p - k). \quad (8.14)$$

Here we use an abbreviation for the quark and the gluon propagator:

$$S(k; m) \equiv \frac{\not{k} + m}{k^2 - m^2 + i0}, \quad (8.15)$$

$$D_{\alpha\beta}(k) \equiv \frac{-i}{k^2 + i0} \left[g_{\alpha\beta} - \xi \frac{k_\alpha k_\beta}{k^2} \right] \quad (8.16)$$

and use the Landau gauge $\xi = 0$. These diagrams all have a common QCD color structure. The common color factor is

$$\sum_{a,b;k,l} (t^a)_{ik} (t^b)_{lj} \delta^{ab} \delta^{kl} = \sum_a (t^a t^a)_{ij} = C_F \delta_{ij}, \quad (8.17)$$

where $C_F = 4/3$ is the $SU(3)$ Casimir invariant.

The complexity of computation for each coefficient as listed in Eq. (8.10) increases from left to right. After the integration-by-parts reduction, we obtain eight masters with a non-vanishing imaginary part (see Appendix C.1).

Corrections to the charm-quark propagator at NLO level have the simplest structure. Only integrals of the sunset-type contribute. The box diagram also has factorizable integrals built from the product of two-loop integrals of the sunset-type and a massive one-loop tadpole. The vertex correction is the most complicated contribution to C_0^{NLO} . It contains all four masters including two non-factorizable ones. In Appendix C we list the required two- and three-loop spectral functions and comment on their calculation. As a cross-check we also calculate C_0 for a massless charm quark. The calculation simplifies drastically if only the bottom quark is massive. The number of masters reduces to three (see Appendix C.2): These are a sunset-type integral with only massless lines, a factorizable master which is the product of a two-loop sunset integral and a massive tadpole, and a non-factorizable master integral.

In order to renormalize the expression from direct computation of the Feynman graphs, we perform an on-shell renormalization by multiplying the bare result of C_0 with

$$Z_2^{\text{OS}} = 1 - C_F \frac{\alpha_s}{4\pi} \left(3 \times \left[\frac{1}{\varepsilon} + \log \left(\frac{\mu^2}{m_b^2} \right) \right] + 4 \right). \quad (8.18)$$

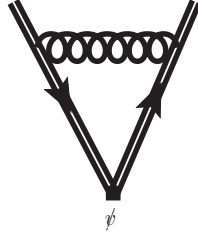
We fix the scale at $\mu = m_b$ for the rest of the calculation. It can be restored if necessary due to the knowledge of the anomalous dimension. The renormalized result of the leading power coefficient is

$$C_0(r) = Z_2^{\text{OS}} \times C_0^{\text{bare}}(r). \quad (8.19)$$

The full analytical expression is given in Eqs. (7.30) and (7.31).

Note that we can also renormalize C_0^{bare} by computing the vertex correction to the heavy-quark current \tilde{C}_0^{NLO} , see also Fig. 8.2. The following combination of coefficient functions also yields the renormalized function C_0 :

$$C_0(r) = C_0^{\text{bare}} - C_0^{\text{LO}} \tilde{C}_0^{\text{NLO}}. \quad (8.20)$$

Figure 8.2: Vertex correction to the heavy-quark current \tilde{C}_0^{NLO} .

8.2 EOM Operator Coefficient

An auxiliary contribution to the chromomagnetic operator is the coefficient C_V of the operator $\mathcal{O}_V = \bar{h}_v(ivD)h_v$. To single out C_V we choose an on-shell bottom quark state and include an additional longitudinal polarized gluon with vanishing momentum. In this way we select the coefficient contribution from the gluon field $A_\mu = v_\mu(vA)$, which is related to vD by gauge invariance. The matching relation is

$$\text{Im} \langle b(p) | \hat{T}_0 | b(p) g(0) \rangle = \frac{C_V}{m_Q} \langle b(p) | \mathcal{O}_V | b(p) g(0) \rangle. \quad (8.21)$$

The perturbative series with NLO accuracy has the form

$$C_V(r) = C_V^{\text{LO}}(r) + \left(\frac{\alpha_s}{\pi}\right) C_F C_V^{\text{NLO}}(r). \quad (8.22)$$

The color factor of the coefficient C_V at NLO level is C_F due to the structure of the corresponding Feynman graphs. At LO level C_V is given by

$$C_V^{\text{LO}}(r) = \frac{1}{\hat{\Gamma}_b} \int_q \text{Tr} \left[P_+ \times \Gamma_{\text{lo},v}^{\mu\nu}(\varepsilon v, p, q; m_c) \right] \times \Pi_{\mu\nu}^{\text{lep}}(q). \quad (8.23)$$

The partonic kernel reads

$$\Gamma_{\text{lo},v}^{\mu\nu} = \gamma^\nu P_L S(p - q; m_c) (\varepsilon v) \not{v} S(p - q; m_c) \gamma^\mu P_L. \quad (8.24)$$

Here, we insert $(\varepsilon v) \not{v}$ to assess the longitudinal part of the background gluon insertion, following $\not{\varepsilon} = (\varepsilon v) \not{v} + \not{\varepsilon}_\perp$, see Fig. 8.3 (a). Alternatively, one can also compute the same contribution using a small momentum expansion near the quark mass-shell

$p \rightarrow p + (kv)v$, i.e.

$$\frac{1}{m_b - \not{p}} \rightarrow \frac{1}{m_b - \not{p}} + \frac{1}{m_b - \not{p}} (kv)\not{p} \frac{1}{m_b - \not{p}}, \quad (8.25)$$

where we keep the linear term in (kv) . Radiative corrections to C_V emerge from four Feynman graphs, see Fig. 8.3 (b) to (e). The introduced background gluons are attached to all possible spots on the graphs. Note that the two vertex corrections are again identical.

From this follows the EOM coefficient at NLO level:

$$C_V^{\text{NLO}}(r) = \sum_j C_V^{\text{NLO};j} = C_V^{\text{NLO};\text{se}} + C_V^{\text{NLO};\text{bx}} + 2 \times C_V^{\text{NLO};\text{vx}}. \quad (8.26)$$

NLO contributions have the general form

$$C_V^{\text{bare, NLO};j}(r) = \frac{1}{\tilde{\Gamma}_b} \sum_n \int_q \int_k \text{Tr} \left[P_+ \times \tilde{\Gamma}_{n;j}^{\mu\nu}(\varepsilon v, p, q, k; m_c) \right] \times \Pi_{\mu\nu}^{\text{lep}}(q). \quad (8.27)$$

For convenience, we introduce the fermion and gluon propagator with a gluon insertion:

$$S^{\text{int}}(q; m_c) = S(q; m_c) \times (\varepsilon v)\not{p} \times S(q; m_c) \quad \text{and} \quad D^{\text{int}}(q) = D(q) \times (\varepsilon v)\not{p} \times D(q). \quad (8.28)$$

The self-energy corrections to the charm quark propagator have four insertions:

$$\begin{aligned} \tilde{\Gamma}_{se;1}^{\mu\nu} &= \gamma^\nu P_L S^{\text{int}}(p - q; m_c) \gamma^\beta S(k - q; m_c) \gamma^\alpha D_{\alpha\beta}(p - k) S(p - q; m_c) \gamma^\mu P_L, \\ &\quad \vdots \\ \tilde{\Gamma}_{se;4}^{\mu\nu} &= \gamma^\nu P_L S(p - q; m_c) \gamma^\beta S(k - q; m_c) \gamma^\alpha D_{\alpha\beta}(p - k) S^{\text{int}}(p - q; m_c) \gamma^\mu P_L. \end{aligned} \quad (8.29)$$

In an analogous way, we determine the contributions from the box and vertex corrections, i.e.

$$\begin{aligned} \tilde{\Gamma}_{bx;1}^{\mu\nu} &= \gamma^\beta S^{\text{int}}(k; m_b) \gamma^\nu P_L S(k - q; m_c) \gamma^\mu P_L D_{\alpha\beta}(p - k) S(k; m_b) \gamma^\alpha, \\ &\quad \vdots \\ \tilde{\Gamma}_{bx;4}^{\mu\nu} &= \gamma^\beta S(k; m_b) \gamma^\nu P_L S(k - q; m_c) \gamma^\mu P_L D_{\alpha\beta}(p - k) S^{\text{int}}(k; m_b) \gamma^\alpha, \end{aligned} \quad (8.30)$$

and

$$\begin{aligned}
\tilde{\Gamma}_{vx;1}^{\mu\nu} &= \gamma^\nu P_L S^{\text{int}}(p-q; m_c) \gamma^\alpha S(k-q; m_c) \gamma^\mu P_L S(k; m_b) \gamma^\alpha D_{\alpha\beta}(p-k), \\
&\quad \vdots \\
\tilde{\Gamma}_{vx;4}^{\mu\nu} &= \gamma^\nu P_L S(p-q; m_c) \gamma^\alpha S(k-q; m_c) \gamma^\mu P_L S(k; m_b) \gamma^\alpha D_{\alpha\beta}^{\text{int}}(p-k). \tag{8.31}
\end{aligned}$$

We obtain the following color factors to the aforementioned contributions: All Feynman graphs with insertions on the quark-gluon loop include the $SU(3)$ Casimir invariant C_A . The color factor for insertions on the charm quark line in the loop yields

$$\sum_{a,c;j,l,m} (t^a)_{ij} (t^b)_{kl} (t^c)_{mn} \delta^{ac} \delta^{jk} \delta^{lm} = \sum_a (t^a t^b t^a)_{in} = \left(C_F - \frac{C_A}{2} \right) t^b \delta_{in}. \tag{8.32}$$

If the background gluon is attached on the gluon line in the loop, we find

$$\sum_{b,c;j,k} i f^{abc} (t^b)_{ij} (t^c)_{kl} \delta^{jk} = \frac{C_A}{2} t^a \delta_{il}. \tag{8.33}$$

Contributions which are proportional to C_A cancel explicitly in total as stated in Eq. (8.27). This is a good crosscheck for our calculation.

Here, the same topology of Feynman diagrams contributes as in the leading power coefficient C_0 and, hence, we have the same set of master integrals.

As for the leading power coefficient, the HQET spinor is free of correction terms, whereas the QCD partner requires additional renormalization. In order to renormalize the bare result, it is not sufficient to multiply C_V^{bare} by the on-shell renormalization constant Z_2^{OS} . Additional divergences stem from corrections to the external bottom quark legs including a single gluon insertion.

To determine all necessary contributions for C_V we consider the skeleton expansion of the total width. In accordance to the inclusive setup the total decay rate can be written in terms of Green's function, namely the quark propagator S and the 1PI kernel Λ :

$$\Gamma \sim (Z_2^{\text{OS}})^{-1} (S \Lambda S)_R. \tag{8.34}$$

For accessing the relevant Feynman graphs, we consider bare fields to write down all contributions and perform the computation. To illustrate the general matching

procedure we expand the Green's functions in kv to linear order:

$$S = \tilde{S}^{(0)} + \tilde{S}^{(1)} \frac{kv}{m_b} = Z_2^{\text{OS}} \frac{P_+}{kv} \left[1 + \Delta Z \frac{kv}{m_b} \right], \quad (8.35)$$

$$\Lambda = \Lambda_0 + \Lambda_1 \frac{kv}{m_b}. \quad (8.36)$$

Due to the operator structure of \mathcal{O}_V the transverse component of k should be neglected. Altogether the Green's function of the longitudinal expression of the total width reads

$$(Z_2^{\text{OS}})^{-1} (S \Lambda S)_R \rightarrow Z_2^{\text{OS}} (\tilde{S}^{(0)} \Lambda_0 \tilde{S}^{(0)} + (\tilde{S}^{(0)} \Lambda_1 \tilde{S}^{(0)} + 2\tilde{S}^{(1)} \Lambda_0 \tilde{S}^{(0)}) \frac{kv}{m_b} + \dots) \quad (8.37)$$

$$= Z_2^{\text{OS}} \left(\frac{P_+}{(kv)} \Lambda_0 \frac{P_+}{(kv)} \right) + Z_2^{\text{OS}} \left[\frac{P_+}{(kv)} \Lambda_1 \frac{P_+}{(kv)} + 2\Delta Z \frac{P_+}{(kv)} \Lambda_0 \frac{P_+}{(kv)} \right] \frac{kv}{m_b} + \dots \quad (8.38)$$

In Eq. (8.38) the first term yields the leading power coefficient C_0 , whereas the second term contributes to C_V . Here, the additional renormalization term $2\Delta Z \Lambda_0$ arises, which is necessary to cancel all divergences of C_V^{bare} . If we expand the quark-propagator in kv , we find

$$S^{-1} = \not{p} + \not{k} - m_0 - \Sigma(p+k) = \not{p} + \not{k} - m + \delta m - \Sigma(p+k) \quad (8.39)$$

$$= -2P_- m + (P_+ - P_-)kv + \delta m - \left[\Sigma + \frac{\partial \Sigma}{\partial (kv)} kv + \frac{\partial^2 \Sigma}{\partial (kv)^2} (kv)^2 \right] \Big|_{kv=0}. \quad (8.40)$$

Here, we introduce the self-energy correction term

$$i\Sigma(p+k) = C_F \frac{\alpha_s}{\pi} \int_l \frac{\gamma_\alpha (l+m) \gamma^\alpha}{[m^2 - l^2][-(l-(p+k))^2]}. \quad (8.41)$$

Expanding in kv we obtain

$$\Sigma \Big|_{kv=0} = \not{p} \Sigma_v + \Sigma_m = \left(\frac{3}{\varepsilon} + 4 \right) m_b P_+ = \delta m_b P_+, \quad (8.42)$$

$$\Sigma' \Big|_{kv=0} = \not{p} \Sigma'_v + \Sigma'_m = - \left(\frac{3}{\varepsilon} + 4 \right) P_+, \quad (8.43)$$

$$\Sigma'' \Big|_{kv=0} = \not{p} \Sigma''_v + \Sigma''_m = - \left(\frac{3}{\varepsilon} + 1 \right) \frac{1}{m_b} P_+, \quad (8.44)$$

where we neglect the P_- component. The mass pole of the propagator is $\delta m_b = \Sigma_v +$

Σ_m . Besides, at NLO level the on-shell quark mass and wave function renormalization constants are identical:

$$Z_m = 1 - \Sigma|_{kv=0} = Z_2^{\text{OS}} = \frac{1}{1 - \Sigma'|_{kv=0}}. \quad (8.45)$$

From the second derivative of Σ with respect to kv we find

$$\Delta Z = -C_F \frac{\alpha_s}{\pi} \left(\frac{3}{\varepsilon} + 1 \right). \quad (8.46)$$

The renormalized EOM coefficient associated to the operator \mathcal{O}_V is given by

$$C_V = Z_2^{\text{OS}} \times \left(C_V^{\text{bare}} + 2\Delta Z \times C_0^{\text{LO}} \right). \quad (8.47)$$

Alternatively, we can determine the renormalized coefficient by taking the difference of the bare C_V coefficient and the linear term of the kv -expanded heavy-quark operator

$$C_V = Z_2^{\text{OS}} \times \left(C_V^{\text{bare}} - C_0^{\text{LO}} \tilde{C}_V^{\text{NLO}} \right) \quad (8.48)$$

$$= C_V^{\text{bare}} - C_0^{\text{LO}} \tilde{C}_V^{\text{NLO}} - C_V^{\text{LO}} \tilde{C}_0^{\text{NLO}}. \quad (8.49)$$

In this manner, we also remove the additional divergence from NLO corrections to the bottom quark legs.

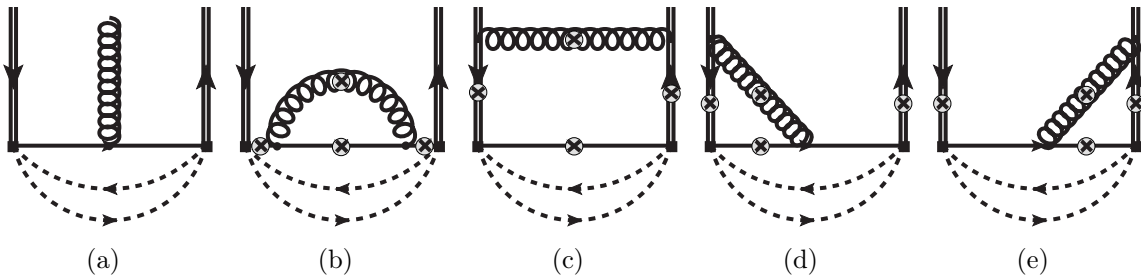


Figure 8.3: Leading-order and next-leading order Feynman graph with single external gluon insertion for C_V and C_G : The bubbles mark possible insertion points.

8.3 Chromomagnetic Operator Coefficient

To determine the chromomagnetic operator coefficient we calculate the difference between the corresponding contributions from direct computation of Feynman graphs of the operator \mathcal{O}_G and the local $\bar{b}\psi b$ operator, see Eq. (7.22). The resulting formula is given by

$$\bar{C}_G \equiv Z_2^{\text{OS}} Z_{\text{mag}} \times \left(C_G^{\text{bare}} - C_0^{\text{bare}} \tilde{C}_G^{\text{bare}} \right). \quad (8.50)$$

Here, we introduce the renormalization constant of the chromomagnetic operator Z_{mag} [144, 145]. The coefficient C_G^{bare} stems from several Feynman graphs: We classify these graphs into the (amputated) 1PI part $C_G^{1\text{PI}}$ and corrections to the external bottom quark leg $\Delta_G^{\text{ext.}}$:

$$C_G^{\text{bare}} = C_G^{1\text{PI}} + \Delta_G^{\text{ext.}} \times C_0^{\text{bare}}. \quad (8.51)$$

In the following, we only require the corrections in the 1PI part due to the cancellation of $\Delta_G^{\text{ext.}}$ when taking the difference of (8.51) and (8.64) (see also Eq. (8.50)).

To single out C_G and \tilde{C}_G we choose on-shell bottom quark states and include an additional transversely polarized gluon with momentum k . The choice of states is associated to the structure of \mathcal{O}_G . The corresponding matching relations are

$$\text{Im} \langle b(p) | \hat{T}_0 | b(p) g(k) \rangle = \frac{C_G}{m_Q^2} \langle b(p) | \mathcal{O}_G | b(p) g(k) \rangle, \quad (8.52)$$

$$\langle b(p) | \bar{b}\psi b | b(p) g(k) \rangle = \frac{\tilde{C}_G}{m_Q^2} \langle b(p) | \mathcal{O}_G | b(p) g(k) \rangle. \quad (8.53)$$

Our aim is to extract expressions proportional to $\not{\epsilon}_\perp \not{k}_\perp$, which is motivated by the structure of the operator $\mathcal{O}_G \sim \bar{h}_v [\gamma_\mu, \gamma_\nu] [D^\mu, D^\nu] h_v$. The coefficient function of \mathcal{O}_G is identical to the coefficient function of $\bar{h}_v \not{A}_\perp \not{\phi}_\perp h_v$ due to gauge invariance.

The coefficient $C_G^{1\text{PI}}$ has the following structure if we use the skeleton expansion:

$$C_G^{1\text{PI}} = \text{Tr} \left[P_+ (\mathcal{S}^{(I)} \times \mathcal{G} \times \tilde{\mathcal{S}}^{(II)}) P_+ \right], \quad (8.54)$$

where the ε_\perp and k_\perp -expanded terms are

$$\mathcal{S}^{(I,II)} = \hat{S}_0 + \hat{S}_{(\varepsilon,k)} + \hat{S}_{\varepsilon k} = S_0 + S_{(\varepsilon,k)}(\not{\epsilon}_\perp, \not{k}_\perp) + S_{\varepsilon k}(\not{\epsilon}_\perp \not{k}_\perp), \quad (8.55)$$

$$\mathcal{G} = \hat{g}_0 + \hat{g}_{(\varepsilon,k)} + \hat{g}_{\varepsilon k} = g_0 + g_{(\varepsilon,k)}(\not{\epsilon}_\perp, \not{k}_\perp) + g_{\varepsilon k}(\not{\epsilon}_\perp \not{k}_\perp). \quad (8.56)$$

Here, $\mathcal{S}^{(I,II)}$ denote the external bottom quark legs, whereas \mathcal{G} is the 1PI part. Relevant contributions which are proportional to $\not{\epsilon}_\perp \not{k}_\perp$ are given by

$$\begin{aligned}
& P_+(\mathcal{S}^{(I)} \times \mathcal{G} \times \tilde{\mathcal{S}}^{(II)})P_+ \\
&= P_+ \left[\hat{S}_0 \hat{g}_0 \hat{S}_{\varepsilon k} + \hat{S}_0 \hat{g}_{\varepsilon k} \hat{S}_0 + \hat{S}_{\varepsilon k} \hat{g}_0 \hat{S}_0 + \hat{S}_\varepsilon \hat{g}_k \hat{S}_0 + \hat{S}_\varepsilon \hat{g}_0 \hat{S}_k + \hat{S}_0 \hat{g}_\varepsilon \hat{S}_k \right] P_+ \\
&= \left[S_0 P_+ \hat{g}_0 P_+ S_{\varepsilon k} + S_0 P_+ \hat{g}_{\varepsilon k} P_+ S_0 + S_{\varepsilon k} P_+ \hat{g}_0 P_+ S_0 \right. \\
&\quad \left. + S_\varepsilon P_- \hat{g}_k P_+ S_0 + S_\varepsilon P_- \hat{g}_0 P_- S_k + S_0 P_+ \hat{g}_\varepsilon P_- S_k \right] (\not{\epsilon}_\perp \not{k}_\perp) \\
&= \left[\underbrace{2S_0 g_{0,++} S_{\varepsilon k}}_1 + \underbrace{2S_\varepsilon g_k S_0}_2 + \underbrace{S_0 g_{\varepsilon k} S_0}_3 + \underbrace{S_\varepsilon g_{0,--} S_k}_4 \right] (\not{\epsilon}_\perp \not{k}_\perp). \tag{8.57}
\end{aligned}$$

The expansion of the 1PI part reads

$$\begin{aligned}
\hat{g} &= \hat{g}_0 + \hat{g}_{(\varepsilon,k)} + \hat{g}_{\varepsilon k} \\
&= \hat{g}_0 + \hat{g}_\mu (\varepsilon_\perp^\mu, k_\perp^\mu) + \hat{g}_{\mu\nu} \varepsilon_\perp^\mu k_\perp^\nu. \tag{8.58}
\end{aligned}$$

In order to determine $\hat{g}_{\mu\nu}$ we consider a gluon insertion with transverse polarization and momentum k_\perp . We expand each line in k_\perp along the momentum flow in the Feynman graph and keep the linear term.

In the following, we will discuss the individual pieces in detail (see also Fig. 8.4):

1. The first set of contributions to C_G is reducible and arises from the 1PI part of the leading power diagrams in combination with $\not{\epsilon}_\perp$ and \not{k}_\perp insertions on each of the external bottom quark legs. Note that P_+ anticommute with $\not{\epsilon}_\perp$ and \not{k}_\perp . Therefore we compute $P_- \hat{g}_0 P_-$, from which follows

$$g_{0,--} = \frac{1}{2} \text{Tr} \left(P_- \hat{g}_0 P_- \right). \tag{8.59}$$

2. The $\not{\epsilon}_\perp$ or \not{k}_\perp insertion is in the 1PI part. Accordingly, the structures proportional to $\not{\epsilon}_\perp$ and \not{k}_\perp , respectively, originate from the external legs. We consider the projector combination $P_- \hat{g}_k P_+$ and $P_+ \hat{g}_\varepsilon P_-$. The projected kernel is

$$g_{\varepsilon,k} = \frac{1}{2(d-1)} \text{Tr} \left(P_+ \hat{g}_\varepsilon^\mu \gamma_\mu P_- \right) = \frac{1}{2(d-1)} \text{Tr} \left(P_- \hat{g}_k^\mu P_+ \gamma_\mu \right). \tag{8.60}$$

3. We consider the combination $\not{\epsilon}_\perp \not{k}_\perp$ in the 1PI part, which is the most complicated calculation. To extract the corresponding combination we choose the projector

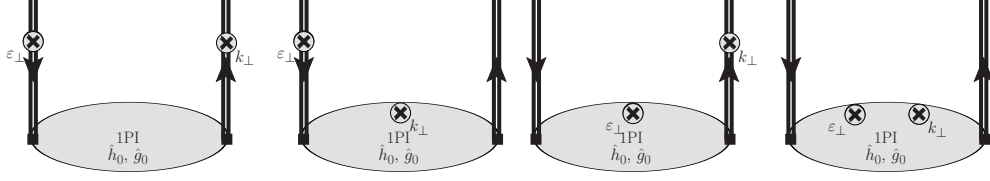


Figure 8.4: Type of insertion diagrams that contribute to C_G and \tilde{C}_G . The crosses mark insertion points and expanded propagators.

$P_+[\gamma_\mu, \gamma_\nu]P_+$. The normalized contribution is given by

$$g_{\varepsilon k} = \frac{-1}{(d-1)(d-2)} \text{Tr} \left(P_+ \hat{g}_{\varepsilon k}^{\mu\nu} P_+[\gamma_\mu, \gamma_\nu] \right). \quad (8.61)$$

4. The insertions of $\not{\varepsilon}_\perp$ and \not{k}_\perp can also be implemented on the external legs only, which leads to $\Delta_G^{\text{ext.}}$ in Eq. (8.51). This case should not be considered, since we compute the difference $C_G^{\text{bare}} - C_0 \tilde{C}_G^{\text{NLO}}$ and, hence, the additional pieces of this type cancel with the corresponding pieces in the coefficient \tilde{C}_G^{NLO} of the $\bar{b}\psi b$ operator.

For example, we explicitly give a single contribution from the left-sided vertex correction in Fig. 8.3 (d) with insertion outside the loop:

$$\Gamma_{vx;1}^{\mu\nu} = \gamma^\nu P_L S^{\text{int}}(p-q+k; m_c) \gamma^\alpha S(k-q; m_c) \gamma^\mu P_L S(k; m_b) \gamma^\alpha D_{\alpha\beta}(p-k), \quad (8.62)$$

where $S_\rho^{\text{int}}(p-q+k; m_c) \equiv S(p-q+k; m_c) \gamma_\rho S(p-q; m_c)$. Note that by expanding the propagator up to $\mathcal{O}(k_\perp)$ the symmetry relation of both vertex corrections that holds in previous cases is now broken. Therefore we have to include both vertex contributions separately. In total there are 16 NLO Feynman graphs. The coefficient function of the operator \mathcal{O}_G at NLO level is given by

$$C_G^{\text{NLO}}(r) = \sum_j C_G^{\text{NLO};j} = C_G^{\text{NLO};\text{se}} + C_G^{\text{NLO};\text{bx}} + C_G^{\text{NLO};\text{vx}} + C_G^{\text{NLO};\text{vxr}}. \quad (8.63)$$

8.4 Heavy-quark Current Operator Coefficient

Similarly to C_G , we determine the coefficient \tilde{C}_G of the $\bar{b}\psi b$ operator and take only the 1PI part into account. The decomposition of $\tilde{C}_G^{\text{bare}}$ is

$$\tilde{C}_G^{\text{bare}} = \tilde{C}_G^{1\text{PI}} + \Delta_G^{\text{ext.}}. \quad (8.64)$$

Using the skeleton expansion for the 1PI part of $\tilde{C}_G^{\text{bare}}$, we obtain

$$\tilde{C}_G^{1\text{PI}} = \text{Tr} \left[P_+ (\mathcal{S}_{\varepsilon k}^{(I)} \times \mathcal{H}_{\varepsilon k} \times \tilde{\mathcal{S}}_{\varepsilon k}^{(II)}) P_+ \right] \quad (8.65)$$

$$= \left[\underbrace{2S_0 h_{0,++} S_{\varepsilon k}}_1 + \underbrace{2S_\varepsilon h_k S_0}_2 + \underbrace{S_0 h_{\varepsilon k} S_0}_3 + \underbrace{S_\varepsilon g_{0,--} S_k}_4 \right] (\not{\varepsilon}_\perp \not{k}_\perp), \quad (8.66)$$

where the expanded kernel is

$$\mathcal{H} = \hat{h}_0 + \hat{h}_{(\varepsilon,k)} + \hat{h}_{\varepsilon k} = h_0 + h_{(\varepsilon,k)} (\not{\varepsilon}_\perp \not{k}_\perp) + h_{\varepsilon k} (\not{\varepsilon}_\perp \not{k}_\perp) \quad (8.67)$$

$$= \left[\underbrace{2S_0 g_{0,++} S_{\varepsilon k}}_1 + \underbrace{2S_\varepsilon g_k S_0}_2 + \underbrace{S_0 g_{\varepsilon k} S_0}_3 + \underbrace{S_\varepsilon g_{0,--} S_k}_4 \right] (\not{\varepsilon}_\perp \not{k}_\perp). \quad (8.68)$$

Three Feynman graphs contribute to $\tilde{C}_G^{1\text{PI}}$, see in Fig. 8.4.

1. We consider an ε_\perp and k_\perp insertion on the external bottom quark legs. The 1PI part is the simple vertex correction.
2. The background gluon is attached to one of the legs, whereas the 1PI part has a k_\perp insertion, and vice versa.
3. Both insertions are in the 1PI part.
4. The insertions of $\not{\varepsilon}_\perp$ and \not{k}_\perp on the external legs only leads to $\Delta_G^{\text{ext.}}$ in Eq. (8.51). This contribution cancels in Eq. (8.50).

The expansion of the 1PI piece reads

$$\begin{aligned} \hat{h} &= \hat{h}_0 + \hat{h}_{(\varepsilon,k)} + \hat{h}_{\varepsilon k} \\ &= \hat{h}_0 + \hat{h}_\mu (\varepsilon_\perp^\mu, k_\perp^\mu) + \hat{h}_{\mu\nu} \varepsilon_\perp^\mu k_\perp^\nu. \end{aligned} \quad (8.69)$$

For the 1PI part without insertions we find

$$\hat{h} = \psi + \frac{\alpha_s}{4\pi} C_F \left[-\psi \left(\frac{1}{\varepsilon} + 2 \right) + m \left(\frac{4}{\varepsilon} + 6 \right) \right]. \quad (8.70)$$

We consider the operator combination $P_- \hat{h} P_- = P_- h P_-$ for insertions outside of \hat{h} . It follows that

$$h = \frac{1}{2} \text{Tr} [P_- \hat{h} P_-] = \frac{1}{2} \left(-1 + \frac{\alpha_s}{4\pi} C_F \left[\frac{5}{\varepsilon} + 8 \right] \right). \quad (8.71)$$

The 1PI part is expanded according to

$$h_{(\varepsilon, k)} = -\frac{\alpha_s}{2\pi} C_F \left[\frac{1}{\varepsilon} + 2 \right]. \quad (8.72)$$

In order to extract the $\varepsilon_\perp k_\perp$ structure we use a specific projector

$$h_{\varepsilon k} = \frac{8}{(d-1)(d-2)} \text{Tr} \left(P_+ \hat{h}^{\mu\nu} P_+ [\gamma_\mu, \gamma_\nu] \right) = -\frac{\alpha_s}{4\pi} \left[6C_F \left(\frac{1}{\varepsilon} + 1 \right) + C_A \left(\frac{1}{\varepsilon} + 5 \right) \right]. \quad (8.73)$$

The final 1PI heavy-quark operator coefficient reads

$$\tilde{C}_G^{1\text{PI}} = -\frac{1}{2} - \frac{5\alpha_s}{4\pi} \left[C_F \left(\frac{3}{2\varepsilon} + 2 \right) + C_A \left(\frac{1}{5\varepsilon} + 1 \right) \right]. \quad (8.74)$$

Summary and Discussion

This thesis is a compendium of three projects¹, which are dedicated to the QCD effects of heavy meson decays. In the first two projects the method of QCD sum rules was used to determine non-perturbative quantities, that is the decay constants of heavy-light mesons. The third and final project considered the calculation of perturbative corrections in inclusive weak heavy-meson decays. The evaluation of analytical and numerical results was performed with the software program `Mathematica`.

Decay Constants of Heavy-Light Mesons

We applied the method of QCD sum rules to estimate the decay constants of vector and pseudoscalar bottom and charmed mesons with light quark content (u, d, s) . Our predicted decay constants have gained state-of-the-art precision by including all known perturbative contributions and new ones for the first time. We also calculated perturbative corrections to the leading power contribution with NLO accuracy in the sum rules. To this end, we constructed a computation routine for one- and two-loop typologies and presented the computational techniques in detail. The numerical values of all decay constants were updated, together with their upper bounds. The resulting central values with their corresponding uncertainties from parameter variation and the upper bounds (in brackets) are:

$f_{B^*} = (210^{+10}_{-12}) [261] \text{ MeV}$	$f_B = (207^{+17}_{-09}) [258] \text{ MeV}$
$f_{B_s^*} = (251^{+14}_{-16}) [296] \text{ MeV}$	$f_{B_s} = (242^{+17}_{-12}) [285] \text{ MeV}$
$f_{D^*} = (242^{+20}_{-12}) [297] \text{ MeV}$	$f_D = (201^{+12}_{-13}) [237] \text{ MeV}$
$f_{D_s^*} = (293^{+19}_{-14}) [347] \text{ MeV}$	$f_{D_s} = (238^{+13}_{-23}) [266] \text{ MeV}$

The relative uncertainties were estimated to 10% and less. Typical errors for $f_{B(s)}$ and f_D are about ± 20 MeV in other sum rules studies [53, 104]. Our results are

¹The list of resulting publications is given on page 181.

consistent with recent predictions based on lattice QCD, see Fig. 5.5, 5.6 and 5.7. Some measurements of leptonic decays, namely $D_{(s)} \rightarrow \ell \bar{\nu}_\ell$ and $B \rightarrow \tau \bar{\nu}_\tau$, also allow determinations for decay constants. In case of $f_{D_{(s)}}$ the experimental values show some tension to our predictions, whereas f_B is consistent within the large experimental uncertainty.

We also evaluated other versions of our sum rules to test the consistency of this method. The other versions include certain weight functions in the OPE formalism to modify the hierarchy of OPE contributions. Their predictions agree with the ones of standard sum rules within the uncertainty intervals.

We finally give the ratios of vector to pseudoscalar and strange to non-strange meson decay constants as estimates for heavy quark spin-violating effects and deviations of the $SU(3)_f$ symmetry. These ratios were determined by dividing both sum rules:

Heavy-Quark Spin Violation		$SU(3)_f$ Violation	
$\frac{f_{B^*}}{f_B} = 1.02^{+0.02}_{-0.09}$	$\frac{f_{B_s^*}}{f_{B_s}} = 1.04^{+0.01}_{-0.08}$	$\frac{f_{B_s}}{f_B} = 1.17^{+0.03}_{-0.04}$	$\frac{f_{B_s^*}}{f_{B^*}} = 1.20 \pm 0.04$
$\frac{f_{D^*}}{f_D} = 1.20^{+0.13}_{-0.07}$	$\frac{f_{D_s^*}}{f_{D_s}} = 1.24^{+0.13}_{-0.05}$	$\frac{f_{D_s}}{f_D} = 1.18^{+0.04}_{-0.05}$	$\frac{f_{D_s^*}}{f_{D^*}} = 1.21 \pm 0.05$

The numbers show a small deviation from the heavy-quark-symmetry limit for bottom mesons. Recently the HPQCD collaboration determined $f_{B^*}/f_B = 0.941 \pm 0.026$ and $f_{B_s^*}/f_{B_s} = 0.953 \pm 0.023$ in lattice QCD [107]. Both values are consistent within the uncertainty intervals of our predictions. Ratios of vector to pseudoscalar charmed meson decay constants are about 20 % off the symmetry limit. This shows substantial influence of mass corrections to this limit value.

Decay Constants of Radially Excited Mesons

In the next step we extended the QCD sum rules formalism to include radial excitations of heavy-light mesons. In the first procedure the ground- and radially excited state resonances were fitted to the OPE expression of the two-point correlation function. We also performed a single fit of the radially excited state for additional validation. Both procedures led to almost identical results. Here we only present the single fit predictions due to the slightly smaller uncertainties:

$f_{B^{*'}} = (165_{-12}^{+46}) [314] \text{ MeV}$	$f_{B'} = (166_{-10}^{+9}) [279] \text{ MeV}$
$f_{B_s^{*'}} = (194_{-18}^{+57}) [325] \text{ MeV}$	$f_{B'_s} = (178_{-17}^{+19}) [320] \text{ MeV}$
$f_{D^{*'}} = (183_{-24}^{+13}) [275] \text{ MeV}$	$f_{D'} = (138_{-22}^{+10}) [189] \text{ MeV}$
$f_{D_s^{*'}} = (178_{-39}^{+20}) [265] \text{ MeV}$	$f_{D'_s} = (146_{-36}^{+12}) [219] \text{ MeV}$

The fit results have smaller central values in comparison to the ground-state decay constants. Our detailed study of $f_{D'}$ shows that the condensate terms lead to a suppression of the resulting decay constants. At the moment there are only a few other studies of radial excitations. A recent determination in lattice QCD estimates $f_{D'} = 117 \pm 25 \text{ MeV}$ which is in good agreement with our value [118].

Inclusive Weak Decays of Heavy Hadrons

In the final part of this thesis we considered inclusive weak decays of heavy hadrons. We applied the heavy quark expansion (HQE) method in the realm of heavy quark effective theory (HQET) to determine the total decay rate of such decays. Our main goal was to compute the radiative corrections to the coefficient function of the power-suppressed (dimension-5) chromomagnetic operator with NLO accuracy. For definiteness we chose inclusive semileptonic $b \rightarrow c$ transitions. At first the charm quark was treated as massless. However, for higher precision we also computed the full mass dependence of all necessary coefficient functions. We automatized the computation of on-shell two- and three-loop Feynman graphs with two different masses. The normalized total decay width for inclusive weak B decays (including the mass ratio $m_c^2/m_b^2 = 0.07$) is given by

$$\Gamma(B \rightarrow X_c \ell \bar{\nu}_\ell) / \tilde{\Gamma}_0 = \left(1 - 1.78 \frac{\alpha_s}{\pi}\right) \left[1 - \frac{\mu_\pi^2}{2m_b^2}\right] - 3.89 \left(1 - 0.92 \frac{\alpha_s}{\pi}\right) \frac{\bar{\mu}_G^2}{2m_b^2}.$$

Our result coincides with the numerical calculation in Ref. [134]. We found out that the coefficient functions are strongly affected by the mass scheme of the charm quark. In addition to the total width we determined the moments over the invariant mass-squared of the leptonic pair q^2 and the partonic invariant mass-squared $(p - q)^2 - m_c^2$. Moments in q^2 show a decreasing influence of radiative corrections compared to the total width. Numerically the partonic moments diminish very quickly.

A prominent application of the computed results is the precision determination of the CKM matrix element V_{cb} . Here we give the shift of $|V_{cb}|$ due to the new correction. In

case of a massive charm quark the relative shift is

$$\frac{\Delta|V_{cb}|}{|V_{cb}|} = -0.14\% .$$

This means that our corrections have roughly the same influence on V_{cb} as the dimension-7 operator contribution at tree-level [135].

General Setup and Properties

In this chapter we briefly discuss general prerequisites and properties of the integration within dimensional regularization, which is used for the computation of Feynman diagrams.

A.1 Regularization

We know that the lowest-order QCD calculation (at tree-level approximation) in quark-gluon processes reproduce just parton model results. To assess the dynamical effects of QCD it is necessary to consider radiative corrections to the tree-level amplitudes. At high transfer energies the strong coupling constant is regarded as weak and perturbation theory can be used. As an example for a Green's function we show a scalar one-loop Feynman diagram in $g\phi^3$ -theory [70], which corresponds to the integral

$$\Pi(q^2) = g^2 \int \frac{d^4k}{(2\pi)^4} \frac{1}{[-k^2][-(q-k)^2]}. \quad (\text{A.1})$$

The integral $\Pi(q^2)$ is logarithmically divergent at large and small momenta (UV & IR-singularity). Hence, it is necessary to regularize the integration by manifesting these singularities. From this follows that divergent integrals can be written in the terms of convergent ones. The singular term is not defined in the physical limit, which restores the original theory. To give the expression a physical meaning one has to perform *renormalization* [8]. This issue will be discussed in Sect. A.3.

There are several methods to regularize the above integral, but some may violate underlying physical requirements such as gauge symmetries or Lorentz invariance. In this thesis we use *dimensional regularization* [148, 149, 8] as a method, which replaces the four-dimensional space-time dimension ($D = 4$) to $D = 4 - 2\varepsilon$. Singularities will appear as $1/\varepsilon$ -poles (with $\varepsilon \rightarrow 0$) combining singularities of UV and IR nature. Properties of the dimensional regularization will be discussed in the next section.

A.2 Definitions and Properties of Feynman Integrals within Dimension Regularization

Within dimensional regularization the dimensionality D can be integer, non-integer or even a complex number. In case of a complex continuation, emerging divergences transform into singularities in the (complex) D -plane. In practice, one changes the integration measure for each loop integral as follows

$$\int \frac{d^4k}{(2\pi)^{4i}} \rightarrow \mu^{4-D} \int \frac{d^Dk}{(2\pi)^{Di}}, \quad (\text{A.2})$$

with μ as an arbitrary scale that conserves the mass dimension of the integral. For further applications, we introduce other factors within the integration measure to avoid a proliferation of constant terms in the final result (see Sect. 4.1). The Dirac-Algebra should also be extended to D dimensions to ensure a consistent calculation beyond the ordinary four dimensions. At first the space-time index μ spans $D - 1$ components, in case of a momentum vector that is

$$k^\mu = (k^0, k^1, \dots, k^{D-1}) . \quad (\text{A.3})$$

Contracted metric tensors and Dirac matrices simplify to

$$g_{\mu\nu}g^{\mu\nu} = D, \quad \gamma_\mu\gamma^\mu = D \cdot \mathbf{1}, \quad (\text{A.4})$$

where $g_{\mu\nu} \equiv \text{diag}(1, -1, -1, -1, \dots)$. Dirac matrices obey the anticommutation relation

$$\{\gamma_\mu, \gamma_\nu\} \equiv \gamma_\mu\gamma_\nu + \gamma_\nu\gamma_\mu = 2g_{\mu\nu} \cdot \mathbf{1}. \quad (\text{A.5})$$

Traces of odd numbers of Dirac matrices vanish. Only An even number of matrices contributes, e.g.

$$\text{Tr} [\gamma_\mu\gamma_\nu] = \text{Tr} [\gamma_\nu\gamma_\mu] = \frac{1}{2}\text{Tr} [\{\gamma_\mu, \gamma_\nu\}] = 4g_{\mu\nu}. \quad (\text{A.6})$$

Other trace relations of strings of Dirac matrices are given in [70]. Here, $\text{Tr}[\mathbf{1}] = 4$ has been adopted.

As dimensional regularization does not break any space-time symmetries, some integration properties are still preserved for D -dimensional integration. If $f(\vec{k})$ and $g(\vec{k})$ are any given functions of a vector \vec{k} and any complex numbers a and b , the following useful properties occur:

- **Linearity**

$$\int d^D k (af(\vec{k}) + bg(\vec{k})) = a \int d^D k f(\vec{k}) + b \int d^D k g(\vec{k}), \quad (\text{A.7})$$

- **Translation invariance**

$$\int d^D k f(\vec{k} + \vec{p}) = \int d^D k f(\vec{k}), \quad (\text{A.8})$$

- **Scaling law**

$$\int d^D k f(\lambda \vec{k}) = \frac{1}{\lambda^D} \int d^D k f(\vec{k}) \quad (\lambda \in \mathbb{C}), \quad (\text{A.9})$$

- **Lorentz invariance**

$$\int d^D k f(\Lambda \vec{k}) = \int d^D k f(\vec{k}), \quad (\text{A.10})$$

where Λ is a Lorentz transformation and an element of the Lorentz group $SO(1, D-1)$.

- **Partial integration**

$$\int d^D k \frac{\partial}{\partial k^\mu} f(\vec{k}) = 0, \quad (\text{A.11})$$

- **Isotropy**

$$\int d^D k k^\mu k^\nu f(\vec{k}^2) = \frac{g^{\mu\nu}}{D} \int d^D k \vec{k}^2 f(\vec{k}^2), \quad (\text{A.12})$$

Scaleless integrals have the property [150]

$$\int d^D k \frac{1}{[-k^2]^\alpha} = \begin{cases} \frac{1}{\Gamma(\frac{D}{2}+1)}, & \text{if } \alpha = \frac{D}{2} \\ 0, & \text{otherwise.} \end{cases} \quad (\text{A.13})$$

This means that any massless vacuum diagram without any scaling mass parameter vanishes with exception for $\alpha = D/2$, which also includes diagrams with detachable scaleless subdiagrams.

A.3 Renormalization and Quark Masses

Divergencies in the QCD Lagrangian originate from loop diagrams based on *bare* fields. In that way all Green's functions are infinite. But QCD is a renormalizable theory from which physical, finite quantities (observables) can be computed. This implies an ab-

sorption of divergencies into QCD parameters, such as coupling constant, quark masses and fields, in order to cancel emerging infinite expressions in the loop corrections to Green's functions. A relevant object for renormalization in QCD is the quark propagator (two-point Green's function)

$$S^0(p, m_0, \alpha_s^0) = i \int dx e^{ipx} \langle 0 | T \{ \psi^0(x) \bar{\psi}^0(0) \} | 0 \rangle = \frac{1}{m_0 - \not{p}} \quad (\text{A.14})$$

where m_0 and ψ^0 are the bare quark mass and bare quark field operator, respectively. α_s^0 denotes the bare strong coupling constant and it is also related to the gauge coupling parameter g (motivated by the electric charge in QED) through $\alpha_s^0 = (g_s^0)^2/4\pi$. The renormalized propagator is constructed as

$$\begin{aligned} S(p, m, \alpha_s, \mu) &= Z_{2\psi}^{-1} \cdot S^0(p, m_0, \alpha_s^0) \\ &= i \int dx e^{ipx} \langle 0 | T \{ \psi(x) \bar{\psi}(0) \} | 0 \rangle = \frac{1}{m_0 - \not{p} - \Sigma} \\ &= \frac{1}{m - \not{p} - \Sigma - \delta m}. \end{aligned} \quad (\text{A.15})$$

Here, we introduce the mass counterterm δm . For renormalization of S^0 we introduce the quantities

$$\psi^0(x) = Z_{2\psi}^{1/2} \psi, \quad m_0 = Z_m m_q, \quad \alpha_s^0 = \mu^{2\varepsilon} Z_\alpha \alpha_s, \quad (\text{A.16})$$

where $Z_{2\psi}^{1/2}$, Z_m and Z_α are renormalization constants to the renormalized field operator ψ , the quark mass m_q and the strong coupling α_s . For convenience, the quark field renormalization constant is defined with a square root to obtain $Z_{2\psi}$ for bilinear fields in the Lagrangian. We also introduced an arbitrary momentum scale μ to generate a dimensionless coupling. In perturbation theory, the renormalization constant has to cancel divergencies order by order, i.e. we can expand these constants according to

$$Z_x = 1 + Z_x^{(1)} \frac{\alpha_s}{\pi} + \mathcal{O}(\alpha_s^2) \quad (x = \{2\psi, m, \alpha_s\}). \quad (\text{A.17})$$

Observables and bare parameters are by definition independent by any renormalization scale that is the key requirement of the *renormalization group equation* (RGE). The RGE determines the scale running of QCD parameters. In case of a general physical

quantity R , which is parametrized by m and α_s , we find

$$0 = \mu \frac{d}{d\mu} R(p; m_0, \alpha_s^0) = \left\{ \mu \frac{\partial}{\partial \mu} + \mu \frac{d\alpha_s}{d\mu} \frac{\partial}{\partial \alpha_s} + \mu \frac{dm}{d\mu} \frac{\partial}{\partial m} \right\} R(p; m, \alpha_s) \quad (\text{A.18})$$

The scale dependence is given by either explicit or implicit dependence (of the parameters). Note that the momentum is an observable and therefore cannot be scale dependent. Based on above equation we define the *renormalization group functions*

$$\beta(\alpha_s) \equiv -\mu \frac{d}{d\mu} \left(\frac{\alpha_s}{\pi} \right) = -\beta_0 \left(\frac{\alpha_s}{\pi} \right)^2 - \beta_1 \left(\frac{\alpha_s}{\pi} \right)^3 + \dots, \quad (\text{A.19})$$

$$\gamma_m(\alpha_s) \equiv -\frac{\mu}{m} \frac{d}{d\mu} m(\mu) = \gamma_m^{(0)} \left(\frac{\alpha_s}{\pi} \right) + \gamma_m^{(1)} \left(\frac{\alpha_s}{\pi} \right)^2 + \dots = \alpha_s \frac{\partial Z_m}{\partial \alpha_s}, \quad (\text{A.20})$$

$$\psi(\mu) \gamma_{2\psi}(\alpha_s) \equiv 2\mu \frac{d}{d\mu} \psi(\mu) = -\psi(\mu) \left[\gamma_{2\psi}^{(0)} \left(\frac{\alpha_s}{\pi} \right) + \gamma_{2\psi}^{(1)} \left(\frac{\alpha_s}{\pi} \right)^2 + \dots \right] = \psi(\mu) \alpha_s \frac{\partial Z_{2\psi}}{\partial \alpha_s}. \quad (\text{A.21})$$

Here, the running coupling is related to the β -function, whereas the quark mass and field operator are governed by the corresponding anomalous dimensions $\gamma_m(\alpha_s)$, $\gamma_{2\psi}(\alpha_s)$. With this function the RGE can be simplified as follows:

$$\left\{ \mu \frac{d}{d\mu} - \beta(\alpha_s) \frac{\partial}{\partial \alpha_s} - \gamma_m(\alpha_s) m \frac{\partial}{\partial m} \right\} R(p; m, \alpha_s, \mu) = 0. \quad (\text{A.22})$$

The renormalized quark propagator to the NLO level is given by the one-loop self-energy diagram. From this diagram we calculate the expressions $Z_m^{(1)}$ and $Z_{2\psi}^{(1)}$. In Landau gauge the self-energy contribution leads to

$$\Sigma(p^2) = -g_s^2 C_F \int \frac{d^d k}{(2\pi)^d i} \frac{\gamma_\mu (\not{p} - \not{k}) \gamma^\mu}{[m_0^2 - (p-k)^2][k^2]} \quad (\text{A.23})$$

$$= m_0 \Sigma_m(p^2) + (m_0 - \not{p}) \Sigma_p(p^2). \quad (\text{A.24})$$

If we insert the self-energy expression in Eq. (A.15), where Σ_m and Σ_p denote the mass and field operator renormalization, we end up with

$$S(p; m_q, \alpha_s, \mu) = \frac{1}{1 - \Sigma_p} \cdot \frac{1}{(m_q - \delta m) \left[1 - \frac{\Sigma_m}{1 - \Sigma_p} \right] - \not{p}}. \quad (\text{A.25})$$

On one-loop level from this follows the renormalization constant

$$Z_{2\psi} = 1 + \Sigma_p \quad \text{and} \quad Z_m = 1 - \Sigma_m. \quad (\text{A.26})$$

Performing the explicit calculations for Σ_p and Σ_m , we obtain for the infinite parts

$$Z_{2\psi}^{(1)} = -\frac{1}{4}C_F\frac{1}{\varepsilon} \quad \text{and} \quad Z_m^{(1)} = -\frac{3}{4}C_F\frac{1}{\varepsilon}. \quad (\text{A.27})$$

In this context, we define the running $\overline{\text{MS}}$ mass

$$m_{\overline{\text{MS}}}(\mu) \equiv (Z_m^{\overline{\text{MS}}})^{-1}m_0 = m_0 \left[1 + \left(\frac{\alpha_s}{\pi}\right)\frac{1}{\varepsilon} + \mathcal{O}(\alpha_s^2) \right] \quad (\text{A.28})$$

where the mass renormalization constant in $\overline{\text{MS}}$ -scheme reads

$$Z_m^{\overline{\text{MS}}} \equiv 1 - \left(\frac{\alpha_s}{\pi}\right)\frac{3}{4}C_F\frac{1}{\varepsilon} \quad (\text{A.29})$$

and analogously the field operator renormalization is defined as

$$Z_{2\psi}^{\overline{\text{MS}}} \equiv 1 - \left(\frac{\alpha_s}{\pi}\right)\frac{1}{4}C_F\frac{1}{\varepsilon}. \quad (\text{A.30})$$

Another common mass definition obeys the condition $S(p)|_{p^2=m_{\text{pole}}^2}$ and from Eq. (A.15) we find

$$m_{\text{pole}} = (Z_m^{\text{pole}})^{-1}m_0 = m_0 \left[1 + \left(\frac{\alpha_s}{\pi}\right)\frac{3}{4}C_F \left(\frac{1}{\varepsilon} + 4 + \log \left(\frac{\mu^2}{m_{\text{pole}}^2} \right) \right) \right] + \mathcal{O}(\alpha_s^2). \quad (\text{A.31})$$

At one-loop order we obtain

$$Z_m^{\text{pole}} = Z_{2\psi}^{\text{pole}} = 1 - \left(\frac{\alpha_s}{\pi}\right)\frac{3}{4}C_F \left(\frac{1}{\varepsilon} + 4 + \log \left(\frac{\mu^2}{m_{\text{pole}}^2} \right) \right). \quad (\text{A.32})$$

Note that for higher order renormalization Z_m^{pole} and $Z_{2\psi}^{\text{pole}}$ are not equal anymore. The ratio Eqs. (A.28) and (A.31) provide the relation between $\overline{\text{MS}}$ and pole mass

$$\frac{m_{\text{pole}}}{m_{\overline{\text{MS}}}(\mu)} = \frac{Z_m^{\overline{\text{MS}}}}{Z_m^{\text{pole}}} = 1 + \left(\frac{\alpha_s}{\pi}\right)C_F \left[1 + \frac{3}{4} \log \left(\frac{\mu^2}{m_{\text{pole}}^2} \right) \right]. \quad (\text{A.33})$$

We will also solve the RGE for $m_{\overline{\text{MS}}}(\mu)$ to present its scale dependence. Since the bare mass is scale-independent, we know

$$\mu \frac{dm_{\overline{\text{MS}}}(\mu)}{d\mu} + \gamma_m(\alpha_s)m_{\overline{\text{MS}}}(\mu) = 0. \quad (\text{A.34})$$

According to Eq. (A.20) the anomalous dimension of the quark mass in $\overline{\text{MS}}$ -scheme reads

$$\gamma_m(\alpha_s) = \frac{\alpha_s}{\pi} + \mathcal{O}(\alpha_s^2). \quad (\text{A.35})$$

Combining Eqs. (A.34) and the β -function as defined in Eq. (A.19), this leads to the solution of the quark mass RGE at one-loop order:

$$m_{\overline{\text{MS}}}(\mu) = m_{\overline{\text{MS}}}(\mu_0) \exp \left\{ \int_{\alpha_s(\mu_0)}^{\alpha_s(\mu)} \frac{d\alpha_s}{\alpha_s} \frac{\gamma_m(\alpha_s)}{2\beta(\alpha_s)} \right\} = m_{\overline{\text{MS}}}(\mu_0) \left(\frac{\alpha_s(\mu)}{\alpha_s(\mu_0)} \right)^{\gamma_m^{(0)}/2\beta_0}. \quad (\text{A.36})$$

Finally, the scaling of the strong coupling can be determined if the beta function is known. The beta function itself originates from the quark-gluon vertex at NLO accuracy, see Ref. [81]. Here, β_0 is function of the number of color N_C and quark flavor n_f :

$$\beta_0 = \frac{11N_C - 2n_f}{6}. \quad (\text{A.37})$$

From this follows in combination with Eq. (A.19)

$$\alpha_s(\mu) = \frac{\alpha_s(\mu_0)}{1 + \alpha_s(\mu_0) \frac{\beta_0}{2} \log \left(\frac{\mu^2}{\mu_0^2} \right)}. \quad (\text{A.38})$$

The starting value $\alpha_s(\mu_0)$ can also be replaced by an specific scale Λ_{QCD} , which marks the scale at which the coupling constant diverges:

$$\alpha_s(\mu) = \frac{2\pi}{\beta_0 \log \left(\frac{\mu^2}{\Lambda_{\text{QCD}}^2} \right)}. \quad (\text{A.39})$$

From measurements we know that Λ_{QCD} is ranged between 200 and 300 MeV [36].

Apart from basic renormalization of Green's functions, we also require the renormal-

ization of *composite operators*. These operators do not get renormalized by the renormalization of QCD parameters (m , α_s and ψ). In the Chaps. 3 and 7 composite operators are discussed in the context of the operator product expansion. Formally, for two operators $\mathcal{O}_A(x)$ and $\mathcal{O}_B(0)$ this expansion takes the form

$$\mathcal{O}_A(x)\mathcal{O}_B(0) \sim \sum_{i=1}^{\infty} C_i(x)\mathcal{O}_i(0) \Big|_{x \rightarrow 0}. \quad (\text{A.40})$$

The operator product is expanded into an infinite sum of local operators $\mathcal{O}_i(0)$ and coefficient functions $C_i(x)$, which reside the spatial dependence. As an example, we give the renormalization constant of the bi-local quark field operator $\mathcal{O}_{\bar{\psi}\psi}(z) \equiv \bar{\psi}\psi$. The explicit calculation is performed by calculating Green's functions with insertions of the composite operator [151]. The result is

$$Z_{\bar{\psi}\psi} = 1 + \frac{3}{4}C_F \frac{\alpha_s}{\pi} \frac{1}{\varepsilon} + \mathcal{O}(\alpha_s) = Z_m^{-1} \quad (\text{A.41})$$

where $(\bar{\psi}\psi)^0 = Z_{\bar{\psi}\psi}(\bar{\psi}\psi)$. One can proof that $Z_{\bar{\psi}\psi} = Z_m^{-1}$ is valid to every order in perturbation theory. Hence, the product $m(\bar{\psi}\psi)$ is a renormalization group invariant quantity.

A.4 Renormalization Group Functions

Following the definition of $\beta(\alpha_s)$ and $\gamma_m(\alpha_s)$ in Sect. A.3, we provide the solutions to the second order in α_s as presented in Ref. [53]. These solutions determine the scale-dependence of the strong coupling and the quark masses. From Eq. A.19 we find

$$\beta_0 = \frac{11C_A - 2n_f}{6}, \quad \beta_1 = \frac{17C_A^2 - 5C_A n_f - 3C_F n_f}{12} \quad (\text{A.42})$$

and Eq. A.20

$$\gamma_m^{(0)} = \frac{3}{2}C_F, \quad \gamma_m^{(1)} = \frac{C_F(97C_A + 9C_F - 10n_f)}{48}, \quad (\text{A.43})$$

following the notations of [53]. With all coefficient terms as stated above, we extend the $\overline{\text{MS}}$ to pole mass relation of Eq. (A.33) to NNLO level:

$$\frac{m_{\text{pole}}}{m_{\overline{\text{MS}}}}(\mu) = 1 + \left(\frac{\alpha_s}{\pi}\right) r_m^{(1)} + \left(\frac{\alpha_s}{\pi}\right)^2 r_m^{(2)} + \mathcal{O}(\alpha_s^3). \quad (\text{A.44})$$

In the equation above, we introduce the coefficient functions

$$\begin{aligned}
 r_m^{(1)} &= C_F + \frac{\gamma_m^{(0)}}{2} \log \left(\frac{\mu^2}{m_{\overline{\text{MS}}}^2(\mu)} \right), \\
 r_m^{(2)} &= r_{m,0}^{(2)} - \frac{1}{2} \left[\gamma_m^{(1)} - C_F(\gamma_m^{(0)} - \beta_0) \right] \log \left(\frac{\mu^2}{m_{\overline{\text{MS}}}^2(\mu)} \right) \\
 &\quad + \frac{\gamma_m^{(0)}}{8} (\gamma_m^{(0)} - \beta_0) \log^2 \left(\frac{\mu^2}{m_{\overline{\text{MS}}}^2(\mu)} \right) - \gamma_m^{(0)} r_m^{(1)}. \tag{A.45}
 \end{aligned}$$

The remaining constant terms read

$$\begin{aligned}
 r_{m,0}^{(2)} &= C_F^2 \left(\frac{7}{128} - \frac{15}{8} \zeta(2) - \frac{3}{4} \zeta(3) + 3 \zeta(2) \log(2) \right) + C_F n_f \left(\frac{71}{192} + \frac{1}{4} \zeta(2) \right) \\
 &\quad + C_A C_F \left(\frac{1111}{384} + \frac{1}{2} \zeta(2) + \frac{3}{8} \zeta(3) - \frac{3}{2} \zeta(2) \log(2) \right) + C_F \left(\frac{3}{8} - \frac{3}{4} \zeta(2) \right), \tag{A.46}
 \end{aligned}$$

where $\zeta(x)$ is the Riemann zeta-function.

OPE and Hadronic Expressions for Two-Point Correlator

In this chapter we further discuss some basics for the sum rules of f_{H^*} and f_H , which we have briefly described in Chap. 3, namely the hadronic spectrum representation and the dispersion relation. Moreover, we present the `LiteRed` basis and solutions of the prototypes for the perturbative spectral functions $\rho_t^{\text{pert,NLO}}$ and $\rho_5^{\text{pert,NLO}}$. Then we give the result of ρ_t^{pert} and ρ_5^{pert} up to NLO in α_s . In the last two sections we present the condensate contributions and the sum rule in the heavy quark limit for decay constants of pseudoscalar mesons.

B.1 Hadronic representation of the two-point correlator

To quantify the hadronic content of $\Pi_{\mu\nu}$ of Eq. (3.2) at $q^2 \geq m_Q^2$, we insert a full subset of hadronic states, corresponding to the quark-flavor and quantum numbers of the interpolating current $j_\mu = \bar{q}\gamma_\mu Q$. For the sake of brevity, we assume exact hadron states, for which the completeness relation reduces to Eq. (3.7). From this follows that the correlation function is

$$\begin{aligned} \Pi_{\mu\nu}(q^2) = \sum_{\lambda,h} i \int d^4x e^{iqx} & \left[\theta(x_0) \langle 0 | j_\mu(x) | h(p_h, \lambda) \rangle \langle h(p_h, \lambda) | j_\nu^\dagger(0) | 0 \rangle \right. \\ & \left. + \theta(-x_0) \langle 0 | j_\nu^\dagger(0) | h(p_h, \lambda) \rangle \langle h(p_h, \lambda) | j_\mu(x) | 0 \rangle \right], \end{aligned} \quad (\text{B.1})$$

where we expand the time-ordered product. The translation operators can be separated from the quark-current $j_\mu(x) = e^{i\hat{p}_h x} j_\mu(0) e^{-i\hat{p}_h x}$. Hence, the matrix element, describing the vacuum-to-hadron transition, is given by

$$\langle 0 | j_\mu(x) | h(p_h, \lambda) \rangle = \langle 0 | j_\mu(0) | h(p_h, \lambda) \rangle e^{-ip_h x}. \quad (\text{B.2})$$

The conjugated partner is

$$\langle h(p_h, \lambda) | j_\mu(x) | 0 \rangle = \langle h(p_h, \lambda) | j_\mu(0) | 0 \rangle e^{ip_h x}. \quad (\text{B.3})$$

Further, we include the definition of the decay constant in Eq. (3.5) and integrate over d^3x :

$$\begin{aligned} \Pi_{\mu\nu}(q^2) = \sum_{\lambda, h \neq H} i \int dx_0 \left[\theta(x_0) e^{i(q^0 - p_h^0)x_0} \tilde{\rho}_{\mu\nu}(p_h, \lambda) \delta^{(3)}(\vec{q} - \vec{k}) \right. \\ \left. + \theta(-x_0) e^{i(q^0 + p_h^0)x_0} \tilde{\rho}_{\mu\nu}^\dagger(p_h, \lambda) \delta^{(3)}(\vec{q} + \vec{k}) \right]. \end{aligned} \quad (\text{B.4})$$

In the equation above, we introduced the function

$$\tilde{\rho}_{\mu\nu}(p_h, \lambda) \equiv (m_{H^*} f_{H^*})^2 \varepsilon_\mu(\lambda) \varepsilon_\nu^*(\lambda) + \langle 0 | j_\mu(0) | h(p_h, \lambda) \rangle \langle h(p_h, \lambda) | j_\nu^\dagger(0) | 0 \rangle$$

which separates the ground-state from all other hadron states. Using the integral representation of the theta function

$$\theta(x_0) = -\frac{1}{2\pi i} \int d\lambda \frac{e^{-i\lambda x_0}}{\lambda + i\varepsilon} \quad (\text{B.5})$$

we can perform the remaining integration according to

$$i \int dx_0 \theta(\pm x_0) e^{i(q^0 \mp p_h^0)x_0} = \mp \frac{1}{q_0 \mp \sqrt{\vec{q}^2 + m_h^2} \pm i\varepsilon}. \quad (\text{B.6})$$

Eqs. (B.5) and (B.6) lead to the propagator

$$\frac{1}{2\sqrt{\vec{q}^2 + m_h^2}} \left[\frac{1}{q_0 + \sqrt{\vec{q}^2 + m_h^2} - i\varepsilon} - \frac{1}{q_0 - \sqrt{\vec{q}^2 + m_h^2} + i\varepsilon} \right] = \frac{1}{m_h^2 - q^2 - i\varepsilon}. \quad (\text{B.7})$$

The two-point correlation now has the form

$$\begin{aligned} \Pi_{\mu\nu}(q^2) &= \left(-g_{\mu\nu} + \frac{q_\mu q_\nu}{m_{H^*}^2} \right) \times \frac{(m_{H^*} f_{H^*})^2}{m_{H^*}^2 - q^2 - i\varepsilon} + \sum_{h \neq H} \frac{\rho_{\mu\nu}(p_h^2)}{p_h^2 - q^2 - i\varepsilon} \\ &= \left(\frac{q_\mu q_\nu}{q^2} - g_{\mu\nu} \right) \times \left\{ \frac{(m_{H^*} f_{H^*})^2}{m_{H^*}^2 - q^2 - i\varepsilon} + \sum_{h \neq H} \frac{\rho_t(p_h^2)}{p_h^2 - q^2 - i\varepsilon} \right\} \\ &\quad + \frac{q_\mu q_\nu}{q^2} \left(\sum_{h \neq H} \frac{\rho_l(p_h^2)}{p_h^2 - q^2 - i\varepsilon} - f_{H^*}^2 \right), \end{aligned} \quad (\text{B.8})$$

where we used the CPT -invariance of QCD [152] stating that $\rho_{\mu\nu}$ is equal to $\rho_{\mu\nu}^\dagger$. For the ground state follows $|H^*\rangle = |\bar{H}^*\rangle$ and therefore $f_{H^*} = f_{\bar{H}^*}$. In the following, we neglect the last line of (B.8) since both terms in the parenthesis have a longitudinal structure, which does not agree to the (transverse) structure of the ground state. The second term has also no pole and a vanishing imaginary part, for positive q^2 and, hence, it does not contribute to the spectral density.

In the general (continuum) case the sum of hadron states characterizes a spectrum of hadronic particles on their mass-shell, i.e. the center of mass energy is $s = m_h^2$. One can use the Källén-Lehmann spectral representation [70] to rewrite

$$\sum_{h \neq H} \frac{\rho_{\mu\nu}(p_h^2)}{p_h^2 - q^2 - i\varepsilon} \rightarrow \int ds \frac{\rho_{\mu\nu}^h(s)}{s - q^2 - i\varepsilon} \quad (s = p_h^2 > 0), \quad (\text{B.9})$$

with

$$\rho_{\mu\nu}^h(s)\theta(p_0) \equiv \sum_h (2\pi)^3 \delta(s - m_h^2) \delta^{(4)}(p - p_h) \langle 0 | j_\mu(0) | h \rangle \langle h | j_\nu(0)^\dagger | 0 \rangle. \quad (\text{B.10})$$

B.2 Details about the Dispersion Relation

The function $\Pi(q^2)$ is analytic for $q^2 \ll m_Q^2$, which should be related to the physical domain ($s = q^2 \geq m_Q^2$) via *Cauchy's integral formula*

$$\Pi(q^2) = \frac{1}{2\pi i} \oint_C ds \frac{\Pi(s)}{s - q^2}. \quad (\text{B.11})$$

The contour C is divided into four sections (see Fig. 3.2): $C_R + C_+ + C_\varepsilon + C_-$. In the limit $R \rightarrow \infty$ and $\varepsilon^+ \rightarrow 0$, integrals along C_ε and C_R vanish:

$$\Pi(q^2) = \frac{1}{2\pi i} \left(\int_{C_R + C_\varepsilon} ds \frac{\Pi(s)}{s - q^2} + \int_{C_+ + C_-} ds \frac{\Pi(s)}{s - q^2} \right) \quad (\text{B.12})$$

$$= \frac{1}{2\pi i} \left(\oint_{|s|=R} ds \frac{\Pi(s)}{s - q^2} + \int_{m_Q^2}^R ds \frac{\Pi(s + i\varepsilon^+) - \Pi(s - i\varepsilon^+)}{s - q^2} \right) \quad (\text{B.13})$$

$$= \lim_{R \rightarrow \infty} \frac{1}{2\pi i} \int_{m_Q^2}^\infty ds \frac{\Pi(s + i\varepsilon^+) - \Pi(s - i\varepsilon^+)}{s - q^2}. \quad (\text{B.14})$$

In general, the condition

$$\lim_{R \rightarrow \infty} \oint_{|s| \rightarrow R} ds \frac{\Pi(s)}{s - q^2} = 0 \quad (\text{B.15})$$

is not given. To guarantee this limit, the integrand must converge according to $\Pi(q^2) \sim \frac{1}{|q^2|^\alpha}$ with $\alpha > 0$. As a result the residual integral reads

$$\Pi(q^2) = \frac{1}{2\pi i} \int_0^\infty ds \frac{\Pi(s + i\varepsilon^+) - \Pi(s - i\varepsilon^+)}{s - q^2}. \quad (\text{B.16})$$

The Schwarz's reflection principle states [71]: *Let f be a function that is analytic in a region S that has a segment of the real axis as part of its boundary B . If $f(z)$ is real whenever z is real, then the analytic continuation g of f into S^* (the mirror image of S with respect to the real axis) exists and is given by*

$$g(z) = \bar{f}(\bar{z}), \quad \text{where } z \in S^*. \quad (\text{B.17})$$

$\Pi(q^2)$ is analytic in the upper complex plane and real on the axis segment $q^2 < m_{H^*}^2$, then we are allowed to continue the function analytically in the lower half plane as the mirror image with respect to the real axis: $\bar{\Pi}(q^2) = \Pi(\bar{q}^2)$. In combination with

$$\Pi(s + i\varepsilon^+) = \text{Re} \{ \Pi(s + i\varepsilon^+) \} + i \text{Im} \{ \Pi(s + i\varepsilon^+) \}, \quad (\text{B.18})$$

$$\Pi(s - i\varepsilon^+) = \text{Re} \{ \Pi(s - i\varepsilon^+) \} - i \text{Im} \{ \Pi(s - i\varepsilon^+) \}, \quad (\text{B.19})$$

this principle leads to the spectral function

$$\rho(s) \equiv \frac{1}{\pi} \text{Im} \Pi(s) = \lim_{\varepsilon^+ \rightarrow 0} \frac{1}{2\pi i} [\Pi(s + i\varepsilon^+) - \Pi(s - i\varepsilon^+)]. \quad (\text{B.20})$$

Eq. (B.16) takes the final form

$$\Pi(q^2) = \int_{m_Q^2}^\infty ds \frac{\rho(s)}{s - q^2}. \quad (\text{B.21})$$

B.3 LiteRed Basis and Master Integrals

In order to create the reduction rules we define a basis which resembles the two-loop off-shell propagator with two massive and three massless lines as presented in Fig. B.1 (a). The basis consists of the functions D_α (inverse propagators), which depend

linearly on the scalar products determined by loop momenta q and k :

$$D_S = \left\{ \begin{array}{l} D_1 = m_Q^2 - (p - q)^2, \quad D_2 = m_Q^2 - (p - k)^2, \\ D_3 = -k^2, \quad D_4 = -q^2, \quad D_5 = -(q - k)^2 \end{array} \right\}. \quad (\text{B.22})$$

Finally, the two-loop propagator typology is built up by five master integrals MIs (see Fig. B.1 (b)-(d)):

$$\text{MIS} = \left\{ V(1, 1, 0, 0, 0), V(0, 1, 0, 1, 1), V(1, 1, 0, 1, 0), V(0, 2, 0, 1, 1), V(1, 1, 1, 1, 0) \right\}. \quad (\text{B.23})$$

The master integral $V(1, 1, 0, 0, 0)$ represents a double massive tadpole with a vanishing imaginary part.

Further, we find $V(0, 1, 0, 1, 1)$ and $V(0, 2, 0, 1, 1)$, which denote the convolution of a massive and massless loop diagram with simple and double power on the massive quark line. The master integral $V(1, 1, 0, 1, 0)$ is the product of a massive tadpole and a simple one-loop. The final integral $V(1, 1, 1, 1, 0)$ represents a double one-loop diagram. All masters are shown in Fig. B.1. We also present the corresponding prototypes to determine the spectral function of the perturbative contribution. Using the notation $G(1, 1) = G/\varepsilon$ it follows:

$$\rho_V(0, 1, 0, 1, 1; z) = \frac{G}{\varepsilon} \times \rho(1, \varepsilon; z) = \frac{s}{2} \left(1 - z^2 + 2z \log(z) \right), \quad (\text{B.24})$$

$$\rho_V(0, 2, 0, 1, 1; z) = \frac{G}{\varepsilon} \times \rho(2, \varepsilon; z) = -1 + z - \log(z), \quad (\text{B.25})$$

$$\begin{aligned} \rho_V(1, 1, 0, 1, 0; z) &= V(1, 1; m_Q^2) \times \rho(1, 1) \\ &= -\frac{G}{\varepsilon} s^{1-2\varepsilon} (1-z) z^{1-2\varepsilon} - s(1-z) z \left(\log(z) - 2\log(1-z) \right), \end{aligned} \quad (\text{B.26})$$

$$\begin{aligned} \rho_V(1, 1, 1, 1, 0; z) &= 2\frac{G}{\varepsilon} z^{-\varepsilon} \times \rho(1, 1) + 2(1-z)^2 \left(\log(z) - \log(1-z) \right) \\ &= 2\frac{G}{\varepsilon} s^{-\varepsilon} (1-z) z^{-2\varepsilon} + 2(1-z) \left(\log(z) - 2\log(1-z) \right) \\ &\quad + 2(1-z)^2 \left(\log(z) - \log(1-z) \right), \end{aligned} \quad (\text{B.27})$$

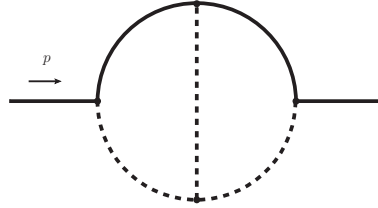
$$\rho_V(1, 1, 0, 0, 0; z) = 0. \quad (\text{B.28})$$

To perform the last step in above equations we considered the following one-loop spectral functions and used Eq. (4.14)

$$\rho(n, \varepsilon; z) = \frac{s^{2-2\varepsilon-n}}{\Gamma(n)\Gamma(\varepsilon)\Gamma(5-n-4\varepsilon)} \int_z^1 dx x^{\varepsilon-1} \bar{x}^{1-2\varepsilon} (x-z)^{2-n-2\varepsilon} \quad (\text{B.29})$$

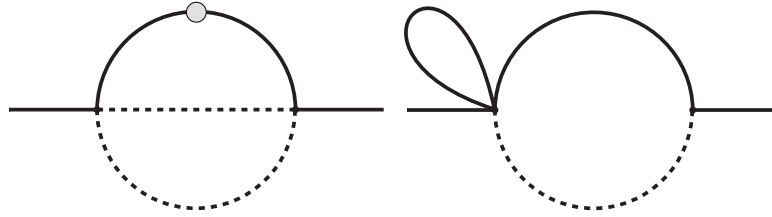
which are finite for $n = 1, 2$. In Eq. (B.26) we used the one-loop on-shell integral with one mass, see also Eq. (4.5), which results in $V(1, 1; m_Q^2) = \Gamma(1 - \frac{d}{2}) \times (m_Q^2)^{\frac{d}{2}-1}$.

Basis of two-loop topology



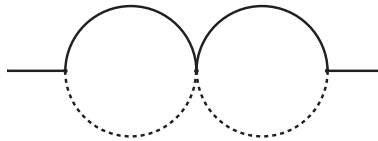
(a) Two-loop basis for LiteRed

Feynman graphs of master integrals



(b) $V(0, \{1, 2\}, 0, 1, 1)$

(c) $V(1, 1, 0, 1, 0)$



(d) $V(1, 1, 1, 1, 0)$

Figure B.1: Basis to generate IBP identities with LiteRed as selected for two-loop Feynman integrals is shown in (a). Master integrals of two-loop off-shell propagator with non-vanishing imaginary part in (b)-(d). Massive $b(c)$ -quark propagators denote solid lines, whereas massless propagators are represented by dashed lines. Dotted lines denote propagators with an additional power.

B.4 Perturbative Spectral Function

In this section we collect the expressions for NLO contributions to the spectral function $\rho_{t(5)}^{(\text{pert})}(s)$ in the $\overline{\text{MS}}$ -scheme for the heavy quark mass m_Q . For the vector heavy-light quark currents, according to our convention for the invariant amplitude $\Pi_t(q^2)$, we extract the coefficient at $-g_{\mu\nu}$ of $\Pi_{\mu\nu}(q)$. The corresponding spectral function reads:

$$\begin{aligned} \rho_t^{(\text{pert, NLO})}(s) = & \frac{3C_F}{16\pi^2} s \left[1 - \frac{5}{2}z + \frac{2}{3}z^2 + \frac{5}{6}z^3 + \frac{1}{3}z(-5 - 4z + 5z^2) \log(z) \right. \\ & - \frac{1}{3}(1-z)^2(4+5z) \log(1-z) + \frac{2}{3}(1-z)^2(2+z) \left(2 \text{Li}_2(z) \right. \\ & \left. \left. + \log(z) \log(1-z) \right) - z(1-z^2) \left(3 \log \left(\frac{\mu^2}{m_Q^2} \right) + 4 \right) \right], \end{aligned} \quad (\text{B.30})$$

where $z \equiv m_Q^2/s$ and $\text{Li}_2(z) = -\int_0^z \frac{\log(1-t)}{t} dt$. For the pseudoscalar heavy-light quark currents we have

$$\begin{aligned} \rho_5^{(\text{pert, NLO})}(s) = & \frac{3C_F}{16\pi^2} (m_Q + m_q)^2 s(1-z) \left[\frac{9}{2}(1-z) + (3-z)(1-2z) \log(z) \right. \\ & - (1-z)(5-2z) \log(1-z) + 2(1-z)(2 \text{Li}_2(z) + \log(z) \log(1-z)) \\ & \left. + (1-3z) \left(3 \log \left(\frac{\mu^2}{m_Q^2} \right) + 4 \right) \right]. \end{aligned} \quad (\text{B.31})$$

NNLO corrections are obtained in [75] in the pole mass scheme. Hence, to properly apply the $\overline{\text{MS}}$ scheme for m_Q to α_s^2 accuracy, we have to add to the corrections to the NNLO part, which arise from expanding the pole mass in the LO and NLO contribution in terms of $\overline{\text{MS}}$ mass. For the vector-current correlation function they are

$$\Delta_1 \rho_t^{(\text{pert, NNLO})}(s) = -\frac{3}{8\pi^2} s z \left[(3 - 7z^2) r_m^{(1)^2} - 2(1 - z^2) r_m^{(2)} \right], \quad (\text{B.32})$$

$$\begin{aligned} \Delta_2 \rho_t^{(\text{pert, NNLO})}(s) = & -\frac{1}{16\pi^2} C_F r_m^{(1)} s \left[-z(1-z^2) \left(24 \text{Li}_2(z) + 12 \log(z) \log(1-z) \right) \right. \\ & - 2z(9 + 6z - 17z^2) \log(z) + 2(1-z)(-4 + 5z + 17z^2) \log(1-z) \\ & \left. - z(1-z)(17 + 15z) \right], \end{aligned} \quad (\text{B.33})$$

respectively, and for the pseudoscalar-current correlation function:

$$\Delta_1 \rho_5^{(\text{pert, NNLO})}(s) = \frac{3(m_Q + m_q)^2}{8\pi^2} s \left[(3 - 20z + 21z^2) r_m^{(1)^2} - 2(1 - z)(1 - 3z) r_m^{(2)} \right], \quad (\text{B.34})$$

$$\begin{aligned} \Delta_2 \rho_5^{(\text{pert, NLO})}(s) = & -\frac{3(m_Q + m_q)^2}{8\pi^2} C_F r_m^{(1)} s \left[(1 - z)(1 - 3z) \left(4 \text{Li}_2(z) \right. \right. \\ & \left. \left. + 2 \log(z) \log(1 - z) \right) + (3 - 22z + 29z^2 - 8z^3) \log(z) \right. \\ & \left. - (1 - z)(7 - 21z + 8z^2) \log(1 - z) + \frac{1}{2}(1 - z)(15 - 31z) \right], \quad (\text{B.35}) \end{aligned}$$

where $r_m^{(1,2)}$ are the coefficients in the perturbative relation between the pole and $\overline{\text{MS}}$ quark masses, given in Sect. A.4.

Light-quark mass correction terms (see Sect. 4.4), after expanding the massive propagators in powers of m_q , read:

$$\delta \rho_T^{(\text{pert, LO, } m_q)}(s) = \frac{3}{8\pi^2} m_q \left[2m_Q(1 - z) - m_q(1 + z^2) \right], \quad (\text{B.36})$$

$$\begin{aligned} \delta \rho_T^{(\text{pert, NLO, } m_q)}(s) = & \frac{3}{8\pi^2} C_F m_q m_Q \left[2(1 - z) (2 \text{Li}_2(z) + \log(z) \log(1 - z)) \right. \\ & \left. + (3 - 4z - z^2) \log(z) - (1 - z)(5 + z) \log(1 - z) + \frac{1}{2}(17 - 26z + z^2) \right. \\ & \left. + 3(1 - 2z) \log \left(\frac{\mu^2}{m_Q^2} \right) \right]. \quad (\text{B.37}) \end{aligned}$$

The analogous corrections to the perturbative part of the pseudoscalar-current correlation function are:

$$\delta \rho_5^{(\text{pert, LO, } m_q)}(s) = \frac{3(m_Q + m_q)^2}{8\pi^2} \left[2(1 - z) m_Q m_q - 2m_q^2 \right], \quad (\text{B.38})$$

$$\begin{aligned} \delta \rho_5^{(\text{pert, NLO, } m_q)}(s) = & \frac{3(m_Q + m_q)^2}{8\pi^2} C_F m_Q m_q \left[(1 - z) \left(4 \text{Li}_2(z) + 2 \log(z) \log(1 - z) \right. \right. \\ & \left. \left. - 2(4 - z) \log(1 - z) \right) + 2(3 - 5z + z^2) \log(z) \right. \\ & \left. + 2(7 - 9z) + 3(2 - 3z) \log \left(\frac{\mu^2}{m_Q^2} \right) \right]. \quad (\text{B.39}) \end{aligned}$$

We include the above corrections only for the s -quark and up to the second (first) power in m_s in LO (NLO).

B.5 Condensate Contributions

We present the condensate contributions in two forms: with an explicit q^2 dependence (needed, e.g. for the power moments) and after Borel transformation.

In the correlation function of vector currents, the total contribution of the quark condensate is:

$$\begin{aligned} \Pi_{\mu\nu}^{\langle\bar{q}q\rangle}(q^2) = \langle\bar{q}q\rangle \frac{m_Q}{m_Q^2 - q^2} & \left[g_{\mu\nu} \left(1 - \frac{m_q m_Q}{2(m_Q^2 - q^2)} + \frac{\alpha_s C_F}{2\pi} f_{V,1}(z) \right) \right. \\ & \left. - \frac{q_\mu q_\nu}{q^2} \frac{\alpha_s C_F}{\pi} f_{V,2}(z) \right]. \end{aligned} \quad (\text{B.40})$$

with the NLO terms given by

$$f_{V,1}(z) = 2 - z + z(1-z)L_z - \frac{z}{z-1} \left(3 \log \frac{\mu^2}{m^2} + 4 \right), \quad (\text{B.41})$$

$$f_{V,2}(z) = 1 - 2z + 2z(1-z)L_z, \quad (\text{B.42})$$

where the short-hand notations $z = \frac{m_Q^2}{q^2}$ and $L_z = \log\left(\frac{z-1}{z}\right)$ are used. In the case of the strange quark as light quark partner the first-order $O(m_q)$ correction is included in (B.40). For our purpose, only the coefficient $\Pi_t^{\langle\bar{q}q\rangle}(q^2)$ of the full vector-current correlation function is needed. The Borel-transformed expression of this amplitude is:

$$\begin{aligned} \Pi_t^{\langle\bar{q}q\rangle}(M^2) = -m_Q \langle\bar{q}q\rangle e^{-\frac{m_Q^2}{M^2}} & \left(1 - \frac{m_q m_Q}{2M^2} + \frac{\alpha_s C_F}{2\pi} \left[1 - 3 \frac{m_Q^2}{M^2} \log\left(\frac{\mu^2}{m_Q^2}\right) - 4 \frac{m_Q^2}{M^2} \right. \right. \\ & \left. \left. + \frac{m_Q^2}{M^2} e^{\frac{m_Q^2}{M^2}} \Gamma\left(-1, \frac{m_Q^2}{M^2}\right) \right] \right), \end{aligned} \quad (\text{B.43})$$

with the incomplete gamma function $\Gamma(a, z) = \int_z^\infty t^{a-1} e^{-t} dt$. The NLO part in (B.40) originating from one-loop diagrams has an imaginary part at $q^2 \rightarrow s \geq m_Q^2$. The latter, in addition to the terms proportional to $\delta(s - m_Q^2)$ and its derivatives, contains also a part which does not vanish at $s > m_Q^2$, that is proportional to $\theta(s - m_Q^2)$. Since we include the latter in the OPE spectral function involved in the quark-hadron

duality approximation, we present also here the spectral function of the condensate contribution:

$$\begin{aligned} \rho_t^{\langle \bar{q}q \rangle}(s) = & -m_Q \langle \bar{q}q \rangle \left(\delta(s - m_Q^2) - \frac{1}{2} m_q m_Q \delta'(s - m_Q^2) + \frac{\alpha_s C_F}{2\pi} \left[\delta(s - m_Q^2) \right. \right. \\ & \left. \left. - m_Q^2 \left(3 \log \frac{\mu^2}{m_Q^2} + 4 \right) \delta'(s - m_Q^2) + \frac{m_Q^2}{s^2} \theta(s - m_Q^2) \right] \right). \end{aligned} \quad (\text{B.44})$$

Here, we introduce the derivative of the Dirac delta function $\delta'(x - x_0) = \frac{d}{dx} \delta(x - x_0)$. In the pseudoscalar-meson channel, the quark condensate contribution to the correlation function in the same approximation reads

$$\Pi_5^{\langle \bar{q}q \rangle}(q^2) = -\langle \bar{q}q \rangle \frac{(m_Q + m_q)^2 m_Q}{m_Q^2 - q^2} \left(1 - \frac{m_q}{2m_Q} - \frac{m_q m_Q}{2(m_Q^2 - q^2)} - \frac{\alpha_s C_F}{2\pi} f_5(z) \right), \quad (\text{B.45})$$

with the coefficient (see also [53])

$$f_5(z) = 3 \frac{z}{z-1} (L_z(2-z) - 1) + \frac{1}{z-1} \left(3 \log \frac{\mu^2}{m^2} + 7 - 3L_z \right). \quad (\text{B.46})$$

The Borel-transform of (B.45) yields:

$$\begin{aligned} \Pi_5^{\langle \bar{q}q \rangle}(M^2) = & -(m_Q + m_q)^2 m_Q \langle \bar{q}q \rangle e^{-\frac{m_Q^2}{M^2}} \left(1 - \frac{m_q}{2m_Q} - \frac{m_q m_Q}{2M^2} \right. \\ & \left. - \frac{\alpha_s C_F}{2\pi} \left[\left(3 \log \frac{\mu^2}{m_Q^2} + 4 \right) \frac{m_Q^2}{M^2} - 7 - 3 \log \frac{\mu^2}{m_Q^2} + 3\Gamma\left(0, \frac{m_Q^2}{M^2}\right) e^{\frac{m_Q^2}{M^2}} \right] \right). \end{aligned} \quad (\text{B.47})$$

The spectral function derived from (B.45) reads

$$\begin{aligned} \rho_5^{\langle \bar{q}q \rangle}(s) = & -(m_Q + m_q)^2 m_Q \langle \bar{q}q \rangle \left(\delta(s - m_Q^2) + \frac{\alpha_s C_F}{2\pi} \left[\left(7 + 3 \log \frac{\mu^2}{m_Q^2} \right) \delta(s - m_Q^2) \right. \right. \\ & \left. \left. - m_Q^2 \left(4 + 3 \log \frac{\mu^2}{m_Q^2} \right) \delta'(s - m_Q^2) - \frac{3}{s} \theta(s - m_Q^2) \right] \right). \end{aligned} \quad (\text{B.48})$$

The expressions for $d \geq 4$ condensate contributions for the vector-current correlation

function read:

$$\Pi_{\mu\nu}^{\langle GG \rangle}(q^2) = \frac{\langle GG \rangle}{12(m_Q^2 - q^2)} g_{\mu\nu}, \quad \Pi_{\mu\nu}^{\langle \bar{q}Gq \rangle}(q^2) = -\frac{m_0^2 \langle \bar{q}q \rangle m_Q^3}{2(m_Q^2 - q^2)^3} g_{\mu\nu}, \quad (\text{B.49})$$

$$\Pi_{\mu\nu}^{\langle \bar{q}q\bar{q}q \rangle}(q^2) = \frac{8\pi\alpha_s r_{vac} \langle \bar{q}q \rangle^2}{81(m_Q^2 - q^2)^4} \left[\left(9m_Q^4 - 16m_Q^2 q^2 + 4q^4 \right) g_{\mu\nu} + \left(10m_Q^2 - 4q^2 \right) q_\mu q_\nu \right]. \quad (\text{B.50})$$

The Borel-transformed expressions are:

$$\Pi_t^{\langle GG \rangle}(M^2) = -\frac{\langle GG \rangle}{12} e^{-\frac{m_Q^2}{M^2}}, \quad \Pi_t^{\langle \bar{q}Gq \rangle}(M^2) = \frac{m_0^2 \langle \bar{q}q \rangle m_Q^3}{4M^4} e^{-\frac{m_Q^2}{M^2}}, \quad (\text{B.51})$$

$$\Pi_t^{\langle \bar{q}q\bar{q}q \rangle}(M^2) = -\frac{32\pi\alpha_s r_{vac} \langle \bar{q}q \rangle^2}{81M^2} \left(1 + \frac{m_Q^2}{M^2} - \frac{m_Q^4}{8M^4} \right) e^{-\frac{m_Q^2}{M^2}}. \quad (\text{B.52})$$

The corresponding condensate contributions to the correlation function with pseudoscalar currents are:

$$\Pi_5^{\langle GG \rangle}(q^2) = \frac{\langle GG \rangle m_Q^2}{12(m_Q^2 - q^2)}, \quad \Pi_5^{\langle \bar{q}Gq \rangle}(q^2) = -\frac{m_0^2 \langle \bar{q}q \rangle m_Q^3}{2(m_Q^2 - q^2)^2} \left(1 - \frac{m_Q^2}{m_Q^2 - q^2} \right), \quad (\text{B.53})$$

$$\Pi_5^{\langle \bar{q}q\bar{q}q \rangle}(q^2) = -\frac{8\pi\alpha_s r_{vac} \langle \bar{q}q \rangle^2 m_Q^2 q^2}{27(m_Q^2 - q^2)^4} \left(2q^2 - 3m_Q^2 \right), \quad (\text{B.54})$$

yielding after Borel transformation:

$$\Pi_5^{\langle GG \rangle}(M^2) = \frac{\langle GG \rangle m_Q^2}{12} e^{-\frac{m_Q^2}{M^2}}, \quad \Pi_5^{\langle \bar{q}Gq \rangle}(M^2) = -\frac{m_0^2 \langle \bar{q}q \rangle m_Q^3}{2M^2} \left(1 - \frac{m_Q^2}{2M^2} \right) e^{-\frac{m_Q^2}{M^2}}, \quad (\text{B.55})$$

$$\Pi_5^{\langle \bar{q}q\bar{q}q \rangle}(M^2) = -\frac{16\pi\alpha_s r_{vac} \langle \bar{q}q \rangle^2 m_Q^2}{27M^2} \left(1 - \frac{m_Q^2}{4M^2} - \frac{m_Q^4}{12M^4} \right) e^{-\frac{m_Q^2}{M^2}}. \quad (\text{B.56})$$

B.6 Sum rules for Pseudoscalar Quark Currents in the Infinite Heavy-Quark-Mass Limit

The rescaled sum rule in the pseudoscalar channel according to the reparametrization rules in Eq. 3.51 is

$$f_H^2 m_H \left(\frac{m_H}{m_Q} \right)^3 e^{-\frac{\bar{\Lambda}}{\tau} - \frac{\bar{\Lambda}^2}{2m_Q \tau}} = \frac{3\tau^3}{\pi^2} \int_0^{\frac{\omega_0}{\tau}} dz e^{-z} \left(\frac{z^2}{1 + \frac{2z\tau}{m_Q}} \right)$$

$$\begin{aligned}
 & \times \left\{ 1 + \frac{2\alpha_s}{\pi} \left[\log\left(\frac{m_Q}{2\tau}\right) + \frac{13}{6} + \frac{2\pi^2}{9} - \log(z) + \frac{2}{3} \mathcal{K}_5\left(\frac{2z\tau}{m_Q}\right) \right] \right\} \\
 & - \langle q\bar{q} \rangle \left\{ 1 - \frac{2\alpha_s}{3\pi} \left(-1 + 3 \frac{2\tau}{m_Q} \int_0^\infty dz \frac{e^{-z}}{1 + \frac{2z\tau}{m_Q}} \right) \right\} + \frac{\langle GG \rangle}{12m_Q} \\
 & + \frac{m_0^2 \langle q\bar{q} \rangle}{16\tau^2} \left\{ 1 - \frac{4\tau}{m_Q} \right\} + \frac{\pi\alpha_s r_{\text{vac}} \langle q\bar{q} \rangle^2}{162\tau^3} \left\{ 1 + \frac{6\tau}{m_Q} - \frac{48\tau^2}{m_Q^2} \right\}.
 \end{aligned} \tag{B.57}$$

We introduced $\mathcal{K}_5(x)$ which is finite in the heavy-quark limit

$$\mathcal{K}_5(x) = 2 \text{Li}_2(-x) + \log(x) \log(1+x) - \frac{x}{1+x} \log(x) + \frac{1+x}{x} \log(1+x) - 1 \tag{B.58}$$

where

$$\lim_{x \rightarrow 0} \mathcal{K}_5(x) = -\frac{3}{2}x + \mathcal{O}(x^2). \tag{B.59}$$

List of Masters of On-Shell Two- and Three-Loop Topology

The total width of inclusive B decays is determined by the heavy quark expansion in Eq. (7.24). In order to calculate the leading power coefficient and coefficients of the power-suppressed operators, we perform a matching computation as described in Chap. 8. This matching computation gives rise to two-loop Feynman diagrams including one massive/massless charm quark and massless fermion lines at the LO level. NLO QCD corrections arise from additional gluon loops on the leading order Feynman diagrams. The calculation of these Feynman diagrams require a computational framework, which reduces scalar two- and three-loop integrals with on-shell b -quarks. For this purpose, we use LiteRed [85, 86] to determine the set of master integrals. In this section we give the corresponding basis for a massive b - and c -quark. We also consider the case of a massless c -quark. The results of prototypes to the given master integrals are also presented in the final parts of Sect. C.1 and C.2. In the final section we calculate the most difficult non-reducible prototype of this thesis.

C.1 LiteRed Basis and Master Integrals with Two Masses

We define a basis D_S with one massive line of the mass m_b , two massive line of the mass m_c and four massless lines. This basis is determined by three loop momenta q , k and l as well as the external momentum p with the condition $p^2 = m_b^2$. D_S is illustrated in Fig. C.1 (d) and reads in terms of inverse propagators:

$$D_S = \left\{ \begin{array}{l} D_1 = m_c^2 - (p - q)^2, \quad D_2 = -(p - k)^2, \\ D_3 = m_b^2 - k^2, \quad D_4 = -q^2, \quad D_5 = -l^2, \\ D_6 = -(l - q)^2, \quad D_7 = m_c^2 - (q - k)^2 \end{array} \right\}. \quad (\text{C.1})$$

154 Appendix C. List of Masters of On-Shell Two- and Three-Loop Topology

We define the two-loop basis

$$D_S' = \left\{ \begin{array}{l} C_1 = -(p-l)^2, \quad C_2 = m_c^2 - (p-q)^2, \\ C_3 = -q^2, \quad C_4 = -l^2, \quad C_5 = -(l-q)^2 \end{array} \right\}, \quad (\text{C.2})$$

which is shown in Fig. C.1 (a). The IBP reduction and other symmetry relations (see Chap. 4.1), employed by the program LiteRed, lead to eight master integrals with a non-vanishing imaginary part for the three-loop basis. We define the scalar integral

$$\begin{aligned} (m_b^2)^{3D/2-n_1-n_2-n_3-n_4-n_5-n_6-n_7} \times J(n_1, n_2, n_3, n_4, n_5, n_6, n_7) \\ \equiv \int_k \int_q \int_l \frac{1}{D_1^{n_1} D_2^{n_2} D_3^{n_3} D_4^{n_4} D_5^{n_5} D_6^{n_6} D_7^{n_7}} \end{aligned} \quad (\text{C.3})$$

from which follows the set of master integrals:

$$MIS = \left\{ \begin{array}{l} J(0, 1, 0, 0, 1, 1, 1), \quad J(1, 0, 0, 0, 1, 1, 1), \quad J(1, 0, 1, 0, 1, 1, 0), \\ J(0, 2, 0, 0, 1, 1, 1), \quad J(2, 0, 0, 0, 1, 1, 1), \quad J(2, 0, 1, 0, 1, 1, 0), \\ J(1, 0, 1, 0, 1, 1, 1), \quad J(2, 0, 1, 0, 1, 1, 1) \end{array} \right\}. \quad (\text{C.4})$$

In case of the two-loop basis we define

$$(m_b^2)^{D-n_1-n_2-n_3-n_4-n_5} \times K(n_1, n_2, n_3, n_4, n_5) \equiv \int_k \int_q \frac{1}{C_1^{n_1} C_2^{n_2} C_3^{n_3} C_4^{n_4} C_5^{n_5}} \quad (\text{C.5})$$

and end up with two master integrals with non-vanishing imaginary part:

$$MIS' = \left\{ K(0, 1, 0, 1, 1), K(0, 2, 0, 1, 1) \right\}. \quad (\text{C.6})$$

Here, $J(0, n, 0, 0, 1, 1, 1)$ denotes a convolution of simple massive and massless one-loop integrals ($n = 1$) including a massless propagator with second power ($n = 2$).

The master integrals $J(n, 0, 0, 0, 1, 1, 1)$ and $J(2, 0, 1, 0, 1, 1, 0)$ are the product of a massive tadpole (either b or c -quark) and a two-loop massive-massless convolution. The most complicated integrals $J(n, 0, 1, 0, 1, 1, 1)$ (with $n = 1, 2$) are non-reducible three-loop integrals with two different masses. Finally, $K(0, n, 0, 1, 1)$ represents a convolution of simple massive and massless one-loop integrals ($n = 1$) including a massless propagator with second power ($n = 2$). As a next step we consider the prototypes following from the imaginary part of all master integrals as stated above.

For this purpose, we apply the one-loop spectral function from Eq. (4.14) to the on-shell condition according to

$$\begin{aligned} \hat{V}(\alpha, \beta) &= V(\alpha, \beta, m_b^2) \Big|_{m_1=0, m_2=m_c} \\ \rightarrow \hat{\rho}(\alpha, \beta; r) &= \frac{s^{d/2-\alpha-\beta}}{\Gamma(\alpha)\Gamma(\beta)\Gamma(1+d/2-\alpha-\beta)} \int_r^1 dx \bar{x}^{d/2-\beta-1} x^{\beta-1} (x-r)^{d/2-\alpha-\beta}. \end{aligned} \quad (\text{C.7})$$

where $r \equiv m_c^2/m_b^2$. Prototypes from two- and three-loop master integrals are denoted by

$$\rho_J(n_1, n_2, n_3, n_4, n_5, n_6, n_7) \equiv \frac{1}{\pi} \times \text{Im} \left\{ J(n_1, n_2, n_3, n_4, n_5, n_6, n_7) \right\} \quad (\text{C.8})$$

and

$$\rho_K(n_1, n_2, n_3, n_4, n_5) \equiv \frac{1}{\pi} \times \text{Im} \left\{ K(n_1, n_2, n_3, n_4, n_5) \right\}. \quad (\text{C.9})$$

Two-Loop Prototypes

Relevant results of both two-loop finite prototypes $K_1 \equiv \rho_K(0, 1, 0, 1, 1)$ and $K_2 \equiv \rho_K(0, 2, 0, 1, 1)$ are given by

$$\begin{aligned} K_1 &= \frac{G}{\varepsilon} \times \hat{\rho}(1, \varepsilon; m_c^2) \\ &= \frac{1}{2} \left(1 - r^2 + 2r \log(r) \right) + \varepsilon \left[4r \text{Li}_2(r) + \frac{5}{4} (1 - r^2) - 2(1 - r^2) \log(1 - r) - \frac{2\pi^2}{3} r \right. \\ &\quad \left. - \frac{1}{2} r \log^2(r) - \frac{1}{2} r(2 + r) \log(r) \right] \end{aligned} \quad (\text{C.10})$$

$$K_2 = \left(-\frac{\partial K_1}{\partial(m_c^2)} \right) = \frac{G}{\varepsilon} \times \hat{\rho}(2, \varepsilon; m_c^2) \quad (\text{C.11})$$

$$\begin{aligned} &= -1 + r - \log(r) + \varepsilon \left[-4 \text{Li}_2(r) + r + 4(1 - r) \log(1 - r) + \frac{2\pi^2}{3} - 1 \right. \\ &\quad \left. + \frac{1}{2} \log^2(r) + (2 + r) \log(r) \right] \end{aligned} \quad (\text{C.12})$$

Three-Loop Prototypes

Here we present the three-loop on-shell prototypes. For brevity the abbreviations $M_{1,\{1,2\}} \equiv \rho_J(\{1, 2\}, 0, 0, 0, 1, 1, 1)$, $M_{2,\{1,2\}} \equiv \rho_J(0, \{1, 2\}, 0, 0, 1, 1, 1)$,

156 Appendix C. List of Masters of On-Shell Two- and Three-Loop Topology

$M_{4,\{1,2\}} \equiv \rho_J(\{1, 2\}, 0, 1, 0, 1, 1, 0)$ and $N_{\{1,2\}} \equiv \rho_J(\{1, 2\}, 0, 1, 0, 1, 1, 1)$ are used. In the following only the relevant expressions in terms of ε are displayed:

$$\begin{aligned} M_{11} &= V(1; m_c^2) \times \rho(1, \varepsilon; m_c^2) \\ &= \frac{1}{2\varepsilon} r (r^2 - 2r \log(r) - 1) + \frac{1}{12} r \left(-48r \operatorname{Li}_2(r) + 9r^2 - 24(r^2 - 1) \log(1 - r) \right. \\ &\quad \left. + 8\pi^2 r + 6 \log(r)(4r + 3r \log(r) + 1) - 9 \right), \end{aligned} \quad (\text{C.13})$$

$$\begin{aligned} M_{12} &= V(1; m_c^2) \times \rho(2, \varepsilon; m_c^2) = V(1; m_c^2) \times \left(-\frac{\partial \rho(1, \varepsilon; m_c)}{\partial(m_c^2)} \right) \\ &= \frac{1}{\varepsilon} r (-r + \log(r) + 1) + \frac{1}{6} r \left(24 \operatorname{Li}_2(r) - 9 \log^2(r) - 24 \log(r) \right. \\ &\quad \left. + 24(r - 1) \log(1 - r) - 4\pi^2 \right), \end{aligned} \quad (\text{C.14})$$

$$M_{21} = \rho(1, 2\varepsilon - 1; m_c^2) = \frac{1}{12} \left(6r(r + 1) \log(r) - (r - 1)(r(r + 10) + 1) \right), \quad (\text{C.15})$$

$$\begin{aligned} M_{22} &= \rho(1, 2\varepsilon; m_c^2) \\ &= \frac{1}{2\varepsilon} \left(r^2 - 2r \log(r) - 1 \right) + \frac{1}{2} \left(-12r \operatorname{Li}_2(r) + 3r^2 + 2r^2 \log(r) \right. \\ &\quad \left. - 6(r^2 - 1) \log(1 - r) + 2\pi^2 r + r \log^2(r) + 4r \log(r) - 3 \right), \end{aligned} \quad (\text{C.16})$$

$$\begin{aligned} M_{41} &= V(1; m_b^2) \times \rho(1, \varepsilon; m_c^2) \\ &= \frac{1}{2\varepsilon} \left(r^2 - 2r \log(r) - 1 \right) + \frac{1}{12} \left(-48r \operatorname{Li}_2(r) + 9r^2 + 6r^2 \log(r) \right. \\ &\quad \left. - 24(r^2 - 1) \log(1 - r) + 8\pi^2 r + 6r \log^2(r) + 24r \log(r) - 9 \right), \end{aligned} \quad (\text{C.17})$$

$$\begin{aligned} M_{42} &= V(1; m_b^2) \times \rho(2, \varepsilon; m_c^2) = V(1; m_b) \times \left(-\frac{\partial \rho(1, \varepsilon; m_c)}{\partial(m_c^2)} \right) \\ &= \frac{1}{\varepsilon} (-r + \log(r) + 1) + 4 \operatorname{Li}_2(r) - \frac{1}{2} \log^2(r) - r \log(r) - 3 \log(r) \\ &\quad + 4(r - 1) \log(1 - r) - \frac{2\pi^2}{3}. \end{aligned} \quad (\text{C.18})$$

Note that we refrain from computing the non-reducible three-loop in the present form. It is more convenient to calculate the sum and difference of N_1 and N_2 :

$$N_{\pm} = N_1 \pm N_2. \quad (\text{C.19})$$

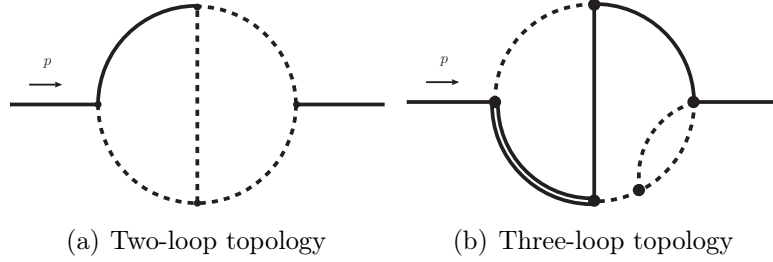
For both prototypes we find finite expressions:

$$\begin{aligned}
 N_+ = & -2(1-r) - (1+r)\log(r) \\
 & + \varepsilon \left[2(5r + 2\pi^2\sqrt{r} - 5) - (1+r)\log(r) + 8(1-r)\log(1-r) \right. \\
 & + \frac{1}{2}(1-r)\log^2(r) + 4(1+r)\log(1-r)\log(r) \\
 & \left. - 4\sqrt{r} \left(4\text{Li}_2^- - \pi^2 - 2\log(r)\log\left(\frac{1+\sqrt{r}}{1-\sqrt{r}}\right) \right) \right], \tag{C.20}
 \end{aligned}$$

$$\begin{aligned}
 N_- = & -\frac{\pi^2}{3}(1-r) - (1-r)\log(r) + r\log^2(r) + 2(1-r)\log(r)\log(1-r) \\
 & + 2(1-r)\text{Li}_2(r), \tag{C.21}
 \end{aligned}$$

where $\text{Li}_2^- \equiv \text{Li}_2(\sqrt{r}) - \text{Li}_2(-\sqrt{r})$. The explicit calculation of N_+ and N_- is presented in Sect. C.3.

Basis of two- and three-loop topology



Feynman graphs of master integrals

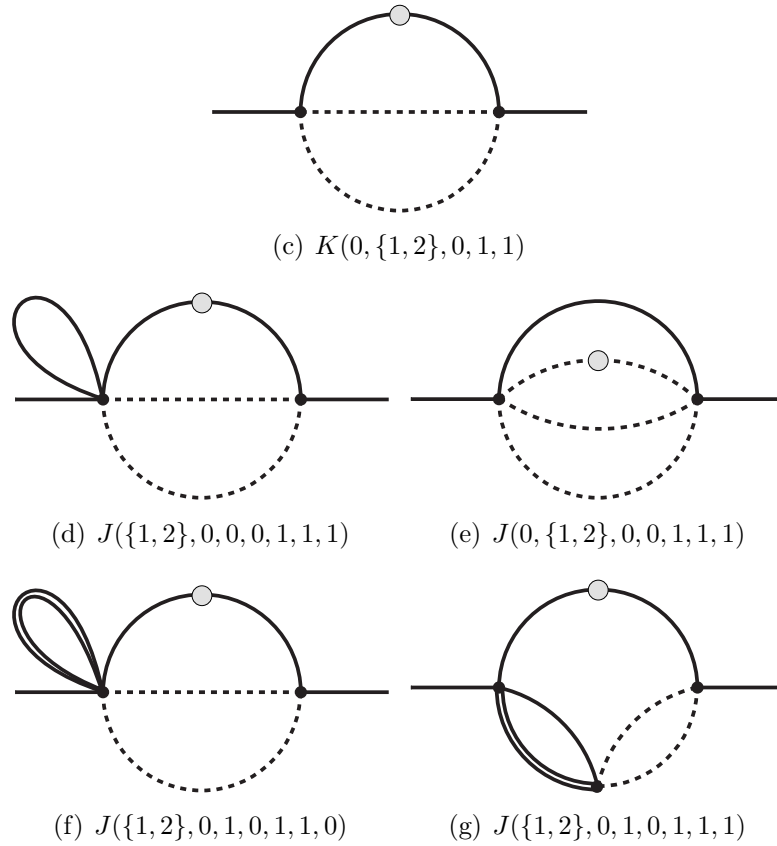


Figure C.1: Basis to generate IBP identities by LiteRed as selected for two- and three-loop Feynman integrals are shown in (a) and (b). Master integrals of two- and three-loop on-shell propagators ($p^2 = m_b^2$) with non-vanishing imaginary part in (c)-(g). Massive b -quark propagators are represented as double lines. Massive c -quark propagators denote solid lines, whereas massless propagators are represented by dashed lines. Dotted lines denote propagators with an additional power.

C.2 LiteRed Basis and Master Integrals with One Mass ($m_c = 0$)

In case of a massless c -quark we define a basis Ds'' with one massive line of the mass m_b and six massless lines. This basis is determined by three loop momenta q , k and l as well as the external momentum p , following $p^2 = m_b^2$. Ds'' is illustrated in Fig. C.2 (d) and reads in terms of inverse propagators:

$$\text{Ds}'' = \left\{ \begin{array}{l} B_1 = -(p-q)^2, \quad B_2 = -(p-k)^2, \\ B_3 = m_b^2 - k^2, \quad B_4 = -q^2, \quad B_5 = -l^2, \\ B_6 = -(l-q)^2, \quad B_7 = -(q-k)^2 \end{array} \right\}. \quad (\text{C.22})$$

We define the two-loop basis

$$\text{Ds}''' = \left\{ \begin{array}{l} A_1 = -(p-l)^2, \quad A_2 = -(p-q)^2, \\ A_3 = -q^2, \quad A_4 = -l^2, \quad A_5 = -(l-q)^2 \end{array} \right\}, \quad (\text{C.23})$$

which is also displayed in Fig. C.2 (a). The IBP reduction and other symmetry relations (see Chap. 4.1) employed by LiteRed lead to eight master integrals with a non-vanishing imaginary part for the three-loop basis. We define the scalar integral

$$\begin{aligned} (m_b^2)^{3D/2-n_1-n_2-n_3-n_4-n_5-n_6-n_7} \times M(n_1, n_2, n_3, n_4, n_5, n_6, n_7) \\ \equiv \int_k \int_q \int_l \frac{1}{B_1^{n_1} B_2^{n_2} B_3^{n_3} B_4^{n_4} B_5^{n_5} B_6^{n_6} B_7^{n_7}} \end{aligned} \quad (\text{C.24})$$

from which follows the set of master integrals:

$$\text{MIs}'' = \left\{ M(0, 1, 0, 0, 1, 1, 1), \quad M(1, 0, 1, 0, 1, 1, 0), \quad M(1, 0, 1, 0, 1, 1, 1) \right\} \quad (\text{C.25})$$

In case of the two-loop basis we define

$$(m_b^2)^{D-n_1-n_2-n_3-n_4-n_5} \times N(n_1, n_2, n_3, n_4, n_5) \equiv \int_k \int_q \frac{1}{A_1^{n_1} A_2^{n_2} A_3^{n_3} A_4^{n_4} A_5^{n_5}} \quad (\text{C.26})$$

and end up with two masters with a non-vanishing imaginary part:

$$\text{MIs}''' = \left\{ N(0, 1, 0, 1, 1), \quad N(1, 1, 1, 1, 0) \right\}. \quad (\text{C.27})$$

$M(0, 1, 0, 0, 1, 1, 1)$ denotes a convolution of massless one-loop integrals.

$M(1, 0, 1, 0, 1, 1, 0)$ is the product of the massive tadpole and a two-loop massive-massless convolution. The most complicated master $M(1, 0, 1, 0, 1, 1, 1)$ is a non-reducible three-loop integral with one mass. $N(0, 1, 0, 1, 1)$ also represents a convolution of simple massless one-loop integrals whereas $N(0, 1, 0, 1, 1)$ is a product of two one-loop massless integrals. Prototypes from above master integrals are denoted by $M(\dots) \rightarrow \rho_M(\dots)$ and $N(\dots) \rightarrow \rho_N(\dots)$.

C.2.1 Two-Loop Prototypes

Both two-loop prototypes $\tilde{K}_1 \equiv \rho_N(0, 1, 0, 1, 1)$, $\tilde{K}_2 \equiv \rho_N(1, 1, 1, 1, 0)$ are finite. The relevant expressions in terms of ε are

$$\tilde{K}_1 = 1 + 4\varepsilon, \quad \tilde{K}_2 = \frac{2}{\varepsilon} - \frac{4\pi^2}{3}\varepsilon. \quad (\text{C.28})$$

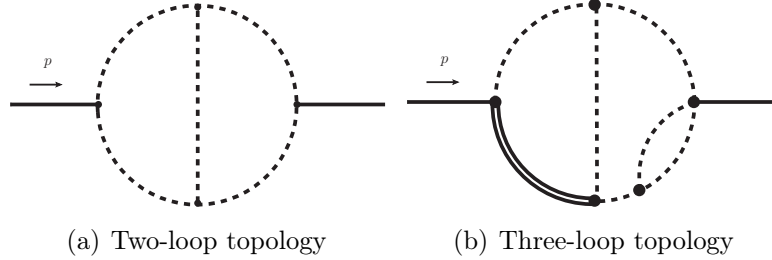
C.2.2 Three-Loop Prototypes

Here we present the three-loop on-shell prototypes. For brevity we use the abbreviations $\tilde{M}_1 \equiv \rho_M(0, 1, 0, 0, 1, 1, 1)$, $\tilde{M}_2 \equiv \rho_M(1, 0, 1, 0, 1, 1, 0)$, and $\tilde{M}_4 \equiv \rho_M(1, 0, 1, 0, 1, 1, 1)$. In the following, only the relevant expressions of the ε -expansion are displayed:

$$\tilde{M}_1 = \frac{1}{12} + \frac{35}{72}\varepsilon, \quad (\text{C.29})$$

$$\tilde{M}_2 = -\frac{1}{2\varepsilon} - \frac{3}{4} + \left(\frac{\pi^2}{4} - \frac{13}{8}\right)\varepsilon, \quad \tilde{M}_4 = \frac{1}{2\varepsilon} + \left(\frac{5}{2} - \frac{\pi^2}{6}\right). \quad (\text{C.30})$$

Basis of two- and three-loop topology



Feynman graphs of master integrals

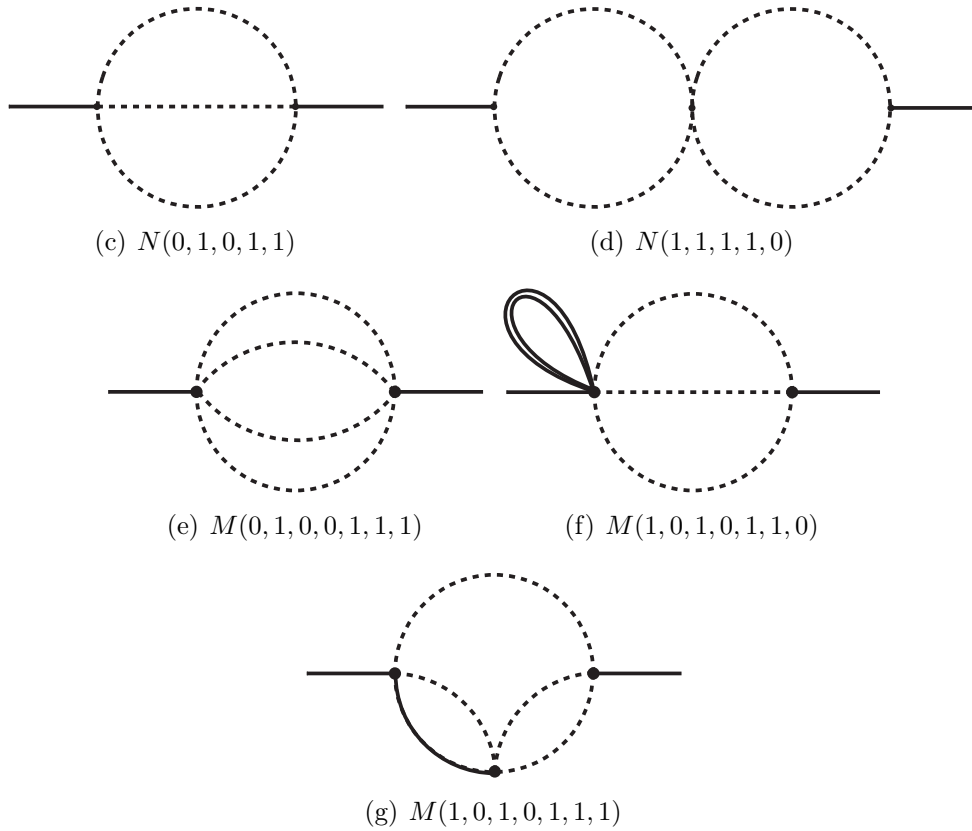


Figure C.2: Basis to generate IBP identities by LiteRed as selected for two- and three-loop Feynman integrals are shown in (a) and (b). Master integrals of two- and three-loop on-shell propagators ($p^2 = m_b^2$) with non-vanishing imaginary part in (c)-(g). Massive b -quark propagators are represented as double lines. Massive c -quark propagators denote solid lines, whereas massless propagators are represented by dashed lines.

C.3 Calculation of N_+ and N_-

In the following, we will compute the non-reducible prototypes N_+ and N_- . For convenience, we define the three-loop integral

$$\hat{J}(a, b, 1, 1, 1) \equiv \int_k \int_q \int_l \frac{1}{[m_b^2 - (p - q)^2]^a [m_c^2 - (q - k)^2]^b [-(l - k)^2] [-(p - l)^2] [m_c^2 - k^2]} \quad (\text{C.31})$$

and their corresponding spectral functions

$$\rho_j(a, b, 1, 1, 1) \equiv \frac{1}{2\pi i} \text{Disc} \left(\hat{J}(a, b, 1, 1, 1) \right). \quad (\text{C.32})$$

If we consider the sum or difference of N_1 and N_2 , this simplifies the problem as follows

$$\begin{aligned} N_{\pm} &= \rho_j(2, 1, 1, 1, 1) \pm \rho_j(1, 2, 1, 1, 1) \\ &= \frac{G}{\varepsilon} \Gamma\left(3 - \frac{d}{2}\right) \int_k \int_0^1 dx \frac{1}{\tilde{\Lambda}^{3-d/2}} \frac{x \pm \bar{x}}{[m_c^2 - k^2] [-(p - k)^2]^\varepsilon}. \end{aligned} \quad (\text{C.33})$$

The parameter $\tilde{\Lambda}$ is an abbreviation of the denominator given by

$$\tilde{\Lambda} = m_b^2 x + m_c^2 \bar{x} - (p - k)^2 x \bar{x} \quad (\text{C.34})$$

after Feynman parametrization. In Eq. C.33 we insert the massless one-loop integral

$$\int_l \frac{1}{[-(l - k)^2] [-(p - l)^2]} = \int_l \frac{1}{[-l^2] [-(l - (k - p))^2]} = \frac{G}{\varepsilon} \frac{1}{[-(p - k)^2]^\varepsilon}. \quad (\text{C.35})$$

We employ the Cutkosky rules to evaluate the discontinuity of N_{\pm} . To this end, we perform the substitutions

$$\frac{1}{m^2 - p^2 - i\varepsilon} \rightarrow (-2\pi i) \delta(p^2 - m^2) \theta(p_0), \quad (\text{C.36})$$

$$\frac{1}{\varepsilon} \times \frac{1}{[-(p - k)^2]^\varepsilon} \rightarrow (-2\pi) \frac{\sin(\pi\varepsilon)}{\pi\varepsilon} \cdot \frac{1}{(p - k)^{2\varepsilon}} \theta((p - k)^2) \quad (\text{C.37})$$

and introduce the prefactor $1/(2i)$. We find

$$N_+ = \rho_j(2, 1, 1, 1, 1) + \rho_j(1, 2, 1, 1, 1)$$

$$= (2\pi i)^2 G \Gamma\left(3 - \frac{d}{2}\right) \int_k \int_0^1 dx \frac{\delta(k^2 - m_c^2) \theta((p-k)^2) \theta(k_0)}{\tilde{\Lambda}^{3-d/3} \cdot (p-k)^{2\varepsilon}}. \quad (\text{C.38})$$

We now choose the rest frame of the b -quark for brevity:

$$p^\mu = \begin{pmatrix} m_b \\ 0 \end{pmatrix}, \quad k^\mu = \begin{pmatrix} k_\parallel \\ k_\perp \end{pmatrix} = \begin{pmatrix} kv \\ k_\perp \end{pmatrix}. \quad (\text{C.39})$$

The integration measure yields

$$d^d k = dk_0 d^{d-1} \vec{k} = dk_0 k^{d-2} dk \Omega_{d-1} = \frac{1}{2} dk_0 dk^2 k^{d-3} \Omega_{d-1} = dt dk_\perp^2 (k_\perp^2)^{\frac{d-3}{2}} \times \frac{\Omega_{d-1}}{2}, \quad (\text{C.40})$$

where $\Omega_d = 2\pi^{d/2}/\Gamma(d/2)$. Here, we introduce the parametrization $m_b t = pk$. The momentum integration has limits due to the delta distribution $\delta(k^2 - m_c^2)$ and the step function $\theta(k_0)$, i.e.

$$\delta(k^2 - m_c^2) \theta(k_0) = \delta(k_0^2 - \vec{k}_\perp^2 - m_c^2) \theta(k_0) = \delta([t^2 - m_c^2] - \vec{k}_\perp^2) \theta(t), \quad (\text{C.41})$$

$$\theta((p-k)^2) = \theta(m_b^2 + m_c^2 - 2m_b \cdot t). \quad (\text{C.42})$$

Both functions give rise to the integration limits

$$m_c \leq t \leq \frac{m_b^2 + m_c^2}{2m_b}. \quad (\text{C.43})$$

We rearrange the denominator $\tilde{\Lambda}$ as follows

$$\begin{aligned} \tilde{\Lambda} &= m_b^2 x + m_c^2 \bar{x} - (m_b^2 + m_c^2 - 2tm_b) x \bar{x} \\ &= m_b^2 x^2 + m_c^2 \bar{x}^2 + 2tm_b x \bar{x} = m_b^2 \bar{x}^2 + m_c^2 x^2 + 2tm_b x \bar{x} \\ &\equiv (1 - ax)(1 - bx) m_b^2. \end{aligned} \quad (\text{C.44})$$

The spectral function N_+ for $m_b = 1$ and $r \equiv m_c^2/m_b^2$ reads

$$N_+ = C_0 \int_{m_c}^{\frac{1-m_c^2}{2}} dt \int_0^1 dx (t^2 - r)^{\frac{1}{2}-\varepsilon} \frac{1}{[(1-ax)(1-bx)]^{1+\varepsilon} (1+r-2t)^{2\varepsilon}}, \quad (\text{C.45})$$

164 Appendix C. List of Masters of On-Shell Two- and Three-Loop Topology

where $C_0 \equiv G \Gamma(3 - d/2) \Omega_{d-1} / (2\pi)$. For further computation we also define

$$a \equiv \sqrt{t^2 - r} - (t - 1), \quad b \equiv -\sqrt{t^2 - r} - (t - 1), \quad (\text{C.46})$$

$$a \equiv 1 - m_c \xi, \quad b \equiv 1 - m_c \xi^{-1}. \quad (\text{C.47})$$

The new parameter ξ has the following properties:

$$\xi = \frac{t - \sqrt{t^2 - r}}{\sqrt{r}}, \quad \xi^{-1} = \frac{t + \sqrt{t^2 - r}}{\sqrt{r}}, \quad \xi \xi^{-1} = 1. \quad (\text{C.48})$$

From this follows $t = \sqrt{r}(\xi^{-1} + \xi)/2$ and $\sqrt{t^2 - r} = \sqrt{r}(\xi^{-1} - \xi)/2 = (a - b)/2$. We do not calculate the whole integral, since only the pole and finite part are essential for computing the coefficient functions in Eq.7.24. Double poles appear at an intermediate level in combinations with N_+ and reducible prototypes. Those prototypes can be expanded in ε in order to obtain finite expressions. Hence, we expand N_+ up to $\mathcal{O}(\varepsilon)$ and get 4 individual integrals. The expanded prototype is

$$\begin{aligned} N_+ &= C_0 (N_+|_{\text{LO}} + \varepsilon N_+|_{\text{NLO}}) \\ &= C_0 \int_{m_c}^{\frac{1-m_c^2}{2}} dt \int_0^1 dx \frac{\sqrt{t^2 - r}}{[(1 - ax)(1 - bx)]} - \varepsilon \frac{\sqrt{t^2 - r}}{[(1 - ax)(1 - bx)]} \\ &\quad \times \left[\log(t^2 - r) + \log((1 - ax)(1 - bx)) + \log(1 + r - 2t) \right]. \end{aligned} \quad (\text{C.49})$$

For the leading order expressions we find

$$\begin{aligned} N_+|_{\text{LO}} &= \int_{m_c}^{\frac{1-m_c^2}{2}} dt \int_0^1 dx \frac{\sqrt{t^2 - r}}{[(1 - ax)(1 - bx)]} \\ &= \int dt \left(\frac{a - b}{2} \right) \int dx \frac{1}{[(1 - ax)(1 - bx)]} \\ &= \int dt \frac{1}{2} \log \left(\frac{b - 1}{a - 1} \right) = \int_1^{m_c} d\xi \frac{dt}{d\xi} \cdot (-1) \log \xi = \frac{1}{2} \left[1 - r + \frac{1}{2} (1 + r) \log(r) \right]. \end{aligned} \quad (\text{C.50})$$

The integration limits are $1 \leq \xi \leq m_c$. We divide the NLO expression in three parts, i.e.

$$N_+|_{\text{NLO}} = N_+|_{\text{NLO}}^{(1)} + N_+|_{\text{NLO}}^{(2)} + N_+|_{\text{NLO}}^{(3)}. \quad (\text{C.51})$$

For the individual terms of $N_+|_{\text{NLO}}$ we find

$$\begin{aligned} N_+|_{\text{NLO}}^{(1)} &= \iint dt dx \frac{\sqrt{t^2 - r}}{[(1 - ax)(1 - bx)]} \log(t^2 - r) \\ &= 2 \int_{m_c}^1 d\xi \frac{dt}{d\xi} \log(\xi) \log\left(\frac{\sqrt{r}}{2}(\xi^{-1} - \xi)\right), \end{aligned} \quad (\text{C.52})$$

$$\begin{aligned} N_+|_{\text{NLO}}^{(2)} &= \iint dt dx \frac{\sqrt{t^2 - r}}{[(1 - ax)(1 - bx)]} \log(1 + r - 2t) \\ &= \int_{m_c}^1 d\xi \frac{dt}{d\xi} \log(\xi) \log\left(1 + r - \sqrt{r}(\xi^{-1} + \xi)\right), \end{aligned} \quad (\text{C.53})$$

$$\begin{aligned} N_+|_{\text{NLO}}^{(3)} &= \iint dt dx \frac{\sqrt{t^2 - r}}{[(1 - ax)(1 - bx)]} \log((1 - ax)(1 - bx)) \\ &= \int_1^{m_c} d\xi \frac{dt}{d\xi} F(a, b) = tF(a, b)\Big|_1^{m_c} - \int_1^{m_c} d\xi t \frac{dF(a, b)}{d\xi}. \end{aligned} \quad (\text{C.54})$$

$$(\text{C.55})$$

where $F(a, b) \equiv \int dx \frac{\sqrt{t^2 - r}}{[(1 - ax)(1 - bx)]} \log((1 - ax)(1 - bx))$. For reasons of normalization we consider

$$\frac{C_0}{G^3} \left(\frac{1}{2}\right)^{\frac{d-4}{2}} = 4(1 - 2\varepsilon). \quad (\text{C.56})$$

Hence, the final result of the non-reducible prototype N_+ is

$$\begin{aligned} N_+/G^3 &= 4(1 - 2\varepsilon)(N_+|_{\text{LO}} + \varepsilon \times N_+|_{\text{NLO}}) \\ &= -\frac{1}{\varepsilon} \left(2(1 - r) + (1 + r) \log(r)\right) \\ &\quad + 4\sqrt{r} \left(\pi^2 - 4\text{Li}_2^- + 2 \log\left(\frac{1 + \sqrt{r}}{1 - \sqrt{r}}\right) \log(r)\right) \\ &\quad + \frac{1}{2}(1 - r) \log^2(r) + 4(1 + r) \log(1 - r) \log(r) \\ &\quad - (1 + r) \log(r) + 8(1 - r) \log(1 - r) - 10(1 - r). \end{aligned} \quad (\text{C.57})$$

166 Appendix C. List of Masters of On-Shell Two- and Three-Loop Topology

For N_- we find the finite expression

$$N_- = \frac{2}{3}(1-r) \left(3\text{Li}_2(r) - \frac{1}{2}\pi^2 \right) + r \log^2(r) + (1-r)(2\log(1-r) - 1)\log(r). \tag{C.58}$$

Bibliography

- [1] Yang C.N. and Mills R.L. *Conservation of Isotopic Spin and Isotopic Gauge Invariance*. Phys. Rev. **96**, (1954), 191–195. (Cited on pages 1 and 9.)
- [2] Glashow S.L. *Partial Symmetries of Weak Interactions*. Nucl. Phys. **22**, (1961), 579–588. (Cited on page 1.)
- [3] Higgs P.W. *Broken Symmetries and the Masses of Gauge Bosons*. Phys. Rev. Lett. **13**, (1964), 508–509. (Cited on page 1.)
- [4] Englert F. and Brout R. *Broken Symmetry and the Mass of Gauge Vector Mesons*. Phys. Rev. Lett. **13**, (1964), 321–323. (Cited on page 1.)
- [5] Guralnik G.S., Hagen C.R. and Kibble T.W.B. *Global Conservation Laws and Massless Particles*. Phys. Rev. Lett. **13**, (1964), 585–587. (Cited on page 1.)
- [6] Weinberg S. *A Model of Leptons*. Phys. Rev. Lett. **19**, (1967), 1264–1266. (Cited on page 1.)
- [7] Salam A. *Weak and Electromagnetic Interactions*. Conf. Proc. **C680519**, (1968), 367–377. (Cited on page 1.)
- [8] 't Hooft G. and Veltman M.J.G. *Regularization and Renormalization of Gauge Fields*. Nucl. Phys. **B44**, (1972), 189–213. (Cited on pages 1 and 131.)
- [9] Gell-Mann M. *Isotopic Spin and New Unstable Particles*. Phys. Rev. **92**, (1953), 833–834. (Cited on page 1.)
- [10] Barnes V.E. et al. *Observation of a Hyperon with Strangeness -3*. Phys. Rev. Lett. **12**, (1964), 204–206. (Cited on page 2.)
- [11] Gell-Mann M. *A Schematic Model of Baryons and Mesons*. Phys. Lett. **8**, (1964), 214–215. (Cited on page 2.)
- [12] Zweig G. *An $SU(3)$ model for strong interaction symmetry and its breaking. Version 2*. In Lichtenberg D. and Rosen S.P. (eds.), *Developments in the Quark Theory of Hadrons. Vol. 1. 1964 - 1978*. (Cited on page 2.)

- [13] Clark A.R., Elioff T., Field R.C., Frisch H.J., Johnson R.P., Kerth L.T. and Wenzel W.A. *Experimental Limits on the Decays $K_L^0 \rightarrow \mu^+\mu^-$, e^+e^- , and $\mu^\pm e^\mp$* . Phys. Rev. Lett. **26**, (1971), 1667–1671. (Cited on page 2.)
- [14] Glashow S.L., Iliopoulos J. and Maiani L. *Weak Interactions with Lepton-Hadron Symmetry*. Phys. Rev. **D2**, (1970), 1285–1292. (Cited on page 2.)
- [15] Aubert J.J. et al. [E598]. *Experimental Observation of a Heavy Particle J*. Phys. Rev. Lett. **33**, (1974), 1404–1406. (Cited on page 2.)
- [16] Augustin J.E. et al. [SLAC-SP-017]. *Discovery of a Narrow Resonance in e^+e^- Annihilation*. Phys. Rev. Lett. **33**, (1974), 1406–1408. [Adv. Exp. Phys.5,141(1976)]. (Cited on page 2.)
- [17] Christenson J.H., Cronin J.W., Fitch V.L. and Turlay R. *Evidence for the 2π Decay of the $k(2)0$ Meson*. Phys. Rev. Lett. **13**, (1964), 138–140. (Cited on page 2.)
- [18] Kobayashi M. and Maskawa T. *CP Violation in the Renormalizable Theory of Weak Interaction*. Prog. Theor. Phys. **49**, (1973), 652–657. (Cited on page 2.)
- [19] Herb S.W. et al. *Observation of a Dimuon Resonance at 9.5-GeV in 400-GeV Proton-Nucleus Collisions*. Phys. Rev. Lett. **39**, (1977), 252–255. (Cited on page 2.)
- [20] Abe F. et al. [CDF]. *Observation of top quark production in $\bar{p}p$ collisions*. Phys. Rev. Lett. **74**, (1995), 2626–2631. arXiv:hep-ex/9503002. (Cited on page 2.)
- [21] Abachi S. et al. [D0]. *Observation of the top quark*. Phys. Rev. Lett. **74**, (1995), 2632–2637. arXiv:hep-ex/9503003. (Cited on page 2.)
- [22] Eberhardt O., Lenz A., Menzel A., Nierste U. and Wiebusch M. *Status of the fourth fermion generation before ICHEP2012: Higgs data and electroweak precision observables*. Phys. Rev. **D86**, (2012), 074014. arXiv:1207.0438. (Cited on page 2.)
- [23] Abe K. et al. [Belle]. *Observation of large CP violation in the neutral B meson system*. Phys. Rev. Lett. **87**, (2001), 091802. arXiv:hep-ex/0107061. (Cited on page 2.)
- [24] Aubert B. et al. [BaBar]. *Observation of CP violation in the B^0 meson system*. Phys. Rev. Lett. **87**, (2001), 091801. arXiv:hep-ex/0107013. (Cited on page 2.)
- [25] Cabibbo N. *Unitary Symmetry and Leptonic Decays*. Phys. Rev. Lett. **10**, (1963), 531–533. (Cited on page 2.)

- [26] Abbiendi G. et al. [OPAL]. *Tests of the standard model and constraints on new physics from measurements of fermion pair production at 189-GeV to 209-GeV at LEP*. Eur. Phys. J. **C33**, (2004), 173–212. arXiv:hep-ex/0309053. (Cited on page 3.)
- [27] Aad G. et al. [ATLAS]. *Observation of a new particle in the search for the Standard Model Higgs boson with the ATLAS detector at the LHC*. Phys. Lett. **B716**, (2012), 1–29. arXiv:1207.7214. (Cited on page 3.)
- [28] Chatrchyan S. et al. [CMS]. *Observation of a new boson at a mass of 125 GeV with the CMS experiment at the LHC*. Phys. Lett. **B716**, (2012), 30–61. arXiv:1207.7235. (Cited on page 3.)
- [29] Fukuda Y. et al. [Super-Kamiokande]. *Evidence for oscillation of atmospheric neutrinos*. Phys. Rev. Lett. **81**, (1998), 1562–1567. arXiv:hep-ex/9807003. (Cited on page 3.)
- [30] Ahmad Q.R. et al. [SNO]. *Direct evidence for neutrino flavor transformation from neutral current interactions in the Sudbury Neutrino Observatory*. Phys. Rev. Lett. **89**, (2002), 011301. arXiv:nucl-ex/0204008. (Cited on page 3.)
- [31] Canetti L., Drewes M. and Shaposhnikov M. *Matter and Antimatter in the Universe*. New J. Phys. **14**, (2012), 095012. arXiv:1204.4186. (Cited on page 3.)
- [32] Sakharov A.D. *Violation of CP Invariance, c Asymmetry, and Baryon Asymmetry of the Universe*. Pisma Zh. Eksp. Teor. Fiz. **5**, (1967), 32–35. [Usp. Fiz. Nauk161,61(1991)]. (Cited on page 3.)
- [33] Chadwick J. *The intensity distribution in the magnetic spectrum of beta particles from radium ($B + C$)*. Verh. Phys. Gesell. **16**, (1914), 383–391. (Cited on page 4.)
- [34] Beneke M., Buchalla G., Neubert M. and Sachrajda C.T. *QCD factorization for exclusive, nonleptonic B meson decays: General arguments and the case of heavy light final states*. Nucl. Phys. **B591**, (2000), 313–418. arXiv:hep-ph/0006124. (Cited on page 5.)
- [35] Kraenkl S., Mannel T. and Virto J. *Three-Body Non-Leptonic B Decays and QCD Factorization*. Nucl. Phys. **B899**, (2015), 247–264. arXiv:1505.04111. (Cited on page 5.)

- [36] Beringer J. et al. [Particle Data Group]. *Review of Particle Physics (RPP)*. Phys.Rev. **D86**, (2012), 010001. (Cited on pages 7, 11, 14, 15, 18, 22, 57, 59, 62, 69, 75, 79, 86 and 137.)
- [37] Schwartz M.D. *Quantum Field Theory and the Standard Model*. Cambridge University Press, 2014. (Cited on page 7.)
- [38] Donoghue J.F., Golowich E. and Holstein B.R. *Dynamics of the standard model*. Camb. Monogr. Part. Phys. Nucl. Phys. Cosmol. **2**, (1992), 1–540. (Cited on page 7.)
- [39] Wolfenstein L. *Parametrization of the Kobayashi-Maskawa Matrix*. Phys. Rev. Lett. **51**, (1983), 1945. (Cited on page 14.)
- [40] Charles J., Hocker A., Lacker H., Laplace S., Le Diberder F.R., Malcles J., Ocariz J., Pivk M. and Roos L. [CKMfitter Group]. *CP violation and the CKM matrix: Assessing the impact of the asymmetric B factories*. Eur. Phys. J. **C41**, (2005), 1–131. arXiv:hep-ph/0406184. (Cited on page 16.)
- [41] Faddeev L.D. and Popov V.N. *Feynman Diagrams for the Yang-Mills Field*. Phys. Lett. **B25**, (1967), 29–30. (Cited on page 17.)
- [42] Cabibbo N., Parisi G. and Testa M. *Hadron Production in $e^+ e^-$ Collisions*. Lett. Nuovo Cim. **4S1**, (1970), 35–39. [Lett. Nuovo Cim.4,35(1970)]. (Cited on page 20.)
- [43] Jeschonnek S. and Van Orden J. *Quark hadron duality* 222–233. arXiv:hep-ph/0209157. (Cited on pages 21 and 36.)
- [44] Gorishnii S.G., Kataev A.L. and Larin S.A. *The $O(\alpha_s^{**3})$ corrections to sigma-tot ($e^+ e^- \rightarrow$ hadrons) and Gamma ($\tau \rightarrow$ tau-neutrino + hadrons) in QCD*. Phys. Lett. **B259**, (1991), 144–150. (Cited on page 22.)
- [45] Shifman M.A., Vainshtein A. and Zakharov V.I. *QCD and Resonance Physics. Sum Rules*. Nucl.Phys. **B147**, (1979), 385–447. (Cited on pages 23, 34 and 58.)
- [46] Aaij R. et al. [LHCb]. *First Evidence for the Decay $B_s^0 \rightarrow \mu^+ \mu^-$* . Phys.Rev.Lett. **110** (2), (2013), 021801. arXiv:1211.2674. (Cited on page 23.)
- [47] Aaij R. et al. [LHCb]. *Measurement of the $B_s^0 \rightarrow \mu^+ \mu^-$ branching fraction and search for $B^0 \rightarrow \mu^+ \mu^-$ decays at the LHCb experiment*. Phys.Rev.Lett. **111**, (2013), 101805. arXiv:1307.5024. (Cited on page 23.)

- [48] Chatrchyan S. et al. [CMS]. *Measurement of the $B(s)$ to $\mu^+ \mu^-$ branching fraction and search for B^0 to $\mu^+ \mu^-$ with the CMS Experiment*. Phys.Rev.Lett. **111**, (2013), 101804. arXiv:1307.5025. (Cited on page 23.)
- [49] Bazavov A. et al. [Fermilab Lattice, MILC]. *B - and D -meson decay constants from three-flavor lattice QCD*. Phys.Rev. **D85**, (2012), 114506. arXiv:1112.3051. (Cited on pages 23, 76 and 77.)
- [50] Davies C., McNeile C., Follana E., Lepage G., Na H. et al. *Update: Precision D_s decay constant from full lattice QCD using very fine lattices*. Phys.Rev. **D82**, (2010), 114504. arXiv:1008.4018. (Cited on pages 23, 76 and 77.)
- [51] Dowdall R., Davies C., Horgan R., Monahan C. and Shigemitsu J. [HPQCD]. *B -Meson Decay Constants from Improved Lattice Nonrelativistic QCD with Physical u , d , s , and c Quarks*. Phys.Rev.Lett. **110** (22), (2013), 222003. arXiv:1302.2644. (Cited on pages 23, 76 and 77.)
- [52] Laiho J., Lunghi E. and Van de Water R.S. *Lattice QCD inputs to the CKM unitarity triangle analysis*. Phys.Rev. **D81**, (2010), 034503. arXiv:0910.2928. (Cited on page 23.)
- [53] Jamin M. and Lange B.O. *f_B and f_{B_s} from QCD sum rules* 056005. arXiv:hep-ph/0108135. (Cited on pages 23, 24, 33, 57, 61, 75, 76, 127, 138 and 150.)
- [54] Narison S. *A fresh look into $m_{c,b}$ and precise $f_{D(s),B(s)}$ from heavy-light QCD spectral sum rules*. Phys.Lett. **B718**, (2013), 1321–1333. arXiv:1209.2023. (Cited on page 23.)
- [55] Lucha W., Melikhov D. and Simula S. *Accurate bottom-quark mass from Borel QCD sum rules for f_B and f_{B_s}* . Phys.Rev. **D88**, (2013), 056011. arXiv:1305.7099. (Cited on page 23.)
- [56] Belyaev V., Braun V.M., Khodjamirian A. and Ruckl R. *$D^* D \pi$ and $B^* B \pi$ couplings in QCD*. Phys.Rev. **D51**, (1995), 6177–6195. arXiv:hep-ph/9410280. (Cited on page 23.)
- [57] Kallen G. *On the definition of the Renormalization Constants in Quantum Electrodynamics*. Helv. Phys. Acta **25** (4), (1952), 417. [509(1952)]. (Cited on pages 24 and 27.)

- [58] Lehmann H. *On the Properties of propagation functions and renormalization constants of quantized fields.* Nuovo Cim. **11**, (1954), 342–357. (Cited on pages 24 and 27.)
- [59] Poggio E., Quinn H.R. and Weinberg S. *Smearing the Quark Model.* Phys.Rev. **D13**, (1976), 1958. (Cited on pages 24 and 36.)
- [60] Shifman M.A. *Quark hadron duality* hf8/013. arXiv:hep-ph/0009131. (Cited on pages 24 and 36.)
- [61] Shuryak E.V. *Hadrons Containing a Heavy Quark and QCD Sum Rules.* Nucl.Phys. **B198**, (1982), 83. (Cited on pages 24 and 39.)
- [62] Neubert M. *Heavy meson form-factors from QCD sum rules.* Phys.Rev. **D45**, (1992), 2451–2466. (Cited on pages 24, 33, 39 and 41.)
- [63] Bagan E., Ball P., Braun V.M. and Dosch H.G. *QCD sum rules in the effective heavy quark theory.* Phys.Lett. **B278**, (1992), 457–464. (Cited on page 24.)
- [64] Broadhurst D.J. and Grozin A. *Operator product expansion in static quark effective field theory: Large perturbative correction.* Phys.Lett. **B274**, (1992), 421–427. arXiv:hep-ph/9908363. (Cited on page 24.)
- [65] Broadhurst D.J. *Chiral Symmetry Breaking and Perturbative QCD.* Phys.Lett. **B101**, (1981), 423–426. (Cited on pages 24 and 32.)
- [66] Generalis S. *QCD sum rules. 1: Perturbative results for current correlators.* J.Phys. **G16**, (1990), 785–793. (Cited on pages 24 and 32.)
- [67] Dominguez C. and Paver N. *Leptonic Decay Constants of Heavy Flavor Mesons of Arbitrary Mass.* Phys.Lett. **B246**, (1990), 493–497. (Cited on pages 24 and 34.)
- [68] Chetyrkin K., Kuhn J.H. and Steinhauser M. *RunDec: A Mathematica package for running and decoupling of the strong coupling and quark masses.* Comput.Phys.Comm. **133**, (2000), 43–65. arXiv:hep-ph/0004189. (Cited on pages 24 and 59.)
- [69] Gelhausen P. *Hadronische Matrixelemente mit schweren Quarks aus QCD-Summenregeln.* Ph.D. thesis, Universität Siegen. (Cited on pages 24, 26, 32, 35 and 63.)

- [70] Peskin M.E. and Schroeder D.V. *An Introduction to quantum field theory*. Westview Press, 1995. (Cited on pages 26, 131, 132 and 143.)
- [71] Hassani S. *Mathematical physics: a modern introduction to its foundations*. Springer, 1999. (Cited on pages 28 and 144.)
- [72] Kniehl B.A. *Dispersion relations in loop calculations*. Acta Phys.Polon. **B27**, (1996), 3631–3644. arXiv:hep-ph/9607255. (Cited on page 28.)
- [73] Radyushkin A. *Introduction into QCD sum rule approach* arXiv:hep-ph/0101227. (Cited on page 28.)
- [74] Colangelo P. and Khodjamirian A. *QCD sum rules, a modern perspective* arXiv:hep-ph/0010175. (Cited on page 30.)
- [75] Chetyrkin K. and Steinhauser M. *Heavy - light current correlators at order α_s^2 in QCD and HQET*. Eur.Phys.J. **C21**, (2001), 319–338. arXiv:hep-ph/0108017. (Cited on pages 31, 32, 55 and 147.)
- [76] Novikov V., Shifman M.A., Vainshtein A. and Zakharov V.I. *Calculations in External Fields in Quantum Chromodynamics. Technical Review*. Fortsch.Phys. **32**, (1984), 585. (Cited on page 33.)
- [77] Aliev T. and Eletsky V. *On Leptonic Decay Constants of Pseudoscalar D and B Mesons*. Sov.J.Nucl.Phys. **38**, (1983), 936. (Cited on page 34.)
- [78] Ioffe B. *Condensates in quantum chromodynamics*. Phys.Atom.Nucl. **66**, (2003), 30–43. arXiv:hep-ph/0207191. (Cited on pages 35, 58 and 62.)
- [79] Neubert M. *Heavy quark symmetry*. Phys.Rept. **245**, (1994), 259–396. arXiv:hep-ph/9306320. (Cited on pages 40, 41, 74 and 75.)
- [80] Manohar A.V. and Wise M.B. *Heavy quark physics*. Camb. Monogr. Part. Phys. Nucl. Phys. Cosmol. **10**, (2000), 1–191. (Cited on page 41.)
- [81] Grozin A. *Lectures on QED and QCD: Practical calculation and renormalization of one- and multi-loop Feynman diagrams*. (Cited on pages 44 and 137.)
- [82] Smirnov V. *Feynman integral calculus*. (Cited on page 44.)
- [83] Huber T. and Maitre D. *HypExp: A Mathematica package for expanding hypergeometric functions around integer-valued parameters*. Comput.Phys.Commun. **175**, (2006), 122–144. arXiv:hep-ph/0507094. (Cited on page 46.)

- [84] Chetyrkin K. and Tkachov F. *Integration by Parts: The Algorithm to Calculate beta Functions in 4 Loops*. Nucl.Phys. **B192**, (1981), 159–204. (Cited on page 47.)
- [85] Lee R. *Presenting LiteRed: a tool for the Loop InTEgrals REDuction* arXiv:1212.2685. (Cited on pages 49 and 153.)
- [86] Lee R.N. *LiteRed 1.4: a powerful tool for reduction of multiloop integrals*. J.Phys.Conf.Ser. **523**, (2014), 012059. arXiv:1310.1145. (Cited on pages 49 and 153.)
- [87] Cutkosky R.E. *Singularities and discontinuities of Feynman amplitudes*. J. Math. Phys. **1**, (1960), 429–433. (Cited on page 51.)
- [88] Khodjamirian A. and Ruckl R. *QCD sum rules for exclusive decays of heavy mesons*. Adv.Ser.Direct.High Energy Phys. **15**, (1998), 345–401. arXiv:hep-ph/9801443. (Cited on pages 55 and 73.)
- [89] Dehnadi B., Hoang A.H., Mateu V. and Zebarjad S.M. *Charm Mass Determination from QCD Charmonium Sum Rules at Order α_s^3* . JHEP **1309**, (2013), 103. arXiv:1102.2264. (Cited on page 57.)
- [90] Chetyrkin K., Kuhn J., Maier A., Maierhofer P., Marquard P. et al. *Precise Charm- and Bottom-Quark Masses: Theoretical and Experimental Uncertainties*. Theor.Math.Phys. **170**, (2012), 217–228. arXiv:1010.6157. (Cited on pages 57 and 73.)
- [91] Chetyrkin K. and Khodjamirian A. *Strange quark mass from pseudoscalar sum rule with $O(\alpha(s)^{**4})$ accuracy*. Eur.Phys.J. **C46**, (2006), 721–728. arXiv:hep-ph/0512295. (Cited on page 57.)
- [92] Jamin M., Oller J. and Pich A. *Scalar K pi form factor and light quark masses*. Phys.Rev. **D74**, (2006), 074009. arXiv:hep-ph/0605095. (Cited on page 57.)
- [93] Bodenstein S., Dominguez C.A. and Schilcher K. *Strange quark mass from sum rules with improved perturbative QCD convergence*. JHEP **1307**, (2013), 138. arXiv:1305.3796. (Cited on page 57.)
- [94] Khodjamirian A., Klein C., Mannel T. and Offen N. *Semileptonic charm decays $D \rightarrow \pi l \nu(l)$ and $D \rightarrow K l \nu(l)$ from QCD Light-Cone Sum Rules*. Phys.Rev. **D80**, (2009), 114005. arXiv:0907.2842. (Cited on page 58.)

- [95] Leutwyler H. *The Ratios of the light quark masses*. Phys.Lett. **B378**, (1996), 313–318. arXiv:hep-ph/9602366. (Cited on pages 58 and 62.)
- [96] Marquard P., Smirnov A.V., Smirnov V.A. and Steinhauser M. *Quark Mass Relations to Four-Loop Order in Perturbative QCD*. Phys. Rev. Lett. **114** (14), (2015), 142002. arXiv:1502.01030. (Cited on page 59.)
- [97] Duplancic G., Khodjamirian A., Mannel T., Melic B. and Offen N. *Light-cone sum rules for $B \rightarrow \pi$ form factors revisited*. JHEP **0804**, (2008), 014. arXiv:0801.1796. (Cited on page 59.)
- [98] Narison S. *On the Laplace Transform of the Weinberg Type Sum Rules and on the Properties of Pseudoscalar Mesons*. Z.Phys. **C14**, (1982), 263. (Cited on page 61.)
- [99] Khodjamirian A. *Upper bounds on $f(D)$ and $f(D(s))$ from two-point correlation function in QCD*. Phys.Rev. **D79**, (2009), 031503. arXiv:0812.3747. (Cited on pages 61 and 64.)
- [100] del Amo Sanchez P. et al. [BaBar]. *Observation of new resonances decaying to $D\pi$ and $D^*\pi$ in inclusive e^+e^- collisions near $\sqrt{s} = 10.58$ GeV*. Phys.Rev. **D82**, (2010), 111101. arXiv:1009.2076. (Cited on pages 69, 70, 79, 83 and 86.)
- [101] Lucha W., Melikhov D. and Simula S. *Decay constants of the charmed vector mesons D^* and D_s^* from QCD sum rules*. Phys.Lett. **B735**, (2014), 12–18. arXiv:1404.0293. (Cited on page 75.)
- [102] Narison S. *$f_{D^*(s)}$, $f_{B^*(s)}$ and f_{B_c} from QCD Laplace sum rules* arXiv:1404.6642. (Cited on page 75.)
- [103] Lucha W., Melikhov D. and Simula S. *Accurate decay-constant ratios f_{B^*}/f_B and $f_{B_s^*}/f_{B_s}$ from Borel QCD sum rules* arXiv:1504.03017. (Cited on pages 75 and 77.)
- [104] Penin A. and Steinhauser M. *Heavy light meson decay constant from QCD sum rules in three loop approximation*. Phys.Rev. **D65**, (2002), 054006. arXiv:hep-ph/0108110. (Cited on pages 75, 76 and 127.)
- [105] Bordes J., Penarrocha J. and Schilcher K. *B and $B(s)$ decay constants from QCD duality at three loops*. JHEP **0412**, (2004), 064. arXiv:hep-ph/0410328. (Cited on page 75.)

- [106] Bordes J., Penarrocha J. and Schilcher K. *D and D(S) decay constants from QCD duality at three loops*. JHEP **0511**, (2005), 014. arXiv:hep-ph/0507241. (Cited on page 75.)
- [107] Colquhoun B., Davies C., Dowdall R., Kettle J., Koponen J. et al. *B-meson decay constants: a more complete picture from full lattice QCD* arXiv:1503.05762. (Cited on pages 75, 76, 77 and 128.)
- [108] Adachi I. et al. [Belle]. *Evidence for $B^- \rightarrow \tau^- \bar{\nu}_\tau$ with a Hadronic Tagging Method Using the Full Data Sample of Belle*. Phys.Rev.Lett. **110** (13), (2013), 131801. arXiv:1208.4678. (Cited on page 75.)
- [109] Khodjamirian A., Mannel T., Offen N. and Wang Y.M. *$B \rightarrow \pi \ell \nu_\ell$ Width and $|V_{ub}|$ from QCD Light-Cone Sum Rules*. Phys.Rev. **D83**, (2011), 094031. arXiv:1103.2655. (Cited on page 75.)
- [110] Becirevic D., Lubicz V., Sanfilippo F., Simula S. and Tarantino C. *D-meson decay constants and a check of factorization in non-leptonic B-decays*. JHEP **1202**, (2012), 042. arXiv:1201.4039. (Cited on pages 76 and 77.)
- [111] Rosner J.L. and Stone S. *Leptonic Decays of Charged Pseudoscalar Mesons - 2013* arXiv:1309.1924. (Cited on page 76.)
- [112] Brodzicka J. et al. [Belle]. *Observation of a new $D(sJ)$ meson in $B^+ \rightarrow \text{anti-}D^0 K^+$ decays*. Phys.Rev.Lett. **100**, (2008), 092001. arXiv:0707.3491. (Cited on page 79.)
- [113] Poluektov A. *Recent results in excited charm and beauty hadron spectroscopy*. PoS **HQL2012**, (2012), 004. (Cited on pages 79 and 84.)
- [114] Bevan A.J. et al. [Belle, BaBar]. *The Physics of the B Factories*. Eur. Phys. J. **C74**, (2014), 3026. arXiv:1406.6311. (Cited on page 79.)
- [115] Aaltonen T.A. et al. [CDF]. *Study of orbitally excited B mesons and evidence for a new $B\pi$ resonance*. Phys. Rev. **D90** (1), (2014), 012013. arXiv:1309.5961. (Cited on page 79.)
- [116] Ebert D., Faustov R. and Galkin V. *Heavy-light meson spectroscopy and Regge trajectories in the relativistic quark model*. Eur.Phys.J. **C66**, (2010), 197–206. arXiv:0910.5612. (Cited on pages 79, 84 and 86.)

- [117] Shah M., Patel B. and Vinodkumar P.C. *Mass spectra and decay properties of D Meson in a relativistic Dirac formalism* arXiv:1412.7400. (Cited on page 79.)
- [118] Becirevic D., Blossier B., Gerardin A., Le Yaouanc A. and Sanfilippo F. *On the significance of B -decays to radially excited D* . Nucl.Phys. **B872**, (2013), 313–332. arXiv:1301.7336. (Cited on pages 79, 89 and 129.)
- [119] Mohler D., Prelovsek S. and Woloshyn R.M. *$D\pi$ scattering and D meson resonances from lattice QCD*. Phys. Rev. **D87** (3), (2013), 034501. arXiv:1208.4059. (Cited on page 79.)
- [120] Moir G., Peardon M., Ryan S.M., Thomas C.E. and Liu L. *Excited spectroscopy of charmed mesons from lattice QCD*. JHEP **05**, (2013), 021. arXiv:1301.7670. (Cited on page 79.)
- [121] Bernlochner F.U., Ligeti Z. and Turczyk S. *A Proposal to solve some puzzles in semileptonic B decays*. Phys.Rev. **D85**, (2012), 094033. arXiv:1202.1834. (Cited on pages 79 and 89.)
- [122] Kuhn J.H. and Santamaria A. *Tau decays to pions*. Z.Phys. **C48**, (1990), 445–452. (Cited on page 85.)
- [123] Bruch C., Khodjamirian A. and Kuhn J.H. *Modeling the pion and kaon form factors in the timelike region*. Eur.Phys.J. **C39**, (2005), 41–54. arXiv:hep-ph/0409080. (Cited on page 85.)
- [124] Bigi I.I.Y., Uraltsev N.G. and Vainshtein A.I. *Nonperturbative corrections to inclusive beauty and charm decays: QCD versus phenomenological models*. Phys. Lett. **B293**, (1992), 430–436. [Erratum: Phys. Lett.B297,477(1993)], arXiv:hep-ph/9207214. (Cited on page 92.)
- [125] Bigi I.I.Y., Shifman M.A., Uraltsev N.G. and Vainshtein A.I. *QCD predictions for lepton spectra in inclusive heavy flavor decays*. Phys. Rev. Lett. **71**, (1993), 496–499. arXiv:hep-ph/9304225. (Cited on page 92.)
- [126] Blok B., Koyrakh L., Shifman M.A. and Vainshtein A.I. *Differential distributions in semileptonic decays of the heavy flavors in QCD*. Phys. Rev. **D49**, (1994), 3356. [Erratum: Phys. Rev.D50,3572(1994)], arXiv:hep-ph/9307247. (Cited on page 92.)
- [127] Manohar A.V. and Wise M.B. *Inclusive semileptonic B and polarized $\Lambda(b)$ decays from QCD*. Phys. Rev. **D49**, (1994), 1310–1329. arXiv:hep-ph/9308246. (Cited on page 92.)

- [128] Benson D., Bigi I.I., Mannel T. and Uraltsev N. *Imprecated, yet impeccable: On the theoretical evaluation of $\Gamma(B \rightarrow X(c) l \nu)$* . Nucl. Phys. **B665**, (2003), 367–401. arXiv:hep-ph/0302262. (Cited on page 92.)
- [129] Alberti A., Gambino P., Healey K.J. and Nandi S. *Precision Determination of the Cabibbo-Kobayashi-Maskawa Element V_{cb}* . Phys. Rev. Lett. **114** (6), (2015), 061802. arXiv:1411.6560. (Cited on pages 92 and 93.)
- [130] Biswas S. and Melnikov K. *Second order QCD corrections to inclusive semileptonic $b \rightarrow X(c) l \text{ anti-}\nu(l)$ decays with massless and massive lepton*. JHEP **02**, (2010), 089. arXiv:0911.4142. (Cited on page 92.)
- [131] Pak A. and Czarnecki A. *Heavy-to-heavy quark decays at NNLO*. Phys. Rev. **D78**, (2008), 114015. arXiv:0808.3509. (Cited on page 92.)
- [132] Becher T., Boos H. and Lunghi E. *Kinetic corrections to $B \rightarrow X_c l \bar{\nu}$ at one loop*. JHEP **12**, (2007), 062. arXiv:0708.0855. (Cited on page 92.)
- [133] Alberti A., Ewerth T., Gambino P. and Nandi S. *Kinetic operator effects in $\bar{B} \rightarrow X_c l \nu$ at $O(\alpha_s)$* . Nucl. Phys. **B870**, (2013), 16–29. arXiv:1212.5082. (Cited on page 92.)
- [134] Alberti A., Gambino P. and Nandi S. *Perturbative corrections to power suppressed effects in semileptonic B decays*. JHEP **1401**, (2014), 147. arXiv:1311.7381. (Cited on pages 92, 111 and 129.)
- [135] Mannel T., Turczyk S. and Uraltsev N. *Higher Order Power Corrections in Inclusive B Decays*. JHEP **11**, (2010), 109. arXiv:1009.4622. (Cited on pages 92, 112 and 130.)
- [136] Bailey J.A. et al. [Fermilab Lattice, MILC]. *Update of $|V_{cb}|$ from the $\bar{B} \rightarrow D^* l \bar{\nu}$ form factor at zero recoil with three-flavor lattice QCD*. Phys. Rev. **D89** (11), (2014), 114504. arXiv:1403.0635. (Cited on page 93.)
- [137] Crivellin A. and Pokorski S. *Can the differences in the determinations of V_{ub} and V_{cb} be explained by New Physics?*. Phys. Rev. Lett. **114** (1), (2015), 011802. arXiv:1407.1320. (Cited on page 93.)
- [138] Georgi H. *An Effective Field Theory for Heavy Quarks at Low-energies*. Phys. Lett. **B240**, (1990), 447–450. (Cited on page 94.)

- [139] Eichten E. and Hill B.R. *An Effective Field Theory for the Calculation of Matrix Elements Involving Heavy Quarks*. Phys. Lett. **B234**, (1990), 511. (Cited on page 94.)
- [140] Grinstein B. *The Static Quark Effective Theory*. Nucl. Phys. **B339**, (1990), 253–268. (Cited on page 94.)
- [141] Isgur N. and Wise M.B. *Weak Decays of Heavy Mesons in the Static Quark Approximation*. Phys. Lett. **B232**, (1989), 113–117. (Cited on page 94.)
- [142] Mannel T., Roberts W. and Ryzak Z. *A Derivation of the heavy quark effective Lagrangian from QCD*. Nucl. Phys. **B368**, (1992), 204–220. (Cited on page 95.)
- [143] Manohar A.V. *The HQET / NRQCD Lagrangian to order α / m^3* . Phys. Rev. **D56**, (1997), 230–237. arXiv:hep-ph/9701294. (Cited on pages 95 and 96.)
- [144] Eichten E. and Hill B.R. *Static Effective Field Theory: $1/m$ Corrections*. Phys.Lett. **B243**, (1990), 427–431. (Cited on pages 96 and 122.)
- [145] Grozin A. and Neubert M. *Higher order estimates of the chromomagnetic moment of a heavy quark*. Nucl.Phys. **B508**, (1997), 311–326. arXiv:hep-ph/9707318. (Cited on pages 96 and 122.)
- [146] Nir Y. *The Mass Ratio $m(c) / m(b)$ in Semileptonic B Decays*. Phys. Lett. **B221**, (1989), 184. (Cited on page 100.)
- [147] Grozin A.G. *Heavy quark effective theory*. Springer Tracts Mod. Phys. **201**, (2004), 1–213. (Cited on page 114.)
- [148] Bollini C.G. and Giambiagi J.J. *Dimensional Renormalization: The Number of Dimensions as a Regularizing Parameter*. Nuovo Cim. **B12**, (1972), 20–26. (Cited on page 131.)
- [149] Breitenlohner P. and Maison D. *Dimensional Renormalization and the Action Principle*. Commun. Math. Phys. **52**, (1977), 11–38. (Cited on page 131.)
- [150] Collins J.C. *Renormalization. An Introduction to renormalization, the renormalization group, and the operator product expansion*. 1984. (Cited on page 133.)
- [151] Pascual P. and Tarrach R. *QCD: Renormalization for the practitioner*. Lect.Notes Phys. **194**, (1984), 1–277. (Cited on page 138.)

- [152] Klein C. *Berechnung hadronischer Übergangsamplituden in der Charm-Physik*.
Ph.D. thesis, Universität Siegen. (Cited on page 143.)

List of Publications

- [A1] Gelhausen P., Khodjamirian A., Pivovarov A.A. and Rosenthal D. *Decay constants of heavy-light vector mesons from QCD sum rules*. Phys. Rev. D88, (2013), 014015. [Erratum: Phys. Rev.D91,099901(2015)], arXiv:1305.5432 (Cited on pages 24, 25, 33, 63 and 74.)
- [A2] Gelhausen P., Khodjamirian A., Pivovarov A.A. and Rosenthal D. *Radial excitations of heavy-light mesons from QCD sum rules*. Eur. Phys. J. C74 (8), (2014), 2979. arXiv:1404.5891. (Cited on page 79.)
- [A3] Mannel T., Pivovarov A.A. and Rosenthal D. *Inclusive semileptonic B decays from QCD with NLO accuracy for power suppressed terms*. Phys. Lett. B741, (2015), 290-294. arXiv:1405.5072. (Cited on page 93.)
- [A4] Mannel T., Pivovarov A.A. and Rosenthal D. *Inclusive weak decays of heavy hadrons with power suppressed terms at NLO* arXiv:1506.08167. (Cited on page 93.)

Acknowledgment

Die letzte Seite meiner Arbeit widme ich den vielen Weggefährten, die mich durch das Studium bis hin zur Promotion begleitet haben.

Zu Beginn möchte ich meinen Betreuern danken, denn ohne sie wären die Projekte nicht entstanden, welche schlussendlich zu dieser Dissertation geführt haben. Ich bin Prof. Dr. Alexander Khodjamirian sehr dankbar, denn er ermöglichte mir die Promotion in diesem außerordentlich interessanten Forschungsgebiet und stand mir während der gesamten Zeit tatkräftig zur Seite. Prof. Dr. Thomas Mannel danke ich, dass mir die Teilnahme an diversen Konferenzen, Workshops oder Teilchenphysikschulen im In- und Ausland ermöglicht wurde. Zu besonderem Dank bin ich Prof. Dr. Alexei A. Pivovarov verpflichtet, da er für sämtliche Projekte der erste Ansprechpartner war. Seine Expertise und Geduld haben maßgeblich zum erfolgreichen Abschluss meiner Dissertation beigetragen. Neben den vielen projektbezogenen Diskussionen waren ebenso die zahlreichen Gespräche über Gott und die Welt sehr anregend und interessant.

Des Weiteren danke ich meinen Kommilitonen. Mein besonderer Dank gilt Patrick Gelhausen, Florian Hartmann, Marco Sekulla und Susanne Kränkl. Wir haben zusammen gelitten und gelacht. Diese gemeinsame Zeit wird mir immer im Herzen bleiben.

Der gesamten Arbeitsgruppe TP1 bin ich für die tolle Arbeitsatmosphäre und die viele Unterstützung sehr dankbar.

Ich möchte auch meinem Mitbewohner Sebastian Schmidt für das erfolgreiche WG-Leben danken.

Desweiteren gilt mein Dank den Korrekturlesern Dr. Sven Faller, Dr. Danny van Dyk, Dr. Björn O. Lange, Susanne Weller, Flo, Paddy und meinem Bruder Oliver, da sie diese Arbeit mit ihren Tipps tiefgreifend geprägt haben.

Zu guter Letzt danke ich meiner Familie und insbesondere meinem Vater. Sie gaben mir seit Beginn des Studiums viel Unterstützung und den nötigen Freiraum damit ich mich meiner Arbeit möglichst unbesorgt widmen konnte.

Siegen, den 21. September 2015 (05:41 Uhr)

